Targeting medulloblastoma: Does subgroup-specific radioresponsiveness affect outcomes?

A thesis submitted to The University of Manchester

for the degree of Doctor of Philosophy in the

Faculty of Biology, Medicine and Health

2021

REBECCA C. MORRIS

School of Medical Sciences

Division of Cancer Sciences

Contents

Final word count – 55,974

List of Figures

List of Tables

List of Abbreviations

AC – astrocytoma
APC –adenomatous polyposis coli
AR – androgen receptor
ATCC – American type culture collection
ATM – ataxia-telangiectasia mutated
ATP – adenosine triphosphate
AUC – area under the curve
BABAM2 – BRISC and BRCA1 A complex member 2, formerly BRE
BBB – blood-brain barrier
BrdU – bromodeoxyuridine
c-myc – MYC proto-oncogene (protein)
CAIX – carbonic anhydrase IX
CCLE – cancer cell line encyclopaedia
CCND1 – cyclin D1
CD133+ - CD133-positive
CI – confidence interval
CK1α – casein kinase 1α
CNS – central nervous system
CON – carbogen and nicotinamide
cpm – counts per million
CSC – cancer stem cell
CSF – cerebrospinal fluid
CSI – craniospinal irradiation
CT – computed tomography
CTG – CellTiter-Glo
DDR – DNA damage response
DMSO – dimethylsulfoxide
DN – Desmoplastic/Nodular
DSB – double strand breaks
Dsh – dishevelled
ECM – extracellular matrix
EEF1E1 – eukaryotic translation elongation factor 1 epsilon 1, formerly AIMP3
EMT – epithelial-mesenchymal transition
FBS – fetal bovine serum
FDA – Food and Drug Administration
FGF20 – fibroblast growth factor 20
FISH – fluorescence *in situ* hybridisation
FZD – Frizzled
G1 – gap 1
G2 – gap 2
GBM – glioblastoma
GEO- Gene Expression Omnibus
GLI1 – Glioma-associated oncogene 1
GLUT1 – glucose transporter 1
GSK3β – glycogen synthase kinase-3β
H&N – head and neck
HCC – hepatocellular carcinoma
HIF – hypoxia-inducible factor
HR – hazard ratio
IdUrd – iododeoxyuridine
IHC – immunohistochemistry
INT – iodonitrotetrazolium violet
LCA – large cell/anaplastic
LEU – leukaemia
LQ – linear quadratic
LUAD – lung adenocarcinoma

M-phase – mitotic phase
MBEN – medulloblastoma with extensive nodularity
MBL – medulloblastoma
MESO – mesothelioma
MM2S – Medullo-Model to Subtypes
MMP – matrix metalloproteinase
mPI – meta-PCNA index
MRE11 – meitotic recombination 11
MRI – magnetic resonance imaging
MYC – Myc proto-oncogene (gene, mRNA)
NBL – neuroblastoma
NBN – nibrin
NSCLC – non-small cell lung cancer
OCRB – Oglesby Cancer Research Building
OER – oxygen enhancement ratio
PBS – phosphate buffered saline
PBT – proton beam therapy
PCNA – proliferating cell nuclear antigen
PCR – polymerase chain reaction
PE – plating efficiency
PF – proliferating fraction
PNET – primitive neuroectodermal tumour
PTCH1 – Patched1
RBE – Relative biological effectiveness
RLU – relative luminescence unit
RO – radius open
RSI – radiosensitivity index
S-phase – synthesis phase
SF2 – surviving fraction at 2 Gy
SHH – Sonic Hedgehog
shRNA – short-hairpin RNA
siRNA – small interfering RNA
SMO – Smoothened
SOBP – Spread out Bragg peak
ssGSEA – single-sample Gene Set Enrichment Analysis
STR – short tandem repeat
SUFU - Suppressor of Fused
TCGA – the cancer genome atlas
Td – population doubling time
TGFβ – Transforming growth factor β
VEGF – vascular endothelial growth factor
VFR – variance filter radius
WHO – World Health Organisation
WNT –Wingless-related integration site
WT – wild-type

SHH cell lines – DAOY, ONS-76, UW228-2
Group 3 cell lines – D283, D425, MED8A

Abstract

Background: Medulloblastoma accounts for 18% of all paediatric brain cancers with between 50 and 100 diagnoses in the UK each year. There are four molecular subgroups with distinct clinical characteristics, cellular origins and identifying mutations. The four molecular subgroups are WNT, SHH, Group 3 and Group 4. The same treatment is given to all patients regardless of subgroup, and the majority of patients over three years receive craniospinal irradiation. The WNT and SHH subgroups are named after the overactive signalling pathways found in these tumours; these signalling pathways are involved in proliferation and response to radiation. The underlying biology of the molecular subgroups could contribute to differences in radioresponsiveness through differences in intrinsic radiosensitivity, proliferative capacity and extent of tumour hypoxia. An understanding of subgroup-specific differences in radioresponsiveness would guide the personalisation of treatment based on a tumour's molecular subgroups.

Aims and Objectives: The aim of this project was to identify factors that might affect differences in the radioresponsiveness of the medulloblastoma subgroups. The specific objectives were to investigate differences in radiosensitivity, proliferation, tumour hypoxia and cell migration between the four molecular subgroups.

Methods: A panel of medulloblastoma cell lines representing the SHH and Group 3 subgroups was used in two radiosensitivity assays (a clonogenic and high-throughput assay) and a migration (gap closure) assay. The clonogenic assay was carried out with the adherent cell lines under normoxic and hypoxic (0.1% oxygen) conditions. The high-throughput assay work was carried out under normoxic conditions only. Radiation survival curves were fitted using a linear quadratic model. *In silico* analyses of publically available clinical cohorts were used to investigate a tumour radiosensitivity signature. Publically available data for clinical cohorts were also used to investigate proliferation measured as the mRNA expression of Ki67 and PCNA, and using a published gene signature. Tumour hypoxia was assessed using CAIX and GLUT1 mRNA expression data and published gene signatures. The gap closure assay was used with the adherent cell lines using barrier (Ibidi insert) and scratch (EssenBio WoundMaker) methods of gap creation. Cells were irradiated immediately, 24 h or 7 days prior to gap creation. Gap closure was monitored using time-lapse microscopy over 24 hours and image analysis carried out using software written for this thesis.

Results: The *in vitro* radiosensitivity assays showed SHH cell lines to be more radiosensitive than Group 3 cell lines. The *in silico* work confirmed this, reporting SHH as the most radiosensitive subgroup, followed by the WNT, Group 3 and Group 4 subgroups. Clinical cohort data showed proliferation was not prognostic in medulloblastoma, and no significant differences in proliferation between the molecular subgroups. The hypoxia biomarkers and gene expression signatures were also not prognostic in medulloblastoma. However, the molecular subgroups were associated with different patterns of hypoxia-associated gene expression. The least hypoxic subgroup was WNT followed by the SHH, Group 4 and Group 3 subgroups. The SHH subgroup cell lines were more migratory within the gap closure assay than the Group 3 cell line. Irradiation produced cell line-specific alterations in gap closure rate but no subgroup-specific alteration of migration following radiation treatment was observed.

Discussion: Subgroup-specific differences in intrinsic radiosensitivity and level of hypoxia are found within medulloblastoma and may contribute to subgroup-specific differences in radioresponsiveness and clinical outcomes. Further clarification of the role of hypoxia in medulloblastoma is required to confirm this relationship.

Declaration

No portion of the work referred to in this thesis has been submitted in support of an application for another degree or qualification of this or any other university or other institute of learning.

Copyright Statement

I. The author of this thesis (including any appendices and/or schedules to this thesis) owns certain copyright or related rights in it (the “Copyright”) and s/he has given the University of Manchester certain rights to use such Copyright, including for administrative purposes.

II. Copies of this thesis, either in full or in extracts and whether in hard or electronic copy, may be made **only** in accordance with the Copyright, Designs and Patents Act 1988 (as amended) and regulations issued under it or, where appropriate, in accordance with licensing agreements which the University has from time to time. This page must form part of any such copies made.

III. The ownership of certain Copyright, patents, designs, trademarks and other intellectual property (the “Intellectual Property”) and any reproductions of copyright works in the thesis, for example graphs and tables (“Reproductions”), which may be described in this thesis, may not be owned by the author and may be owned by third parties. Such Intellectual Property and Reproductions cannot and must not be made available for use without the prior written permission of the owner(s) of the relevant Intellectual Property and/or Reproductions.

IV. Further information on the conditions under which disclosure, publication and commercialisation of this thesis, the Copyright and any Intellectual Property and/or Reproductions described in it may take place is available in the University IP Policy (see http://documents.manchester.ac.uk/DocuInfo.aspx?DocID=24420), in any relevant Thesis restriction declarations deposited in the University Library, the University Library’s regulations (see http://www.library.manchester.ac.uk/about/regulations/) and in The University’s policy on Presentation of Theses.

Acknowledgements

I would first like to thank my main supervisor, Professor Catharine West, for providing support, advice, motivation and inspiration. I cannot express just how much her belief and encouragement has meant, but without it I would not have been able to navigate the complications and challenges of this PhD.

I would also like to express my gratitude and appreciation for the assistance of the rest of my supervisory team, Dr Martin McCabe, Professor Karen Kirkby and Dr Amy Chadwick. Specifically, I would like recognise the support and guidance provided by Martin and his understanding during the changes to the project and supervisory roles. Without his knowledge and contributions this work could not have been completed.

Dr Suzanne Johnson from CCG provided relentless and unparalleled support and I was incredibly lucky to work with her during this project. Her belief in my abilities and ability to provide a blend of positivity, realism and inspiration for any and all situations was invaluable. I would also like to thank Mr Christopher Smith for his advice and support, both technical and general. Although the latter was not always practical, my time in the laboratory would not have been half as much fun without it.

This work would also not have been possible without the support of Dr Elham Santina. Her practical advice and expertise were invaluable, and having her as a mentor and friend has been a true highlight of the past five years. I cannot thank her enough for her support, honesty and for keeping everything in perspective.

I would like to thank my father for his advice and proof-reading services, my brother for making coding more biologist-friendly and my mother for everything else! I would also like to thank my family for their love, support and understanding over the past five years, for more tolerance than I deserved and for providing me with the opportunities to get here.

1. Introduction

Cancer causes 25% of all UK deaths[1], and it is predicted that half of the population will receive a cancer diagnosis during their lifetime[2]. Across all cancer types, the 10-year survival rate is 50%, but this varies from 95% (melanoma[3] and testicular[4]) to <5% (pancreatic[4] and lung[3]). Paediatric cancers account for <1% of cancer diagnoses each year[5] and 5-year overall survival is 84%[5] (ranging from 25% for certain brain tumours to almost 100% for retinoblastoma[6]). Although the most common paediatric cancer is leukaemia (LEU), brain and central nervous system (CNS) tumours are the most common cause of paediatric cancer death[5]. Cancer treatments require a balance between maximising tumour control to increase survival and minimising normal tissue damage to reduce side effects. For paediatric patients, these side effects can have a severe impact on quality of life for survivors as developing tissues are more vulnerable to cancer treatments such as radiotherapy and patients have a longer potential lifespan following successful treatment.

For the paediatric brain tumour medulloblastoma (MBL), side effects of treatment include learning disabilities[7–9], sensorineural hearing loss[7,10] and growth hormone deficiency[11,12]. The classification of MBL has been re-assessed following a series of gene expression studies revealing distinct molecular characteristics that define four major molecular subgroups[13–18]. The four molecular subgroups have different clinical characteristics, including significantly different overall survival[13–18]. A natural hypothesis from this re-classification was that treatment could be re-optimised in order to reduce side effect severity in groups being over-treated, to increase survival in groups being under-treated, or to include targeted therapies based on underlying molecular biology. One facet of MBL treatment that is a candidate for these adjustments is radiotherapy. Radiotherapy contributes to 40% of all cancer cures[19], and irradiation of the brain and spinal cord is used for almost all MBL patients[20,21]. The reduction of radiation dose to these vulnerable regions based on subgroup status could produce real gains in terms of managing side effects by reducing normal tissue damage. Patient cohorts and clinical trial opportunities in MBL are limited due to small patient numbers and the typically young age of patients. Pre-clinical *in vitro* work to better

understand interactions between molecular features and cancer treatment is vital to maximise the information gained from these clinical resources.

In 2018, the Proton Beam Centre at The Christie hospital started treating UK patients with proton beam therapy (PBT)[22]. PBT is hypothesised to provide a better side effect profile due to the physics of proton energy deposition and is of particular interest for use in paediatric populations such as MBL patients. The radiobiology of PBT is not fully elucidated but certain differences between conventional high-energy x-ray radiotherapy and PBT are beginning to be reported. The different underlying biology of the MBL molecular subgroups suggests potentially different radioresponses between conventional x-rays and PBT. Several biological processes and characteristics (including intrinsic radiosensitivity, proliferation and hypoxia) affect radioresponse, and these can be investigated by either *in vitro* or *in silico* methods.

1.1 Medulloblastoma

1.1.1 Epidemiology and diagnosis

MBL is the most common malignant paediatric brain tumour and accounts for 18% of all paediatric brain tumours[20,23]. In the UK, there are between 50 and 100 MBLs diagnosed each year[24]; in the USA, between 250 and 500 children are diagnosed[25]. Certain genetic disorders, such as Li-Fraumeni[26]., Gorlin[26,27]. and Turcot[26]. syndromes (associated with mutations in the *TP53*, *PTCH* and DNA repair or *APC* genes respectively), are associated with an increased risk of MBL and are found in approximately 5% of MBLs[28]. Most cases of MBL, however, have no associated increased genetic risks and the causes are unknown[28,29].

MBLs originate in the cerebellum and metastasis usually occurs along the craniospinal axis[30]. However, as MBL tumours are multiclonal in origin these metastases may represent a different predominate clone than the primary tumour[31]. Because tumours are multiclonal in origin, metastases may contain different predominating clones to the primary tumour. Tumours are classified as low/standard- or high-risk based on the extent of resection[30,32] and the presence or absence of metastases[30,32]. Tumours with *MYC* amplification or anaplastic

histology are also classified as high-risk[32]. Treatment is based on standard- or high-risk status[30]. Other characteristics known to influence survival and used to define MBLs include histological and/or molecular subgroups and *TP53* mutation status – although these do not currently directly influence treatment decisions. Diagnostic tools for MBL include physical examination, brain magnetic resonance imaging (MRI), brain computed tomography (CT), histology and lumbar puncture[33].

1.1.2 Treatment

The treatment of MBL involves a combination of surgery, chemotherapy and radiotherapy. Standard- and high-risk patients over 3 years of age uniformly receive craniospinal irradiation (CSI)[20,21]. CSI targets the whole brain and the spine in order to irradiate the cerebrospinal fluid (CSF) through which MBL can metastasise[30,34]. For standard-risk disease the standard treatment protocol involves 23.4 Gy CSI followed by a posterior fossa and/or tumour bed boost[30,32]. For high-risk patients most regimens increase the CSI dose to either 36.0 or 39.6 Gy[30,32]. CSI is often given concurrently with cisplatin and/or cyclophosphamide-based chemotherapy regimens[30,32,35–38]. While these treatment protocols are not selected based on molecular subgroup status, personalised treatment regimens are currently under investigation (although these represent the minority of clinical trials; only 11 out of 287[39,40]). These include reducing CSI and/or chemotherapy regimens for WNT (Wingless-related integration site) subgroup tumours[41–45], including targeted therapy to inhibit Sonic Hedgehog (SHH) pathway activation in SHH subgroup tumours[41,45–49] and trialling alternative chemotherapy regimens for non-WNT/non-SHH subgroup tumours[41,45,50,51].

1.1.3 Survival

The 5-year overall survival rate for MBL increased over the past sixty years, from 29% in 1959[52] to current rates of 70-80% for standard-risk and 60-65% for high-risk patients[53,54]. Significant contributors to survival include patient age, tumour location, extent of resection, metastatic status, molecular subgroup and adjuvant treatment status[55,56].

Radiotherapy significantly contributes to both overall and progression-free survival in MBL patients, but CSI is associated with severe side effects such as decline in neurocognitive function[9,57,58], dementia or learning disability[7–9] and sensorineural hearing loss[7,10]. The age of a patient during treatment correlates well with subsequent learning ability, sociability, hobbies and relationships, with younger patients displaying larger deficits[59]. The irradiation of the endocrine system can result in growth hormone deficiency[11,12], hypothyroidism[11,12,60–62] and early[12,63–65] or delayed[66] puberty. Spinal irradiation combined with growth hormone deficiency can significantly reduce adult height[64,65]. Additionally, children who survive MBL have a higher mortality rate than their healthy peers and an increased risk of a secondary malignancy, which often occur in areas that received radiation[64,67].

1.1.4 Histological subgroups of medulloblastoma

In 2002, the Pediatric Oncology Group[68] described a histologically based classification of MBL defining four histological subgroups which were subsequently incorporated into the WHO classification[69]: Classic, Desmoplastic/Nodular (DN), MBL with Extensive Nodularity (MBEN), and Large Cell/Anaplastic (LCA). The majority of tumours show classic histology (74%), followed by DN (16%), LCA (7%) and MBEN (2.5%)[70]. Classic tumours have relatively round nuclei[71,72], no increase in cell size[71,72], no increase in mitotic activity or mitoses[71] and frequent Homer-Wright rosettes[71] (a pathological feature where differentiated tumour cells are grouped around a central point[73]). DN tumours have nodules of differentiated cells[68,71,72] within the tumour forming rows of cells with irregular nuclei[68] and show desmoplasia[72], where collagen is deposited around the cells[71]. MBEN tumours are a subtype of these DN tumours[71] where over 95% of the tumour contains irregular and coalesced nodules[68,72] (i.e. extensive nodularity). The LCA histological subgroup is a conventional grouping of two distinct histologies[71] with anaplastic features: anaplastic tumours and large cell tumours[71]. Anaplastic tumours have increased and irregular cell sizes[68,71,72], excess mitotic activity[68] and apoptotic bodies[71] and increased nuclear moulding[68,71] (where the shape of adjacent nuclei show conformity). Large cell tumours have increased cell sizes with a round cell morphology and prominent nucleoli[68] as well as the anaplastic features of frequent mitotic activity and apoptotic bodies[71]. The identification of

the histological subgroups using immunohistochemistry (IHC) allows this classification to be highly compatible with clinical use. The different histological subgroups are associated with slightly different survival outcomes, with DN or MBEN tumours having the best survival (82%), closely followed by classic tumours (78%)[70]. LCA tumours have only a 44% 5-year progression-free survival rate[70]. If the histological features are taken more generally, desmoplasia, which occurs in 22% of MBLs, was found to have no connection with clinical outcomes[68]. On the other hand anaplasia, found to some extent in 32% of MBL tumours, was found to be significantly associated with a worse overall survival, with a worse outcome with a greater extent of anaplasia[68].

1.1.5 Molecular subgroups of medulloblastoma

In 2016, the World Health Organisation (WHO) classification of CNS tumours was updated, classifying MBL using molecular subgroup, *TP53*-mutation status and histology[74]. The four molecular subgroups used in this classification were the consensus of international studies using large genomic data sets[13–18]. These subgroups were named WNT, SHH, Group 3 and Group 4 at a consensus meeting of the International Medulloblastoma Working Group[35]. Each subgroup has a distinct clinical profile, cellular origin, tumour location and identifying mutations[14,75–77]. The WNT subgroup is the least common, but has the best overall survival, Group 3 tumours have the worst outcome, while SHH and Group 4 have intermediate survival rates[15].

So far, no subgrouping method is in widespread routine clinical practice. The preferred method for assigning a molecular subgroup to a patient sample uses expression or methylation profile clustering, however this is expensive, requires technical expertise and the application of clustering algorithms require large sample cohorts (though reference cohorts are available)[13–18,38,76,78–83]. Alternative subgrouping methods using more clinically compatible techniques include IHC[13,76,79,80,84], fluorescence *in situ* hybridisation (FISH)[56,79,80], mass spectrometry[85] and MRI[86,87].

Alternative subgrouping classification schemes are regularly described, usually incorporating the four consensus subgroups to a greater or lesser extent (Table 1). These later classifications will likely lead to a new, better informed scheme in the future, taking into account clinical characteristics such as patient age or clinical outcomes[88]. The incorporation of clinical characteristics is not applicable to established MBL cell lines, limiting *in vitro* research to the current consensus subgroups.

TP53 status is included in the 2016 WHO classification[74]. *TP53* codes the protein p53, a transcription factor involved in stress responses and cell cycling[89]. *TP53* mutations occur in 10% to 45%[90–92] of MBL patients and are associated with significantly worse overall survival, 55% compared to 80% for *TP53* wild-type (WT) patients[91,92].*TP53* mutations most commonly occur in the WNT and SHH subgroups, with almost all of the germline *TP53* mutations (found in 2% of all MBLs) occurring within the SHH subgroup[90,91]. Interestingly, *TP53* mutations have different implications for survival depending on the subgroup. Within the SHH subgroup *TP53* mutations are associated with worse survival outcomes, while in WNT subgroup tumours *TP53* mutation status has no effect on the excellent survival outcomes[91,92].

Table 1: Summary of studies reporting subgrouping classifications of medulloblastoma

Study	Cohort size	Subgroup details
Thompson *et al*. 2006[79]	46	Group A, Group B (WNT), Group C, Group D (SHH), Group E
Kool *et al*. 2008[14]	62	WNT, SHH, Group C (neuronal differentiation genes), Group D (neuronal differentiation genes and by photoreceptor genes), Group E (photoreceptor genes)
Northcott *et al*. 2011[13]	103	WNT, SHH, Group C (NPR3-positive tumours), Group D (KCNA1-positive tumours)
Cho *et al*. 2011 [93]	194	Cluster 1 (*MYC*), Cluster 2 (Neuronal), Cluster 3 (SHH), Cluster 4 (mixed), Cluster 5 (photoreceptor), Cluster 6 (WNT)
Remke *et al*. 2011[17]	28[1]	WNT, SHH, Subtype D (non WNT/SHH)
WHO 2016[74]	NA	WNT-activated, SHH-activated and *TP53*-mutant, SHH-activated and *TP53*-wild-type, Non-WNT/non-SHH - Group 3, Non-WNT/non-SHH - Group 4
Schwalbe *et al*. 2017 [94]	428[2] 276[3]	WNT, SHH-Infant, SHH-Child, Gp3-High Risk*, Gp4-High Risk*, Gp3-Low Risk*, Gp4-Low Risk*
Cavalli *et al*. 2017 [95]	763	WNTα (children, monosomy 6), WNTβ (older patients, no monosomy 6), SHHα (children, worst prognosis, *MYCN* amplification, *GLI2* amplification. *TP53* mutations), SHHβ (infant, metastatic, *PTEN* deletions), SHHγ (less metastatic, no recurrent amplifications, enriched for MBEN histology), SHHδ (adults, TERT promoter mutations), Group 3α (metastatic), Group 3β (older, infrequently metastatic), Group 3γ (metastatic, worst prognosis, i17q, increased *MYC* copy numbers), Group 4α (*MYCN* amplification), Group 4β (higher median age), Group 4γ
Archer *et al*. 2018[96]	45	WNT, SHHa, SHHb, Group 3a (*MYC* activated), Group 3b (Group 3/4), Group 4
Lastowska *et al*. 2018[97]	68	WNT, SHH, Group 3, Group 3/4 (Intermediate), Group 4
Castillo-Rodriguez *et al*. 2018[98]	237	WNT, SHH, Group 3, Group 4α, Group 4β
Sharma *et al*. 2019[99]	1501	WNT, SHH, GpI (infants, classic, *GFI1/GFI1B* activation, *OTX2* amplification), GpII (child, majority metastatic, *MYC* amplification, *GFI/GFI1B* activation, *KBTBD4*, *SMARCA4*, *CTDNEP1*, *KMT2D* mutation), GpIII (child, mostly metastatic, mostly classic, *MYC/MYCN* amplification), GpIV (infant and child, mostly classic, mostly metastatic, no driver events), GpV (child, mostly class, mostly male, mostly metastatic, *MYCN* amplification), GpVI (child, mostly classic, *PRDM6* activation, *MYCN* amplification), GPVII (child, classic, *KBTBD4* mutation), GpVIII (child, male, classic, *PRDM6* activation, *KDM6A*, *ZMYM3*, *KMT2C* mutation)

*WHO – World Health Organisation; CNS – central nervous system; NA – not available; * risk based on MYC amplification, chromosome 13 loss, 5-year overall survival; 1 adult only cohort; 2 discovery cohort; 3 validation cohort*

1.1.6 WNT subgroup – clinical features

WNT tumours overexpress WNT pathway genes[13,14] (see Section 1.1.7 for a description of the WNT signalling pathway). It is the rarest molecular subgroup accounting for approximately 10% of patients[15,83,100,101]. These tumours respond well to surgery and CSI with survival rates over 90%[15,38,102,103], although survival in adult patients is significantly worse than those under 16[17]. WNT tumours are more common in children and adults than in infants, and there is a roughly equal proportion of male and female patients[101]. WNT tumours are rarely LCA with generally classic histology[101]. The age distribution and histology characteristics of these tumours are favourable because non-infant patients and classic histology are associated with better survival.

There are three identifying markers for the WNT subgroup: nuclear β-catenin, mutated *CTNNB1*, and monosomy 6[16,76,83,104,105]. The first two result in or from uncontrolled signalling through the WNT pathway. *CTNNB1* encodes the β-catenin protein, which is translocated to the nucleus upon WNT pathway activation and many of the reported *CTNNB1* mutations result in more stable nuclear localisation of β-catenin[100]. The third hallmark, monosomy 6, is detected in approximately 80% of cases but its biological impact is unclear[15,16].

Upregulated WNT signalling in MBL results in a disrupted blood-brain barrier (BBB) for WNT subgroup tumours[106]. The disrupted BBB gave chemotherapeutic agents better access to tumour cells in mouse models, resulting in a better chemotherapeutic response and contributing to better survival outcomes within this subgroup[106].

1.1.7 WNT subgroup – signalling pathway

The WNT signalling pathway, outlined in Figure 1, is an important developmental pathway in humans, regulating neuronal differentiation and proliferation[107]. In resting cells, β-catenin is bound in a complex with axin, GSK3β (Glycogen synthase kinase-3β), APC (adenomatous polyposis coli) and CK1α (casein kinase 1α)[108–110]. This complex targets β-catenin for degradation[108–110]. WNT signalling proteins bind to Frizzled (FZD) receptors and their co-

receptors LRP-5/6[110,111]. Activation of these receptors recruits Dishevelled (Dsh) and axin, thereby breaking up the axin/GSK3β/APC/CK1α complex[112]. β-catenin is released and translocates to the nucleus where it acts as a transcription factor[109,110]. Targets of the WNT signalling pathway include the genes *FGF20* (fibroblast growth factor 20)[111], *CCND1* (cyclin D1)[111,113] and *MYC* (c-myc)[111,114]. The upregulated WNT signalling in WNT subgroup tumours increases expression of *MYC* mRNA and c-myc protein in these tumours[115]. The expression of c-myc protein is as high in WNT tumours as in Group 3, in which *MYC* amplification is characteristic and associated with worse survival outcomes (see Section 1.1.10). Unlike Group 3 tumours however, *MYC* amplification is extremely rare in the WNT subgroup and this increased expression is attributed to c-myc being a downstream target of WNT signalling[116]. The negative survival implications of *MYC* amplification are, therefore, not observed in WNT tumours[116].

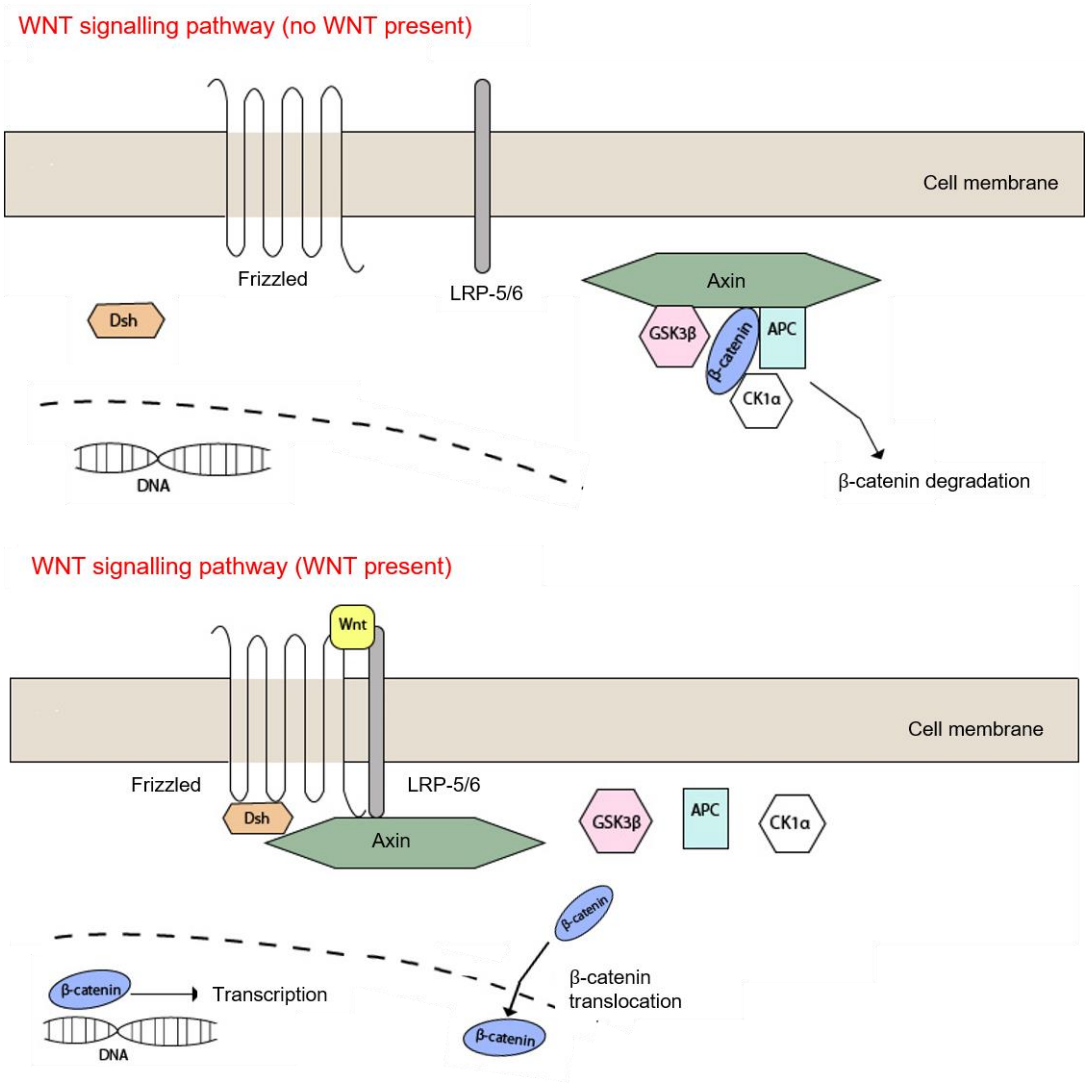

Figure 1: The WNT signalling pathway. *In the resting cell, β-catenin is targeted for degradation by a complex of Axin, GSK-3β, APC and CK1α. WNT signalling through the receptor Frizzled and the co-receptor LRP-5/6 activates Dishevelled. Activated Dishevelled causes the β-catenin degradation complex to break up. B-catenin is then free to translocate to the nucleus and act as a transcription factor. Adapted from Huse and Holland, 2010*[112]*. Dsh – Dishevelled, GSK3β – Glycogen synthase kinase-3 beta, APC – adenomatous polyposis coli, CK1α – casein kinase 1 alpha, WNT – Wingless-related integration site, LRP-5/6 – low-density lipoprotein receptor-related protein 5/6.*

1.1.8 SHH subgroup – clinical features

The SHH group contains the 30% of MBLs with overactive SHH pathways[13,15] (see Section 1.1.9 for a description of this pathway). The 5-year overall survival in the SHH subgroup is 60%[15,38,101,117]. SHH tumours are predominantly found in infant or adult patients[13,15,17,118], rarely occurring in children outside of infancy, and there is an equal representation of male and female patients[15,101]. Some classifications further divide the SHH subgroup based on patient age, as survival rates for adult patients are better than those for younger patients,

and adult SHH MBLs have different expression profiles[56,95,118]. SHH tumours are not linked to any particular histological subgroup, and can have classic, DN or LCA histology[101]. *TP53* mutations are the most important independent risk factor in the SHH subgroup, above age, sex, histology and the presence of metastases[91]. Patients with somatic *TP53*-mutated SHH MBL have a worse prognosis than those without, with 5-year overall survival rates of 41% and 81% respectively[91,103].

There are no clear, defining markers of SHH MBLs as described for the WNT subgroup. The most commonly used identifier is loss of the *PTCH1* gene by gene deletion or monosomy 9[14,76,83,118–120]. Loss of *PTCH1* only occurs in 40-50% of SHH tumours however and therefore cannot be used as a universal marker for this subgroup[14,76,83,118–120].

1.1.9 SHH subgroup – signalling pathway

The Hedgehog signalling pathway is implicated in the activation of cancer stem cells (CSCs) and subsequent tumour maintenance[121]. Activation of the SHH pathway has been associated with worse overall survival in non-small cell lung cancers (NSCLC)[122], breast cancer[123] and pancreatic adenocarcinomas[124]. Hepatocellular carcinoma (HCC) tissues have significantly increased mRNA levels of *SHH*, *PTCH1* (Patched1), *SMO* (Smoothened) and *GLI1* (Glioma-associated oncogene 1) compared to non-cancerous tissues[125].

The canonical SHH signalling pathway is implicated in MBL and is shown in Figure 2. Canonical signalling requires activation of the receptor PTCH1 by SHH ligand (non-canonical activation occurs independently of these proteins)[121]. In a resting cell, the surface membrane receptor PTCH1 inhibits the surface membrane protein SMO, and intracellularly Suppressor of Fused (SUFU) inhibits the GLI transcription factors (GLI1, GLI2 and GLI3). When SHH ligand binds the surface receptor PTCH1, the inhibition of SMO by this receptor is inhibited. SMO is then able to inhibit SUFU. Disinhibited GLI translocates to the nucleus to cause gene transcription. GLI1 targets include *CCND2* (cyclin D2)[126], *BCL-2*[127,128] and matrix metalloproteinases (MMPs)[127–130].

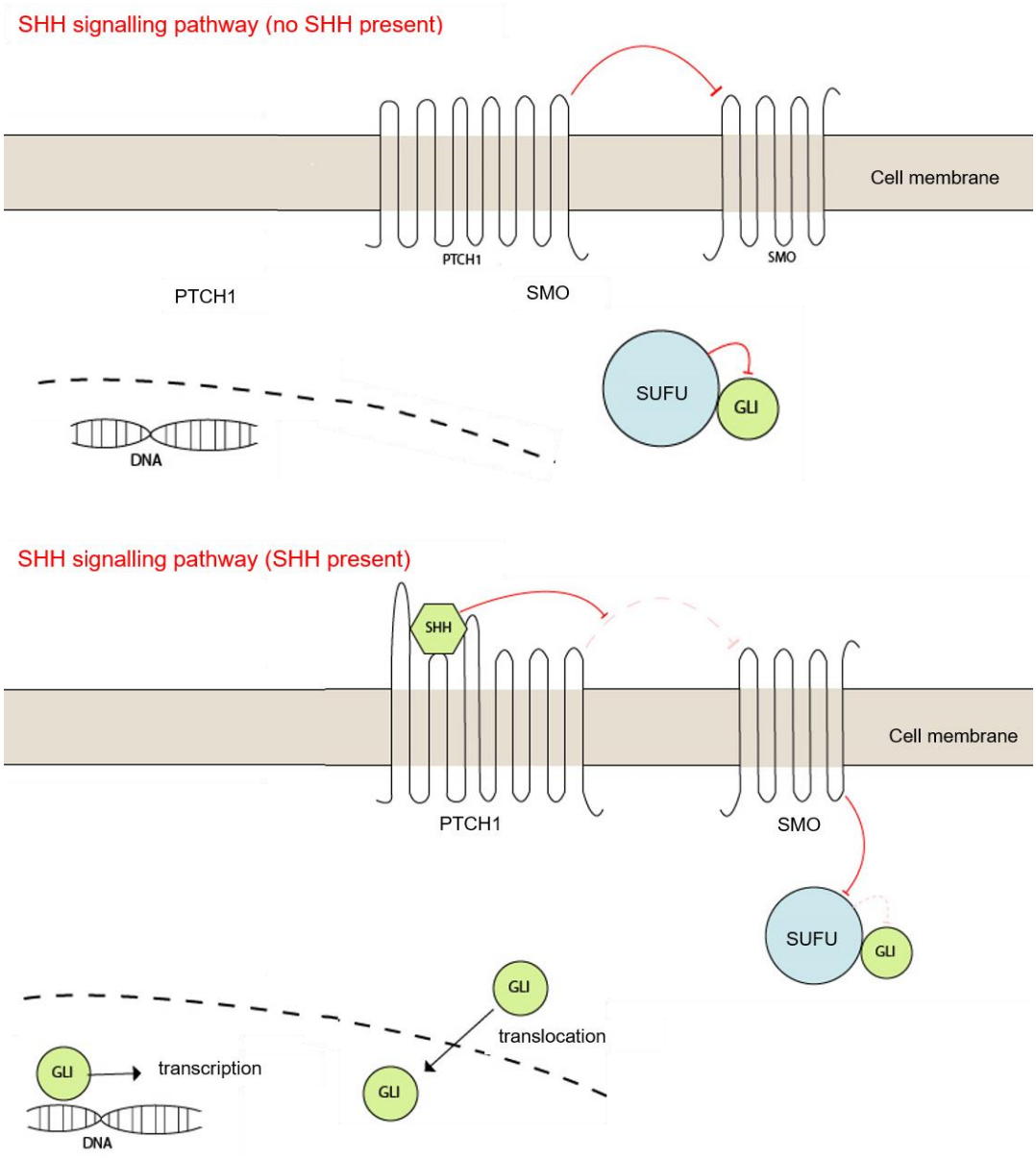

Figure 2: The SHH signalling pathway. *When activated, SHH binds the surface receptor PTCH1 which disinhibits the cell surface protein SMO leading to the disinhibition of Gli. Free Gli translocates to the nucleus and acts as a transcription factor. Adapted from Huse and Holland 2010[112]. PTCH1 – Patched1, SHH – Sonic Hedgehog, Gli – glioma-associated oncogene, SMO – Smoothened, SUFU – Suppressor of Fused homolog*

1.1.10 Group 3 subgroup – clinical features

The non-WNT/non-SHH subgroups have not yet been associated with specific aberrations or signalling pathways and are referred to by the names Group 3 and Group 4. Confirmation of Group 3 or Group 4 status is carried out using expression or methylation microarrays[71]. Approximately 30% of MBLs are Group 3, and this subgroup has the worst overall survival[15,131]. Group 3 is the most common subgroup in children, and contains twice as many

male patients as female[13,101]. The classic and LCA histological subgroups are more represented within Group 3 tumours[101]. Patients with Group 3 tumours often present with metastases[131]. *MYC* amplification which is almost exclusive to Group 3 tumours, is present in 60% of cases and is indicative of a worse overall outcome[13,15,16].

1.1.11 Group 4 subgroup – clinical features

Group 4 MBLs are the most common molecular subgroup, accounting for ~35% of cases and have intermediate survival outcomes[15]. Group 4 tumours are more common in child and adult patients and there are three times as many male as female patients[101]. The major histological subgroups within Group 4 are classic and LCA[101].

In a study investigating irradiation-sparing or irradiation-avoiding treatment strategies in MBL patients, Group 4 tumours treated with irradiation-sparing regimens all had subsequent disease progression[132]. Although this was a small study of only nine patients, it is known that infant Group 4 patients, who are not routinely treated with radiotherapy, show significantly worse survival outcomes compared to older patients and it is possible that radiotherapy is a requirement for optimal treatment of this subgroup[56].

1.2 Radiotherapy

Radiotherapy uses ionising radiation to target and kill (cancer) cells. The most common modality for radiotherapy uses high-energy x-ray (photon) irradiation. A photon deposits energy throughout its transition through the tissue[133]. Energy deposition produces energised electrons which leave and hence ionise atoms[134]. As energised electrons repel other electrons, further ionisations may be caused by these electrons repelling and removing additional electrons from other atoms[134].

The major process by which ionising radiation causes cell death is DNA interaction and damage[135]. Photons can cause direct DNA damage by interacting with DNA itself or, more commonly, indirect DNA damage through interactions with water, producing free

radicals[134,136–139]. The fatal DNA damage resulting from x-ray irradiation is the small proportion of double strand breaks (DSBs) which are incorrectly or incompletely repaired[137,139]. Cell death may result soon after irradiation, or it can be delayed if the cell survives the initial damage but the repair is inadequate[138,140]. A cell that has undergone reproductive cell death and is no longer able to divide to form daughter cells is deemed to have been killed by radiation treatment. Radiation damage is not restricted to cancer cells, and the side-effects of radiotherapy are a result of damage to normal tissues. Side-effects from radiotherapy can be acute, occurring during or within 90 days of treatment, or late, occurring months or years after treatment[141,142]. Acute side-effects include dermatitis or skin reactions at the radiation site, nausea, cystitis, hair loss and bone marrow suppression[116,142,143]. Late side-effects include radiation-induced fibrosis, vascular damage, hormone deficiencies and secondary malignancies[116,142,143]. Generally, acute side effects occur in rapidly or actively proliferating tissues such as skin or the gastrointestinal tract while late effects occur in more slowly proliferating tissues such as the kidney, CNS or heart[142].

Fractionation is where the total radiotherapy dose is delivered in multiple smaller fractions. The biology of fractionation, and how effective fractionated treatment is, depends upon the '4 R's of radiotherapy' first described by Withers in 1975[144] - Repair, Repopulation, Reoxygenation and Redistribution. The *in vivo* benefits of fractionation include: providing normal tissue with a chance to **repair** irradiation-induced damage; reducing side effects resulting from normal tissue damage; allowing cells to **repopulate** and hence regenerate normal tissues, thus reducing acute side-effects; allowing time for previously hypoxic regions in tumours to undergo **reoxygenation** and become more radiosensitive (Section 1.5.1); and allowing tumour cells previously in a more radioresistant phase of the cell cycle to **redistribute** to a more radiosensitive phase (Section 1.4.1). Disadvantages of fractionation are that proliferation of the surviving cancer cells can repopulate the tumour mass and tumour cells are also given time to repair damage. Damage is repaired by DNA damage response (DDR) pathways, such as Homologous Recombination or Non-Homologous End-Joining. These DDR pathways are frequently disrupted in tumours compared to normal tissues[140] and therefore tumour cells are likely to repair DNA damage less efficiently than

normal tissues. A fifth R, radiosensitivity, was added in a 1989 paper, radiosensitivity, which also contributes to fractionation response[145] (see Sections 1.2.2 and 1.2.4).

1.2.1 Radioresponsiveness

The extent to which a patient or tumour responds to radiotherapy treatment is described as the 'radioresponsiveness' of that patient or tumour. It has been established that different cancer types have different radioresponses and tumours generally show a similar level of radioresponsiveness as the tissues from which they originate[146]. More radioresponsive tissues include testis, ovary, lymphatic tissue, foetal tissue and foetus-like blast cells[146]. More radiounresponsive tissues include bone, large blood vessels, fatty tissue and muscle[146].

Radioresponsiveness of a tumour results from a combination of individual characteristics, with those considered the most important being intrinsic radiosensitivity, proliferative capacity and the level of hypoxia. Other factors include tumour histology, genetic mutations such as p53 or Bcl-2 and CSC abundance[146–148]. These individual factors could be targeted to increase a tumour's response to radiotherapy.

Across any given patient cohort, a range of individual radioresponses are observed. Most radiation treatment regimens, and the maximal tolerated doses within them, are limited by the most radiosensitive patients within a population as these patients would be more susceptible to more severe side effects at lower radiation doses[149]. More radioresistant patients who could tolerate higher radiation doses may, therefore, be missing out on maximal tumour control following radiotherapy[149]. Identifying the radioresponsiveness of a patient prior to treatment would allow for either increases or decreases in dose to maximise tumour kill and minimise associated side-effects[150].

1.2.2 Intrinsic radiosensitivity

Radiosensitivity describes how susceptible a cell is to death following exposure to radiation. Cells that are more susceptible to death following irradiation exposure are more radiosensitive, while cells that are more likely to survive irradiation exposure are less radiosensitive, i.e. more radioresistant. The intrinsic radiosensitivity of an individual cell is genetically determined and therefore an inherent cellular characteristic. The intrinsic radiosensitivity of a tumour or cell culture, while still genetically determined, is reflective of the intrinsic radiosensitivities of the component individual cells. The actual (observed) radiosensitivity of a tumour or culture is affected by external factors such as oxygen concentration, pharmacological agents or immune cell activation. Radiosensitivity can be measured *in vitro*, and was correlated with observed clinical radioresponsiveness[151,152]. Some studies have shown that tumour radiosensitivity was prognostic for survival outcomes following radiotherapy[153,154]. Analyses of multiple cell lines showed that the best measures of tumour radiosensitivity were parameters that reflected the initial part of the radiation survival curves, namely surviving fraction at 2 Gy (SF2), α (parameter describing the initial slope of the survival curve) and Dbar (area under the survival curve)[151,152,155] (see Sections 1.2.3 and 1.2.4).

A survey of radiosensitivity studies using human tumour cell lines or patient-derived fibroblasts by Fertil and Malaise in 1981 demonstrated that intrinsic radiosensitivity varies not only between but also within cancer type[151]. At doses of 8 Gy, within-type radiosensitivity variation was large enough to obscure any differences between cancer types; differences were significant at 2 Gy[151]. This within-type variation has been reported by other cancer cell panel work[151,152,156,157].

Deacon *et al.* assigned cancers to categories ranging from most to least radiocurable/radioresponsive[152]. This categorisation, shown in Table 2, was based on both observed clinical responses and the total prescribed dose, as a higher prescribed dose is likely to be associated with a less radioresponsive tumour type[152]. This study also reported the radiosensitivity of cell lines derived from the different tumour types. Cell line

radiosensitivity was measured *in vitro* using clonogenic assays and reported as SF2 as the measure of intrinsic radiosensitivity (see Section 1.2.3). The lower the SF2 value, the greater the intrinsic radiosensitivity.

Table 2: Radioresponsiveness of tumours as defined by Deacon

	Cancer types	SF2*
Radioresponsive	Neuroblastoma. Lymphoma, Myeloma	0.187
	Medulloblastoma, Small-cell lung carcinoma	0.218
	Breast, bladder, cervix carcinoma	0.460
	Pancreas, colo-rectal, squamous lung carcinoma	0.428
Radiounresponsive	Melanoma, osteosarcoma, glioblastoma, renal carcinoma	0.518

*Adapted from Deacon et al.[152]. SF2 – surviving fraction at 2 Gy. *Mean SF2 value reported in paper*

As illustrated in Table 2, while more radioresponsive cancer types do generally have higher intrinsic radiosensitivity (i.e. lower SF2 values) and there is a correlation, there is not a direct relationship. The Deacon *et al.* publication led to interest in measuring tumour radiosensitivity as a potential prognostic factor for radiotherapy outcomes[152]. As with radioresponsiveness, if intrinsic sensitivity could be determined prior to radiotherapy then treatment could be personalised to the patient or tumour. *In vitro* radiosensitivity assays have been applied to patient-derived cells to define patients as radioresistant or radiosensitive.

The gold standard radiosensitivity assay, a clonogenic assay, has been applied to patient-derived samples but the long time frame of approximately 4 weeks and low success rate (~70%) prohibits the use of this assay clinically[148,153,158–161]. Other assays used with varying levels of success include those measuring chromosome or DNA damage (e.g. γH2AX-phosphorylation), cell kill and apoptosis[153,154,161–163]. These assays use cell cultures established from patient biopsy samples. A study of cervical cancer patients demonstrated tumour cells with lower SF2 values were associated with better patient survival outcomes[153], but in glioma patients there was no direct correlation between the two[161]. In head and neck (H&N) cancer patients, while SF2 values were not predictive of patient outcome, the calculated cell growth fraction was (i.e. the ratio of cells capable of dividing on day zero, calculated by extrapolation of the tumour growth curve of cells that subsequently did divide,

over the number of cells initially plated)[154]. A second study of H&N cancer patients again found that SF2 values were not predictive of overall survival rates, but reported lower SF2 values were associated with higher local control rates[159]. A study of over 500 patients with either breast or H&N cancer showed that radiosensitive patients did not have significantly different rates of apoptosis or γH2AX-phosphorylation staining compared to non-radiosensitive patients[162].

It is unlikely that any *in vitro* assay for measuring radiosensitivity will be clinically useful, as the majority have limitations of technical difficulty, long-time courses and/or high costs[148]. Biomarkers and gene signatures present a more practical solution, as, being rapid and high-throughput, they enable quick reporting of results, which is vital if they are to inform treatment decisions. Reported biomarkers include MRE11 (meitotic recombination 11, predictive for survival in bladder cancer[164–166]), EEF1E1 (Eukaryotic translation elongation factor 1 epsilon 1, formerly called AIMP3, predictive for survival in bladder cancer[167]), NBN (nibrin, predictive for survival in prostate cancer[168]) and BABAM2 (BRISC and BRCA1 A complex member 2, formerly BRE, predictive for survival in breast cancer[169]). Published gene signatures for intrinsic radiosensitivity include the radiosensitivity index (RSI)[170–172], Danish Breast Cancer Cooperative Group Radiotherapy Profile[173] and Interferon-related DNA Damage Resistance signature[174]. While gene signatures have greater applicability in a clinical setting and may be non-cancer-type specific (at least in the case of RSI), they are not in routine use.

1.2.3 Measuring radiosensitivity using a clonogenic assay

The clonogenic assay is considered to be the gold standard radiosensitivity assay[175]. Following irradiation, cells are cultured at very low cell numbers for a prolonged period of time until colonies have formed. Only cells that have survived irradiation and successfully repaired resulting DNA damage will divide enough times to form a visible colony. These colonies are counted and described as the fraction of cells that survived compared to the expected number of colonies that would be produced by the number of cells seeded under control conditions. The advantages of clonogenic assay include simple methodology,

moderate throughput, and the ability to use combinations of treatment (e.g. drug + radiation, hypoxia + radiation). The long time-course provides an advantage over other methods of assessing radiosensitivity. After radiation, a cell may divide once or twice before undergoing reproductive cell death; assays with a short time-course may therefore underestimate treatment effect. On the other hand, after irradiation, a cell may take time to repair the DNA damage before it begins to divide, and therefore short time-course assays may overestimate treatment effect. The required long time-course of the clonogenic assay is, however, a practical disadvantage; not only is a long time required to produce results, but also the long incubation period increases the chance that colony formation will be disrupted. Other disadvantages are that: a clonogenic assay is labour intensive and not amenable for high-throughput applications; the fixed number of cells seeded per well provides a limited range of output; optimisation of the assay is labour intensive; cell lines must be able to survive low cell density environments; and significant methodological modifications are required for suspension cell lines. Additionally, different laboratories or authors can report significantly different surviving fractions implying a lack of reproducibility[151]. Despite this, there is a positive correlation between the survival fraction as reported by a clonogenic assay and the tumour control dose[151,152].

1.2.4 The linear quadratic model

The radiation survival curve produced from a clonogenic assay plots the surviving fraction as a function of dose and can be fit using a linear quadratic (LQ) equation, a mechanistic model of cell kill (Equation 1)[176]. The initial linear portion of the survival curve is described by the α parameter and the subsequent quadratic portion by the β parameter[177].

Equation 1

$$SF = e^{-(\alpha D + \beta D^2)}$$

SF = Surviving fraction; D = dose

Higher α values indicate the cells from which the curve is derived are more radiosensitive[178]. A greater bend to the survival curve indicates the cells are less radiosensitive[151,179]. The ratio

between the α and β parameters, α/β, indicates the fractionation sensitivity. Lower ratios (e.g. α/β = 3 Gy) predict that fractionation of radiotherapy will produce a greater sparing effect, where there is less overall cell kill following fractionated treatment[177,178,180,181]. Tumours almost always have an α/β greater than that of late-responding normal tissue, indicating that fractionation will result in greater sparing of late-responding normal tissue than tumours[180]. Notable exception to this rule are prostate[182] and breast cancers[183], where studies over the past decade reported the α/β ratios are low in these cancers.

The LQ model includes the assumption that DNA damage is produced proportionally to the dose[176]. This DNA damage includes lethal lesions and DSBs[176]. In the LQ model, DSBs are assumed to be repaired with first-order rate kinetics, that is a constant proportion of DSBs are repaired over each period of time[176]. Where two DSBs occur spatially and temporally close to one another the ends may be switched during the repair process and misrepair may occur[176]. Misrepaired DSBs can be lethal to a cell[176]. Misrepair requires two 'hits' of irradiation to the DNA at separate points and is therefore proportional to the square of the dose[176].

When the LQ model is applied to experimental data, occasionally the α and β parameters are reported to be negative[151]. Fertil and Malaise recommended in these circumstances to assign a value of 0 if this falls within the 95% confidence interval (CI) for the curve[151].

1.2.5 A high-throughput radiosensitivity assay

The advantages of the clonogenic assay have kept it as the gold standard since it was first described in 1956[184]. However, the incompatibility of the assay for use in high-throughput screens has hindered large-scale assessments of intrinsic radiosensitivity across a range of cell lines or conditions. In 2013, a high-throughput intrinsic radiosensitivity assay was described, where cells are seeded and irradiated in a 384-well plate then given an extended incubation before the end of the assay and where the colony formation endpoint is replaced by the CellTiter-Glo (CTG) luminescence assay[185]. The CTG assay adds an intermediate step between the cell's radiosensitivity and the assay output. In the clonogenic assay,

colonies are fixed and stained with a DNA dye and then counted. As each surviving cell forms only one colony there is a direct link between cell survival, colony formation and assay output. The luminescence method used in the high-throughput assay reflects the concentration of adenosine triphosphate (ATP) present within the test well. In the CTG assay, cells are lysed to release ATP from the intracellular compartment, at which point ATP can catalyse the reaction of luciferin by luciferase to produce photons of light, i.e. produce luminescence[186]. The biggest source of error within the ATP luminescence assay comes from manual pipetting errors, as the assay reaction itself is highly reproducible and sensitive[187]. ATP is a marker of viable cells, and therefore the more cells that are proliferating, i.e., those cells that have not undergone reproductive cell death, the more ATP that is present[187]. The assumption of the CTG assay is that there is a linear relationship between the number of cells present and the amount of ATP produced[188]. The assumption of the high-throughput assay is that this relationship is unaffected by irradiation. If the rate of ATP production is reduced by irradiation, the high-throughput assay may report more cell death than actually occurred, and *vice versa*. To date, the effect of irradiation on ATP production is unclear. Following a single dose of irradiation, cellular ATP production has been reported to be increased, decreased or unchanged in a variety of cell lines[189–194]. Each experiment used different methods to measure ATP production changes, different radiation doses and different cell lines, which may be obscuring any trends in response. The changes were reported at 10 minutes, 24 h and 32 h after the exposure in different cell lines, with no results reported to suggest long-term changes in ATP production compared to control cells[190,191]. Although using an indirect measure of cell survival is a caveat of the high-throughput assay and should be kept in mind during optimisation, if the high-throughput assay accurately reproduces the clonogenic SFs it is a viable alternative to the clonogenic assay.

The high-throughput assay was developed using a panel of 18 lung cancer cell lines, only 15 of which were compatible with the clonogenic assay as one cell line grew in suspension and the remaining two did not form colonies[185]. All 18 cell lines were used in the high-throughput assay, demonstrating its compatibility with cell line phenotypes excluded from the clonogenic

assay[185]. The high-throughput assay reports proliferating fraction (PF) as opposed to SF, and PF is calculated as the relative luminescence unit (RLU) value at X Gy divided by the RLU value at 0 Gy[185]. The clonogenic assay was carried out at 2, 5 and 8 Gy while the high-throughput assay used 1, 2, 3, 4, 5, 6, 8 and 10 Gy, and there was a weak correlation between PF and SF across all dose points used[185]. The authors reported a stronger correlation between the area under the curve (AUC) for the two assays and selected this as their output metric[185]. The reason for the all-doses comparison is unclear as, if the high-throughput assay has the purpose of providing an alternative to the clonogenic assay, a direct comparison between the SF and PF values at the same dose is of most interest. A stronger correlation may be observed when using the direct comparison and in this case the AUC metric would not be necessary.

The highest correlation between the clonogenic and the high-throughput assay was found when a nine day incubation was used in the high-throughput assay, although the corresponding incubation time in the clonogenic assay is not reported[185]. A nine day incubation period was subsequently used in a screen of 533 Cancer Cell Line Encyclopaedia (CCLE) cell lines[156]. The long incubation period is similar to that of a clonogenic assay and should take into account any delayed reproductive cell death. The results of the CCLE screen reported a wide variation in radiosensitivity within each of the 26 cancer types represented by the panel, but across all 533 cell lines radiosensitivity was normally distributed[156]. This work indicated the high-throughput assay method was compatible with a wide range of established cell lines across a wide range of cancer types.

1.2.6 The Radiosensitivity Index

A gene signature is a set of genes that show a characteristic gene expression pattern as a result of a biological state, e.g. presence/absence of a disease, susceptibility to a therapeutic intervention or expression of a particular disease or cellular phenotype[195,196]. If a gene signature can provide information regarding disease outcomes, it is prognostic[197]. If a gene signature can provide information about the response to a therapeutic intervention, it is predictive[197]. The *in vitro* methods of determining radiosensitivity are not readily transferable

to clinical use due to labour and time requirements. In order to provide a clinically compatible method to predict patient benefit from radiotherapy, a gene signature was derived using *in vitro* radiosensitivity data (SF2) from a panel of 35 cell lines[198]. Using a linear regression modelling approach to identify genes with expression levels that correlated with radiosensitivity, the RSI was identified and shown to predict SF2 values for a patient sample[198]. Initial validation showed that in rectal and oesophageal cancer cohorts, patients who responded to radiotherapy had significantly lower RSI scores than non-responding patients[171]. Subsequent work further validated the signature in H&N patients, where low RSI scores were associated with lower loco-regional recurrence rates[171]. Importantly, the RSI is prognostic only in cohorts treated with radiotherapy where the factor being measured could have an effect on survival. In breast cancer patients treated with surgery and radiotherapy, low RSI scores were associated with better recurrence-free and distant-metastasis-free survival, but this was not the case in patients treated with surgery alone[172]. Similar results have been reported in endometrial[199], melanoma[200], pancreatic[201] and glioblastoma (GBM) patients[202].

The published RSI cohorts use two main methods to classify tumours as radioresistant or radiosensitive – the first is a defined cut-off point of 0.3745[199–201,203–206] and the second is the 25th percentile score within the cohort[171,172,202,207]. The cut-off of 0.3745 was defined based on a cohort of colon cancer patients[208] and a second containing 10,000 primary solid tumours[204] where the RSI scores had a bi-modal distribution. The two peaks were assigned to be radiosensitive and radioresistant populations, and the cut-off was selected to separate the two.

1.2.7 Radioresistant and radiosensitive cancers

As the RSI was derived from *in vitro* SF2 values and produces predicted SF2 values for a tumour, its success suggests that the results of the clonogenic assay are applicable to radiotherapy outcomes in patients[198]. If the RSI values are interpreted as predicted SF2 values, then comparisons can be carried out with published SF2 values derived from *in vitro* studies. Figure 3 shows the results of a literature search for published SF2 or RSI values,

separated by cancer type/tissue of origin and ranked in order of radiosensitivity. Each data point represents the mean value of all reported values for that particular cancer type. As some articles only reported a mean or calculated SF2 or RSI value for a set of samples, error bars could not be calculated. The raw data can be found in Appendix 1. A value of 1 indicates high radioresistance and 0 indicates high radiosensitivity. The RSI cut off of 0.3745 is represented by a dashed line to indicate which cancer types would be classed as radiosensitive or radioresistant. From the perspective of clinical application, this fixed cut-point approach would not prove effective at stratifying patients in some cancer types. While only mean values are published and available for inclusion, Figure 3 suggests that in some cancers entire sample sets could be classed as radioresistant (e.g. astrocytoma [AC]) or radiosensitive (e.g. LEU and neuroblastoma [NBL]). As the aim of classifying patients into radioresistant and radiosensitive populations is the adjustment of radiation treatments, and standard radiotherapy protocols vary between cancer types presumably taking into account their different radiosensitivities, there is a need for a cohort/disease specific method. For example, the 25th percentile cut off was used in rectal or oesophageal cohorts giving a cut-off point of 0.46[171], in GBM cohorts giving a cut-off point of 0.54[202] and in H&N cohort with a cut-off point of 0.023[171].

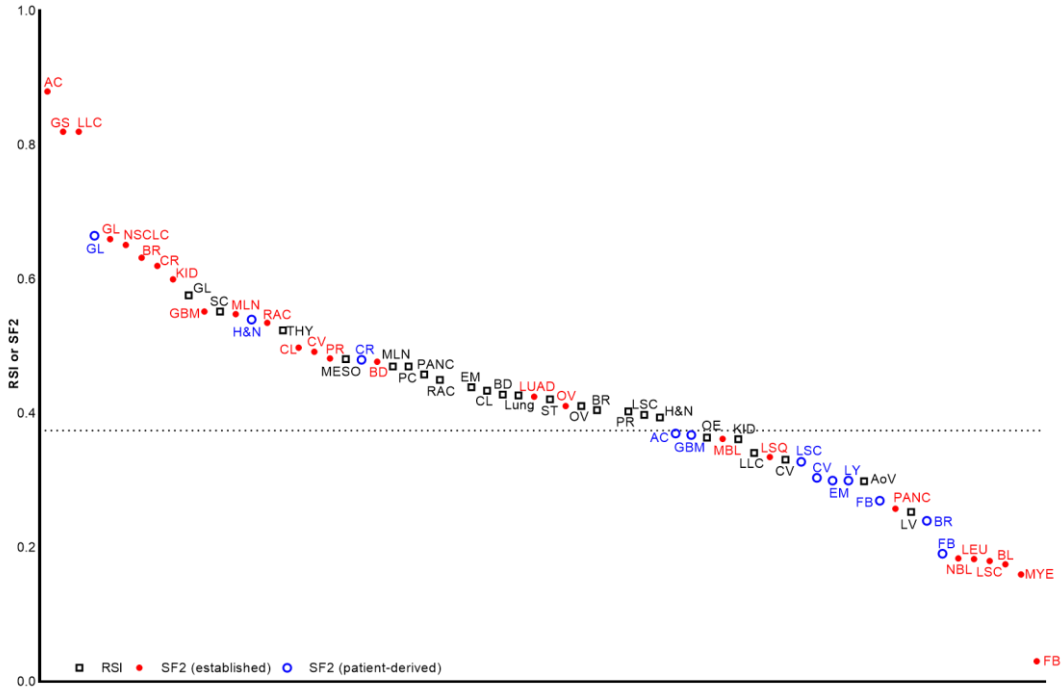

Figure 3: Literature radiosensitivity assay results grouped by different cancer types and ranked by radiosensitivity. *Results of a literature search for articles reporting surviving fraction at 2 Gy (SF2) or radiosensitivity index (RSI) values. SF2 values were taken from stated clonogenic assays using established cell lines [SF2 (established)] or from cultures derived from patient samples [SF2 (patient-derived)]. All RSI studies used patient samples. A detailed results table including study references and raw data used to generate this figure can be found in Appendix 1. Each point represents the mean value for that cancer type. Cancer types are located along the x-axis and ranked from least to most radiosensitive.*
AC – astrocytoma; AoV – Ampullar of Vater adenocarcinoma; BD – bladder; BL – Burkitt lymphoma; CL – colon; CR – colorectal; CV – cervical; EM – endometrial; FA – follicular adenoma; FB – fibroblast; GBM – glioblastoma; GL – glioma; GS – gliosarcoma; H&N – Head and Neck; KID – kidney; LEU – leukaemia; LLC – lung large cell carcinoma; LSC – lung small cell carcinoma; LSQ – lung squamous cell carcinoma; LUAD – lung adenocarcinoma; LV – liver; LY – lymphoma; MBL – medulloblastoma; MLN – melanoma; MESO – mesothelioma; MYE – myeloma; NBL – Neuroblastoma; NSCLC – non-small cell lung cancer; OE – oesophageal; OV – ovarian; PANC – pancreatic; PC – penile carcinoma; PR - prostate; RAC – rectal adenocarcinoma; SC – sarcoma; ST – stomach; THY – thyroid

1.2.8 WNT and radiosensitivity

The WNT signalling pathway is activated in response to irradiation, causing increased nuclear β-catenin and FZD mRNA expression[209–211]. Activation of the WNT signalling pathway is associated with decreased radiosensitivity, although exactly how WNT signalling results in radioresistance is unknown[111]. Mimicking pathway activation by transfection with β-catenin resulted in decreased radiosensitivity in the MBL cell line UW228[92] and the epithelial cell line RPE-1[212]. In the H&N cancer cell line, CNE-2 overexpression of β-catenin significantly increased SF2 compared to control cells (0.58 vs 0.34)[213]. The tankyrase

inhibitor XAV939 is used to inhibit the WNT signalling pathway by increasing β-catenin degradation, and WNT inhibition in this manner significantly increased radiosensitivity in GBM[214] and epithelial cell lines[212]. Inhibition of WNT signalling by preventing WNT ligand secretion using LGK-974 also significantly increased radiosensitivity in HCC cells[211]. Direct inhibition of β-catenin using siRNA targeting β-catenin significantly increased radiosensitivity in colorectal cell lines[212]. Radioresistant cell lines can be generated through repeat radiation exposure and culture of the surviving cells. These radioresistant cell lines have increased mRNA expression of β-catenin and the WNT pathway targets c-myc and cyclin D1, have increased β-catenin protein levels and show an increased response in WNT signalling reporter assays compared to parental cell lines[209,212,215]. Underlying activation of the WNT signalling pathway may therefore contribute to greater radioresistance.

1.2.9 SHH and radiosensitivity

Irradiation activates the SHH signalling pathway. Irradiation of prostate cancer xenografts significantly increased protein expression of the pathway components GLI1 and PTCH1, to 260% and 150% of levels in unirradiated controls respectively[216]. In cell lines, irradiation increased protein expression of SHH and GLI1 and increased the activity in a GLI1 reporter assay, demonstrating increases in the SHH pathway signalling activity[217–220].

Activation of the SHH signalling pathway decreases radiosensitivity. Using SHH ligand to stimulate the pathway decreased radiosensitivity in HCC[217,220] and GBM cell lines[218]. The SHH pathway can be pharmacologically inhibited using the GLI1 antagonist GANT61, which specifically inhibits GLI, or the SHH pathway inhibitor cyclopamine. Pharmacological inhibition of the SHH pathway increased radiosensitivity in prostate[216], GBM[218], oesophageal[221], HCC[217] and lung cancer cell lines[222]. In HCC cells, cyclopamine treatment alone had no effect on either DNA damage as measured by γH2AX foci or the number of apoptotic cells, but when used in combination increased the levels produced by radiation[217]. These data suggest that SHH signalling acts to decrease the amount of DNA damage and apoptotic cell death resulting from irradiation exposure, and this might contribute to the observed radioresistance. Radioresistant cell lines derived from the oesophageal line

ECA109[223] and from the osteosarcoma line MG63[224] expressed higher baseline levels of the SHH pathway proteins GLI1, PTCH1, SMO and SHH compared to the parental cell lines. As for the WNT signalling pathway, higher baseline SHH signalling may contribute to decreased intrinsic radiosensitivity. The SHH subgroup would then be expected to be less radiosensitive due to overactive SHH signalling pathway. In a study investigating the effects of irradiation-sparing or irradiation-avoiding treatment strategies, patients under ten years of age within the SHH subgroup were shown to have a 10-year overall survival rate of >90% if treated with chemotherapy alone, showing that these treatment strategies did not have a detrimental effect on survival[132]. This finding was not influenced by the histological subgroup, however it should be noted that TP53 status was unknown for these patients[132].

Some contradictory evidence has been published using cell lines with abnormal baseline SHH signalling, specifically the MBL cell line DAOY[127] and the prostate cell lines 22Rv1[216], PC3[127,216] and DU145[216]. DAOY is categorised as belonging to the SHH subgroup and expresses high levels of SHH pathway proteins indicating an overactive pathway[225,226]. All three prostate cell lines express increased GLI1 and PTCH1 mRNA compared to control prostate cells, indicating an active SHH pathway[227]. The SHH signalling pathway is activated in prostate cancer and appears to be involved in proliferation and metastasis in this disease[228–231]. Unlike in MBL where aberrant pathway proteins occur due to gene mutations[230], SHH signalling in prostate cancer is thought to result from overexpression and secretion of the SHH ligand[229–231].. GANT61 decreased the expression of PTCH1, GLI1 and GLI2 in PC3, DU145 and DAOY, indicating that the SHH signalling pathway was being inhibited by GANT61 treatment[127,216]. Combination of SHH pathway inhibition with irradiation significantly increased radiosensitivity in 22Rv1 only, while no effect was seen in PC3, DU145 or DAOY[127,216]. The prostate cell lines PC3 and DU145 are androgen-irresponsive and 22Rv1 is androgen-responsive[227]. The androgen receptor (AR) is reportedly involved in non-canonical SHH signalling through interactions with the GLI transcription factors[232]. AR-positive prostate cancers have significantly higher SHH protein expression than AR-negative tumours[229]. Increased SHH signalling in the AR-positive cell line 22Rv1 may be through the non-canonical pathway, while in the AR-negative cell lines aberrant signalling is through a

different mechanism or mutation. As GANT61 is a GLI antagonist, pathway inhibition will still occur for AR-mediated non-canonical signalling. Although pathway inhibition by GANT61 was demonstrated to occur, it had no effect on radiosensitivity in the three cell lines where the cause of constitutive SHH signalling has not been defined[127,216]. It may be the case that constitutively active SHH pathways, as found in the SHH subgroup, do not act to decrease radiosensitivity.

1.2.10 *TP53* status and radiosensitivity

The *TP53* gene, which codes the p53 protein, is a tumour suppressor gene and the most frequently mutated gene in all human cancers[233]. At the simplest level, activation of p53 via phosphorylation allows the protein to become more stable and translocate to the nucleus[234]. Functions of p53 in response to DNA damage include activation of DNA repair proteins, control of the cell cycle and initiation of apoptosis[235–239]. Which function results from p53 activation depends on several factors including the means by which p53 is activated, the intracellular environment and presence or absence of transcription cofactors[240]. *TP53* mutations resulting in inactive p53 protein therefore leave a cell without a key tumour suppressor.

One trigger for the activation of p53 is ionising radiation. There is a potentially complex relationship between p53 mutation status and radiosensitivity. In normal cells, p53 is stabilised in response to ionising radiation, increasing protein expression and coordinating the cellular response to the resulting DNA damage[241–243]. If the p53 response of a cell is not available, then cell cycle arrest or an apoptotic response would not be available to the cell[244]. If the DNA damage resulting from irradiation is severe enough to completely prevent a cell's survival unless repaired, then increased radiosensitivity with *TP53* mutations would be expected. Some human and mouse cell lines with mutated *TP53* are more radiosensitive than the corresponding WT controls[245]. On the other hand, if the *TP53* mutation prevents an apoptotic or DNA repair response to be initiated following DNA damage, there will be an increase in radioresistance and genomic instability. Bone marrow cells derived from transgenic mice with mutated *TP53* were used in a clonogenic assay to show that, compared

to non-transgenic litter mates, *TP53* mutations increased radioresistance[246]. H1299 cells transfected with WT p53 were significantly more radiosensitive than the parental cell line and had a significantly increased percentage of apoptotic cells[247]. However, HCT166 cells with mutant p53 protein showed similar clonogenic survival to p53 WT cells[248]. In H&N cancer cell lines no correlation between the presence of a *TP53* mutation and the SF2 was observed[249]. These observations demonstrate that the specific nature of the *TP53* mutation can contribute to how it affects radiosensitivity. The osteosarcoma cell line Saos-2 was transfected with a range of point mutations in *TP53*, and depending on the location of the mutation, radiosensitivity was either significantly increased or decreased compared to WT cells[250]. The point mutations in *TP53* that resulted in more radioresistant cells correspond to those found more frequently in human cancers[250].

1.2.11 MYC and radiosensitivity

MYC is a proto-oncogene, encoding c-myc protein, which is persistently active in a subset of cancers through copy number alterations or gene amplification[251–257]. *MYC* mRNA is expressed highly within Group 3 tumours, and *MYC* amplification, where a cell contains multiple copies of the *MYC* gene, is a common characteristic of Group 3 MBL[116]. C-myc is a transcription factor for a range of pro-proliferative genes, and is a target of the WNT and SHH signalling pathways[114,258–260]. Having previously established that these pathways are activated following irradiation exposure, it is not surprising that c-myc expression is increased following irradiation in MBL[261], prostate[262] and osteosarcoma[263] cell lines. Overexpression of *MYC* in normal human fibroblasts was shown to increase DNA damage, measured by γH2AX foci, in irradiated compared to unirradiated control cells[264]. The induction of DSBs in cells overexpressing *MYC* resulted in more apoptotic cell death[264]. Increased susceptibility to DNA damage and subsequent apoptotic cell death would suggest that *MYC* overexpression causes cells to be more radiosensitive. However, a study using a panel of small cell lung cancer cell lines in mouse xenografts found no relationship between the level of *MYC* mRNA and the radiosensitivity of the tumours[265]. Alternatively, *MYC* overexpression has also been associated with radioresistance. In a study using H&N cancer patient-derived cell cultures, clinically assigned as either ‘radioresistant’ or ‘radiosensitive’,

radioresistant cells were found to have more expression of c-myc protein compared to the radiosensitive group[266]. Radioresistant MCF-7 cells generated following exposure to 60 Gy or 80 Gy in 5 Gy fractions, show copy number gain of *MYC* compared to non-irradiated cells[267]. Radioresistant lines derived from cervical[215], lung[268] and oesophageal[209] cancer cells have higher c-myc protein and *MYC* mRNA expression than the parental cells, although this could be attributed to increased WNT signalling. It is difficult to determine whether increased expression of c-myc is contributory to or results from the mechanisms of radioresistance.

1.2.12 Medulloblastoma and radiosensitivity

No assessment of the intrinsic radiosensitivity of MBL patient samples has been published. While there are some data available for MBL cell lines, almost all has been published as controls within wider studies of MBL radiobiology. The intrinsic radiosensitivity of MBL has only been directly investigated in two studies, published in 1980[269] and 1993[270]. The first of these used a cell line no longer available, TX-7[269].The second used the cell lines DAOY and D283 and compared the radiosensitivity of MBL with their previous study using glioma cell lines[270]. There is, therefore, a lack of information regarding the intrinsic radiosensitivity of MBL cell lines, both in general and in the context of the molecular subgroups. Data from the literature is reported in Table 3, which contains both stated parameters and those determined from figures within publications.

Table 3: Summary of published medulloblastoma radiosensitivity data

Subgroup	Cell line	SF2	SF8	Linear quadratic parameters
SHH	DAOY	0.40[271] 0.44[270] 0.61[272]	0.018[272]	α – 0.039[127] β – 0.047[127]
	ONS-76	0.42[271] 0.64[273]		α – 0.13[273] β – 0.05[273]
	UW228-2	-	0.11[274]	
Group 3	D283	0.17[272] 0.18[270]	0.0016[272]	
	D425	-	0.09[274]	
	MED8A	0.34[272]	0.00068[272]	

Published SFs suggest that Group 3 cell lines are more radiosensitive than SHH cell lines. This agrees with a study using a panel of cell lines which reported the *TP53* mutant SHH cell lines UW228 and DAOY to be the least radiosensitive, followed by the *TP53* WT SHH cell line ONS-76, with the Group 3 cell lines D283 and MED8A the most radiosensitive[92]. Transfection of ONS-76, which is WT *TP53*, with mutant *TP53* increased the radioresistance of this cell line compared to untransfected cells[92]. There are some caveats to this study. First, the use of the semi-adherent cell line D283 in a standard clonogenic assay, a methodology not compatible with suspension cells. Second, the survival curves using the full panel of cell lines only extended up to a 5 Gy irradiation dose producing a cell kill below 0.1 in only one of the five cell lines. Without extending the curve to cover multiple-log cell killing the β-portion of the survival curve cannot satisfactorily be represented. Last, the survival curves were not fitted with a LQ model and therefore the associated radiosensitivity parameters were not calculated and reported.

1.3 Proton Radiation

Proton therapy was first suggested in 1946 and the first patients were treated in the 1950s [275]. Protons produce a more restricted, higher ionisation density compared to x-rays[276]. The key difference between proton and x-ray radiation is the Bragg peak phenomenon, where the amount of energy deposited by a proton is inversely proportional to its energy, so most energy is deposited at the end of the path[133,277–281]. In order for the whole depth of a tumour to be treated with the same radiation dose, a spread-out Bragg peak (SOBP) is used. To produce a SOBP the initial energy of the proton is altered, changing the depth of the Bragg peak[278]. Multiple Bragg peaks are thus combined to produce a plateau of uniform energy deposition which covers the tumour[278]. The tissue located behind the tumour is exposed to practically no radiation, and tissue before the tumour is exposed to a lower dose than with x-ray radiation. If a lower dose can be given to normal tissue, this will decrease the risk of damage to normal tissue[282]. Alternatively, if side effects and tissue tolerability are already acceptable with conventional x-ray therapy, a higher proton therapy dose which irradiates normal tissue to the same extent could be given, increasing the tumour dose[282].

As of June 2021, 98 proton facilities were in operation worldwide[283]. PBT has been trialled in a range of other cancers, including lung cancer[284–286], breast cancer[281], brain tumours[63,287], oesophageal cancer[288] and sarcomas[289]. These studies show PBT to be well tolerated, with the most common side effects being dermatitis and skin toxicity[281,286]. The tumour types with the most evidence for a clinical advantage of PBT over x-ray therapy are ocular melanoma and chordomas due to the higher irradiation doses that are possible[290]. A 2009 review by the Agency for Healthcare Research and Quality looking at 243 clinical trial reporting articles concluded that there was no evidence showing PBT to be superior to x-ray therapy in terms of clinical outcomes or side effects[291].

5-year progression-free survival for MBL patients following PBT is 85% for standard-risk and 70% for high-risk patients, similar to the survival rates with x-ray radiotherapy[287]. Despite the apparent lack of advantage in survival time, there is interest in using PBT for MBL patients due to the tumour location, typical patient age and the potential to reduce the risk of long-term side-effects[292,293]. Several clinical studies have used simulations or treatment plans to draw conclusions of the potential benefits of PBT in comparison to x-ray beam therapy in MBL. A simulated cohort of 5-year old patients treated with surgery, chemotherapy and either x-ray radiotherapy or PBT was used to evaluate cost-effectiveness of treatment[294]. Taking long-term side effects and quality-of-life adjusted years into account, proton therapy had a lower cost and a better effect[294]. Although this could be used to argue for the use of PBT, there are several concerns with the simulation cohort approach taken, specifically the lack of long-term follow-up patient data which is required to produce a reliable model[294]. Real patient data has been used to design both x-ray and proton treatment plans, although these plans have not both been carried out[295,296]. The proton plans had a statistically significant reduction in healthy tissue irradiation compared to the x-ray plans[295,296]. The problem with theoretical treatment plans is that, because they are not applied to patients, any benefits of reducing the healthy tissue dose cannot be clinically demonstrated and remains theoretical.

An evidence-based review of PBT, carried out in 2012 by ASTRO's Emerging Technology Committee, highlighted the need for more clinical trials in order to determine the clinical

benefits of PBT[290]. A 2016 systematic review of the use of PBT in paediatric cancers including MBL concluded that based on the available evidence, neither the use nor disuse of proton therapy could be justified[293]. Despite this overall lack of clear clinical evidence, around 15% of paediatric MBLs are given PBT due to the theoretical advantages[297]. A clinical trial investigating reduced side effects following PBT in MBL was opened in 2010 with the aim of recruiting 90 patients[298]. The primary endpoints were ototoxicity, endocrine dysfunction and neurocognitive effects, and results are expected in November 2021[298].

1.3.1 Protons vs x-rays

An identical level of biological effect will be produced by differing doses of different radiations[299]. The Relative Biological Effectiveness (RBE) is the ratio between the dose of a test radiation type compared to the dose of x-ray radiation when an identical biological effect is achieved[134,137,299,300]. A RBE greater than 1 indicates that radiation is more effective per unit dose than x-ray[299]. The clinically used RBE value for protons compared to x-rays is 1.1[133,278,300,301]. Protons therefore provide a small improvement in biological effect at any given dose[133,278,300,301]. Though used clinically, this RBE value was derived as an average of many separate experiments over a wide dose range including a large number of irrelevant, non-human cell lines and RBE values ranged from 0.86 to 2.1[302]. The RBE of 1.1, which is currently used in treatment planning, may not be representative leading to over- or under-dosing[303]. Cell line studies have reported RBE values ranging from 1.01 to 1.77[303,304]. These studies, among others, raise questions regarding the general application of a proton RBE of 1.1, and, of note, very few tissue specific RBE values have been determined[276,305].

As with x-ray radiation, proton therapy causes cell death through DNA damage. Proton radiation appears to result in slightly more robust DNA damage and cell apoptosis than x-ray radiation[276,306]. This could be due to the larger numbers of reactive oxygen species that are generated following proton radiation, shown in lung[276] and GBM[306] cancer cells. Additionally, DNA repair may be altered in proton-irradiated cells, although this is not consistently reported[135,306,307]. Other differences in DNA damage and repair seen with proton radiation include altered cell cycle progression and G2 arrest recovery, altered phosphorylation

kinetics of the cell cycle enzymes Chk1 and Chk2, and decreased colony forming capabilities[276,306].

1.4 Proliferation

The process by which a cell grows and divides is called proliferation. In healthy tissue, cell proliferation is carefully regulated in order to maintain normal tissue function, while a hallmark of cancer is uncontrolled cellular proliferation leading to a rapidly expanding population of cells forming the tumour mass[244,308,309]. A higher proliferation rate within a tumour has been shown to be associated with worse survival outcomes in CNS[310] (including MBL[311]), breast[312], bladder[313], pancreatic[314], gastrointestinal[314], lung[315,316], cervical[317] and H&N cancers[318].

There are various mechanisms by which cancer cells gain the ability to proliferate indefinitely, including growth factor independence and overproduction of growth factor ligands and/or receptors[309]. The processes a cell undergoes to divide into two daughter cells form the cell cycle. There are two broad stages to the cell cycle in eukaryotic cells, interphase and mitosis[319]. During mitosis (M-phase) the cell divides into two daughter cells[319]. During interphase the cell is actively growing in size and replicating the intracellular and DNA content[319]. There are several sub-stages during interphase, termed Gap1 (G1) phase, Synthesis (S) phase, and Gap2 (G2) phase[319]. M-phase occurs after G2 and before the start of the next cycle at G1[319]. There are distinct processes that occur during each phase – cell mass increases during the G1- and G2-phases while DNA is replicated during the S-phase[319–321]. Cells in the S-phase of the cell cycle are more radioresistant, likely due to increased abundance of DNA synthesis enzymes, and more radiosensitive in the M-phase[143,322]. The cell cycle is a tightly regulated process and monitoring takes place at cell cycle checkpoints where the progress through the cell cycle can be halted if necessary[319]. These occur at the end of G1 and G2 and are highly choreographed signalling events between proteins such as cyclins, cyclin-dependent kinases and p53[323,324].

Cellular proliferation can be determined *in vitro* by comparing the proportion of cells at each stage in the cell cycle using flow cytometry to determine the relative amount of DNA per cell[308]. During the initial phase of the cell cycle, G1, there is one complete copy (1X) of DNA present within a single cell[321]. During S-phase, where the cell is replicating the DNA, the amount varies between 1X and 2X depending on how far through the process the cell is[321]. In G2, which follows on from DNA replication, a single cell contains 2X DNA[321]. The relative proportion of DNA per cell can be determined and the number of cells per cell cycle phase can be calculated[308]. Other techniques include counting the number of living cells in a culture to monitor increases resulting from cell proliferation or measuring the conversion of a substrate by metabolically active cells to monitor for increasing cell number. In patient or tissue samples, the BrdU (bromodeoxyuridine) or IdUrd (Iododeoxyuridine) assays can be used. BrdU[325] and IdUrd[326] are analogs of the DNA base thymidine which are incorporated into newly synthesised DNA during S-phase. IHC staining for BrdU is used to see where and how many cells have proliferated since the infusion was administered[325,327]. The protein and mRNA expression levels of proteins associated with proliferation, such as Ki67[328,329] and PCNA[329], can also be used to determine whether a tissue is actively proliferating.

Ki67 is a 359 kDa protein that is involved in the control of cell proliferation[314,329]. Ki67 was first detected in a screen of antibodies produced against a range of nuclear antigens where the Ki67 antibody only stained cells known to be proliferative[330] and therefore has been used subsequently as a marker of proliferation[329]. The expression of Ki67 mRNA is positively correlated with Ki67 protein expression[331,332], therefore both mRNA and protein expression are indicative of the level of Ki67 in a sample. Ki67 protein expression is found throughout all stages of the cell cycle but reaches a maximum during the G2- and M-phases[314,329]. The exact protein function has not been fully elucidated, and inhibition of Ki67 does not prevent or alter cellular proliferation in *in vivo*[314,329,333]. Ki67 positivity is significantly associated with clinical staging and lymphatic metastasis in breast cancer[334]. The Ki67 proliferation/labelling index is the percentage of cells in a sample which have positive nuclear staining for Ki-67[328] and forms part of the diagnostic criteria for gastrointestinal and pancreatic cancers[314]. The

Ki-67 labelling index has been significantly associated with local control but not survival rates in H&N cancer[335].

PCNA (proliferating cell nuclear antigen) is a 29 kDa protein involved in several processes during cell proliferation, including during DNA replication where it acts to increase the efficiency of DNA polymerases by acting as a scaffold protein[329,336]. PCNA is frequently used as a cell cycle marker as the expression increases during S-phase, and while PCNA protein and mRNA levels are not significantly correlated, both correlate with clinical outcomes[329,337,338]. NSCLC[338], breast[334] and prostate[339] tumour samples had significantly higher PCNA protein and mRNA expression compared to adjacent normal tissue. Higher PCNA expression is associated with shorter overall survival in NSCLC[338,340], ampullar of Vater carcinoma[341] and breast cancer[342]. The PCNA labelling index was significantly associated with local-control but not survival rate in H&N cancer[335]. Meta-analyses of studies in gastric cancer[343] and osteosarcoma[344] concluded that, again, PCNA expression was significantly correlated with overall survival.

1.4.1 Proliferation and radioresponse

The impact of a proliferative phenotype on radiotherapy outcomes is not straightforward. *In vitro*, immediately following exposure to ionising radiation, a dose-dependent growth delay is observed in cultured cells, although the subsequent growth rate is unaffected compared to unirradiated control cells[265].This growth delay is a result of radiation-induced cell cycle arrest, and occurs to allow the cells to repair the DNA damage before continuing to proliferate and divide.

Although cell kill and a reduction in viable/proliferating cells is a direct result of radiation exposure, surviving cells proliferate to replace the dead cells and repopulate the tumour[241,345]. Subsequent treatment fractions must kill these repopulated cells before any further impact on the original tumour volume can be made[241]. The reduction in total cell number following irradiation treatment also reduces the burden of the tumour on its microenvironment, increasing the availability of oxygen, glucose, nutrients and space and

resulting in conditions more optimal for cell proliferation[241]. If a cancer is fast growing with rapidly proliferating cells there may be significant regrowth between treatment fractions, thus reducing the impact on the original tumour mass that each fraction can have[241,346]. Faster growing tumours would therefore be expected to show reduced local control and a faster recurrence if treated identically to slower growing tumours[346]. In patients with H&N cancer, a higher BrdU labelling index indicating more proliferative tumours was significantly associated with worse local control[347]. In a cohort of bladder cancer patients, a better response to radiation therapy occurred for patients with lower proliferation rates, as determined by Ki67 expression[348]. In a selection of 'radiounresponsive' or 'radioresponsive' patient-derived cell cultures, radiounresponsive cultures showed a significantly greater increase in Ki67 staining following a 2 Gy radiation dose than the radiosensitive cell lines[266]. In these studies, high cellular proliferation was associated with radioresistance. Survival outcomes in more proliferative H&N cancers were significantly improved by the use of a partly accelerated radiotherapy regimen, which increased fraction size and reduced time between fractions[318]. The partly accelerated regimen reduced the time period over which re-population could occur and increased the amount of dose available to target the original tumour mass once re-populated cells had been killed.

Alternatively, rapidly proliferating tumours are expected to contain a larger number of individual cells in the more radiosensitive stages of the cell cycle at any one time. They therefore have a larger proportion of potential target cells than a slowly proliferating tumour[241,328]. Irradiation of more rapidly proliferating tumours could therefore result in a larger cell kill compared to slowly proliferating tumours. In oral squamous cell carcinoma, radiotherapy treatment of highly proliferative tumours, as determined by Ki67 staining, resulted in improved local control and better overall survival[349]. Ki-67 positivity in small cell lung cancer was found to correlate with complete response following irradiation treatment, but not overall survival in a small patient cohort, indicating that a higher proliferation rate within a tumour could produce a greater radioresponse[328].

1.4.2 The meta-PCNA index and proliferative-informative cancers

The meta-PCNA index (mPI) is the median gene expression across the meta-PCNA gene signature[350]. A higher mPI indicates a higher level of proliferation within that sample. The meta-PCNA signature is composed of 131 genes, which are the 1% of genes most associated with PCNA mRNA expression[350]. The data to generate the signature was taken from a set of microarray data for 36 normal tissue types[350]. The gene signature originated as part of a survey of published gene signatures and their application in breast cancer patients in an investigation into whether signatures remained prognostic when proliferation was taken into account[350]. Subsequently, the mPI was applied to cancer cohorts within The Cancer Genome Atlas (TCGA) database[351]. mPI was significantly higher in tumour tissue compared to adjacent normal tissue, and varied between tumours by up to ten-fold (5 counts per million (cpm) for kidney carcinoma to 50 cpm for cervical carcinoma[351]). The survival analysis within this study found that mPI was significantly associated with survival for only a subset of cohorts[351]. These cancers were categorised as 'proliferative informative' by the study, and included kidney, adenoid cystic carcinoma, low-grade gliomas, mesothelioma (MESO), pancreatic and lung adenocarcinoma (LUAD)[351]. Perhaps counterintuitively, these cancers were those with the lowest mPI scores, indicating they were less proliferative[351]. Pathway analysis of the proliferative informative cancers showed enrichment of proliferation-related pathways (cell cycle, cell division and DNA replication), while non-proliferative informative cancers were enriched for cell metabolism, angiogenesis and immune-related pathways[351]. The authors suggest that the influence increasing proliferation of a tumour has on survival outcomes is limited, and once a certain rate of proliferation has been exceeded other processes, such as invasion or immune suppression, become more influential[351].

1.4.3 WNT and proliferation

Activation of the WNT signalling pathway has been reported to both increase and decrease proliferation. Pharmacological activation of the WNT signalling pathway caused an increased percentage of proliferating BrdU-positive cells compared to untreated controls in non-cancerous Sertoli cells[115]. A rat model using transplanted HCC cells found treatment with the

WNT pathway inhibitor WNT-C59 significantly reduced tumour weights compared with those given sham treatment, again suggesting that the WNT pathway was increasing proliferation[352]. In contrast, activation of the WNT signalling pathway in the MBL cell line UW228-1 significantly reduced cell growth and Ki67 staining, suggesting reduced proliferation[353]. The UW228-1 cell line is a SHH cell line, however, and as the other MBL cell lines investigated in this study were not successfully transfected with β-catenin, whether the overactive SHH signalling pathway in this cell line confounded these results is unclear[353].

1.4.4 SHH and proliferation

The *in vitro* evidence connecting the SHH signalling pathway to proliferation repeatedly demonstrates that activation increases and inhibition decreases proliferation. Activation of the SHH signalling pathway using exogenous SHH or GLI1 significantly increased cell proliferation[221,354,355]. Using shRNA (short-hairpin RNA) to inhibit SHH signalling in HCC cell lines resulted in a significant decrease of proliferating cells[356], and siRNA (small interfering RNA) against GLI1 significantly decreased the number of proliferating cells in the GBM cell line U87[354]. The SHH pathway inhibitor cyclopamine reduced cellular proliferation in bladder cancer[355], oesophageal cancer[221] and renal cell carcinoma cells[357]. The SMO antagonist vismodegib significantly decreased proliferation in NSCLC cells[122]. The results are not replicated in *in vivo* studies, and treatment of mouse A549 xenografts with a SHH antagonist had no effect on Ki67 staining, showing that inhibition of the SHH signalling pathway did not alter the proliferation of these tumours[222]. Additionally, it is unclear whether a constitutively active SHH signalling pathway, as occurs in the MBL subgroup, would have the same effect as temporary activation using pharmacological agents.

1.4.5 MYC and proliferation

MYC is pro-proliferative and increased c-myc expression increases cellular proliferation. Increased c-myc activity sped up the progress of transfected cells through the cell cycle, increased cellular proliferation and decreased Td in rat fibroblasts[358] and human stromal cells[359]. In a mouse model of gastric cancer, overexpression of c-myc resulted in increased

cell growth and tumour weight compared to control tumours[360]. Treatment of cells with siRNA against *MYC* caused a reduction in cell growth compared to control cells[361]. *MYC* inhibition using a *MYC* inhibitor or siRNA significantly decreased cell viability of two osteosarcoma cell lines in a dose-dependent manner[362].

1.4.6 Medulloblastoma and proliferation

In a study of primitive neuroectodermal tumour (PNET) samples, which included a proportion of MBL patients, Ki67 positivity was 30% and PCNA was 65%, values which indicate high proliferative activity[363]. The meta-PCNA signature has not been investigated in a MBL cohort. If MBL is identified as a proliferative informative cancer by the mPI, differential rates of proliferation between the molecular subgroups could be influencing their different survival outcomes. Some *in vitro* work includes control data suggesting different proliferative activity between the subgroups. The SHH cell line DAOY is reported to have higher Ki67 protein expression (99%) compared to the Group 3 cell lines D341 (14%) and D283 (42%), indicating more proliferation within the SHH subgroup[364]. If MBL is identified as a non-proliferative cancer, suggesting that the rate of proliferation is not affecting survival outcomes, differences between the subgroups would not be expected to influence their differential survival rates, however there would potentially be indirect effects on survival through influencing the radioresponsiveness.

1.5 Hypoxia

Hypoxia is the presence of reduced molecular oxygen concentrations and is generally, though relatively arbitrarily, defined as oxygen concentrations under 2%[365–367]. For reference, atmospheric oxygen is 21% and physiological oxygen concentrations range from 2-9%[366–368]. Hypoxia is known to be present in various disease states (such as stroke, ischemia and inflammation), and it is well-established that solid tumours contain regions of hypoxia [244,365,366]. Hypoxic conditions can cause cells to reduce proliferation, undergo differentiation or undergo cell death via apoptosis or necrosis[367]. It might be anticipated that this would hinder tumour survival, however the opposite is usually the case. The adaptations a cell

undergoes to survive hypoxia, such as resistance to apoptosis and decreased DNA repair, allow cells to take on a more aggressive phenotype, encouraging tumour survival[365,369,370]. In glioma and AC, more aggressive and faster growing tumours were shown to have higher levels of hypoxia[371]. A worse prognosis for patients with lower tumour oxygen levels has been reported for H&N carcinoma[372], uterine carcinoma[373], soft tissue sarcoma[374], prostate cancer[375,376] and cervical carcinoma[377].

There can be different biological consequences of hypoxia depending on the exposure time. 'Acute hypoxia' results from temporary obstructions of microvessels, cutting off the oxygen supply to a region[365]. Acute hypoxia occurs on a scale of minutes to hours, and causes increases in genomic instability, metastasis, and treatment resistance, mainly via the activation of Hypoxia-Inducible Factor (HIF) 1α[367,369]. Under normoxic conditions, the α subunit of HIF undergoes degradation by oxygen-dependent mechanisms; under hypoxic conditions stabilised HIF1α forms a heterodimer with HIF1β to form the HIF1 transcription factor[378]. Targets of the HIF1 transcription factor include glycolysis enzymes[379], vascular endothelial growth factor (VEGF)[380,381], transforming growth factor β (TGFβ)[380] and MMPs[382,383]. 'Chronic hypoxia' occurs when a large tumour diameter causes large distances between cells and their nearest blood vessel, leading to long-term deficiencies in oxygen supply to that region[365]. Chronic hypoxia occurs over days and causes long term cellular adaptations such as decreased translation, altered transcription, decreased DNA repair and increased genomic instability[367,369]. Both acute and chronic hypoxic conditions can be re-capitulated *in vitro* by altering the length of time cells are cultured in a hypoxic environment.

There are several methods for the detection of hypoxia within a tumour, including protein expression, gene signature expression and oxygen electrode measurements[384–391]. Identifying whether a patient has a hypoxic tumour can be used to inform treatment decisions, such as the inclusion of a hypoxia-modifying element[392–398]. A meta-analysis of hypoxia-modifying treatment in combination with radiotherapy in H&N cancer showed significantly improved loco-regional control and disease specific survival[393].

While the gold standard method for measuring oxygen concentrations is the use of Eppendorf oxygen electrodes, there are prohibitive disadvantages as measurements can only be taken from accessible tumours, the process is highly invasive and it is difficult to implement into the clinic[399,400]. A more clinically applicable though indirect method to measure oxygen concentration detects proteins upregulated by the HIF1 transcription factor through IHC or mRNA expression. Frequently used protein markers of hypoxia are carbonic anhydrase IX (CAIX) and glucose transporter 1 (GLUT1). Protein markers are easily applicable to tumour tissue samples and can be assessed on routine biopsy samples, however they are less specific due to expression by hypoxia-independent processes (e.g. via oncogenic activation), and protein detection can vary depending on the IHC method and antibody specificity[400]. As the oxygen level within a tumour is not homogeneous, depending on which regions of the tumour are sampled there is the potential for under- or over-reporting the true extent of hypoxia.

CAIX is a zinc metalloproteinase involved in the maintenance of pH through hydration of carbon dioxide[401]. CAIX is normally expressed in stomach, intestinal and gall bladder tissue, however hypoxia increases the expression of CAIX through the HIF1α signalling pathway[401]. CAIX protein significantly correlated with HIF1α protein expression[402–405]. CAIX mRNA and protein expression are significantly correlated[406]. Higher CAIX protein staining is associated with worse survival outcomes in breast[404,407] and NSCLC[405,407]. Some studies using cohorts of H&N cancer patients report significantly worse survival outcomes associated with CAIX staining[408409], but this is not always the case[402]. In one study, a significant correlation between CAIX expression and Eppendorf electrode measurements was reported in cervical cancer, and CAIX was a significant prognostic factor for metastasis-free survival[410]. In others, positive staining for CAIX was not significantly associated with measurements taken using the Eppendorf oxygen electrode method, disease-free or overall survival in cervical cancers[411,412].

GLUT1 (coded by the *SLC2A1* gene), is a membrane glucose transporter and acts to transport glucose into cells. Reduced levels of glucose result in an upregulation of GLUT1.

GLUT1 is also upregulated under hypoxic conditions through the HIF1α signalling pathway[401]. GLUT1 protein and mRNA expression levels are significantly correlated[413]. It is highly expressed in the endothelial cells of the BBB[414,415]. In breast cancer, HIF-1a protein expression is significantly correlated with GLUT1 expression[403]. The overexpression of GLUT1 in tumours was associated with worse survival outcomes in H&N[416], ovarian[417], gallbladder[418], rectal[419] and breast[420] cancer and PNET[421]. There was no correlation between GLUT1 expression and overall survival in pancreatic[418,422] and cervical carcinomas[423] although GLUT1 expression was correlated with metastasis-free survival in cervical carcinoma[423]. Meta-analyses of studies investigating GLUT1 expression and outcomes in solid tumours[424], human cancers[425], breast carcinoma[425] and lung cancer[426] all concluded that GLUT1 overexpression is significantly correlated with worse overall survival.

Hypoxia gene signatures are gene sets where the expression level is indicative of the level of hypoxia within a tumour microenvironment. As with protein markers, this data is generated from a sample of the whole tumour and so may not be reflective of the entire tumour microenvironment. However, hypoxia gene signatures are easier to place into clinical practice than probe measurements and are more reliable than protein markers with respect to hypoxia. There are a large number of hypoxia gene signatures in the literature, however, following development, few are validated and translated into clinical practice. Hypoxia gene signatures identified through a literature search are summarised in Table 4. Of note, hypoxia gene signatures are, on the whole, not transferable across multiple cancer types, requiring them to be derived for each new cancer type or site of origin[389]. This is illustrated by the components of the 21 gene signatures. If the gene signatures were transferable between cancer types, genes that were used to identify hypoxic tumours would be expected to be represented in multiple signatures. Across all signatures listed in Table 4, a total of 394 unique genes are included, and only 72 of these are found in more than one signature. Only 15 genes, 4%, occurred in at least five of the signatures. The most frequently used genes were *VEGFA* and *NDRG1*, but these were only found in nine of 21 signatures. The differences between the gene signatures suggest that different cancer types have different genetic responses to a hypoxic microenvironment.

Table 4: Published hypoxia-associated gene signatures

Study	Cancer	No. genes	Signature score	Cut-off	Outcome*
Yang 2017[391]	Bladder	24	Median gene expression	Cohort median signature score	Prognostic; predictive of benefit from CON
Wang 2020[427]	Breast	14	Gene coefficient equation	Cohort median signature score	Prognostic
Seigneuric 2007[428]	Breast	79	None	Overall gene expression	Prognostic
Hu 2009[429]	Breast	13	Average gene expression	Two cut-offs -0.63 and 0.08	Prognostic (also lung and glioma)
Ghazoui 2011[430]	Breast	70	Median gene expression	NS	Not reported
Halle 2012[431]	Cervix	31	Median gene expression	Unsupervised clustering	Prognostic
Fjeldbo 2016[432]	Cervix	6	None	Compare to previously defined hypoxic tumours	Prognostic
Dekervel 2014[433]	CR	6	Gene coefficient equation	Optimal cut-off for cohort (Youden's Index)	Prognostic
Wang 2020[388]	GBM	5	Gene coefficient equation	Cohort median signature score	Prognostic
Tardón 2020[434]	GBM	36	None	k-means clustering	Prognostic - univariate analysis only
Lin 2020[435]	Glioma	5	Gene coefficient equation	NS	Prognostic
Van Malenstein 2010[386]	HCC	7	Gene coefficient equation	0.35	Prognostic
Eustace 2013[436]	H&N Bladder	26	Median gene expression	Cohort median signature score	Not prognostic; predictive of benefit from CON in H&N
Toustrup 2011[437]	H&N	15	None	Compare to previously defined hypoxic tumours	Prognostic; predictive of benefit from nimorazole
Sun 2020[438]	LUAD	16	Gene coefficient equation	Cohort median signature score	Prognostic
Buffa 2010[387]	Metagene	51	Median gene expression	Ranking method	Prognostic (H&N, breast, lung)
Fardin 2010[389]	NBL	32	None	k-means clustering	Prognostic
Ragnum 2015[439]	Prostate	32	Median gene expression	Unsupervised clustering	Prognostic
Yang 2018[440]	Prostate	28	Gene coefficient equation	Cohort median signature score	Prognostic; predictive of benefit from CON (bladder)
Yang 2017[441]	Sarcoma	24	None	Compare to previously defined hypoxic tumours	Prognostic
Winter 2007[390]	Metagene	99	RNA expression distribution	Clustering and ranking of scores	Prognostic (H&N)

**outcome in cohort of patients with cancer the signature was derived in, unless otherwise stated; CON – carbogen and nicotinamide treatment; NS – not stated; GBM – glioblastoma; NBL – Neuroblastoma; H&N – head and neck; HCC – hepatocellular carcinoma; LUAD – lung adenocarcinoma; CR – colorectal; NS – not stated*

The majority of the signatures are prognostic, meaning that their use can identify patients with high hypoxia and worse survival outcomes. A few have been shown to be predictive of benefit from the hypoxia-modifying therapies carbogen and nicotinamide (CON)[391,436,440] or nimorazole[437]. Carbogen is a gas mixture of 98% oxygen with 2% carbon dioxide which is inhaled during the administration of radiotherapy. Nicotinamide is a pharmaceutical intervention that increases blood flow to tumours, administered several hours prior to treatment. The combination of the two treatments work to increase oxygen within a tumour, making the environment less hypoxic and more susceptible to radiation damage. Treatment with CON significantly increased the median tumour pO2 values in the majority of a cohort of bladder cancer patients[397]. Nicotinamide decreased the total x-ray dose required for local control, and when combined with carbogen this dose was reduced even further[395]. Nimorazole is a hypoxia-targeted radiosensitizer[442]. Combining nimorazole with radiotherapy in a cohort of H&N patients significantly increased loco-regional control and disease-specific survival compared to patients treated with placebo and radiotherapy[392]. The predictive gene signatures can identify the patients who will benefit from treatment and those where hypoxia-modifying treatments will provide no additional clinical benefit.

1.5.1 Hypoxia and radioresponse

Under normoxic conditions, DNA is ionised and damaged by the free radicals produced by radiation. Ionised DNA then reacts with free molecular oxygen to form a stable but damaged DNA molecule. In this way, oxygen makes the DNA damage permanent, although it is important to note this damage may still be repaired by DNA repair pathways. Under hypoxic conditions, the lack of free molecular oxygen means that the fixation of DNA damage cannot occur. Instead, ionised DNA, R·, is reduced to form RH, and DNA is restored to its original, undamaged, state[304,365,369,443,444]. This is the basis of the oxygen fixation hypothesis, which explains relative radioresistance under hypoxia. Tissue sections from tumour regions irradiated under high pressure oxygen conditions showed a greater extent of damage compared to sections from matched tumour regions irradiated under atmospheric oxygen conditions[445]. Clinically, an hypoxic tumour has been shown to be a negative prognostic indicator for survival following radiotherapy in multiple cancers including H&N[372,446,447], cervical[448] and soft tissue sarcoma[374].

The oxygen enhancement ratio (OER) is a term used in radiobiology to describe changes in radiosensitivity resulting from different oxygen concentrations[449]. The radiation dose required to produce a certain biological effect in hypoxic cells is greater than that required for normoxic cells; OER is the ratio of these doses[444,449,450]. For x-rays the OER is usually between 2.5 and 3.0[451]. The greatest increase in OER and radiosensitivity occurs between 0-3% oxygen, and very little change in OER occurs at concentrations above 21%[444,450,452–456].

1.5.2 Medulloblastoma and hypoxia

MBLs are assumed to contain regions of hypoxia because they are solid tumours[457–459]. Very few studies have been published examining markers of hypoxia within MBL patient samples. One used a small cohort containing both MBL (n=28) and PNET (n=7) utilising IHC staining for the expression of CAIX[460]. Across the whole cohort, 23% of samples had positive CAIX staining, and these tumours had worse overall survival[460]. While this study provides evidence for the occurrence of hypoxia within MBL tumours, it was conducted prior to the establishment of the molecular subgroups of MBL and so is unable to indicate whether subgroup and hypoxia status are linked. A study reporting that the WNT subgroup showed leakier BBBs compared to the remaining three subgroups investigated the expression of GLUT1. GLUT1 expression was significantly lower in WNT tumours compared to the remaining subgroups[106]. This study also showed that WNT tumours had significantly higher blood vessel density with significantly more vessel branch points than the remaining molecular subgroups[106]. A more comprehensive blood supply in WNT tumours suggest that these would be better oxygenated, which is in agreement with the low GLUT1 staining.

1.6 Migration

Migration is the movement of cells across a surface allowing cells to change their position based on external information, either individually or as a collective cell front[461–464]. Cellular migration is required during embryonic development, tissue repair and immune responses[462–464]. Migration also contributes to the development of cancer metastasis[462–464]. In order to migrate, an external stimulus causes a cell to polarise in the desired direction of movement[463]. This external stimulus could be a chemokinetic signalling molecule (telling the cell to be more migratory), a chemotactic/haptotatic

gradient (telling the cell to move along said gradient) or simply a lack of contact with surrounding cells[463]. The cell extends a protrusion in the direction of movement and sets down adhesion molecules to attach to the surface, then contraction of the cell body along with release of adhesion molecules towards the rear cause the whole cell to be dragged towards the destination[463]. This process will be repeated while the external stimulus is present. The speed with which a cell progresses through this cycle is cell type dependent – for example fibroblasts are slow migratory cells while leukocytes are much faster[463].

Migration of cells can be easily and simply measured *in vitro* using assays such as the gap closure/wound healing or transwell migration assays (see Section 1.6.1 and Figure 4). These assays can be adapted to measure another metastatic process, invasion. The invasion process requires cells to travel through a 3D membrane or matrix, and this process combines degradation of the matrix of the matrix with cell migration[464]. Patient samples can be examined for protein markers of the epithelial-mesenchymal transition (EMT), a process by which cells gain a more migratory, metastatic phenotype[461]. The EMT process is required in cancer metastasis to allow cells to migrate and invade into other tissues. Markers of EMT include low or decreased expression of proteins associated with epithelial cells, such as E-cadherin, and high or increased expression of proteins associated with mesenchymal cells, such as N-cadherin or vimentin. These markers can also be studied *in vitro* and levels correspond to the results of *in vitro* migration and invasion assays. For example, in a study of 28 cancer cell lines representing a variety of disease sites, cells with a high baseline expression of E-cadherin showed very little cell invasion while those with low E-cadherin expression had high rates of invasion[465].

1.6.1 Migration and radiation

Radiation is generally thought to promote the processes of cellular migration and invasion[466]. This relationship has been demonstrated *in vivo*, where mouse models of implanted lung tumours repeatedly demonstrate a significant increase in the number of metastases following radiation treatment compared to no radiation treatment[467–469]. However, *in vitro* studies are less conclusive. Table 5 presents a summary of published studies on the effect of radiation on migration and invasion in a range of cell lines.

While a substantial number of studies report an increase in migration and/or invasion, in concordance with the observations *in vivo*, the majority found either no change or a reduction in migration/invasion. There may be a contribution of the assay methodologies to these contradictory results, as several different protocols with experimental parameters are described.

Table 5: Summary of published studies investigating the effect of radiation on migration/invasion

	Cell Line	Dose (Gy)	Result (Migration)	Result (Invasion)*
Breast	LM2-4	2.3	No change[+ 470]	
	MCF-7	2.3	No change[+ 470]	
	MDA-MB-231	2.3 10	No change[+ 470] Increased[W 471]	 Increased[471]
CR	CaR1	5	Increased[W 472]	Increased[472]
	DLD1	5	Increased[W 472]	Increased[472]
GBM	U87MG	1 3 6	No change[+ 473] No change[+ 473] Increased[+ 473]	No change[473] Increased[473] Increased[473]
	LN-18	1 3, 6	No change[+ 473] Increased[+ 473]	No change[473] Increased[473]
	LN-229	1, 3 6	Increased[+ 473] Increased[+ 473]	No change[473] Increased[473]
	LN229	2 10	Increased[+ 474] No change[+474]	
	U87MG	2 10	Increased[+ 474] No change[+ 474]	
Glioma	GaMg	10	Reduced[S 475]	
	U87	5	Reduced[S 475]	
H&N	BHY	2, 5, 8	Increased[W 476]	
	Cal27	2, 5, 8	Increased[W 476]	
	DDP	8		Reduced[477]
	HLAC	8		Reduced[477]
	HN	8 2, 5, 8	 Increased[W 476]	Reduced[477]
	HT1080	2	No change[C 478]	No change[478]
	UD5	8		Reduced[477]
HC	Hep3B	7.5		Increased[479]
	HepG2	7.5		Increased[479]
	Huh7	7.5		Increased[479]
Lung	A549	2 10 2.2,	Reduced[+ 480] Reduced[+ 480] No change[W 481]	No change[480] Reduced[480]
	EBC-1	2, 10	No change[+ 480]	No change[480]
	LLC-LM	2.5, 7.5		Increased[468]
MBL	DAOY	8	Increased[W 243]	Increased[243]
	D283	8		Increased[243]
OS	MG63	2, 4, 6	Reduced[W 224]	Reduced[224]
Pancreatic	Panc-1	3, 5, 10	Reduced[+ 482]	Increased[482]
	Suit-2	3, 5, 10	Reduced[+ 482]	Increased[482]

**All invasion assays carried out using the Transwell/Matrigel invasion assay*
+ transwell migration assay; W – Wound healing assay; C – chemotaxis assay; S – spheroid assay
CR – colorectal; GBM – glioblastoma; H&N – Head and Neck; HC – hepatocellular; MBL – medulloblastoma; OS - osteosarcoma

On the largest scale, the method of initiating cell migration varies greatly. The most commonly used assay is the transwell assay (Figure 4, top panel). The transwell assay uses a porous membrane within a well through which cells can move – cells are seeded on the top of the membrane, incubated and then the number of cells that have travelled through the membrane are counted to show the migration rate. All invasion studies were conducted using an adaptation of this set up, where a layer of Matrigel is added between the cell layer and the membrane (therefore cells have to invade through the Matrigel before migrating through the membrane)[464]. The chemotaxis assay uses the transwell membrane method but places a chemotactic agent in the bottom section of the well in order to create a chemotactic gradient and a motive for cell movement[464]. The second most commonly used methodology was the wound healing/gap closure assay (Figure 4, middle panel). In this assay, cells are seeded to form a confluent monolayer and then a section of this monolayer is physically removed, for example by scratching a pipette tip across the well. The scratched monolayer is then incubated and gap closure monitored. Often this is done by imaging the well immediately after the scratch has been created and then again at 12 h or 24 h post-scratch. The amount of gap closure can then be calculated. The final method used was the spheroid migration assay (Figure 4, bottom panel), where cells are grown in 3D cell culture before individual spheroids are plated in 96-well plates and the dispersion of cells from the spheroid is monitored[464].

The different protocols measure different aspects of migration. In the transwell assay, cells travel across a membrane either at random or towards a chemotactic stimulus in the chemotaxis variation of the protocol. Cells move from areas of high to low confluency, and cell movement is vertical (from the top to the bottom chamber). The assay monitors single cell or chemotactic migration, but is not a model of collective cell migration or the EMT[464]. The transwell assay outputs the number of moving cells but does not allow for measuring the rate of migration. Additionally, while the chemotaxis assay initially provides cells with a chemotactic gradient towards the bottom chamber, due to the porous membrane required to allow cell movement to occur, this gradient becomes more diffuse over the course of the assay[464]. In the wound healing assay, cell movement is collectively away from a mass of cells and towards a mass of cells. Additionally, if used, the physical scratch will cause physical damage to the cells, causing intracellular signalling responses

that may influence the behaviour of the cell monolayer. While the two gap edges close the gap through co-ordinated cell movement, it is possible to track individual cells throughout the assay and monitor single-cell movement as well as collective cell movement.

The spheroid migration assay monitors the movement of cells away from a cell mass. As cells detach and move away from the spheroid, they do not travel at a uniform speed in a straight line. Radiation has been reported to significantly increase the displacement of cells from a starting point but not the total distance travelled[470]. While live-cell imaging combined with single-cell tracking can be applied to the spheroid migration assay, as the assay measures cell displacement rather than distance travelled single images at set time points may be adequate to detect radiation-induced alterations in cell movement.

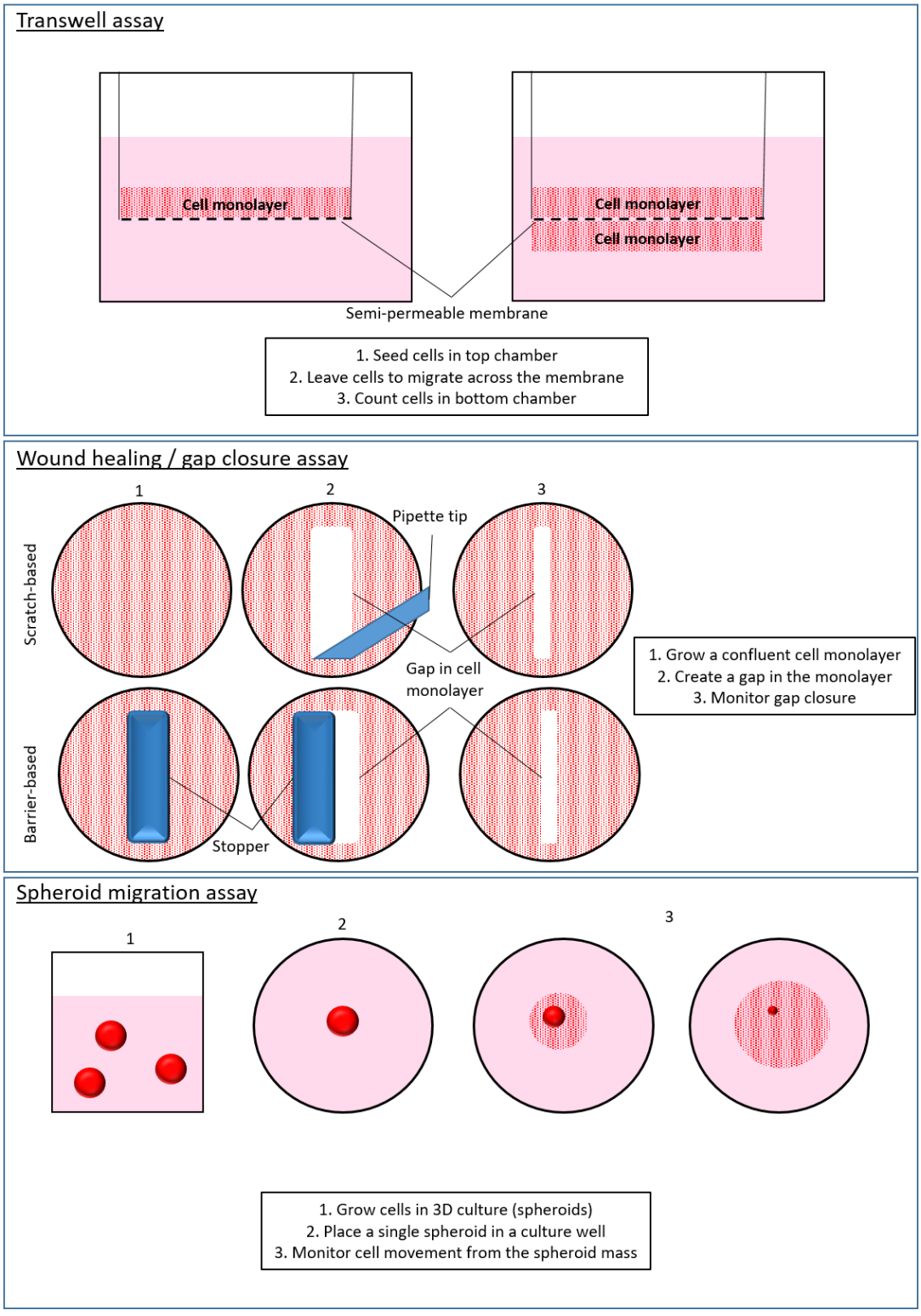

Figure 4: *In vitro* methods for investigating cell migration. *Three common set ups for monitoring cell movement are the transwell (TW) assay, the wound healing/gap closure (WH) assay and the spheroid migration (SM) assay. In the TW assay, cells are seeded in the top chamber of the insert and movement across a semi-permeable membrane is monitored. This set-up can be adapted for a chemotaxis assay by placing the chemotactic agent in the bottom chamber. In the WH assay, cells are seeded as a confluent monolayer, a gap is created and the closure of the gap is monitored. The assay can be scratch based, where cells are physically scraped off the surface, and barrier based, where cells are prevented from growing in a particular area using a removable stopper. In the SM assay cells a single spheroid is placed in a culture vessel. As the spheroid disaggregates, cell movement away from the spheroid is monitored.*

A parameter that varies widely across the studies is the radiation dose used, ranging from 1 to 10 Gy (Table 5). In some studies, changes in migration are dose-dependent, while in others an effect seen at lower doses is lost at higher doses or *vice versa*. It is difficult to take into account the relative effects on cell survival of these different doses within the migration assay. For example, a decreased migration rate at higher doses may actually be a result of increased cell death or longer periods of growth delay.

Another important factor in the analysis of cell movement *in vitro* with regards to radiation-induced changes is a time delay between irradiation exposure and assay initiation. Significant alterations in migration were not observed until 24 h following irradiation[470], while invasion alterations occurred 40 h after exposure[468]. Alterations to the cellular biology can take hours to manifest following irradiation. By assessing cell movement immediately following irradiation there may not be enough time for the biological process of migration to be altered by radiation exposure.

The precise mechanisms by which radiation increases cellular migration are under some debate and not clear. Of the studies reported in Table 5, no conclusions were drawn with regards to the mechanisms. A subset of the studies had the aim only of investigating the effect of irradiation on migration/invasion within particular cell lines rather than the elucidation of underlying biological changes and processes that would cause such a change. The most commonly implicated proteins in radiation-induced motility changes are MMPs. MMPs are enzymes known to degrade the extracellular matrix (ECM), suggesting a mechanism by which cells become more motile[466]. The protein expression of MMP-9 is increased following irradiation of MBL cell lines[483]. Exogenous MMP-2 caused faster gap closure in the wound healing assay[484], as did transfection with MMP-7[485]. Inhibition of MMP-2 or MMP-9 in retinoblastoma cells significantly slowed the gap closure[486].

A wide range of studies across various cell lines, have reported that irradiation affects the expression of EMT markers within cell lines. Specifically, the expression of the epithelial marker E-cadherin is decreased while the expressions of mesenchymal markers vimentin and/or N-cadherin are increased by irradiation in colorectal[472], MBL[487] and lung[481] cancer cell lines. After chemoradiotherapy, tissue from patients with rectal cancer express significantly greater levels of

vimentin and fibronectin, but significantly less E-cadherin[472]. This may also help explain the contradictory results gained from cell line studies, as conditions in which migration and invasion are studied *in vitro* may not be conducive to EMT-driven changes, such as the loss of adhesion molecules or increased ECM degradation.

There is some evidence that radioresistance is linked to migration. In radioresistant cell lines derived from established cervical[215] and oesophageal[209] cell lines (HeLa, ECA109 and Kyse150), E-cadherin protein and mRNA expression was significantly decreased while N-cadherin and vimentin protein and mRNA expression was significantly increased. The radioresistant cell lines were more mesenchymal (and therefore more migratory/metastatic) than the parental cell lines.

As the only methods available for determining cellular migration were *in vitro* monolayer based, only the SHH and Group 3 subgroups were the focus of the work presented in this thesis.

1.6.2 SHH and migration

Activation of the SHH signalling pathway is implicated in increased cellular migration. Activating the SHH pathway increases migration in cell lines representing NSCLC[488,489], LUAD[490], gastric cancers[491], HCC[125,492], ovarian cancers[130], GBM[493] and in synoviocytes[494] (normal cells located within joints). Inhibition of the pathway decreases cell migration in NSCLC[489], breast carcinoma[123] and cervical carcinoma cell lines[495]. SHH pathway activation also causes increases in metastases and components of the metastatic pathway. Overexpression of SHH *in vivo* in an orthotopic model of pancreatic cancer significantly increased the percentage of mice with metastases compared to control subjects[129]. More metastatic breast[123] and HCCs[125] have significantly higher expression of the SHH signalling pathway components SHH, PTCH1, SMO and GLI1 compared to non-metastatic tumours[123,125]. Expression of MMPs at both the protein and mRNA levels are increased by SHH signalling in ovarian cancer cell lines (MMP-7)[130], HCC cell lines (MMP-2 and MMP-9)[125,492], GBM cell lines (MMP-2, MMP-9)[493]. Activation also caused a positive response for EMT protein markers, with decreased expression of E-cadherin and increased expression of N-cadherin and vimentin in bladder cancer[355] and NSCLC cell lines[489]. Inhibition of GLI1 or SMO in lung[490] or pancreatic[496] cancer cells caused an increase in E-cadherin expression. This suggests that the

activation of the SHH pathway promotes a more migratory phenotype through the induction of EMT and increasing expression of MMPs.

1.6.3 *MYC* and migration

MYC staining is significantly higher in metastatic compared to non-metastatic osteosarcoma[362], and c-myc expression inhibits E-cadherin in an immortalized epithelial cell line[497]. Inhibiting the expression and/or activation of c-myc significantly inhibited migration in MBL[498], osteosarcoma[362] and breast cancer[499] cell lines. *MYC* amplification may therefore cause increased *in vitro* cell migration.

1.6.4 Medulloblastoma and migration

Several MBL cell lines have been assessed in *in vitro* migration assays, although rarely as part of a panel of MBL cell lines to allow for comparisons. Additionally, there is infrequent quantification of the rate of migration within these assays, making it difficult to compare between publications. Assays that do use the same cell lines do not report similar results. In one study, the MBL cell line Madsen showed the greatest invasion of a panel of MBL cell lines, followed by UW228-2, UW228-3, DAOY then UW228-1[500]. However, in a transwell assay, ONS-76 cells migrated faster than DAOY or UW228 cells[501]. DAOY cells are more positive for EMT marker expression than ONS-76 cells, suggesting a more migratory phenotype which was reflected by faster gap closure in the gap closure assay[502].

In the transwell assay, the SHH cell line DAOY[127] and Group 3 cell lines MED8A[503] and D425[503] showed reduced cell migration following irradiation. Irradiation also decreased migration of DAOY cells in the gap closure assay[504]. Inhibition of the SHH pathway using GANT61 in combination with irradiation resulted in a greater decrease in cell migration in the gap closure assay – although the study does not comment on the effect of GANT61 treatment alone[127]. In contrast, the cell lines DAOY and D283 (SHH and Group 3 respectively) showed increased invasion following irradiation[504]. These results illustrate one of the difficulties of *in vitro* migration assessment – the

lack of reproducibility for a cell line across different experimental set ups, quantification approaches, experimenters and laboratories.

1.7 Project Aims

The majority of MBL patients are not given subgroup-specific therapy with the majority are prescribed the same treatment. The different clinical outcomes between subgroups demonstrate these therapies achieve different levels of success within each subgroup, and there is potential to improve outcomes using personalised treatment. Current clinical trials focus on the (arbitrary) reduction of treatment severity in the WNT subgroup and targeted treatment for the SHH subgroup using previously discovered SHH pathway antagonists. Knowledge of differential chemotherapeutic and radiotherapeutic responses of the molecular subgroups could be used to design future clinical trials based on empirical evidence.

There is some evidence that the chemotherapeutic response differs across the molecular subgroups based on underlying biological mechanisms[106]. No studies have investigated whether the underlying biology affects radioresponsiveness. Based on survival outcomes it was hypothesised that the WNT subgroup is the most radioresponsive, followed by SHH, Group 4 and Group 3. Major contributing factors to radioresponsiveness are intrinsic radiosensitivity, proliferative capacity and the presence of hypoxia. It was predicted that the molecular subgroups would show significant differences in these factors causing the different radioresponsiveness.

Activation of the WNT and SHH signalling pathways decrease radiosensitivity and therefore these subgroups were hypothesised to be relatively less radiosensitive than Groups 3 and 4. This pathway activation can also increase proliferation and therefore these subgroups were also hypothesised to be more proliferative. Low radiosensitivity and higher proliferation would indicate a lower radioresponsiveness, however these subgroups were initially hypothesised to be more radioresponsive. To account for this discrepancy, it was hypothesised that Group 3 and 4 tumours would contain more extensive hypoxia. Tumour hypoxia is a known and significant factor in decreasing radioresponsiveness and therefore this would account for the initial hypothesis based on survival outcomes.

Data from the literature indicates MBL is a radioresistant and proliferative tumour type, however, no direct comparisons between molecular subgroup with regard to their intrinsic radiosensitivity, proliferative capacity or level of hypoxia have been published. The project hypotheses can be supported by inferences drawn from separate publications which report the SHH subgroup as less radiosensitive than Group 3 and that the WNT subgroup is the least hypoxic. Investigations designed to specifically test these characteristics across subgroups would provide more complete datasets containing more robust and conclusive data. The radiosensitivity, proliferative capacity and extent of tumour hypoxia across the molecular MBL subgroups were investigated using publically available patient cohorts downloaded from Gene Expression Omnibus (GEO).

As the panel of MBL cell lines available for this study only represented SHH and Group 3 cell lines, the migration analysis was limited to these subgroups and MBL as a whole. The activation of the SHH signalling pathway in SHH subgroup cell lines was predicted to result in a higher baseline rate of cell migration compared to the Group 3 cell line. Irradiation of MBL cell lines *in vitro* was predicted to result in increased cell migration.

The overall aim of this project was to identify factors that might lead to differences in the radioresponsiveness of the four MBL molecular subgroups and could potentially be used in the future to personalise treatments.

The specific objectives were to investigate whether there were differences between MBL molecular subgroups in:

1. Radiosensitivity
2. Proliferation
3. Hypoxia
4. Cell migration.

2. Materials and methods

2.1 Cell culture

2.1.1 Medulloblastoma cell line panel

The cell line panel comprised six MBL cell lines (Table 6). The cell lines D425Med, MED8A, ONS-76 and UW228-2 were obtained from Dr David Jones (Heidelberg German Cancer Research Centre, Germany). D283Med and DAOY were purchased from American Type Culture Collection (ATCC) cell biology collection (Manassas VA, USA). Cultures were tested for mycoplasma contamination on a bimonthly basis.

2.1.2 Cell line authentication

Cell lines were authenticated using Short Tandem Repeat (STR) DNA profiling upon receipt and on each cell thaw through the Molecular Biology Core Facilities at the Cancer Research UK – Manchester Institute. STRs are regions in the DNA profile of 1-6 base pairs, which can be used to create a unique profile of a cell line[505]. DNA from the cell line to be authenticated is extracted, amplified using the polymerase chain reaction (PCR), then sequenced[505]. The STR profile of the sample is compared to that of the original cell line and the test cell line is considered to be authentic if there is at least an 80% match between the two[505].

Table 6: Characteristics of the six cell line panel

Cell Line	Subgroup	p53 Status	MYC Status	Phenotype	Derivation	Split Ratio
D283	Group 3[506] Group 4[507]	WT[508–510]	HLG[511]	Semi-adherent	Peritoneal metastasis from 6-year old Caucasian male patient[512]	$5x10^5$ cells/mL
D425	Group 3[506]	M[510,513]	Amp[514]	Semi-adherent	Cerebellar tumour from 5 year old male patient[514]	$3x10^5$ cells/mL
DAOY	SHH[226]	M[508–510,513]	-	Adherent	Posterior fossa tumour from 4-year old Caucasian male patient[515]	1:3 - 1:10
MED8A	Group 3[16]	WT[513]	Amp[511]	Adherent	-	1:5
ONS-76	SHH[226]	WT[513]	-	Adherent	Tumour from 2-year old east Asian female patient[516]	1:10 - 1:15
UW228-2	SHH[226]	M[508,513]	-	Adherent	Posterior fossa tumour from 9-year old female patient[517]	1:3 – 1:10

SHH – Sonic Hedgehog, WT – wild-type, M- mutant, HLG – high level gain, Amp – amplified

2.1.3 Tissue culture conditions

Cell lines were maintained in RPMI-1640 (Sigma Aldrich, Poole, UK) with 0.3 g/L L-glutamine (Sigma Aldrich) and 10% Fetal Bovine Serum (FBS, Lot~ BCBW1009, Sigma Aldrich), henceforth referred to as 'complete medium'. Cultures were maintained at 37°C in a 95% humidified air and 5% CO_2 incubator. Cell culture was conducted using aseptic technique and following the British Journal of Cancer Guidelines for the use of cell lines in biomedical research[518]. Adherent cell lines were maintained in Corning Cell Culture Flasks with Vent Cap (Corning, Corning, USA) and passaged at 70-80% confluency. Semi-adherent cell lines were maintained in CytoOne Non-Treated flasks (Star Labs, Milton Keynes, UK) at optimal cell concentrations specific to each cell line (Table 6). Where required, hypoxia was maintained using a Whitley H35 Hypoxystation (Don Whitley Scientific, Bingley, UK) to provide the required O_2 concentration in a humidified atmosphere with 5% CO_2 at 37°C.

2.1.4 Subculture of adherent cell lines

Subculturing was carried out to maintain cells in the exponential growth phase. The spent cell culture medium was removed and discarded to waste. A Phosphate Buffered Saline (PBS) wash was carried out, using approximately 2 mL PBS per 10 cm^2 culture surface area and gently rocking the culture vessel several times. The wash solution was removed and discarded and a pre-warmed dissociation reagent was added (~0.5 mL per 10 cm^2 culture surface area). For MED8A the reagent Accutase (Sigma Aldrich) was used; for all other cell lines trypsin-EDTA (0.5 g trypsin, 0.2 g EDTA, Sigma Aldrich) was the dissociation reagent. The vessel was gently rocked to ensure complete coverage of the cell layer, before incubation at 37˚C for 5 min. When over 90% of cells had detached, pre-warmed complete medium was added using at least twice the volume of dissociation reagent present. This cell suspension was then transferred into daughter culture flasks using appropriate dilutions and complete medium added up to the recommended volume for the flask size. Passage numbers were recorded at each split to monitor the total number of passages for each cell line. After a maximum of 20 passages, new cells were thawed.

2.1.5 Subculture of semi-adherent cell lines

The subculture of the semi-adherent cell lines was carried out in accordance with the following protocols, previously optimised by the group. Spent medium containing suspension cells was transferred to a Falcon tube. The culture vessel was washed with PBS, using approximately 2 mL per 10 cm^2 culture surface area, and the PBS wash added to the spent medium and centrifuged for 5 min at 400 x *g*. After centrifugation the supernatant was discarded and the pellet was resuspended in an appropriate amount of pre-warmed complete medium using gentle pipette mixing. The cell suspension was counted as described in Section 2.1.6. For D283, the cell suspension was diluted to $5x10^5$ cells/mL and for D425 the final concentration was $3x10^5$ cells/mL. Two days after subculturing, flasks containing semi-adherent cell lines were fed with a volume of complete medium equal to half that already in the flask.

2.1.6 Harvesting cells and haemocytometry

Adherent cells were washed with PBS, detached from the culture vessel and diluted with complete medium as detailed previously (Section 2.1.4). The cell suspension was centrifuged at 400 x *g* for 5 min to produce a cell pellet. The supernatant was discarded and cells re-suspended in appropriate volumes of pre-warmed complete medium and vortexed to produce a single cell suspension. Semi-adherent cells were prepared as detailed in Section 2.1.5. The trypan blue exclusion assay was used to count viable cells by adding 10 µL of cell suspension to 10 µL of 0.4% trypan blue solution (Sigma-Aldrich), of which 10 µL was placed under a coverslip on a haemocytometer (Neubauer Improved Haemocytometer Counting Chamber, Hawksley, London, UK). As trypan blue is only taken up by non-viable cells, unstained cells were counted to obtain a viable cell concentration. Cells across the four outer grids of the haemocytometer were counted, including cells touching the top and left side of each square but excluding those touching the bottom or right sides. The total number of cells was divided by four, multiplied by 10^4, and then multiplied by the trypan blue dilution factor (2) to calculate the concentration in cells/mL. The number of dead cells was recorded by counting the stained blue cells.

2.1.7 Seeding cells

After cells had been harvested and counted, the volume of cell suspension containing the required number of cells for each experiment could be calculated. This volume was added to the appropriate culture vessel, such as a 6-well plate or petri dish, and cells incubated under the required experimental conditions.

2.1.8 Preparation of frozen cell stocks

After initial receipt and authentication of each established culture of each cell line, frozen stocks were prepared in freezing medium containing 90% FBS and 10% dimethylsulfoxide (DMSO, Sigma-Aldrich). Cells in the exponential growth phase with a viability of greater than 80% were harvested and counted as described in Section 2.1.6. After a second centrifugation at 400 x *g* for 5 min, the cell pellet was resuspended in the volume of freezing

medium required to make a $2x10^6$ cells/mL suspension. Cryovials (1.8 mL Cryovial with Internal Thread, E3110-6122, Star Labs) containing 1 mL of cell suspension in freezing medium were placed at -80˚C in a controlled rate freezing apparatus (Nalgene Mr. Frosty or Cool Cell), producing a freezing rate of -1°C per minute. At least 24 h later, vials were transferred to storage in liquid nitrogen.

2.1.9 Thawing of frozen cell stocks

Cryovials were quickly thawed using a 37˚C water bath and the contents transferred to a 15 mL Falcon tube containing 4 mL of pre-warmed complete medium. After centrifugation at 400 x *g* for 5 min, the pellet was resuspended in 4 mL of pre-warmed complete medium in a T25 culture flask (for semi-adherent cell lines) or 15 mL of pre-warmed complete medium in a T75 culture flask (for adherent cell lines). Cells were placed in the incubator and monitored until subculturing was required.

2.2 Irradiation of cells

X-ray irradiation was carried out using either an XStrahl CIX3 irradiator (XStrahl, GA, USA) with a dose rate of 2.14 Gy/min (OCRB experiments) or a Faxitron x-ray (Faxitron Bioptics, AZ, USA) with a dose rate of 0.95 Gy/min (Stopford experiments) or 1.37 Gy/min (Paterson). Cells were irradiated at room temperature under normoxia or under hypoxic conditions (0.1% oxygen), which were maintained throughout irradiation using a Micro Pelicase (Peli, CA, USA).

Proton irradiation was carried out in The Christie Proton Beam Research Room using a Varian Probeam cyclotron (Varian, CA, USA). A dose rate of 0.81 Gy/min was used for the 2 and 4 Gy doses with 230 meV and 26 nA. A dose rate of 0.78 Gy/min was used for the 6 and 8 Gy doses with 230 meV and 51 nA. As the proton irradiation experiments were conducted during the beam commissioning and testing in the Research Room, only an energy of 230 meV at the entrance of the SOBP had been fully commissioned and tested. Sample plates were therefore positioned and exposed to this energy and cells were irradiated at room

temperature under normoxia. Following irradiation, samples were isolated until the activation levels had decreased to a safe level, at which point they were transferred to the incubator. RBE values were calculated using Equation 2.

Equation 2

$$Relative\ Biological\ Effectiveness = \frac{x-ray\ dose\ producing\ a\ set\ biological\ effect}{proton\ dose\ producing\ the\ same\ biological\ effect}$$

2.3 Cell growth assay

Exponentially growing cells were seeded in 6-well plates (Corning Costar Flat Bottom Cell Culture Plates, Corning) on day 0 and maintained in 0.1% or 21% oxygen for 96 h. The trypan blue exclusion assay (Section 2.1.6) was used to count cells every 24 h. For each cell line, one independent experiment was carried out, with three replicate wells for each condition each day. GraphPad Prism v 8.1.2 (GraphPad Software, CA, USA) was used to plot growth curves and calculate population doubling times (Td). Statistical analysis (t-tests) was carried out using GraphPad Prism v 8.1.2.

2.4 Clonogenic assay

The protocol used for the clonogenic survival assay was adapted from Franken *et al.* (2006)[175].

2.4.1 Colony formation tests

Exponentially growing cells were seeded into 6-well plates in 4mL of pre-warmed RPMI-1640 and incubated for up to 14 days. Complete medium was used for all cell lines excluding MED8A, where medium containing 20% FBS was used. Seeding densities ranged from 100 to 1000 cells/well. For each cell line, one independent experiment was carried out, with two technical replicates at each seeding density. Plates were inspected on days seven, 11 and 14 to check colony formation. The endpoint was reached when colonies contained over 50

cells and hence were observable by eye. Once suitable colonies had formed, plates were fixed, stained and counted (Section 2.4.3).

2.4.2 Clonogenic assays

Exponentially growing cells were seeded into plug-seal T25 flasks (CytoOne, Star Labs) at seeding densities optimized for each cell line and allowed to adhere for 24 h in an incubator. After 24 h, flasks for irradiation under hypoxia were transferred to the hypoxia cabinet and exposed to 0.1% oxygen for 24 h. Flasks for irradiation under normoxic conditions remained in the incubator. Before removal from the hypoxia cabinet the plug-seal lids were secured to maintain the oxygen concentration during irradiation. Cells were irradiated with 0, 1, 2, 4, 6, 8, 10, 12, 16 or 20 Gy of x-rays. Immediately following radiation exposure, cells were counted and seeded into 6-well plates using varying seeding densities. Complete medium was used for all cell lines excluding MED8A, where medium containing 20% FBS was used. At least three biological replicates for each dose point were carried out for each cell line, containing three technical replicates per seeding density. Plates were incubated for up to 14 days until colonies containing over 50 cells had formed, at which point cells were fixed, stained and counted (Section 2.4.3).

2.4.3 Fixing, staining and counting of colonies

For DAOY, ONS-76 and UW228-2 plates, medium was decanted from each well and a PBS wash using 2-3 mL per well applied. As the cell line MED8A produced weakly attached colonies, the PBS wash step was omitted for this cell line. 2 mL of 0.1% crystal violet solution (Sigma-Aldrich) in 50% methanol (Fisher Chemical, Loughborough, UK) was added to each well and plates were incubated at room temperature for no more than 1 h. Crystal violet solution was removed for re-use or inactivated using sodium hydroxide pellets. Plates were washed by submerging in a water bath and then air dried overnight. Inactivated crystal violet waste was discarded down a sink. Colonies were counted manually using a colony counting pen (eCount Colony Counter Pen, Heathrow Scientific, IL, USA). Alternatively, the

plates were scanned on a GelCount colony and spheroid counter (Oxford Optronix, Oxford, UK) and the software used to manually identify and count colonies.

2.4.4 Analysis

Wells with fewer than 10 colonies or too many colonies to count were excluded from analysis. The mean number of colonies for each seeding density at each dose was calculated. Plating efficiency (PE) was then calculated using Equation 3, and wells that displayed a loss of linearity for that dose were also excluded from analysis.

Equation 3

$$Plating\ Efficiency = \frac{number\ of\ colonies\ counted}{number\ of\ cells\ seeded} x\ 100$$

The SF for each seeding density at each dose was calculated using Equation 4 and the average 0 Gy PE, then the mean SF value at each dose was reported for that experiment.

Equation 4

$$Surviving\ Fraction = \frac{Number\ of\ colonies\ counted}{Number\ of\ cells\ seeded\ x\ \left(\frac{0\ Gy\ Plating\ Efficiency}{100}\right)}$$

GraphPad Prism was used to plot the survival curves using an LQ model (Equation 5). Survival curve parameters were calculated using GraphPad Prism and the in-house alpha_beta software. Statistical analyses, including F-tests and t-tests, were carried out using GraphPad Prism v 8.1.2.

Equation 5

$$Surviving\ Fraction\ at\ Dose\ (D) = e^{-(\alpha D + \beta D^2)}$$

The OER was calculated using Equation 6 using the dose to produce a specific biological effect following irradiation under hypoxia or normoxia.

Equation 6

$$Oxygen\ Enhancement\ Ratio = \frac{Dose\ in\ hypoxia}{Dose\ in\ normoxia}$$

2.5 CellTiter-Glo assay

2.5.1 Reagent preparation

The CellTiter-Glo Luminescent Cell Viability Assay kit (Promega, WI, USA) was used. The reagent was prepared according to the manufacturer's protocol by transferring 100 mL of CTG buffer to the CTG substrate and vortexing until a homogeneous solution was obtained. The reagent was then stored at -20°C and thawed in the fridge overnight before each assay.

2.5.2 Response linearity test

Exponentially growing cells were seeded in increasing cell densities in a 96-well flat clear bottom white polystyrene TC-treated microplate (Corning) and incubated for 24 h. The CTG reagent and seeded plate were allowed to equilibrate to room temperature for 30 min before either 100 µL or 50 µL of reagent was added to each well. Plates were mixed on an orbital shaker for 2 min then incubated at room temperature for 10 min. A VarioScan Lux plate reader (Thermo Fisher Scientific) was used to record luminescence in RLUs. The number of cells seeded was plotted against the RLU value, and the upper and lower limits of the linear response were recorded. These were used as cut-off values for the CTG assay, as the number of cells present at the point of the assay was not determinable.

2.5.3 CellTiter-Glo assay

Exponentially growing cells were seeded at low but increasing cell densities in a 96-well flat clear bottom white polystyrene TC-treated microplate (Corning) and incubated for 48 h. The range of cell densities used across all cell lines was 20 cells/well – 320 cells/well. Following the incubation period cells were irradiated with 0, 2, 4, 6 or 8 Gy of x-ray irradiation before being returned to the incubator. After a nine day incubation, the CTG reagent and plates were allowed to equilibrate to room temperature for 30 min before 50 µL of reagent was added to each well. Plates were mixed on an orbital shaker for 2 min then incubated at room

temperature for 10 min. The Varioscan Lux plate reader was used to record luminescence (in RLU).

2.5.4 Analysis

For each plate, the 0 cells/well RLU values were used to calculate the background luminescence, which was then subtracted across the plate. Individual RLU values that did not lie within the linear response range for that cell line, as calculated in Section 2.5.2, were excluded in accordance with the manufacturer protocol. A plot of seeding density against RLU was used to identify which seeding densities lay within the linear response range for each radiation dose. A single seeding density which lay within the linear response range for all doses within that experiment was used to calculate the PF (Equation 7).

Equation 7

$$Proliferating\ Fraction = \frac{RLU\ value\ at\ Dose\ X}{RLU\ value\ at\ 0Gy}$$

Response curves were plotted and the AUC calculated using GraphPad Prism. A lower AUC value indicates a more radiosensitive cell line. Statistical analyses, including F-tests and t-tests, were carried out using GraphPad Prism v 8.1.2.

2.6 Bioinformatics analysis

2.6.1 Data processing and analysis

Processing and analysis of the gene expression data were carried out using RStudio (R version 4.0.3). The packages used for analysis were affy[519], affycoretools[520], AnnotationDbi[521], Biobase[522], dplyr[523], GEOquery[524], ggplot2[525], gplots[526], hgu133plus2.db[527], hgu133plus2cdf[528], hugene11sttranscriptcluster.db[529], hugene20sttranscriptcluster.db[530], matrixStats[531], MM2S[532], oligo[533], pheatmap[534], stringr[535], survminer[536], survival[537] and writexl[538]. Probeset IDs were annotated with gene symbols using the relevant annotation package for each platform. Where multiple probesets mapped to a single gene symbol, the median gene expression value of these probesets was used for analysis. Statistical analyses

including the generation of descriptive statistics, ANOVAs and unpaired t-tests were carried out using GraphPad Prism v 8.1.2.

2.6.2 Patient cohorts

Four patient cohorts were downloaded from the GEO database –GSE109401, GSE85217, GSE37382 and GSE37418. All cohorts had subgrouping data available. Data were downloaded as processed, normalised .CEL files. A cohort containing 34 patients was also available (McCabe). Raw data for this cohort were processed and normalised using the RMA algorithm. Patient cohort details are shown in Table 7 and Table 8.

Table 7: Details of the patient cohorts used in this study

Cohort	Sample preparation	Microarray	Probe pairs per sequence*	Number of genes	Normalisation method	Subgroup classification method	Number of samples	Sample number
GSE37418 Finkelstein, St Jude, 2012 cohort [539,540]	100 ng of snap-frozen RNA	Affymetrix Human Genome U133 Plus 2.0 Array	11[541]	38500[541]	Mas5	mRNA expression profiling & immunohistochemistry	73	8 WNT 10 SHH 16 Group 3 39 Group 4
GSE109401 Rivero-Hinojosa, Washington, 2018 cohort[542]	15 µg of cRNA from frozen primary tissue	Affymetrix Human Gene 2.0 ST Array	21[543]	48000[543]	RMA	Methylation profiling classifier from MolecularNeuropathology.org	19	5 WNT 5 SHH 5 Group 3 4 Group 4
GSE85217 Cavalli, Toronto, 2016 cohort[95,544]	400 ng of total RNA from fresh frozen tissue	Affymetrix Human Gene 1.1 ST Array	26[545]	28875[545]	RMA	Integrated gene expression & DNA methylation data, followed by spectral clustering	763	70 WNT 223 SHH 144 Group 3 326 Group 4
GSE37382 Northcott, DKFZ, 2012 cohort[16]	400 ng of total RNA from frozen tissue biopsies	Affymetrix Human Gene 1.1 ST Array	26[545]	28875[545]	RMA	Custom Nanostring codeset	285	0 WNT 51 SHH 46 Group 3 188 Group 4
McCabe, unpublished cohort	500ng of total RNA from frozen primary tissue	Affymetrix Human Genome U133 Plus 2.0 Array	11[541]	38500[541]	RMA	22-probeset signature[78]	32	3 WNT 10 SHH 8 Group 3 11 Group 4

Sample preparation, microarray, normalisation method and subgroup classification methods reported in cohort papers. Probe pairs per sequence and number of genes are details of the microarrays.
**25-mer probe length for each probe*

Table 8: Patient characteristics for the five cohorts

		GSE37418		GSE109401		GSE85217		GSE37382		McCabe	
		n (76)	%	n (19)	%	n (763)	%	n (285)	%	n (32)	%
Subgroup	WNT	8	11	5	26	70	9	0	0	3	9
	SHH	10	13	5	26	223	29	51	18	10	31
	Group 3	16	21	5	26	144	19	46	16	8	25
	Group 4	39	51	4	21	326	43	188	66	11	34
Age Group	Infant (<3)	0	0	4	21	98	13	21	7	19	59
	Child (3-16)	76	100	13	68	520	68	238	84	8	25
	Adult (>16)	0	0	0	0	111	15	69	24	5	16
Gender	Male	54	71	10	52	472	62	202	71	16	50
	Female	22	29	7	37	247	32	80	28	16	50
Histology	Anaplastic	17	22	-	-	0	0	0	0	0	0
	Classic	51	67	-	-	387	51	200	70	32	100
	Desmoplastic	6	8	-	-	109	14	21	7	0	0
	Large Cell Anaplastic	0	0	-	-	72	9	30	11	0	0
	MBEN	0	0	-	-	18	2	6	2	0	0
	Medulloblastoma	0	0	-	-	0	0	27	9	0	0
	Myo	2	3	-	-	0	0	0	0	0	0
M Stage	M0	56	74	13	68	397	52	-	-	28*	88
	M+	20	26	3	16	176	23	-	-	4⁺	13

*MBEN – Medulloblastoma with extensive nodularity. *M0/1; ⁺M2/3*

2.6.3 Subgroup analysis

Subgroup classification data were available for all five patient cohorts. As the method for determining tumour subgroup was not consistent between cohorts, the open-source Medullo-Model to Subtypes (MM2S) R package was used[532]. During MM2S analysis, single-sample Gene Set Enrichment Analysis (ssGSEA) is performed. The algorithm then selects out any enriched genesets that are subgroup specific, and ranks these based on their enrichment scores. This procedure produces a ranking matrix for the sample, which is processed by the algorithm in a k-nearest neighbour classification model. The sample is assigned to a subgroup based on the subgroups of the five nearest neighbours identified using this classification model.

2.6.4 Radiosensitivity index analysis

The RSI is calculated from the gene expression values of 10 genes (Equation 8). Details of the 10 genes are given in Table 9.

Equation 8

$$\textit{Radiosensitivity Index (RSI)} = (HDAC1 * -0.020469) + (JUN * 0.0128283) + (PAK2 * -0.0092431) + (PRKCB * -0.0017589) + (RELA * -0.0038171) + (STAT1 * 0.0254522) + (SUMO1 * -0.0002509) + (IRF1 * -0.0441683) + (ABL1 * 0.1070213) + (AR * 0.0098009)$$

Table 9: The 10 genes of the Radiosensitivity Index Signature

Gene Name	Gene Symbol	Ensembl ID
Histone deacetylase 1	HDAC1	ENSG00000116478
Jun proto-oncogene	JUN	ENSG00000177606
p21 activated kinase 2	PAK2	ENSG00000180370
Protein kinase C beta	PRKCB	ENSG00000166501
Rela proto-oncogene	RelA	ENSG00000173039
Signal transducer and activator of transcription 1	STAT1	ENSG00000115415
Small ubiquitin like modifier 1	SUMO1	ENSG00000116030
Interferon regulatory factor 1	IRF1	ENSG00000125347
ABL proto-oncogene 1	ABL1	ENSG0000097007
Androgen receptor	AR	ENSG00000169083

2.6.5 Meta-PCNA index analysis

The mPI is calculated as the median gene expression value of the 131 genes in the meta-PCNA signature. The full list of genes in the signature can be found in Appendix 1.

2.6.6 Hypoxia signatures

No published hypoxia gene signatures have been derived or validated using MBL cell lines or patients. A literature search identified 21 published hypoxia gene signatures (Table 4, Section 1.5). Of these, 12 were selected for use with the patient cohorts. The three signatures derived for brain cancers were included in analyses, as was the NBL signature, because these cancers are expected to be more closely related to MBL. Of the remaining identified signatures, those that classified patients as high- or low-hypoxia based on the median cohort score were included. Signatures that used more complex clustering or comparison methods were excluded. Finally, signatures derived in cancer types that were not represented in the already selected panel (i.e. a HCC signature and a metagene signature) were included in our panel. The 12 included signatures are described in Table 10.

Table 10: Published hypoxia signatures used in this study

Signature	Number of genes	Cancer of origin	Signature Score Generation
Yang, 2018[440]	28	Prostate	Signature score generated using gene coefficients determined from a Cox survival model. Median signature scores stratified patients into high and low hypoxia groups.
Yang, 2017[391]	24	Bladder	Signature score generated as the median of the 24 gene expression values. The median signature score for the cohort is used to divide samples into high and low hypoxia groups.
Tardón, 2020[434]	36	Glioblastoma	Patients were grouped into 'high-risk' or 'low-risk' categories based on signature expression by k-means clustering (one minus Pearson correlation metric, k=2).
Eustace, 2013[436]	26	Head and neck Bladder	Signature score generated as the median of the 26 gene expression values. The median signature score for the cohort is used to divide samples into high and low hypoxia groups.
Sun, 2020[438]	16	Lung adenocarcinoma	Signature score generated using gene coefficients generated by a LASSO Cox model. The median signature score for the cohort is used to divide samples into high and low hypoxia groups.
Lin, 2020[435]	5	Glioma	Signature score generated using gene coefficients generated by a multivariable Cox analysis.
Fardin, 2010[389]	32	Neuroblastoma	Patients were grouped into high or low hypoxia categories based on signature expression by k-means clustering (Euclidean distance, 100 iterations, k=2).
Buffa, 2010[387]	51	Metagene	Signature score was generated using the median gene expression of the 51 gene expression values.
Van Malenstein, 2010[386]	7	Hepatocellular	Signature scores were generated by subtracting the mean gene expression of downregulated genes (n=3) from the mean gene expression of the upregulated genes (n=4). Patients were grouped in high or low hypoxia groups using a cut off value of 0.35.
Wang, 2020[427]	14	Breast	Signature scores were generated using gene coefficients calculated by Cox regression analysis. The median signature score for each cohort was used to classify patients as high or low hypoxia.
Wang, 2020[388]	5	Glioblastoma	Signature scores were generated using gene coefficients calculated by multivariate Coz regression analysis. Median signature scores were used to classify patients as high or low hypoxia.

2.6.7 Survival analysis

Clinical outcome data were available for GSE85217. Survival analyses, including generation of Kaplan-Meier curves, univariable and multivariable analysis, was carried out in R using the survival package[537]. Only factors that were found to be significant in univariable analysis were included in multivariable analysis with one exception. In the case of the hypoxia gene signatures, the gene signature with the lowest p-value in univariable analysis was used in the multivariable model.

2.7 IncuCyte assays

2.7.1 Gap closure assay (WoundMaker)

This assay was used with the adherent cell lines only. Exponentially growing cells were harvested and seeded in a 96-well plate. Plates were incubated for 24 h and then irradiated at 0 Gy, 2 Gy or 8 Gy and the medium changed to one containing only 1% FBS. For experiments requiring a 24 h delay between irradiation and gap creation, another 24 h incubation was then carried out. For experiments monitoring gap closure immediately following irradiation, this incubation step was omitted. The IncuCyte WoundMaker (Essen Biosciences, Sartorius) was washed once with sterile distilled water and once with 70% ethanol for five min each. It was then used to create a scratch in all wells of one plate simultaneously. Between plates, the WoundMaker was soaked in sterile distilled water for 5 min. After scratching, wells were washed twice with PBS to remove any cell debris before fresh medium containing 1% FBS was added. Plates were transferred to an IncuCyte Zoom (Essen Biosciences, Sartorius) and images taken every 1 h for a period of 24 h to monitor gap closure. For gap measurement at 0 h, immediately following gap creation the wells were washed with PBS and fixed with formalin for 10 min. Two more PBS washes were carried out, then fixed plates were stored at 4°C until imaging on the IncuCyte Zoom. After use the WoundMaker was washed with 0.5% Alconax, 1% Virkon S, sterile distilled water and 70% ethanol for five min each.

2.7.2 Gap closure assay (Ibidi inserts)

This assay was used with the adherent cell lines only and used re-usable ‘Culture-Insert 2 Well for self-insertion’ (‘Ibidi inserts’, Ibidi, Germany). The Ibidi inserts were sterilised by soaking in 100%

ethanol and then left to air dry under sterile conditions. Once dry, the inserts were placed in the centre of each well in a 12-well plate, where they adhered to the culture surface. Exponentially growing cells were harvested and seeded into both sides of the insert. Plates were incubated for 24 h before the inserts were carefully removed using sterilised tweezers from each well to generate the gap. Either complete medium or medium containing 1% FBS was added to each well and irradiation with either 0, 2 or 8 Gy was carried out. Plates were transferred to an IncuCyte Zoom and images taken every 1 h for a period of up to 24 h to monitor gap closure. For experiments requiring a delay in gap creation, cells were seeded into a T75 flask, incubated for 24 h and then irradiated at 0 Gy, 2 Gy or 8 Gy. For a 24 h delay between irradiation and gap creation, cells were harvested, counted and seeded into both sides of the insert. For a 7 day delay between irradiation and gap creation, flasks were returned to the incubator for six days before the cells were seeded into the inserts. Plates were incubated for 24 h before the inserts were carefully removed from each well to generate the gap. Medium containing 1% FBS was added to each well, then plates were transferred to an IncuCyte Zoom and images taken every 1 h for a period of 24 h to monitor gap closure. After use the Ibidi inserts were washed in distilled water, sterilised with 100% ethanol and left to air dry before being stored for future use.

2.7.3 Analysis

Images were cropped prior to analysis to select the centre of each scratch and therefore only horizontal gap closure. Each image provided data for one timepoint. Cropped images were analysed using a Python script developed for this thesis. A user interface was designed and implemented with the assistance of a Python specialist, Nathaniel Morris. The code is available at https://github.com/rcmorris11/Migration-Analysis-Code/. Images were converted to greyscale and a mask was applied to assign a value of 0 to any pixels containing cells and a value of 1 to any pixels that did not. The mask settings were optimised for each cell line to ensure accurate identification of gap or cell pixels. The total of each row within each image was calculated and converted to distance using a scaling factor to produce at least 100 measurements of gap width per timepoint. The mean gap width for each time point was plotted and the linear period of gap closure was determined and used to calculate the gap closure rate. The mean gap closure rate for each assay was calculated. Statistical analysis was carried out using GraphPad Prism v 8.1.2.

3. Results

3.1 Cell growth curves

Figure 5 shows the growth curves for the six MBL cell lines studied (Table 6, Section 2.1.1). Growth curves were completed over 96 h with cells grown in 21% (normoxia) or 0.1% (hypoxia) oxygen concentrations (Section 2.3). The maximum length of time over which cells were required to be incubated under hypoxic conditions was 24 h prior to irradiation, and therefore the 96 h time frame confirmed that the cells survived under these conditions for the duration of the experiments.

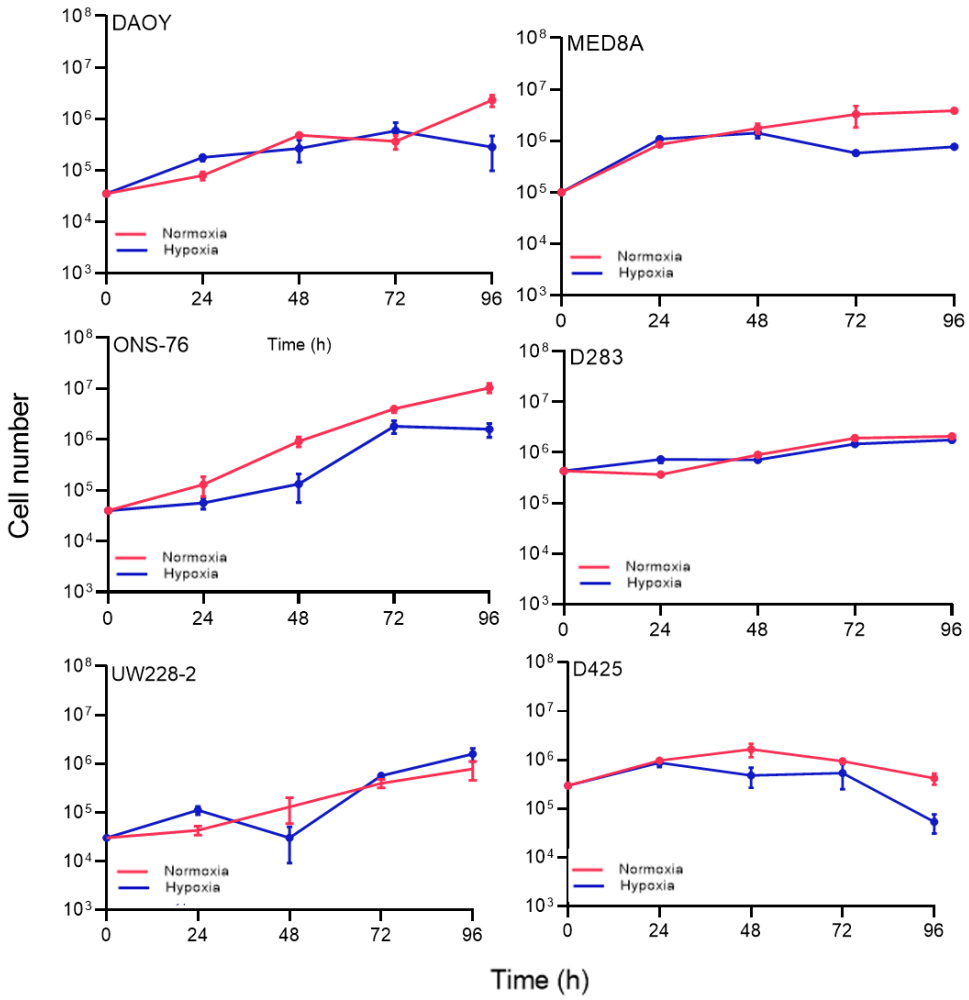

Figure 5: Growth curves for the six medulloblastoma cell lines under normoxic and hypoxic conditions. *Cell lines were seeded in triplicate in 6-well plates in RPMI-1640 with 10% FBS and exposed to normoxic or hypoxic (0.1% oxygen) conditions for the duration of the experiment. Cell counts were made every 24 h for a total of 96 h, counting three wells at each time point. Data points represent the mean ± SEM of three technical repeats.*

Under both normoxic and hypoxic conditions, the four adherent cell lines had an exponential growth phase. A plateau phase was seen for ONS-76 (72-96 h) and MED8A (24-48 h) under hypoxia only. Under hypoxic conditions, the beginning of a death phase was observed for DAOY at 72 h and for MED8A at 48 h. The growth of the semi-adherent cell line D283 was relatively unaffected by oxygen concentration over the course of the experiment, resulting in a similar live cell count at 96 h at 21% and 0.1% oxygen. The semi-adherent cell line D425 showed cell death after 48 h under normoxia; under hypoxia loss of viability was seen after 24 h. For both semi-adherent cell lines the medium is regularly changed in routine culture to allow for their continued growth. Under the conditions of the growth curve experiment, medium changes were not carried out, which may explain the premature death phase of D425 cells. D283 cells have a longer Td so the death phase of the growth curve was not reached during this experiment. The calculated Tds are listed in Table 11. The rapid onset of the death phase for D425 and MED8A under hypoxia meant Tds could not be calculated.

Table 11: The population doubling time for six MBL cell lines

Cell line	Condition	Doubling time (h)
D283*	Normoxia	40
	Hypoxia	46
D425*	Normoxia	NC
	Hypoxia	NC
DAOY^{+}	Normoxia	16
	Hypoxia	18
MED8A*	Normoxia	18
	Hypoxia	NC
ONS-76^{+}	Normoxia	12
	Hypoxia	13
UW228-2^{+}	Normoxia	20
	Hypoxia	17

*NC – not calculable; * indicates cell line belongs to Group 3; + indicates cell line belongs to SHH*

The relative proportions of adherent and suspension cells for the two semi-adherent cell lines were recorded (Figure 6). The percentage of suspension D425 cells was higher when cells were cultured in hypoxia compared to normoxia. For the D283 cell line, the percentage of suspension cells was unchanged by hypoxic conditions. Regardless of oxygen concentration, the relative proportions of suspension to adherent cells within a culture remained constant over time, which was also observed in routine cell culture.

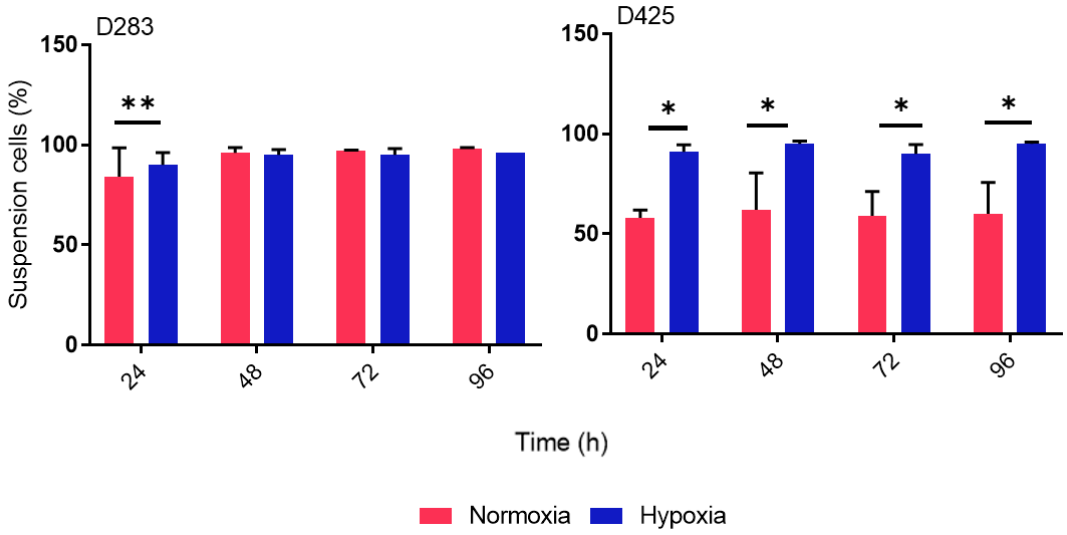

Figure 6: Hypoxia increases the proportion of suspension cells in D425 but not in D283. *Cell lines were seeded in triplicate in 6-well plates in RPMI-1640 with 10% FBS and exposed to normoxic or hypoxic (0.1% oxygen) conditions. The standard cell culture plates were used, as opposed to the suspension cell culture vessels used in continuous cell culture. Cell counts were completed every 24 h for a total of 96 h. For the two semi-adherent cell lines, the percentage of live cells in suspension was monitored. For D283, most cells grew in suspension whether cultured in normoxia or hypoxia. Under normoxic conditions >50% of D425 cells were in suspension, while under hypoxic conditions suspension cells made up >90% of live cells. No time dependence was observed. Data points represent the mean ±SEM of three technical repeats. *p<0.05, **p<0.01 (t-test).*

3.2 Intrinsic radiosensitivity

Intrinsic radiosensitivity was assessed in cell lines using a clonogenic assay and a high-throughput proliferation-based assay, and in patient cohorts using the RSI.

3.2.1 Clonogenic assay – method development

The clonogenic assay (Section 2.4) was optimised to measure radiosensitivity for the four adherent cell lines (DAOY, MED8A, ONS-76, UW228-2). Figure 7 shows representative images of the colonies formed by the four adherent cell lines at three radiation doses and stained with crystal violet before being scanned using the GelCount colony counter.

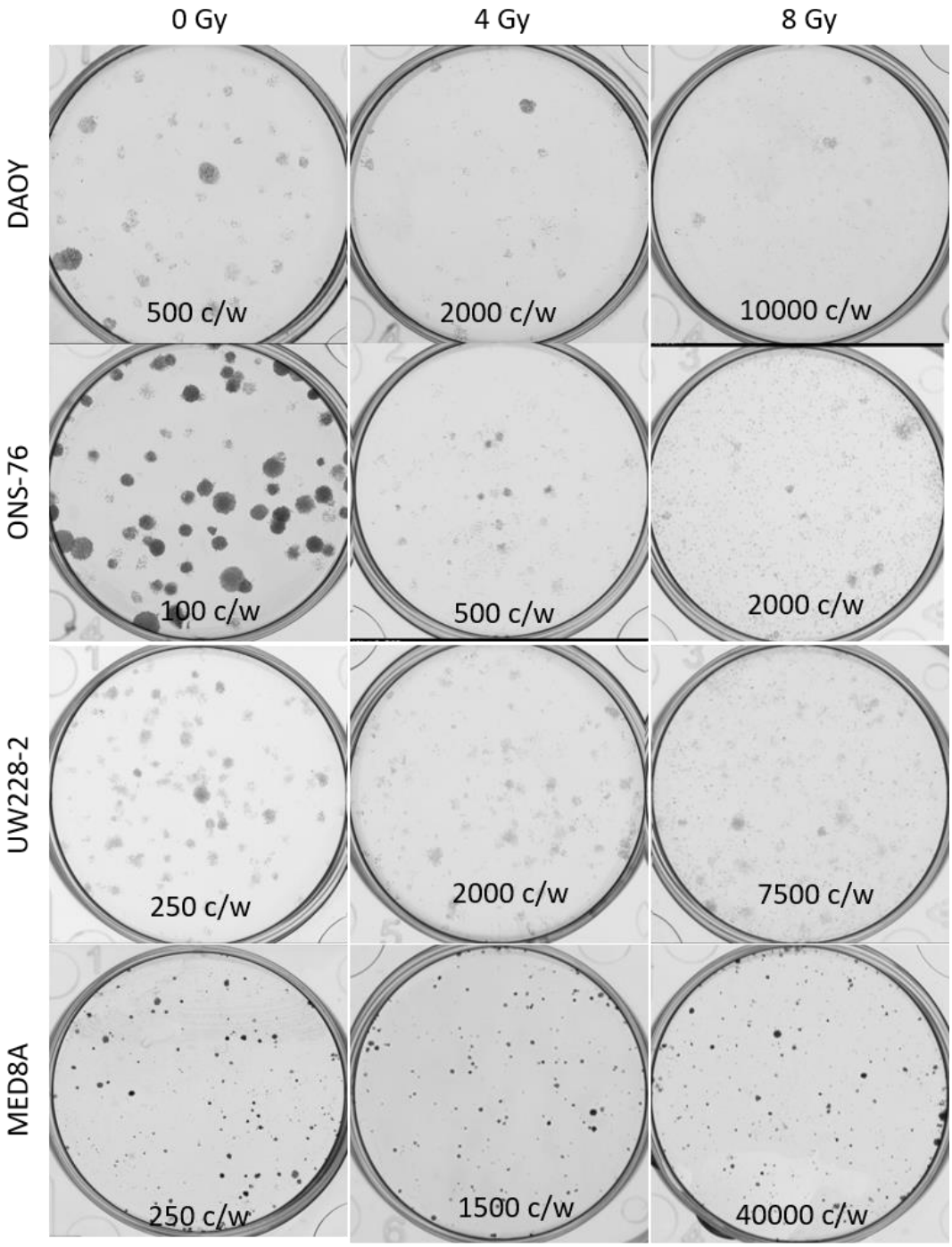

Figure 7: Representative GelCount images of stained colonies for the four adherent cell lines. *Plates containing fixed and stained colonies were scanned using the GelCount colony counter prior to manual counting. Representative images following 0 Gy, 4 Gy or 8 Gy of irradiation under normoxic conditions are shown for each of the four adherent cell lines. Due to the faint nature of the scanned, stained colonies for DAOY and UW228-2 and irradiated ONS-76 plates, the GelCount colony counter software could not accurately count the stained colonies, whereas the distinction between the purple stained colonies and the clear plastic wells was clearly visible for manual counting. c/w = cells per well.*

All four cell lines formed countable colonies across the dose range used, although the characteristics of the colonies varied between cell lines. Under control conditions, the staining of ONS-76 and DAOY colonies produced clearly defined colonies, compared to the more diffuse and faint colonies seen with UW228-2. MED8A colonies tended to form in a three-dimensional manner away from the culture surface, with cells attaching to each other rather than to the cell culture dish. MED8A had darkly stained colonies with a much smaller diameter than seen with the other cell lines. Colony definition decreased with radiation dose for DAOY, ONS-76 and UW228-2, shown by the fainter colonies, due to increased cell spreading following irradiation. The colonies formed by MED8A cells did not change in appearance following irradiation. Each cell line required different initial seeding densities in order to form a countable number of colonies, reflecting the different plating efficiencies and survival characteristics of each cell line. The number of colonies formed increased linearly with seeding density for all four cell lines, although a plateau in colony formation was reached at 700 cells/well for MED8A (Figure 8).

Exceeding the linear range for the cell lines DAOY, ONS-76 and UW228-2 resulted in overcrowding of colonies within a well. Colony overcrowding prevented an accurate colony count, and so data outside of the linear range are not available for these cell lines. The small diameter of the colonies formed by MED8A allowed the linear range of colony formation to be exceeded while the colonies were still countable, which is shown as a plateau at seeding densities over 750 cells/well. The four adherent MBL cell lines routinely showed low plating efficiencies (PEs). Here, the PE for DAOY, ONS-76 and UW228-2 was 15% and for MED8A it was 10%.

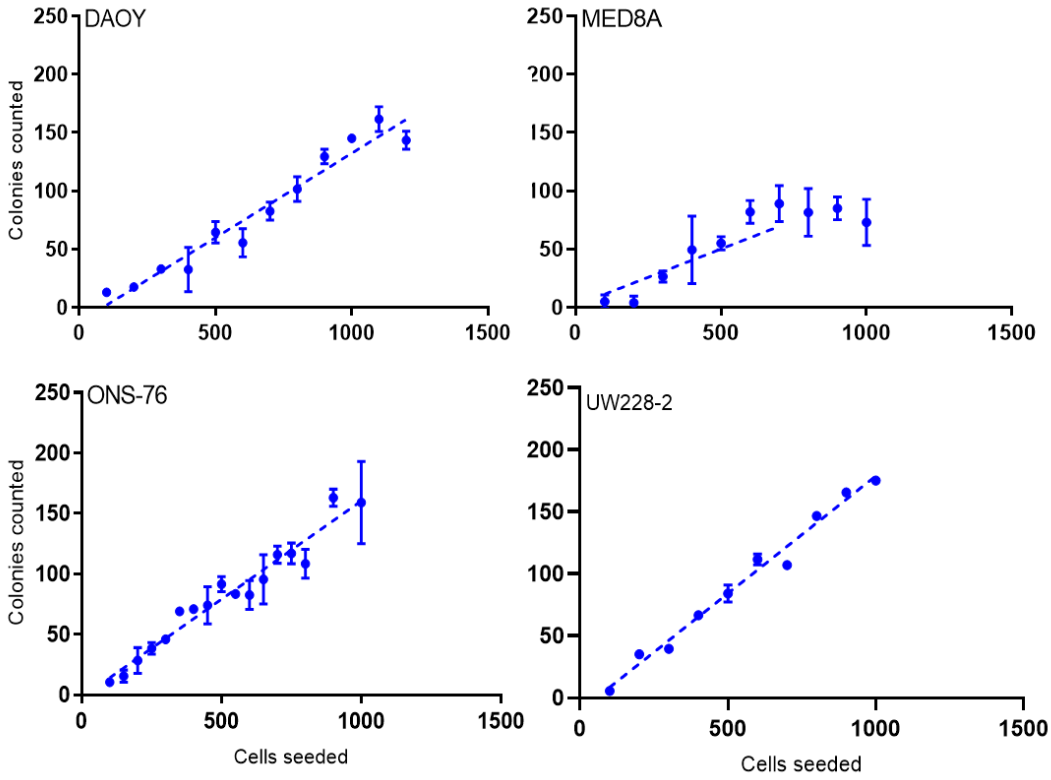

Figure 8: Colony formation increases linearly with cell seeding number for the four adherent cell lines. *Cell lines were seeded in duplicate wells in 6-well plates in RPMI-1640 with 10% FBS, apart from MED8A which used 20% FBS and incubated until colonies containing at least 50 cells formed (up to 11 days). At this point, colonies were fixed and stained with 0.1% crystal violet in 50% methanol, and counted manually. Data points represent the mean ± SEM of two technical repeats from a single experiment. A linear trend line was fitted using GraphPad Prism.*

Colony formation in MED8A cells was improved by using medium containing 20% FBS because lower concentrations of serum reduced the attachment of the MED8A colonies to the culture vessel surface and allowed colonies to be washed off during the staining procedure. To investigate if increased serum concentration affected colony formation, ONS-76 cells were seeded into medium containing either 10% or 20% FBS and incubated until colonies formed. The PE was not affected by the serum concentration of the medium (Figure 9). Clonogenic assays were carried out using the optimal FBS concentration for each cell line.

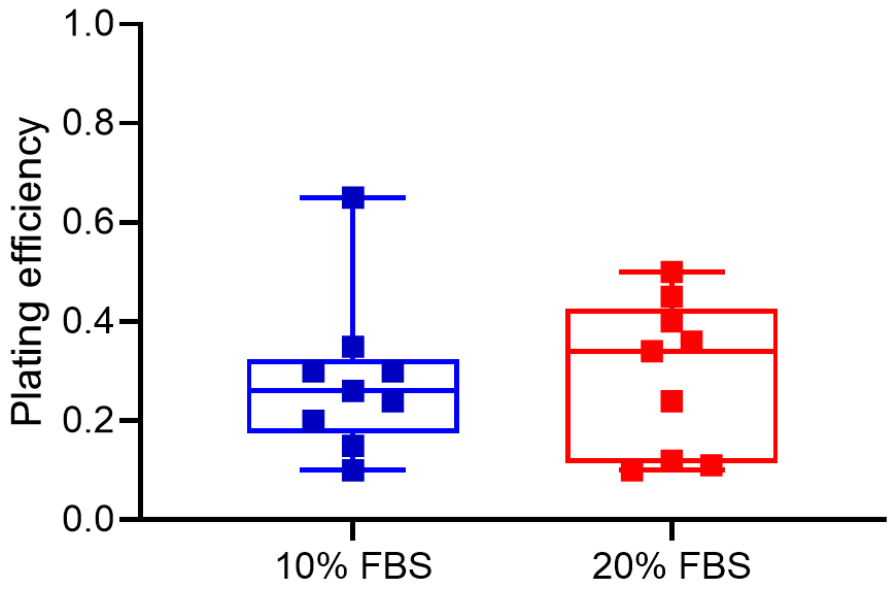

Figure 9: Increasing the medium serum concentration has no effect on plating efficiency. *Unirradiated ONS-76 cells were seeded into 6-well plates in media containing either RPMI-1640 with 20% foetal bovine serum (FBS) or RPMI-1640 with 10% FBS and incubated for 9 days until colonies containing at least 50 cells had formed. Colonies were fixed and stained with 0.1% crystal violet in 50% methanol and counted manually using a Colony Counting pen. Box and Whisker plots show unirradiated cells incubated in medium containing 20% serum did not form significantly more colonies than cells incubated in medium containing 10% serum (p=0.31, t-test). Data points are nine replicates per serum concentration from a single experiment.*

Over the course of the project, three separate laboratories with different irradiator set-ups were used. Figure 10 shows survival curves generated at the three locations (Paterson building, Stopford building and Oglesby Cancer Research Building [OCRB]) for two of the adherent cell lines, ONS-76 and UW228-2. No significant difference between the survival curves was observed, and therefore data from the three locations were pooled for each cell line.

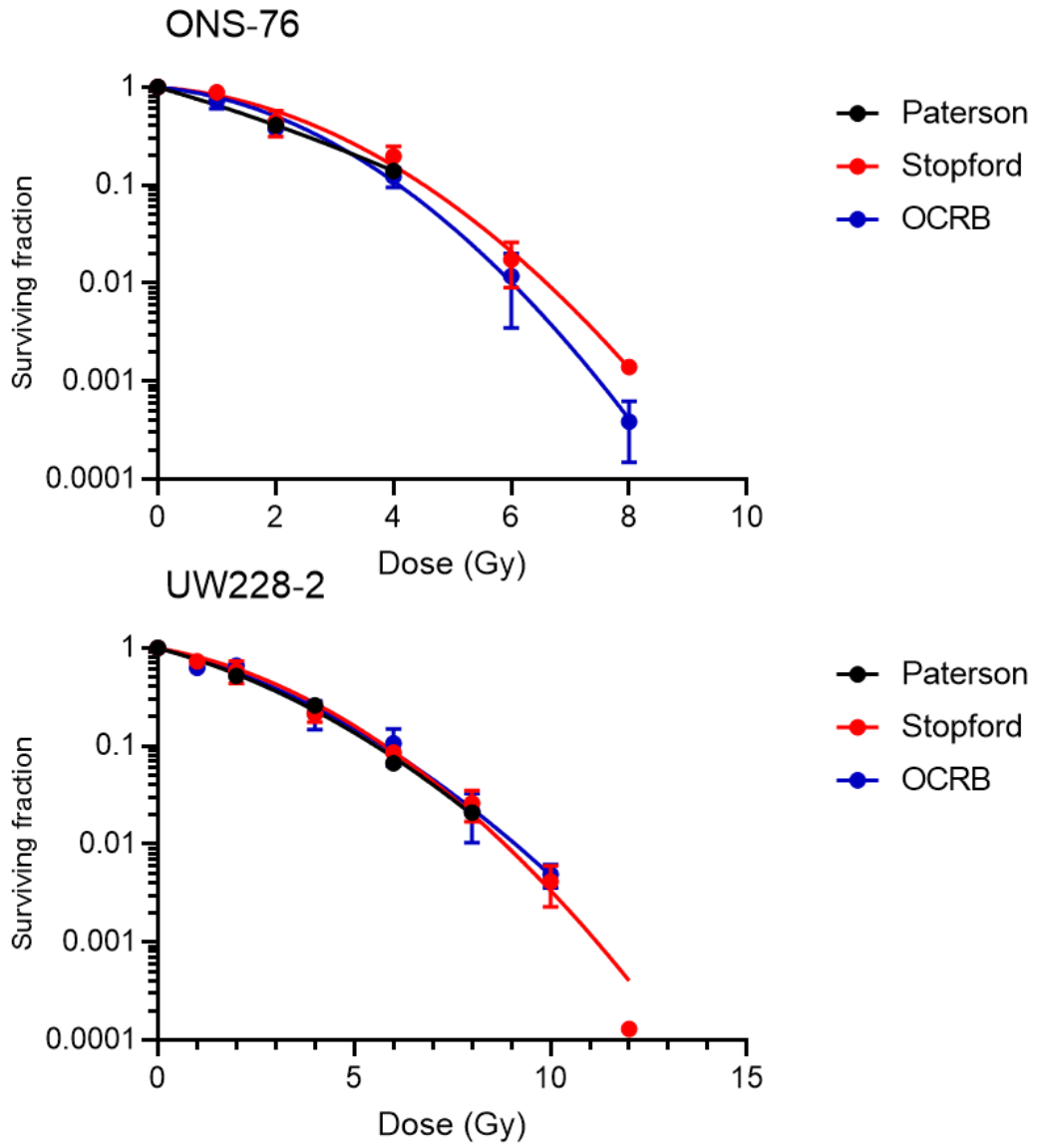

Figure 10: Survival curves generated in three different laboratories for two cell lines are not significantly different. *Clonogenic assays were carried out using three separate irradiator set-ups in the Paterson, Stopford and Oglesby (OCRB) buildings. Survival data at each location were compared, and no significant difference was found between the survival curves generated in each location for ONS-76 (p=0.32, F-test) or UW228-2 (p=0.90, F-test). Data points represent the mean ± SEM survival fraction for ≥2 (Stopford and OCRB) or a single (Paterson) independent experiment/s with ≥2 replicates per dose point in each experiment.*

An automated colony counting set-up was available and was investigated as a high-throughput alternative to manual counting. Figure 11A shows a comparison of the number of colonies counted by the two methods. Each data point represents a single well and the solid lines show the line of concordance. The majority of the data points for all three cell lines lie beneath this line, indicating that the GelCount was routinely over counting the number of colonies present in each well. The over reporting is reflected by the survival curves, where

the manual counts resulted in lower cell survival at higher radiation doses than the GelCount ones. Due to the more diffuse nature of the colonies at higher doses, the algorithm settings required also detected background dirt, dead cells or scratches on the plastic as colonies. The number of these additional colonies remained relatively consistent across doses. However, the low number of colonies formed at higher doses did not exceed background noise levels, causing falsely elevated colony counts and reported radioresistance at these doses. This over counting was a major problem for the fourth cell line MED8A, which produced colonies with a very small diameter. While these stained colonies could be easily differentiated by eye, the GelCount software was unable to correctly isolate colonies from artefacts. It was, therefore, decided to use the manual counting method for all clonogenic assays to ensure a more accurate set of results.

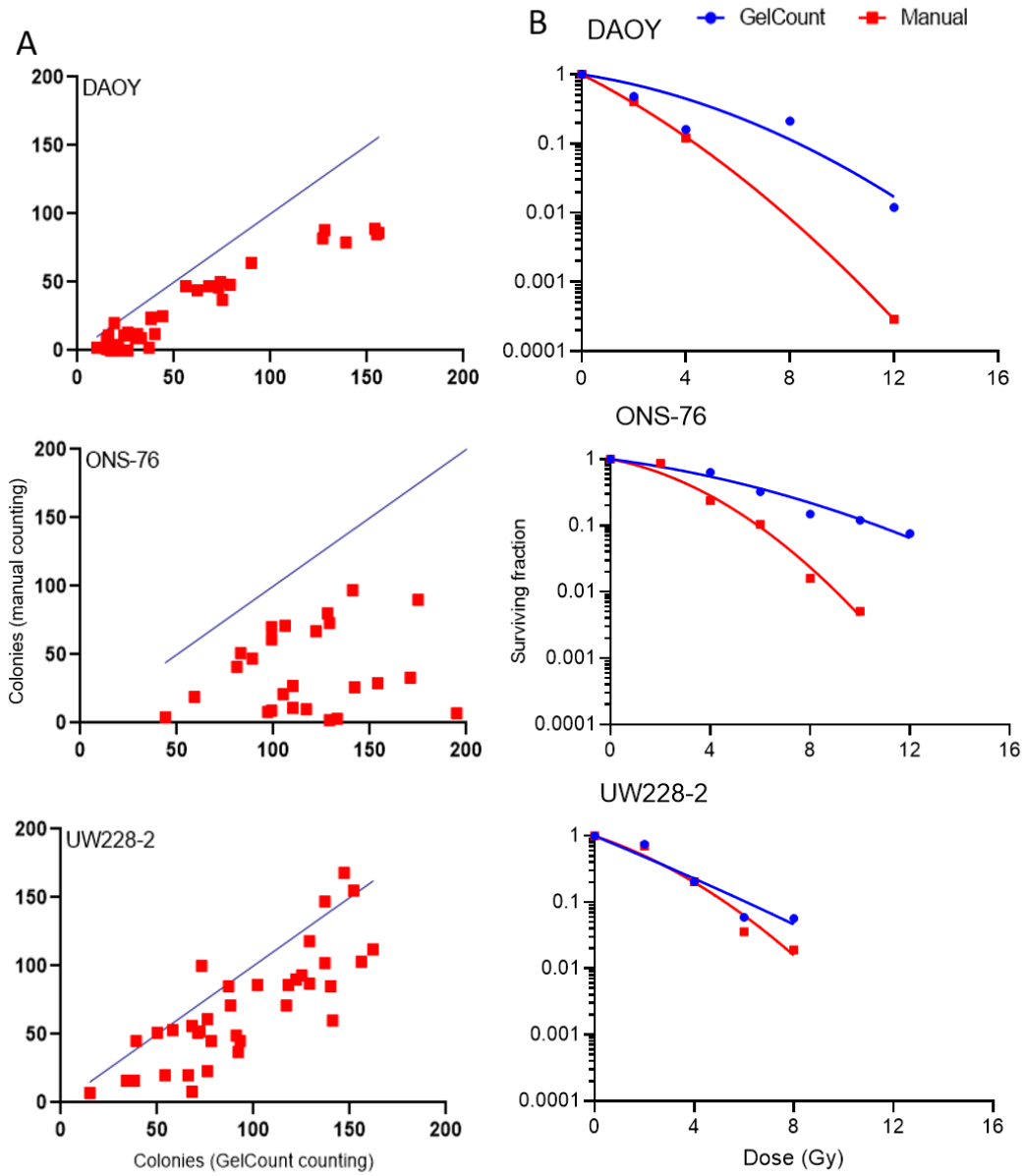

Figure 11: The automated cell counter reported higher colony counts and surviving fractions than manual counting across all three cell lines tested. *Test plates containing fixed and stained colonies were processed using the GelCount colony counter and manual counting. The number of colonies in each well as reported by the GelCount software was plotted against the number counted manually (A). The solid line indicates where the colony counts match for the two methods. For all three cell lines, the automated counting reported higher colony numbers. Data points represent colony counts from each individual well within a biological replicate and include all countable wells regardless of cell seeding density or irradiation dose. The reported colony counts were used to generate surviving fractions and plot survival curves (B). The automated colony counter reported the cell lines to be more radioresistant than when colonies were counted manually but was only significant for ONS-76 and DAOY ($p<0.05$, F-test). Data points represent the surviving fraction calculated from ≥ 2 technical replicate wells per dose within a single experiment.*

3.2.2 Radiosensitivity measured using a clonogenic assay

The results of the clonogenic assays (Section 2.4) following irradiation under normoxia or hypoxia for the four adherent cell lines are shown in Figure 12. Table 12 summarises the radiation survival curve parameters for the four cell lines. All survival curves were fitted using the LQ model. The Group 3 cell line MED8A was the least radiosensitive with the highest SF2 value under normoxia. For all four cell lines, irradiation under hypoxic conditions decreased radiosensitivity, with the OER for all four cell lines between two and three (as expected for x-ray irradiation).

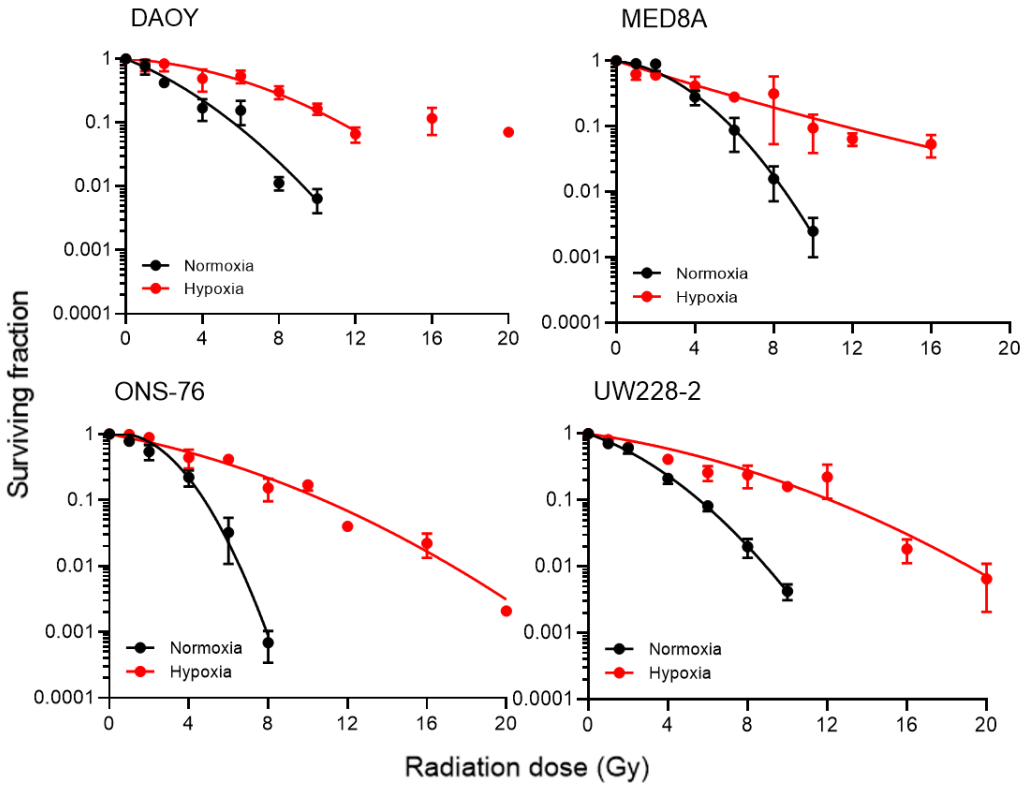

Figure 12: Survival curves for the four adherent cell lines irradiated under normoxic and hypoxic conditions. *Cells were irradiated under normoxic or hypoxic conditions then seeded into 6-well plates in media containing either RPMI-1640 with 20% serum or RPMI-1640 with 10% serum and incubated for up to 11 days until colonies containing at least 50 cells had formed. Colonies were fixed and stained with 0.1% crystal violet in 50% methanol and counted manually using a Colony Counting pen. For all four cell lines, radiosensitivity is significantly decreased following irradiation under hypoxia ($p<0.05$, F-test). Data points represent the mean ± SEM of three biological repeats apart from the 1 Gy and 10 Gy (n=2, MED8A) and 20 Gy (n=1, all cell lines) points. Each biological repeat contained >2 technical replicate wells per dose point.*

Table 12: Summary of radiation survival curve parameters for the four adherent cell lines

	SF2[1]	SF2[2]	α^1 ±SEM (Gy^{-1})	α^2 ±SEM (Gy^{-1})	AUC[1] (Gy)	AUC[2] (Gy)	OER
DAOY+	0.42	0.84	0.280 ±0.084	0.042±0.040	2.58	5.67	2.67
MED8A	0.89	0.61	0.086±0.077	0.220±0.062	3.52	4.56	2.00
ONS-76+	0.54	0.89	0.078*±0.11	0.130±0.029	2.60	5.35	2.20
UW228-2+	0.61	0.63	0.240±0.050	0.100±0.056	2.76	5.11	2.17

SF2 values experimentally derived, OER manually calculated, other parameters calculated using GraphPad PRISM.
1 – Normoxia; 2-Hypoxia; *absolute value of α reported as calculated value based on linear quadratic fit is negative.
+ indicates cell line belongs to SHH subgroup, otherwise Group 3

Figure 13 shows the same survival curves plotted onto single graphs for normoxia and hypoxia to allow comparisons between cell lines. No significant difference was detected between the four adherent cell lines under either normoxia or hypoxia. Of the three SHH cell lines, ONS-76 appears the most radiosensitive under normoxic conditions at radiation doses over 4 Gy. Under hypoxia, this difference in radiosensitivity is not observed. Survival curve analyses were also carried out using the in-house alpha_beta software, to perform 1000 Monte Carlo simulations to produce theoretical datasets with statistical parameters that match those of the experimental dataset. From these theoretical datasets, the alpha values are plotted against the beta values producing ellipses containing 1000 data points (Figure 13B & D). Ellipses that overlap indicate no statistically significant difference between the experimental datasets. Under normoxic conditions, the radiosensitivities of the *TP53* mutant SHH cell lines DAOY and UW228-2 are not significantly different from one another, but do differ from the *TP53* WT SHH cell line ONS-76. The Group 3 cell line MED8A is significantly different from all three SHH cell lines. Under normoxic conditions the separation of the ellipses is mainly due to differences in the β value, seen by greater separation along the y-axis. The β value describes the quadratic component of the curve. At higher dose points of the experimentally defined survival curves (Figure 13A), ONS-76 and MED8A begin to curve away from the DAOY and UW228-2 curves and extrapolation of the curve beyond the maximum experimental dose may reflect the results of the Monte Carlo simulation. Under hypoxic conditions, these differences in radiosensitivity are not observed and all four ellipses overlap.

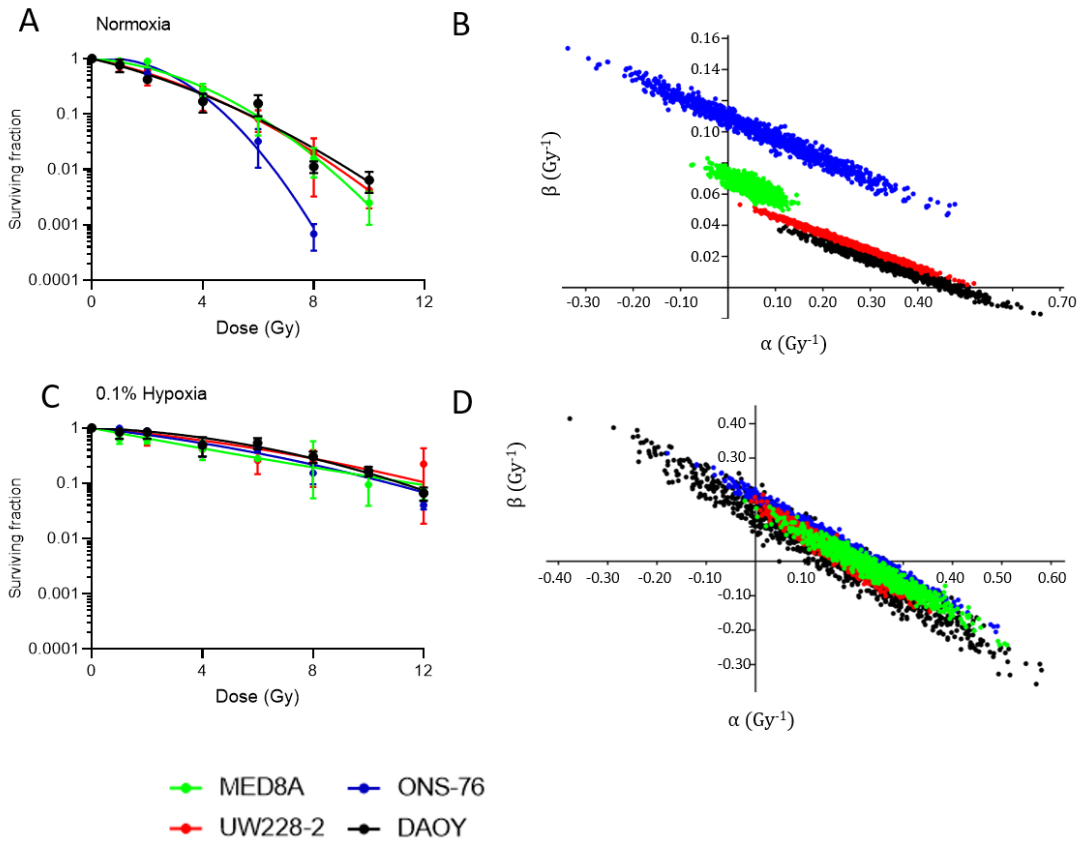

Figure 13: Survival curves and alpha_beta Monte Carlo simulation results for the four adherent cell lines. *Cells were irradiated under normoxic or hypoxic conditions then seeded into 6-well plates in media containing either RPMI-1640 with 20% serum or RPMI-1640 with 10% serum and incubated for up to 11 days until colonies containing at least 50 cells had formed. Colonies were fixed and stained with 0.1% crystal violet in 50% methanol and counted manually using a Colony Counting pen. Figures A and C show survival curves for the four cell lines following irradiation under normoxia or 0.1% hypoxia respectively. Data points represent the mean ± SEM of ≥ 3 biological repeats apart from at 1 Gy and 10 Gy (n=2, MED8A) and 20 Gy (n=1, all cell lines). There was no significant difference between the cell lines in normoxia (p=0.40, F-test) or hypoxia (p=0.14, F-test). The Monte Carlo simulation carried out by alpha_beta analysis results are shown for normoxia (B) and hypoxia (D). Alpha_beta analysis calculated theoretical datasets fitting the statistical characteristics of the experimental datasets. Each α was plotted against β for a simulation, and 1000 simulations were carried out for each dataset. The ellipses produced indicate statistical significance (p<0.05) when they do not overlap.*

3.2.3 Radiosensitivity measured using a high-throughput assay

The luminescent response to CTG reagent increases linearly with seeding density until a saturation point is reached (Figure 14). The saturation point varies between the cell lines. As the high-throughput assay requires an 11-day incubation period between seeding and analysis, the number of cells in a well on the day of analysis will not be known. Therefore, the relative luminescence unit (RLU) value at which saturation begins to occur for each cell

line was used as an upper limit during analysis (Table 13). Any individual wells that reported RLU values above these upper limits were excluded from analysis.

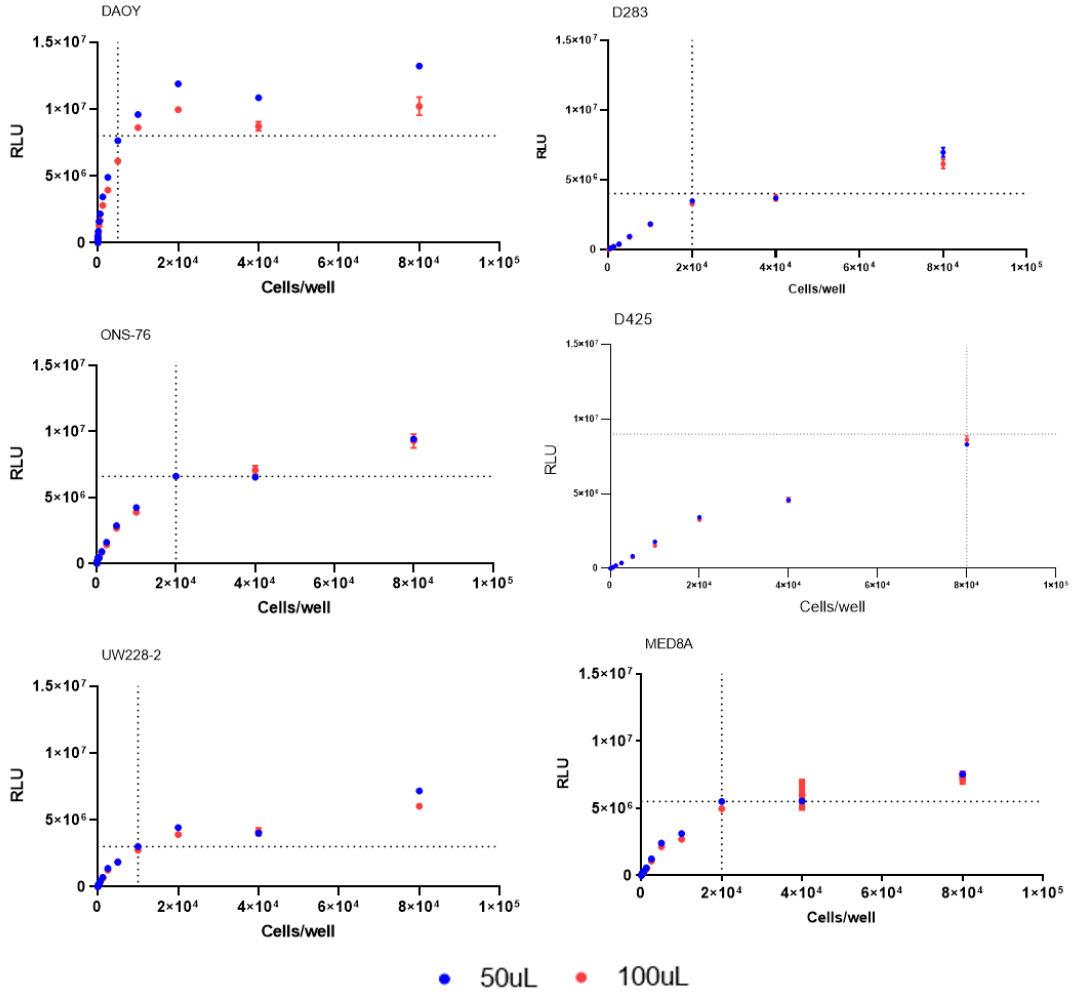

Figure 14: Response to CellTiter-Glo reagent increases linearly with cell seeding density. *Cells were seeded in increasing cell densities in duplicate 96-well plates one day prior to the addition of the CellTiter-Glo reagent. One plate was treated with 50 µL of CellTiter-Glo reagent, while the other was treated with 100 µL of CellTiter-Glo reagent. RLUs were background-subtracted, and plotted against cell seeding density. Reducing the CellTiter-Glo reagent volume by 50% had no effect on the reported values for any of the six cell lines. For all six cell lines, RLU output increases linearly with seeding density for a range of cell seeding densities, before plateauing. The upper limit for each cell line is shown by the dotted lines. Data points represent the mean ± SEM of three technical replicate wells. RLU = Relative luminescence unit.*

Table 13: Upper limits of detection for luminescence in the CellTiter-Glo assay

Cell line	Upper limit of detection (RLU)
D283*	$4.0x10^6$
D425*	$8.3x10^6$
DAOY+	$8.0x10^6$
MED8A*	$5.5x10^6$
ONS-76+	$6.6x10^6$
UW228-2+	$3.0x10^6$

** indicates cell line belongs to Group 3, + indicates cell line belongs to SHH subgroup*

The survival curves for the remaining three adherent cell lines were compared between the clonogenic and high-throughput assay to confirm that the proliferation-based approach was able to replicate the clonogenic assay results in MBL cell lines (Figure 15).

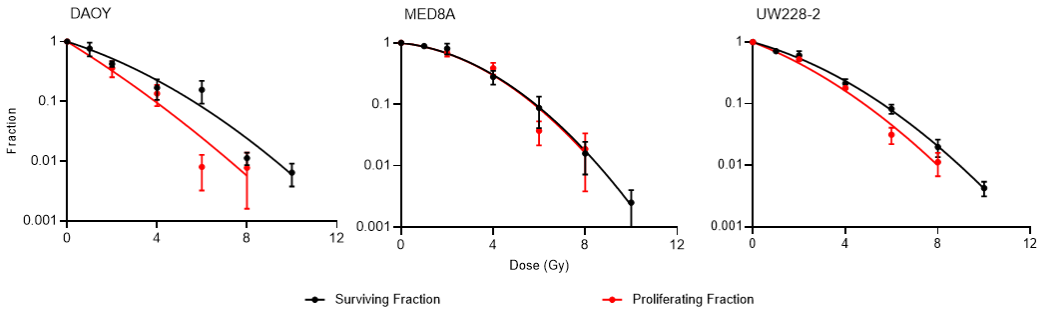

Figure 15: Radiation survival curves generated using the high-throughput assay recreate the clonogenic survival curves. *Cells were irradiated under normoxic conditions in 96-well plates. The 96-well plates were incubated for 9 days then 50 µL CellTiter-Glo reagent was added. For clonogenic assays, the surviving fraction at each dose is plotted. For the high-throughput assay, the proliferating fraction at each dose is plotted. An F-test confirmed survival curves were not significantly different for DAOY (p=0.20, F-test), MED8A (p=0.57, F-test) and UW228-2 (p=0.55, F-test). Proliferating fraction data points represent the mean ± SEM of three biological repeats. Each biological replicate contained four technical replicates at each dose point. Surviving fraction data points represent the mean ± SEM of three biological repeats apart from 1 Gy and 10 Gy for MED8A where n=2. Each biological repeat contained ≥ 2 technical replicate wells per dose point.*

For all three cell lines, the survival curves produced by the high-throughput assay were not significantly different from those generated by the clonogenic assay (F-test, $p>0.05$). The high-throughput assay was better able to replicate the clonogenic results at lower radiation doses (<4 Gy). Attempts to generate PFs at doses greater than 8 Gy were unsuccessful. As the PF is generated as the fraction of luminescence at the dose compared to the control (0 Gy), and the seeding density must be consistent between doses, a seeding density that produced a response for the higher doses while also producing a response within the linear range at 0 Gy was not possible.

As the high-throughput assay was found to adequately measure radiosensitivity for the adherent cell lines, the radiosensitivity of the two semi-adherent cell lines was investigated (Figure 16). Although no clonogenic assay results were available for comparison, data

generated for these cell lines can be fitted with the LQ equation. Doses greater than 6 Gy (D283) and 8 Gy (D425) were not achievable with the current experimental parameters.

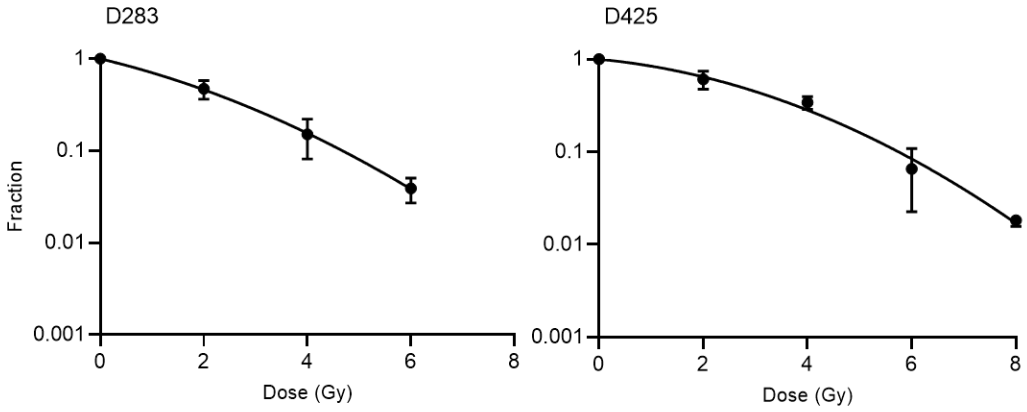

Figure 16: Radiation survival curves generated using the CellTiter-Glo assay for the semi-adherent cell lines D283 and D425. *Cells were irradiated under normoxic conditions in 96-well plates. The 96-well plates were incubated for 9 days then 50 µL CellTiter-Glo reagent was added. Proliferating fraction was calculated as the proportion of luminescence at each dose compared to the control (0Gy) plate. Data points represent the mean ± SEM of three biological repeats. Each biological replicate contained four technical replicates for each dose point.*

The radiation survival curves for all five cell lines produced by the high-throughput proliferation-based assay are shown in Figure 17. These radiation survival results suggest that the SHH subgroup is more radiosensitive than the Group 3 subgroup. The two SHH cell lines (DAOY and UW228-2) did not significantly differ in terms of radiation survival (F-test, $p>0.05$). Two of the Group 3 cell lines (MED8A and D425) did not significantly differ in terms of radiation survival (F-test, $p>0.05$). The third Group 3 cell line, D283, showed more similarity to the SHH cell lines than the other Group 3 cell lines. D283 has also been classified as Group 3/4.

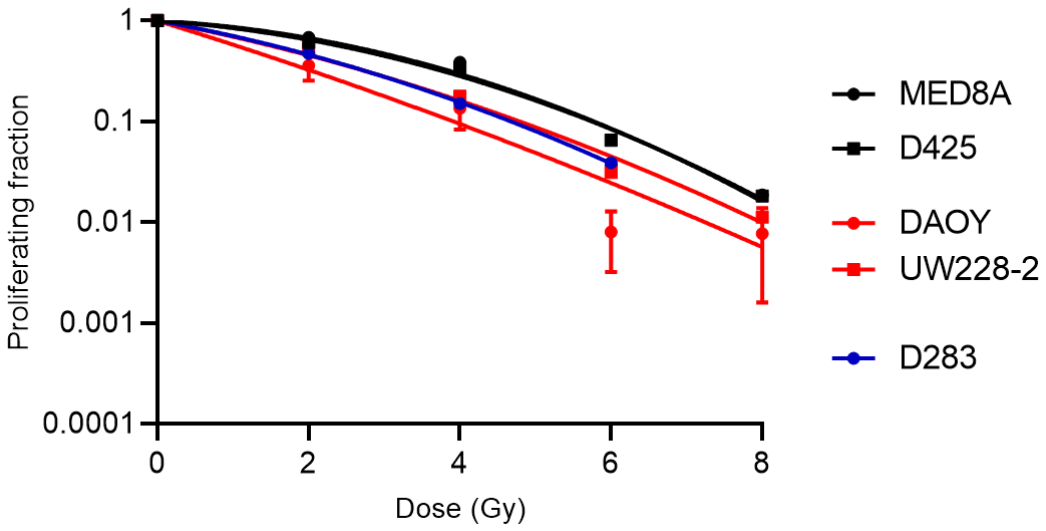

Figure 17: Survival curves under normoxic conditions determined using the CellTiter-Glo assay. *Cells were irradiated in 96-well plates and incubated for 9 days. 50 µL of CellTiter-Glo reagent was added, then plates were mixed on an orbital shaker for 2 min and incubated at room temperature for 10 min. Luminescence was read using a VarioScan Lux Plate Reader. There was no significant difference between the curves within each of the subgroups ($p>0.05$, F-test). The SHH cell lines (red) were more radiosensitive than the Group 3 cell lines MED8A and D425 (black) ($p<0.0001$, F-test on pooled datasets). The cell line D283 is more similar to the SHH cell lines in terms of radiosensitivity, despite being classified as a Group 3/4 cell line. Data points represent the mean ±SEM of three biological repeats. Each biological replicate contained four technical replicates for each dose point.*

Table 14 lists the parameters of the radiation survival curves calculated by GraphPad Prism. The SF2 and PF2 values are generated by the clonogenic and proliferation-based assays respectively. For D283 and D425, only data from the proliferation-based assay is available; for ONS-76, only clonogenic data were available.

Table 14: Parameters for the radiation survival curves

Cell Line	SF2	AUC (Clonogenic) (Gy)	PF2	AUC (CellTiter-Glo) (Gy)
D283*	-	-	0.47	2.284
D425*	-	-	0.61	3.051
DAOY+	0.42	2.581	0.36	2.013
MED8A*	0.89	3.378	0.69	3.241
ONS-76+	0.54	2.534	-	-
UW228-2+	0.61	2.760	0.53	2.483

*SF2/PF2 experimentally derived, AUC calculated using GraphPad PRISM. * indicates cell line belongs to Group 3, + indicates cell line belongs to SHH subgroup*

As no significant difference was shown between the two methods for the three adherent cell lines, a combination of the two methods was used to generate radiosensitivity rankings. A

commonly reported output of the clonogenic assay is the SF2 which was used to rank the cell lines in terms of radiosensitivity (Figure 18A). The most resistant cell line was MED8A, followed by D425, both Group 3 cell lines. The most radiosensitive cell lines were D283 (Group 3/4) and DAOY (SHH, *TP53* mutant). The output parameter of the high-throughput proliferation-based assay is the AUC. The resulting radiosensitivity rankings using the AUC are shown in Figure 18B.

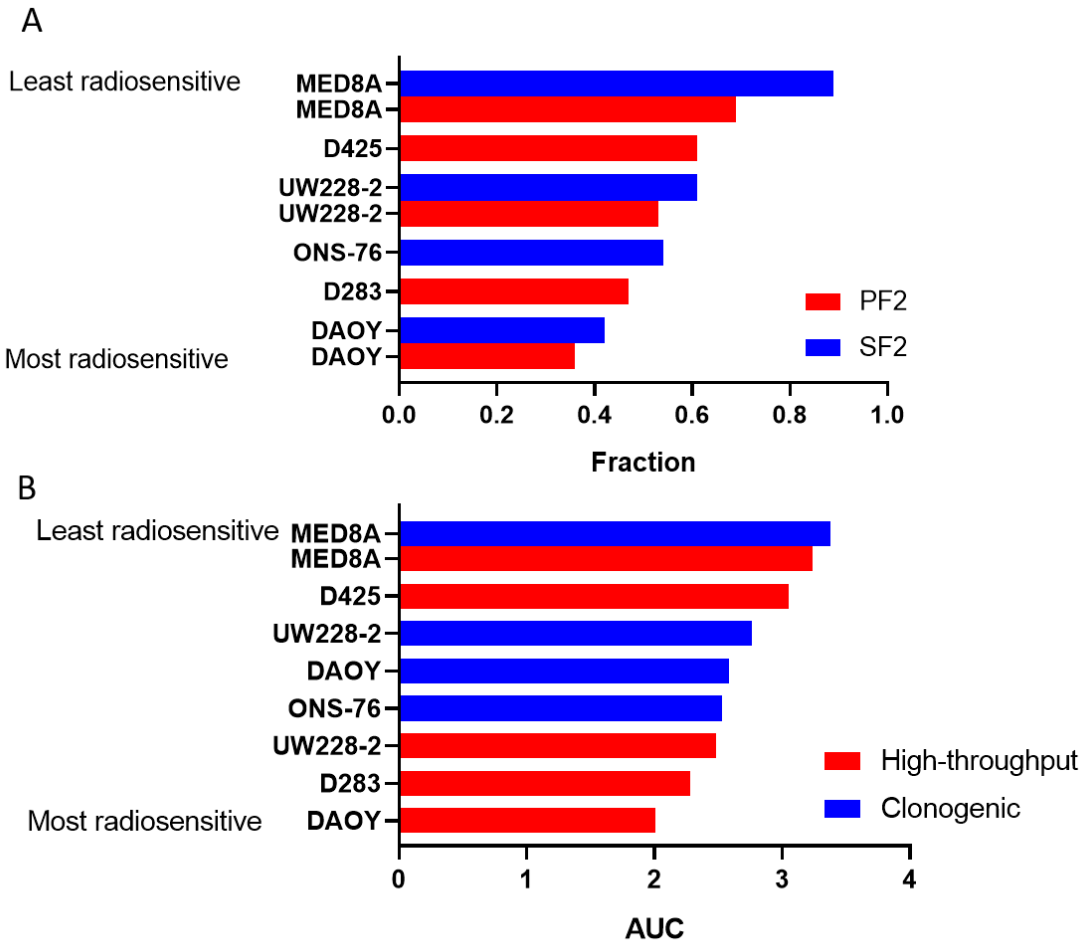

Figure 18: MED8A is the least radiosensitive cell line according to both radiosensitivity assays and rankings. *Cell lines were ranked based on the surviving/proliferating fraction (A) or the area under the curve (AUC; B). For cell lines where both the clonogenic and high-throughput assay had been used, ranking by fraction placed both assay results together. When the AUC parameter was used, the clonogenic assay results rankings were higher than the high-throughput assay. For both assays, regardless of the parameter used, MED8A was the least radiosensitive cell line. SF2 – surviving fraction at 2 Gy; PF2 – proliferating fraction at 2 Gy.*

Unlike SF2, the AUC rankings separate two of the three cell lines with replicate data (UW228-2 and DAOY). With AUC, the most resistant cell line was MED8A, followed by the Group 3 cell line D425. The most radiosensitive cell lines were D283 (Group 3/4) and DAOY (SHH, *TP53* mutant), as measured by the high-throughput assay.

Results from a single biological replicate using proton irradiation were generated for two of the cell lines, representing the SHH (DAOY) and Group 3 (MED8A) subgroups (Figure 19). . The RBE at 50%, 10% and 1% cell survival for DAOY was calculated 1.01, 1.08 and 1.16 respectively. The RBE at 50%, 10% and 1% cell survival for MED8A was 1.11, 1.34 and 1.36 respectively. At higher radiation doses, protons produced a higher cell kill than x-ray irradiation in both cell lines.

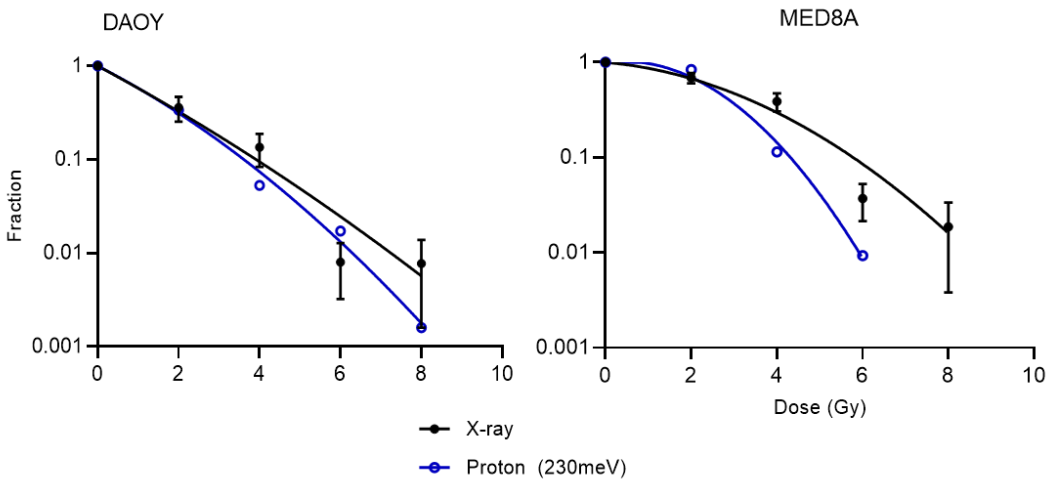

Figure 19: Radiation survival curves using the proliferating fraction for DAOY and MED8A generated using either x-ray or proton irradiation. *Cells were irradiated under normoxic conditions in 96-well plates and incubated for 9 days. 50 µL of CellTiterGlo reagent was added. X-ray irradiation was carried out using an Xstrahl CIX3 irradiator. Proton irradiation was carried out using a Varian cyclotron. Proton (230meV) irradiation increased cell killing compared to x-rays, although not significantly. X-ray data points represent the mean ± SEM of three biological repeats. Each biological replicate contained four technical replicates for each dose point. Proton data points represent a single biological repeat with four technical replicates for each dose point. The average of the four technical replicates was used to calculate the proliferating fraction at each dose.*

3.2.4 Radiosensitivity measured using the radiosensitivity index

To assess the radiosensitivity of clinical samples, the RSI was applied to five patient cohorts (Table 7 and Table 8, Section 2.6.2). Most publications using the RSI signature dichotomise

into radioresistant or radiosensitive tumours using a single cut-off value of 0.3745[199–201,203–206]. In the five patient cohorts used in the current study, only two samples had RSI values less than 0.3745 (GSE37418, samples SJMB089 and SJMB001), classifying most tumours as radioresistant. An alternative cut-off point in the literature is the 25th percentile[171,172,202,207]; with the bottom quartile deemed to have low RSI scores and to be radiosensitive. When applied to GSE85217, patients with low RSI scores had a reduced risk of death compared to those with high RSI scores (Hazard ratio [HR] = 0.67, 95% CI = 0.45-1, p=0.048, Figure 20). Survival outcome data were not available for the other four patient cohorts. This analysis confirmed the relevance of using RSI to measure the radiosensitivity of MBL.

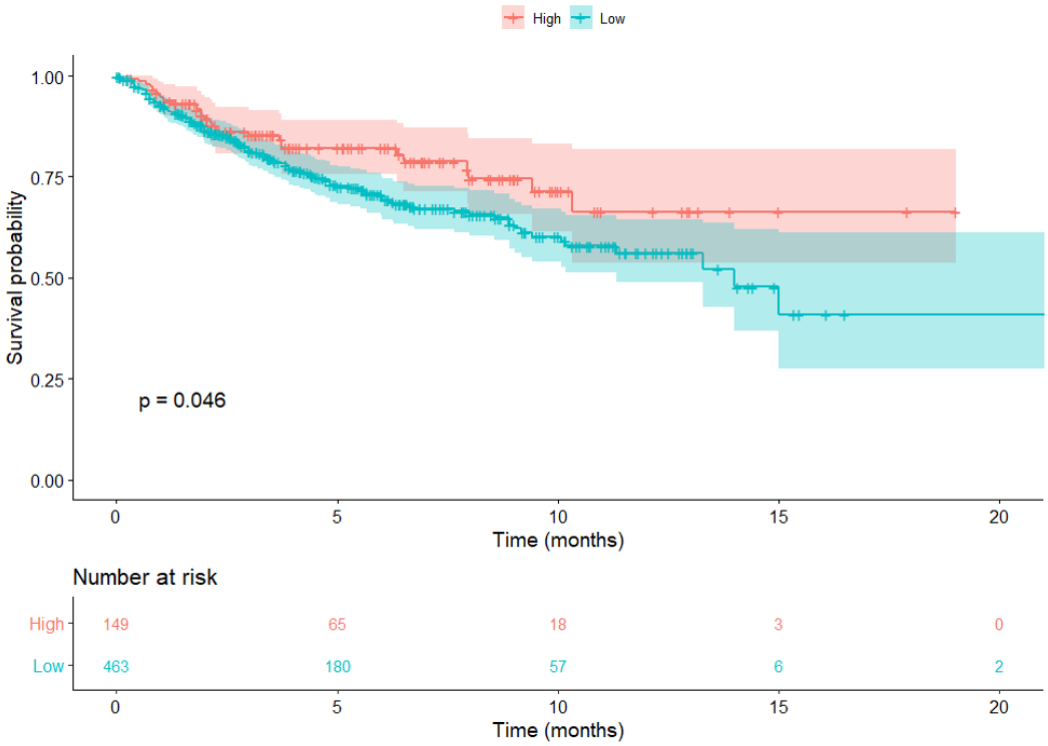

Figure 20: Medulloblastoma patients with radiosensitive tumours have better overall survival. *The 25th percentile RSI score within the cohort was used to dichotomise patients into low and high tumour radiosensitivity groups. Patients with low RSI scores had a significantly decreased risk of death compared to patients with high RSI values (HR 0.67, 95% CI 0.45-1, p=0.048).*

The five patient cohorts used different methods to assign samples to the four molecular subgroups of MBL. The R package 'MM2S' was applied across all cohorts to re-assign samples to the molecular subgroups (Section 2.6.3. The classifications from the cohort data and MM2S are shown in Figure 21. For 92% of samples the subgroup assignment by MM2S

matched the cohort classification. Over half of the samples that changed subgroup using the MM2S package moved from Group 3 to Group 4 or *vice versa*.

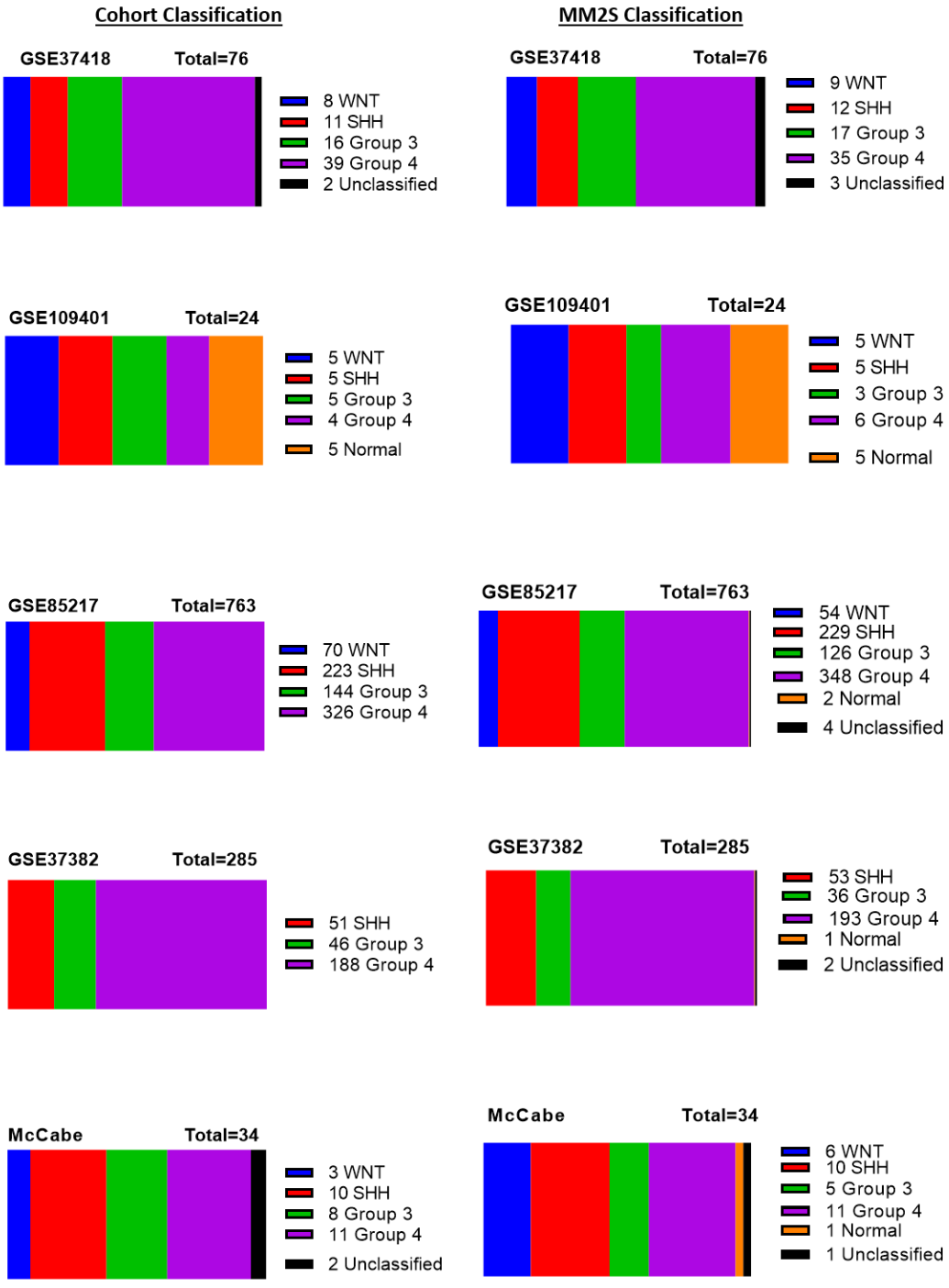

Figure 21: The distribution of samples across the molecular subgroups using the provided and re-classified groupings. *Subgroup classification data were provided with the patient cohorts (Cohort Classification) and generated using the Medullo-Model to Subtypes (MM2S) R package (MM2S Classification). For the majority of samples (92%) the subgroup assignment provided was confirmed by re-analysis. Both subgroup assignments for each sample were used in the remaining analyses, but did not affect the results.*

Both the provided (cohort) and MM2S classifications were used to investigate the percentage of radiosensitive tumours using the 25th percentile for each cohort (Table 15 and Table 16 respectively). The cut-off points varied from 0.4903 to 0.6824 across the five cohorts. The highest cut-off point was found in the cohort with no WNT representation (GSE37382). The lowest was in GSE37418, which was consistent with the lower gene expression scores reported across this cohort. It is not possible to determine whether the cut-off point was consistent within each microarray platform with the limited number of cohorts used. Across all cohorts the SHH subgroup contained the highest percentage of low RSI tumours (Table 15), i.e. the group was the most radiosensitive. Group 4 samples consistently had the highest proportion of high RSI tumours, followed by Group 3. Although WNT subgroup tumours had a higher representation of high scoring tumours overall indicating radioresistance, in GSE37418 most of the subgroup were classed radiosensitive.

Table 15: Percentage of medulloblastoma classified as radioresistant* within each of the molecular subgroups (cohort classification) in the five patient cohorts

Cohort	Microarray	N	25th Percentile	WNT	SHH	Group 3	Group 4
GSE85217	1.1 ST[1]	763	0.6535	51	46	77	97
GSE37382	1.1 ST[1]	285	0.6824	N/A	37	50	91
GSE37418	U133[2]	76	0.4903	38	30	93	87
GSE109401	2.0 ST[3]	19	0.6361	100	50	80	100
McCabe	U133[2]	32	0.6714	67	50	88	100
All Cohorts	N/A	1175	N/A	59	44	73	95

**Samples with RSI scores above the 25th quartile cut point within each cohort were classed as radioresistant.*
[1]Affymetrix Human Gene 1.1 ST Array; [2]Affymetrix Human Genome U133 Plus 2.0 Array; [3]Affymetrix Human Gene 2.0 ST Array

Table 16: Percentage of medulloblastoma classified as radioresistant* within each of the molecular subgroups (MM2S classification) in the five patient cohorts

Cohort	Microarray	N	25th Percentile	WNT	SHH	Group 3	Group 4
GSE85217	1.1 ST[1]	763	0.6535	59	47	79	95
GSE37382	1.1 ST[1]	285	0.6824	N/A	36	35	94
GSE37418	U133[2]	76	0.4903	44	42	94	86
GSE109401	2.0 ST[3]	19	0.6361	100	60	100	100
McCabe	U133[2]	32	0.6714	50	50	100	100
All Cohorts	N/A	1175	N/A	59	46	71	95

**Samples with RSI scores above the 25th quartile cut point within each cohort were classed as radioresistant. [1]Affymetrix Human Gene 1.1 ST Array; [2]Affymetrix Human Genome U133 Plus 2.0 Array; [3]Affymetrix Human Gene 2.0 ST Array*

The different molecular subgroups also had significantly different RSI scores, with both the cohort and MM2S subgrouping classifications (Figure 22 and Figure 23). In all cohorts, the SHH subgroup was significantly more radiosensitive than Group 4 tumours. The SHH subgroup was also significantly more radiosensitive than Group 3 tumours in all cohorts except GSE37382. In the four cohorts containing the WNT subgroup, these were significantly more radiosensitive than Group 4. In the larger two cohorts, GSE37418 and GSE85217, WNT tumours were significantly more radiosensitive than Group 3 tumours. Only the two largest cohorts found significantly reduced radiosensitivity in Group 3 tumours compared to Group 4. Overall, these results indicate the WNT and SHH subgroups were more radiosensitive than the Group 3 and 4 subgroups, with SHH tumours being most sensitive and Group 4 most resistant.

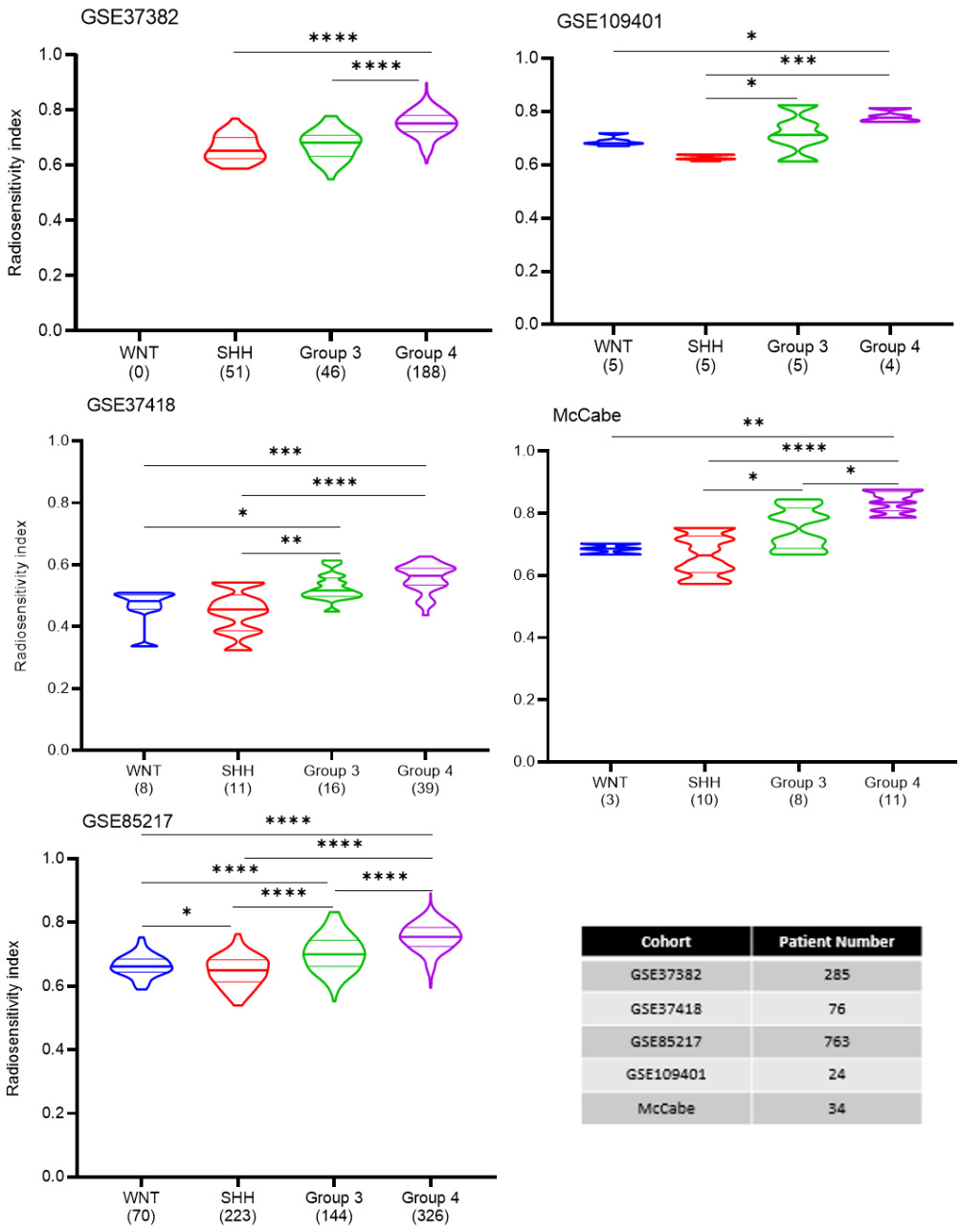

Cohort	Patient Number
GSE37382	285
GSE37418	76
GSE85217	763
GSE109401	24
McCabe	34

Figure 22: Radiosensitivity differs between molecular subgroups (cohort classification) of medulloblastoma. *Violin plots shown the distribution of radiosensitivity scores for the four subgroups within the five patient cohorts, along with the total sample number for each cohort. The subgroup assignment was taken from the cohort data. The central line of the violin plot indicates the median. The most radiosensitive subgroup in all cohorts is the SHH group, followed by WNT (where represented). The least radiosensitive subgroup was Group 4. * p<0.05, ** p<0.01, *** P<0.001, **** p<0.0001, One-Way ANOVA.*

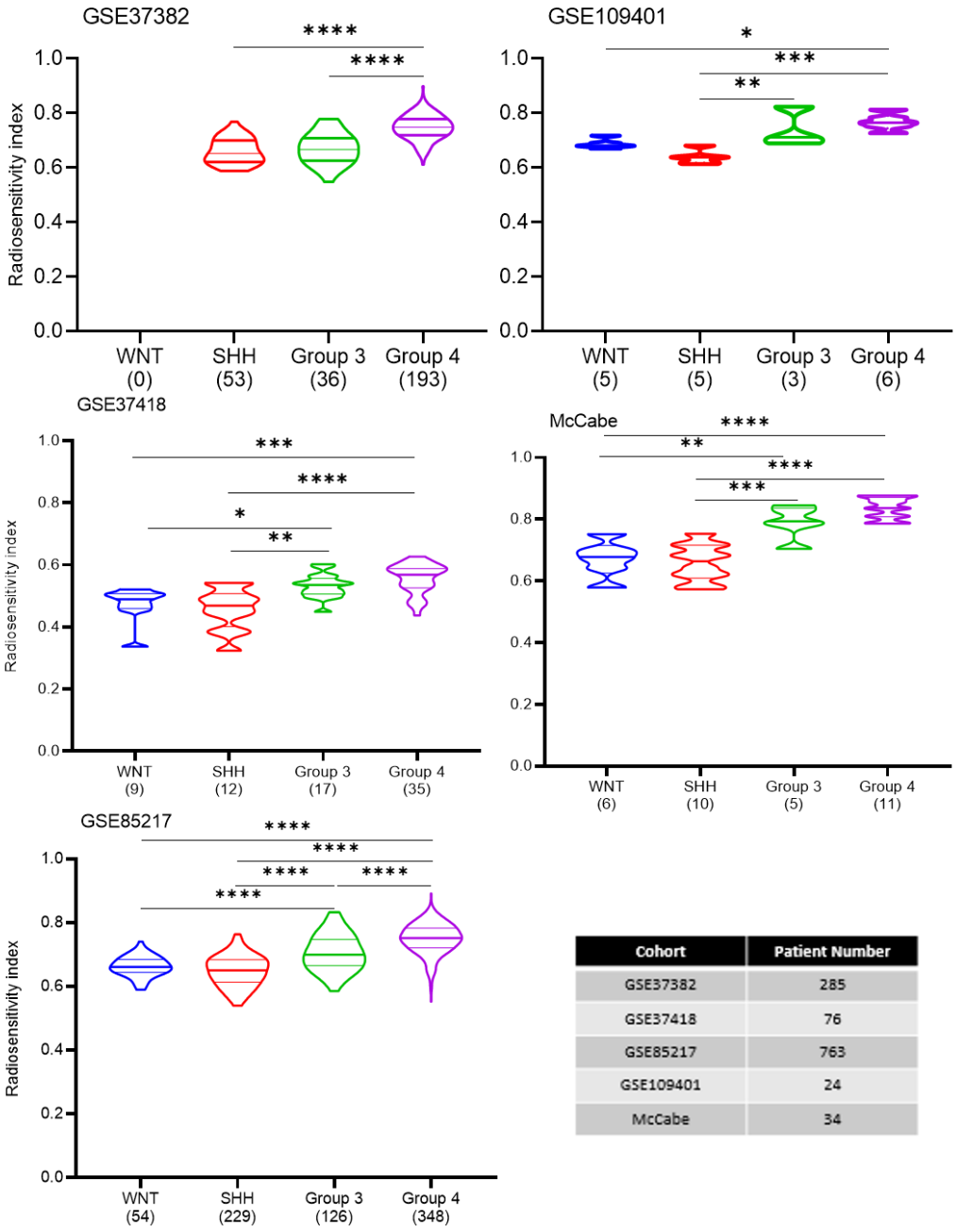

Cohort	Patient Number
GSE37382	285
GSE37418	76
GSE85217	763
GSE109401	24
McCabe	34

Figure 23: Radiosensitivity differs between molecular subgroups (MM2S classification) of medulloblastoma. *Violin plots show the distribution of radiosensitivity scores for the four subgroups as assigned by the MM2S classification method. The central line of the violin plot indicates the median. The most radiosensitive subgroup in all cohorts is the SHH group, followed by WNT. The least radiosensitive subgroup was Group 4. * p<0.05, ** p<0.01, *** P<0.001, **** p<0.0001, One-Way ANOVA.*

For cohorts where the data were available, other patient characteristics were investigated in relation to the RSI scores. Higher scores were observed in patients who were male (Figure 24), younger (3-16 years; Figure 25) and had classic histology tumours (Figure 26). The molecular subgroup proportions of the whole cohort were not reflected in these analyses, particularly in comparisons where statistical significance was detected. Specifically, in GSE37382, the infant and adult groups as well as the group of LCA tumours showed underrepresentation of Group 4 but an overrepresentation of SHH tumours compared to the cohort as a whole. Cohort GSE37418 had an overrepresentation of WNT tumours and underrepresentation of Group 3 tumours in the female patient population. Five of the six desmoplastic tumours within GSE37418 fell into the SHH subgroup, and half of the LCA tumours were classified as Group 3. In GSE85217, the infant and adult age groups were enriched for SHH tumours. Desmoplastic and MBEN tumours within GSE85217 mostly belong to the SHH subgroup, while the LCA tumours contained a high proportion of Group 3 tumours. In cohort GSE109401, three quarters of the female population were classified as SHH subgroup, while almost half of the male population were classified as Group 3 tumours.

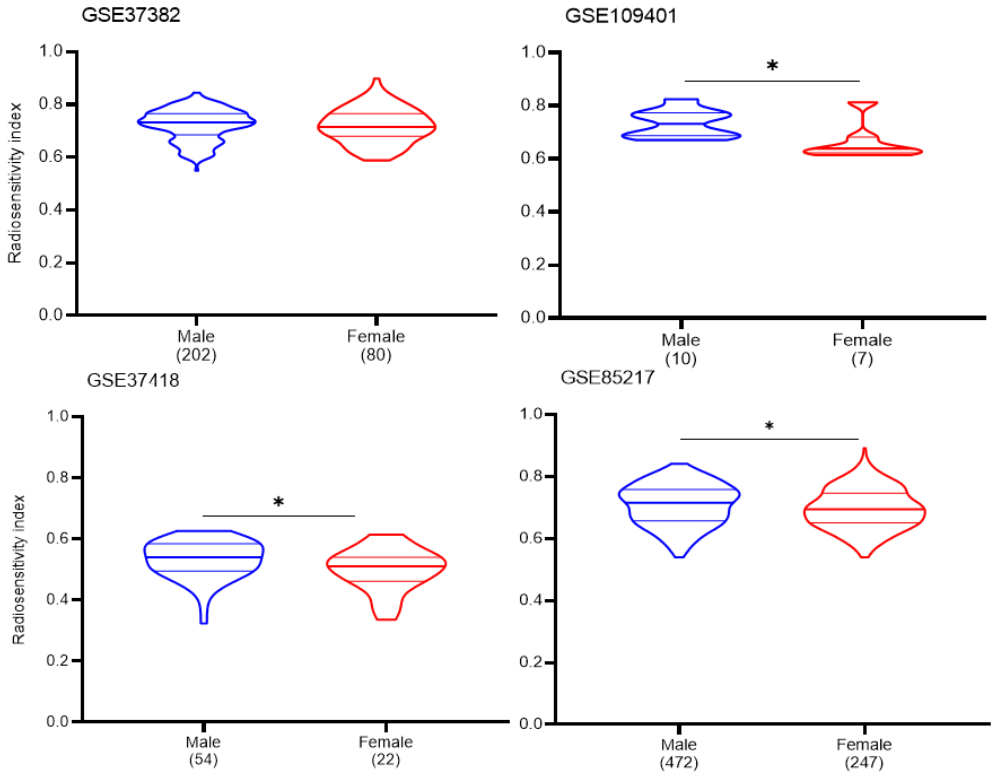

Figure 24: Medulloblastoma is more radiosensitive in female versus male patients. *Violin plots show a significantly higher radiosensitivity index was found in male patients compared to female patients in three of four cohorts analysed. In all cohorts, there were more male than female patients. * p<0.05, unpaired t-test.*

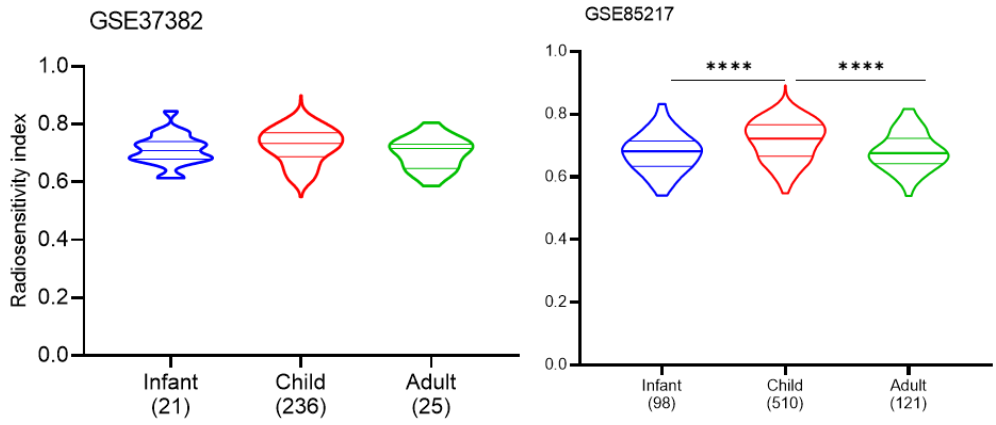

Figure 25: Medulloblastoma is less radiosensitive in children, but only in one cohort. *For both cohorts there were at least twice as many 'child' patients than 'infant' or 'adult'. In GSE37382, no significance was found between age categories and radiosensitivity index and age group. In GSE85217, a higher radiosensitivity index was observed for children compared to infants (<3) and adults (>16). **** p<0.0001, One-Way ANOVA.*

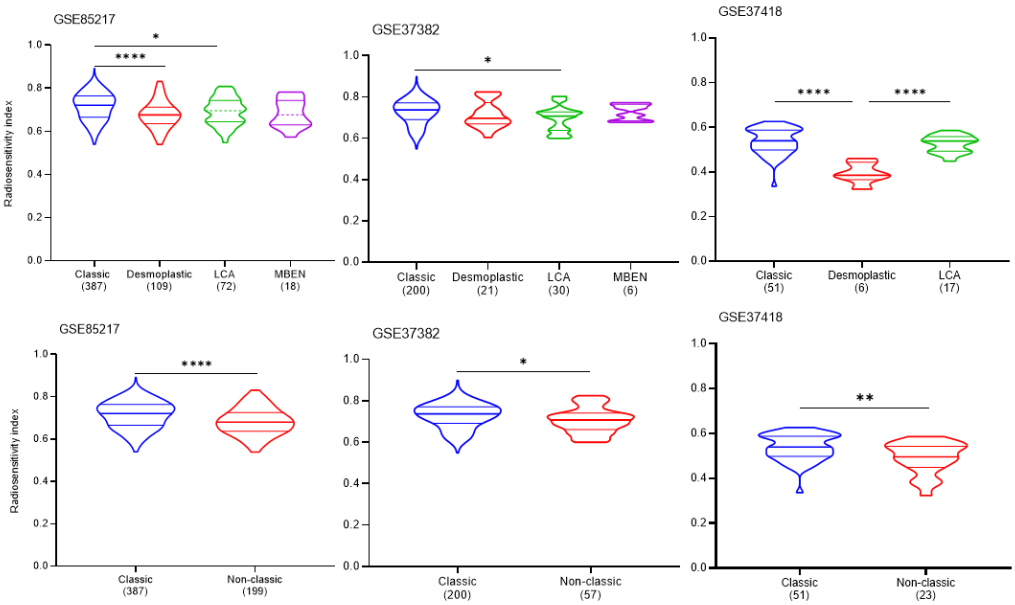

Figure 26: Classic histology medulloblastoma is less radiosensitive than non-classic histology medulloblastoma. *For cohorts where histological subgroup status was available, no pattern was observed between the radiosensitivity index scores and the histological subgroups. In GSE85217 and GSE37418, classic medulloblastomas were significantly less radiosensitive than desmoplastic medulloblastomas. In GSE85217 and GSE37382, classic medulloblastomas were significantly less radiosensitive than LCA medulloblastomas. In GSE37418, LCA tumours were significantly less radiosensitive than desmoplastic tumours. There were a much greater number of classic histology tumours than the remaining histological subgroups in all three patient cohorts. * p<0.05, **** p<0.0001, One-Way ANOVA. MBEN – medulloblastoma with extensive nodularity. LCA – large cell-anaplastic.*

The results of univariable and multivariable analyses are shown in Table 17 and Table 18 using the cohort and MM2S subgroup classifications respectively. Due to the limited clinical data known for this cohort a multivariate analysis, which would strengthen this work by investigating the significance of RSI in relation to other risk factors, was not available. Metastatic stage was prognostic in both multivariable analyses, as was the cohort classification subgroups. The MM2S classification subgroups lost prognostic significance in multivariable analyses. Although prognostic in univariable analysis, RSI was not a significantly prognostic factor in multivariable analysis.

Table 17: Univariable and multivariable analyses for GSE85217 using the cohort subgroup classification

			Univariable		Multivariable	
Variable		N	HR (95% CI)	p-value	HR (95% CI)	p-value
Age Group	Infant	119	1.00			
	Child	499	0.82 (0.54-1.30)	0.371		
	Adult	111	0.56 (0.30-1.10)	0.072		
Gender	Female	247	1.00			
	Male	472	1.20 (0.83-1.60)	0.368		
Metastatic stage	M0	397	1.00		1.00	
	M+	176	1.60 (1.20-2.30)	**0.004**	1.50 (1.09-2.20)	**0.015**
RSI quartile	High	191	1.00		1.00	
	Low	572	1.50 (1.00-2.20)	**0.048**	1.40 (0.85-2.20)	0.191
Subgroup (Cohort)	WNT	70	1.00		1.00	
	SHH	223	5.30 (1.60-17.00)	**0.006**	4.80 (1.48-15.8)	**0.009**
	Group 3	144	10.9 (3.40-35.00)	**<0.001**	7.40 (2.29-24.0)	**<0.001**
	Group 4	326	6.00 (1.90-19.00)	**0.002**	3.70 (1.13-11.9)	**0.031**

**values in bold were significant (p<0.05)*

Table 18: Univariable and multivariable analyses for GSE85217 using the MM2S subgroup classification

			Univariable		Multivariable	
Variable		N	HR (95% CI)	p-value	HR (95% CI)	p-value
Age Group	Infant	119	1.00			
	Child	499	0.82 (0.54-1.30)	0.371		
	Adult	111	0.56 (0.30-1.10)	0.072		
Gender	Female	247	1.00			
	Male	472	1.20 (0.83-1.60)	0.368		
Metastatic stage	M0	397	1.00		1.00	
	M+	176	1.60 (1.20-2.30)	**0.004**	1.60 (1.12-2.30)	**0.009**
RSI quartile	High	191	1.00		1.00	
	Low	572	1.50 (1.00-2.20)	**0.048**	1.20 (0.73-1.90)	0.487
Subgroup (MM2S)	WNT	54	1.00		1.00	
	SHH	229	4.20 (1.30-13.0)	**0.018**	3.60 (1.12-11.9)	**0.032**
	Group 3	126	8.60 (2.70-28.0)	**<0.001**	5.70 (1.75-18.7)	**0.004**
	Group 4	348	5.00 (1.60-16.0)	**0.006**	3.20 (0.98-10.3)	0.054

**values in bold were significant (p<0.05)*

3.3 Proliferation

The proliferation of MBL tumours was investigated using the same cohorts studied to investigate radiosensitivity. The gene expression data were used to analyse markers of proliferation (Ki67, PCNA) and the meta-PCNA signature (Section 2.6).

3.3.1 Gene expression markers of proliferation

The RNA expression levels of Ki67 and PCNA were assessed in the five patient cohorts. IHC staining is generally used to determine the protein levels of these markers and there is no convention regarding cut-off point for mRNA expression. For Ki67 the 75th percentile was used[546]. For PCNA the median was used[547]. In cohort GSE85217, neither Ki67 (HR = 1.1, 95% CI = 0.8-1.6, p=0.484; Figure 27) nor PCNA (HR = 0.80, 95% CI = 0.58-1.1, p=0.15; Figure 28) was prognostic for overall survival.

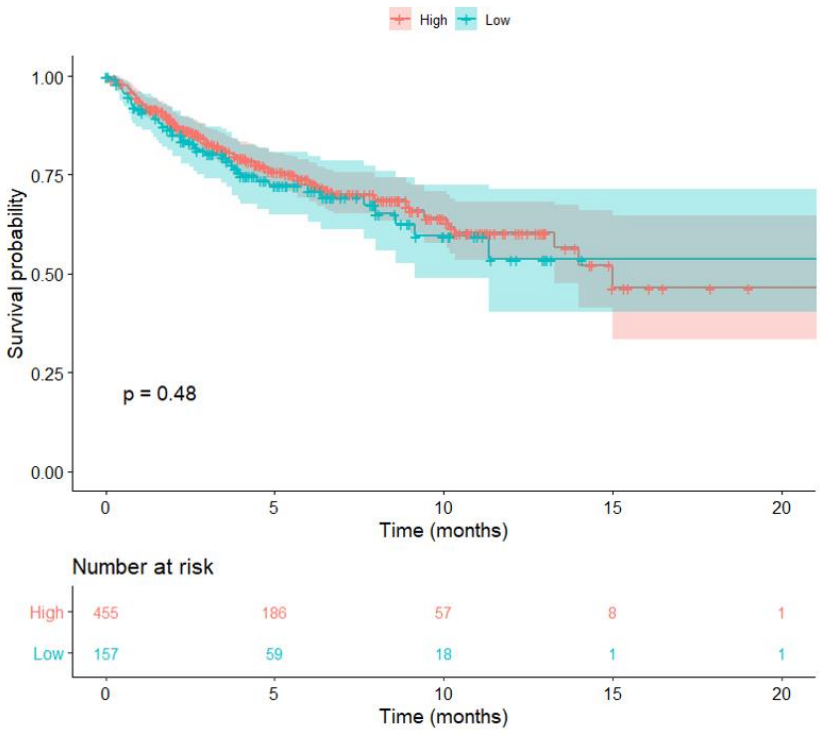

Figure 27: Ki67 gene expression is not prognostic in the GSE85217 cohort. *The Kaplan-Meier curves compare samples with high and low Ki67 expression, dividing samples using the 75th percentile as a cut-off. The survival outcomes are not significantly linked to Ki67 gene expression (HR 1.1, 95% CI 0.8-1.6, p=0.484).*

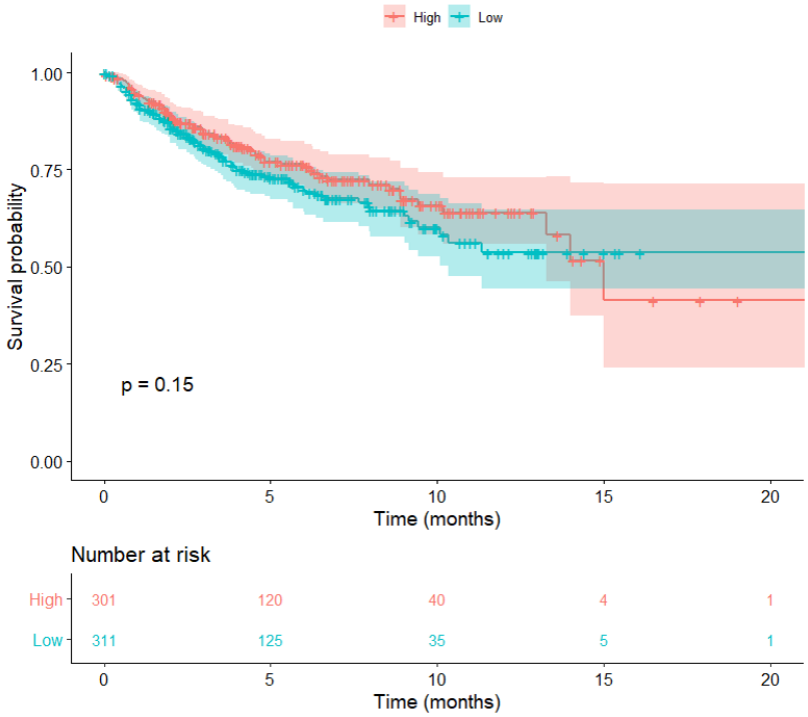

Figure 28: PCNA gene expression is not prognostic in the GSE85217 cohort. *The Kaplan-Meier curve comparing samples with high PCNA expression and low PCNA expression, dividing samples using the median as a cut-off. The survival outcomes are not significantly linked to PCNA gene expression (HR 0.80, 95% CI 0.58-1.1, p=0.15).*

The gene expression of Ki67 differed significantly between the molecular subgroups in the three larger patient cohorts using both the cohort (Figure 29) and MM2S (Figure 30) classifications. In GSE37382, the SHH subgroup had the highest Ki67 expression, followed by Group 4 and Group 3. In GSE37418, Group 4 tumours had significantly lower expression than the other three subgroups, between which no difference was detected. In GSE85217, the WNT subgroup had significantly higher gene expression of Ki67 than the other three subgroups. Again, no difference was detected between these other subgroups. There was no consistency across cohorts as to which subgroups had greater Ki67 expression and therefore which subgroups were consistently more or less proliferative. The gene expression of PCNA was also found to differ significantly between the molecular subgroups in the three larger patient cohorts, GSE37382, GSE37418 and GSE85217 (Figure 31, given subgroups; Figure 32, MM2S subgrouping).

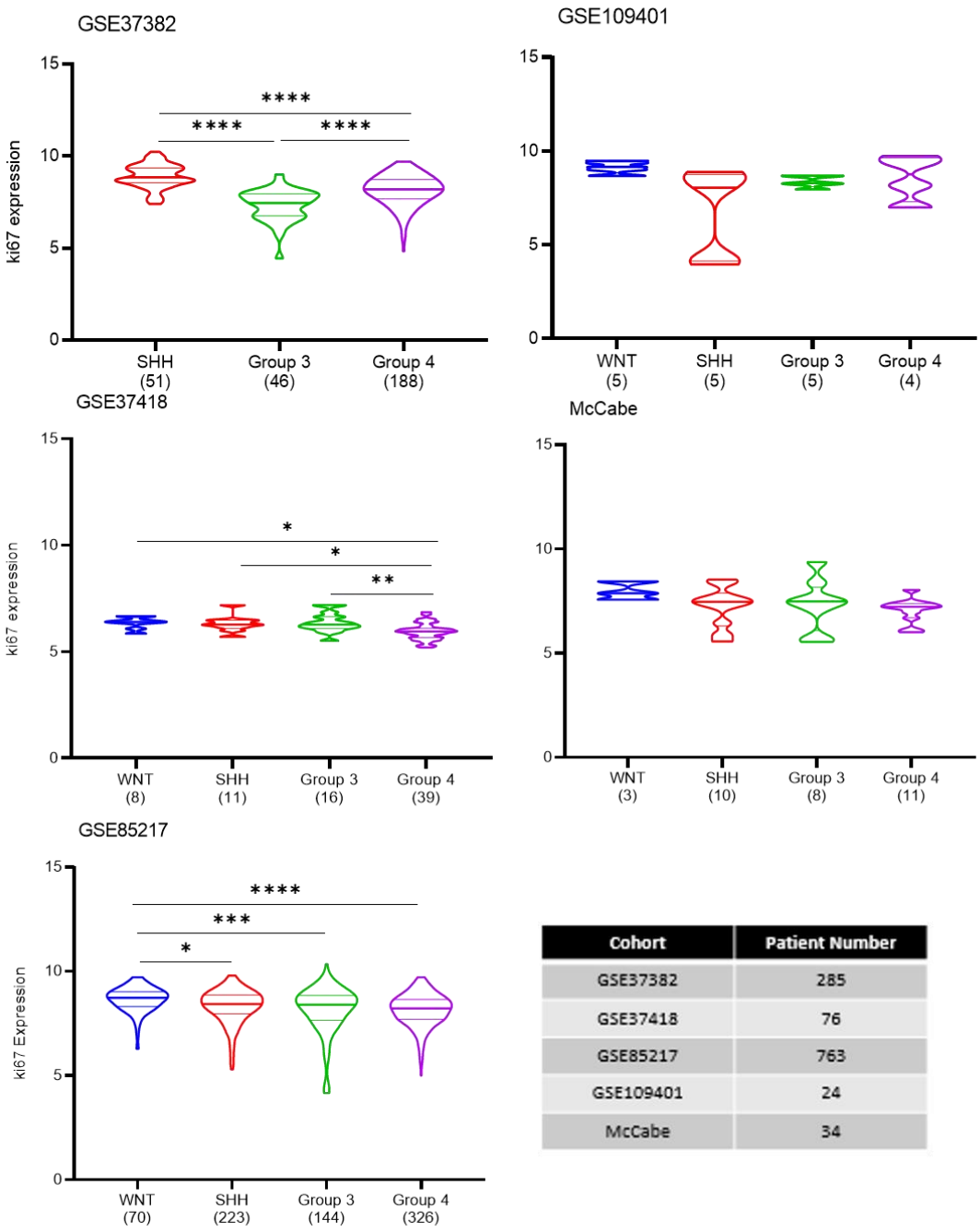

Cohort	Patient Number
GSE37382	285
GSE37418	76
GSE85217	763
GSE109401	24
McCabe	34

Figure 29: No consistent association between molecular subgroup (cohort classification) and Ki67 expression. *The distribution of Ki67 expression for the four subgroups within the five patient cohorts. The central line of the violin plot indicates the median. Although some significant differences between Ki67 gene expression and molecular subgroups were detected within individual cohorts, no cross-cohort pattern in Ki67 expression in relation to subgrouping was observed. * p<0.05, ** p<0.01, *** P<0.001, **** p<0.0001 One-Way ANOVA.*

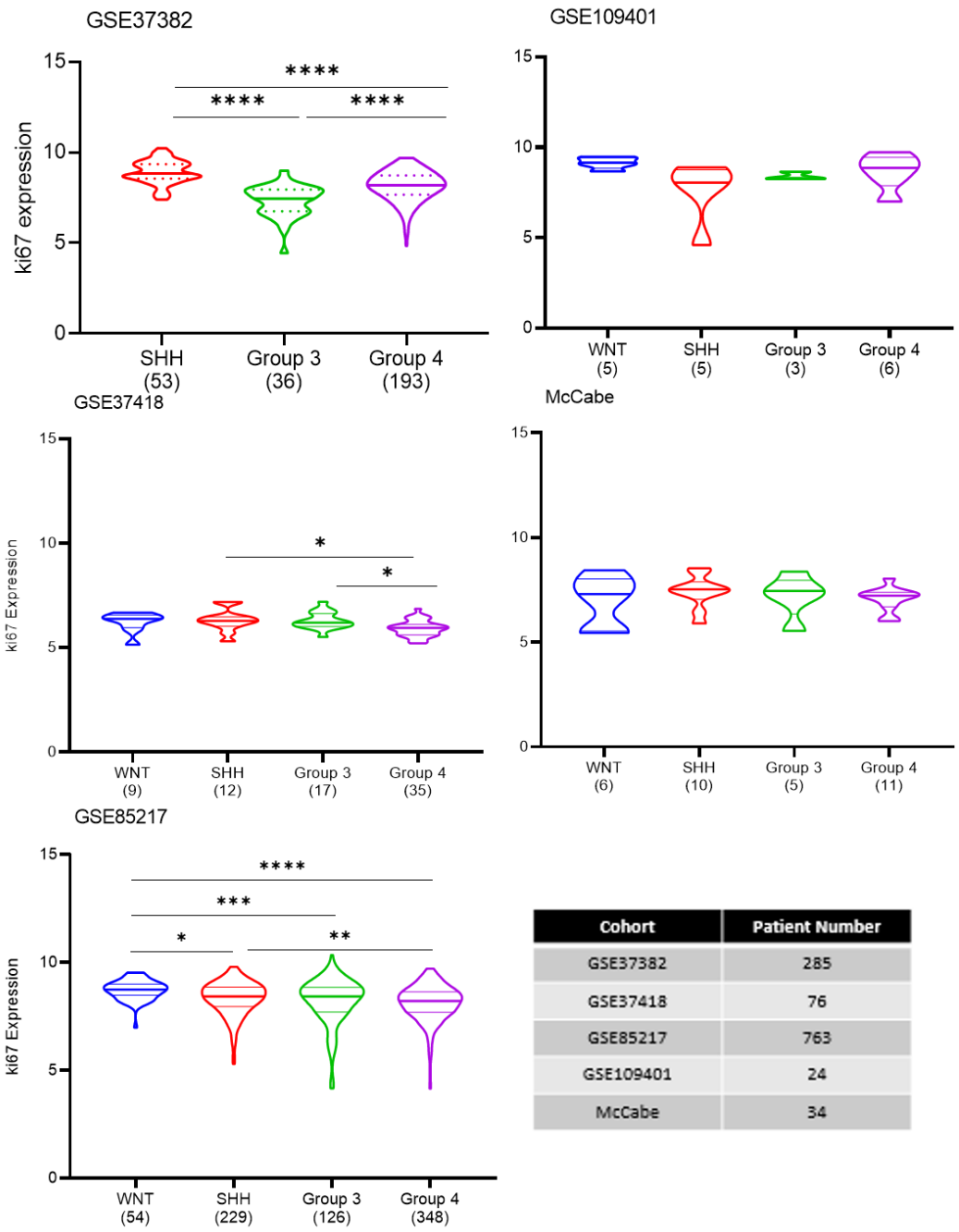

Cohort	Patient Number
GSE37382	285
GSE37418	76
GSE85217	763
GSE109401	24
McCabe	34

Figure 30: No consistent association between molecular subgroup (MM2S classification) and Ki67 expression. *The distribution of Ki67 expression for the four subgroups as determined by the MM2S algorithm within the five patient cohorts. The central line of the violin plot indicates the median. No cross-cohort pattern in Ki67 expression and subgroups was observed. * p<0.05, ** p<0.01, *** P<0.001, **** p<0.0001 One-Way ANOVA.*

In GSE37382, the same pattern as Ki67 expression was observed for PCNA, with SHH tumours displaying higher gene expression, followed by Group 4 and Group 3. In GSE37418, a significant difference was only observed for expression being higher in Group 3 than in Group 4. In GSE85217, the SHH subgroup was found to have the lowest PCNA gene expression, while no difference was observed between the three remaining subgroups. As with Ki67 expression, no consistent pattern of increased or decreased PCNA gene expression was observed in relation to the molecular subgroups. In GSE37382 both Ki67 and PCNA expression indicates SHH to be the most proliferative subgroup. In GSE37418 Ki67 expression indicated Group 4 tumours were the least proliferative with no difference in the other subgroups, while PCNA expression showed that only Group 3 tumours were significantly more proliferative than Group 4 tumours. In GSE85217 PCNA expression showed SHH tumours were less proliferative than the other three subgroups, while Ki67 expression suggested WNT tumours were more proliferative than the other three subgroups.

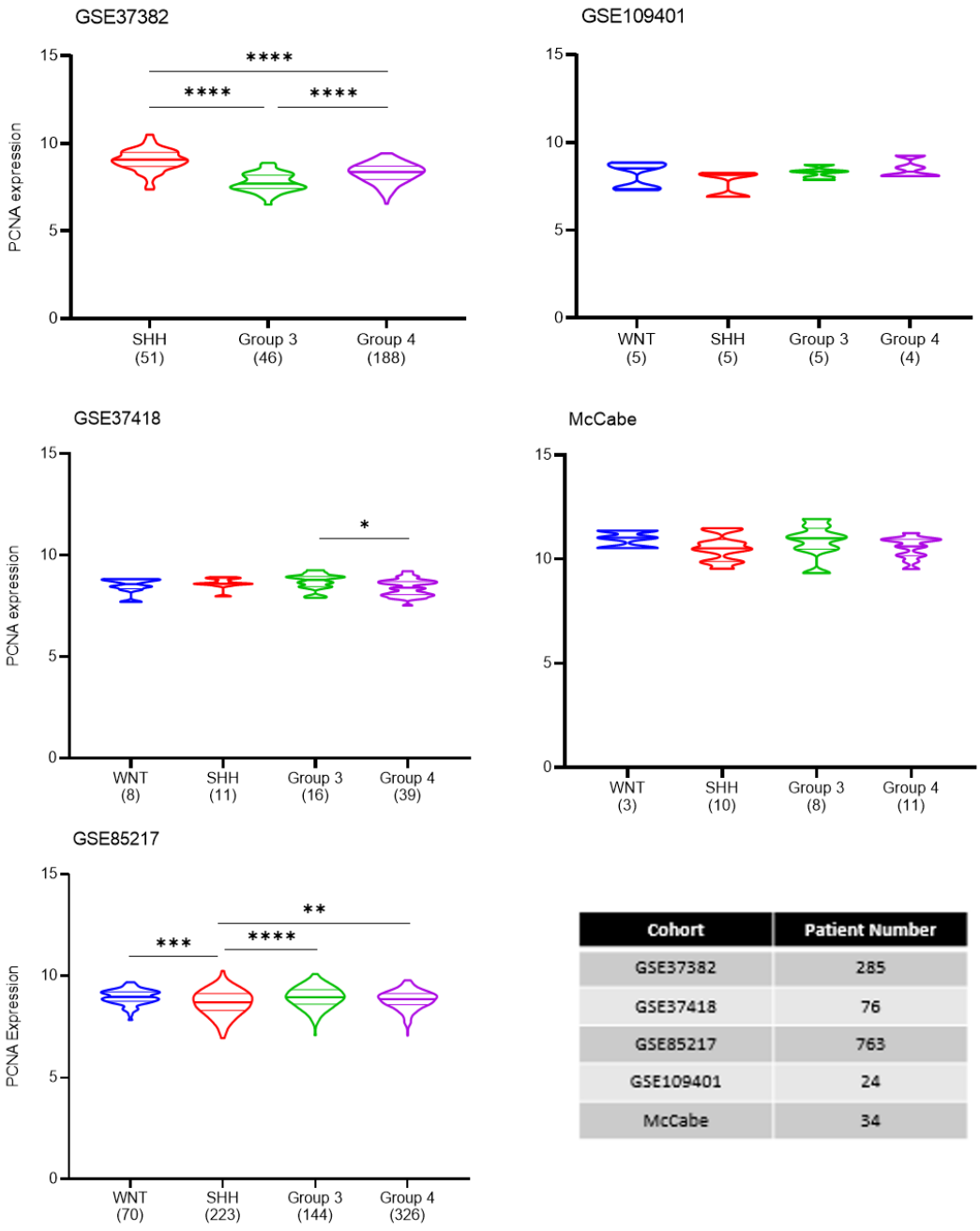

Cohort	Patient Number
GSE37382	285
GSE37418	76
GSE85217	763
GSE109401	24
McCabe	34

Figure 31: No consistent association between molecular subgroups (cohort classification) and PCNA expression. *The distribution of PCNA expression for the four subgroups within the five patient cohorts. The central line of the violin plot indicates the median. No cross-cohort pattern in PCNA expression and subgroups was observed. * p<0.05, ** p<0.01, *** P<0.001, **** p<0.0001 One-Way ANOVA.*

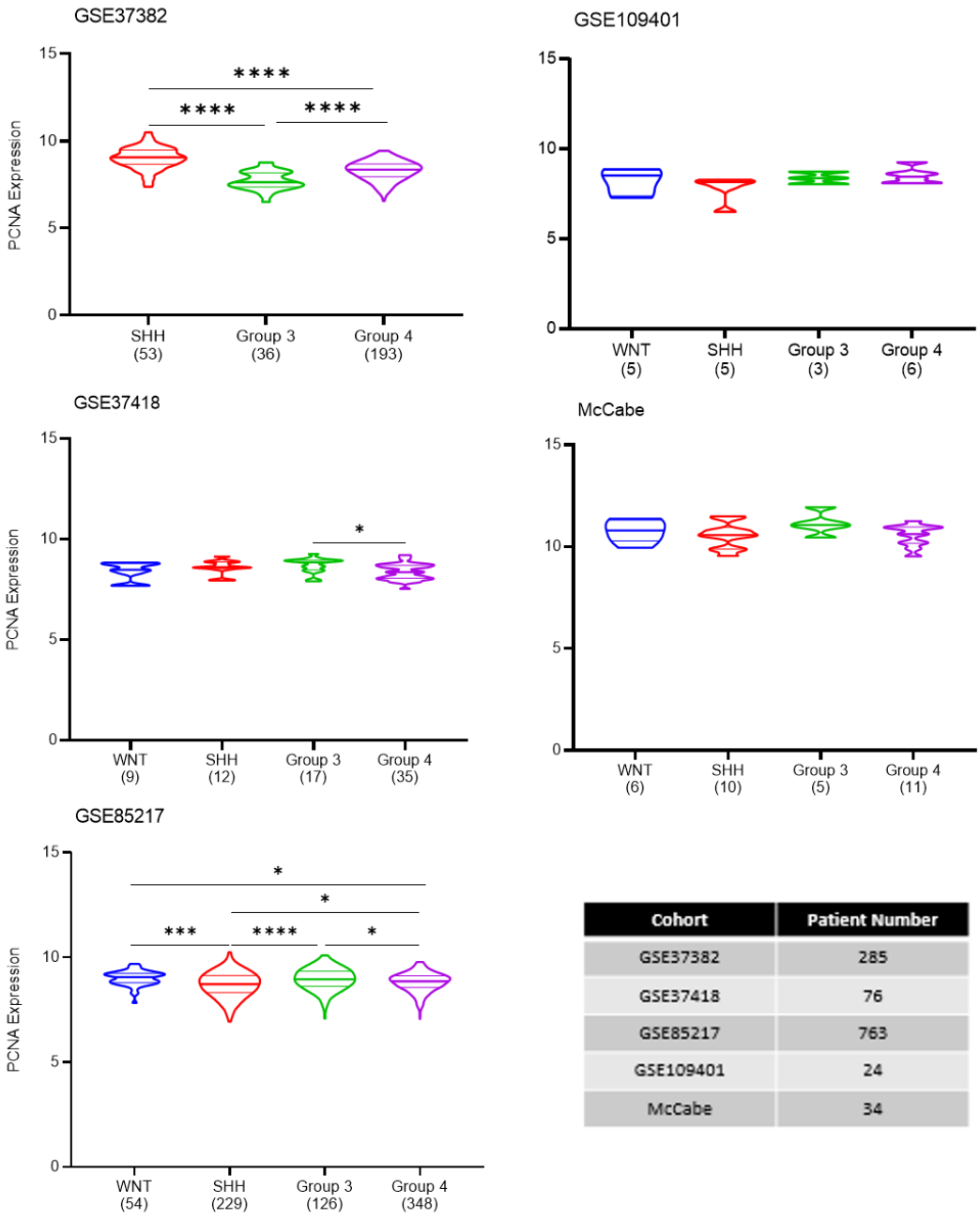

Cohort	Patient Number
GSE37382	285
GSE37418	76
GSE85217	763
GSE109401	24
McCabe	34

Figure 32: No consistent association between molecular subgroup (MM2S classification) and PCNA expression. *The distribution of PCNA expression for the four subgroups within the five patient cohorts. The central line of the violin plot indicates the median. No cross-cohort pattern in PCNA expression and subgroups was observed. * p<0.05, ** p<0.01, *** P<0.001, **** p<0.0001 One-Way ANOVA.*

3.3.2 Meta-PCNA index as a marker of proliferation

The mPI[350] has been used to assess proliferation in TCGA cohorts[351]. The meta-PCNA signature showed MBL to be non-proliferative informative, as the top and bottom quartiles of the cohort are not prognostic (HR = 0.82, 95% CI = 0.51-1.3, p=0.393; Figure 33). The meta-PCNA score does not consistently differ between subgroups in different cohorts (Figure 34 and Figure 35).

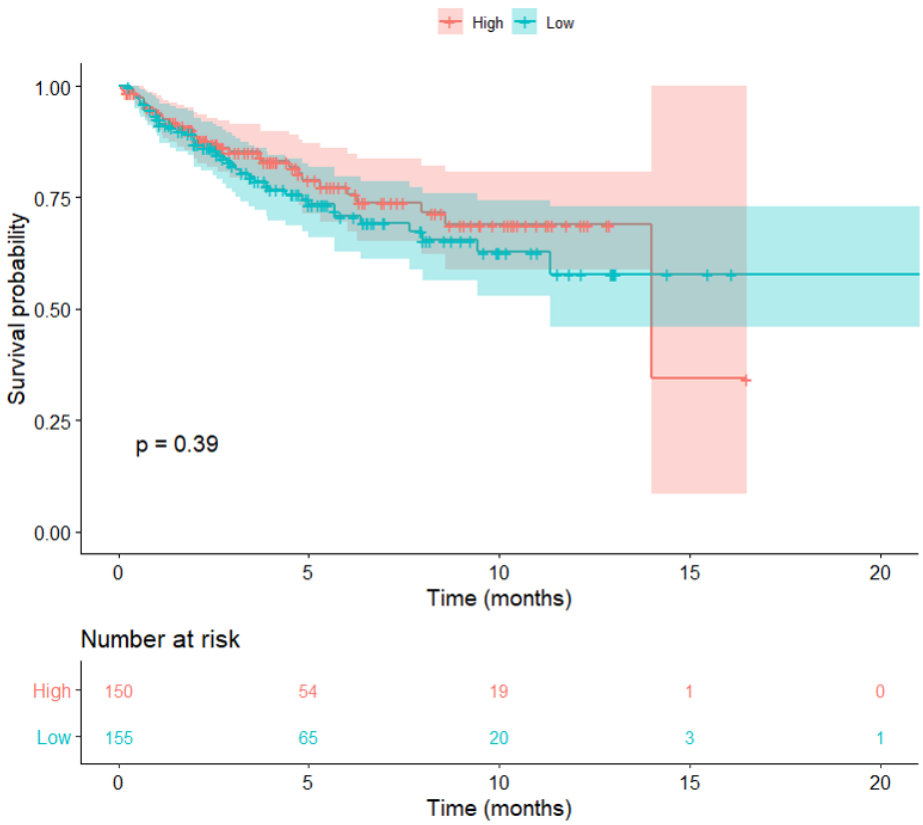

Figure 33: Medulloblastoma is a non-proliferative informative cancer, as determined by the meta-PCNA index. *The Kaplan-Meier curve for the meta-PCNA index (mPI) for GSE85217, comparing survival outcomes for the top (High) and bottom (Low) quartiles. A cancer is designated as 'proliferative informative' if the top and bottom quartiles of the mPI rankings are prognostic on Kaplan-Meier analysis. In the GSE85217 cohort, these two groupings are not significantly separated (HR 0.82, 95% CI 0.51-1.30, p=0.39), designating medulloblastoma as non-proliferative informative.*

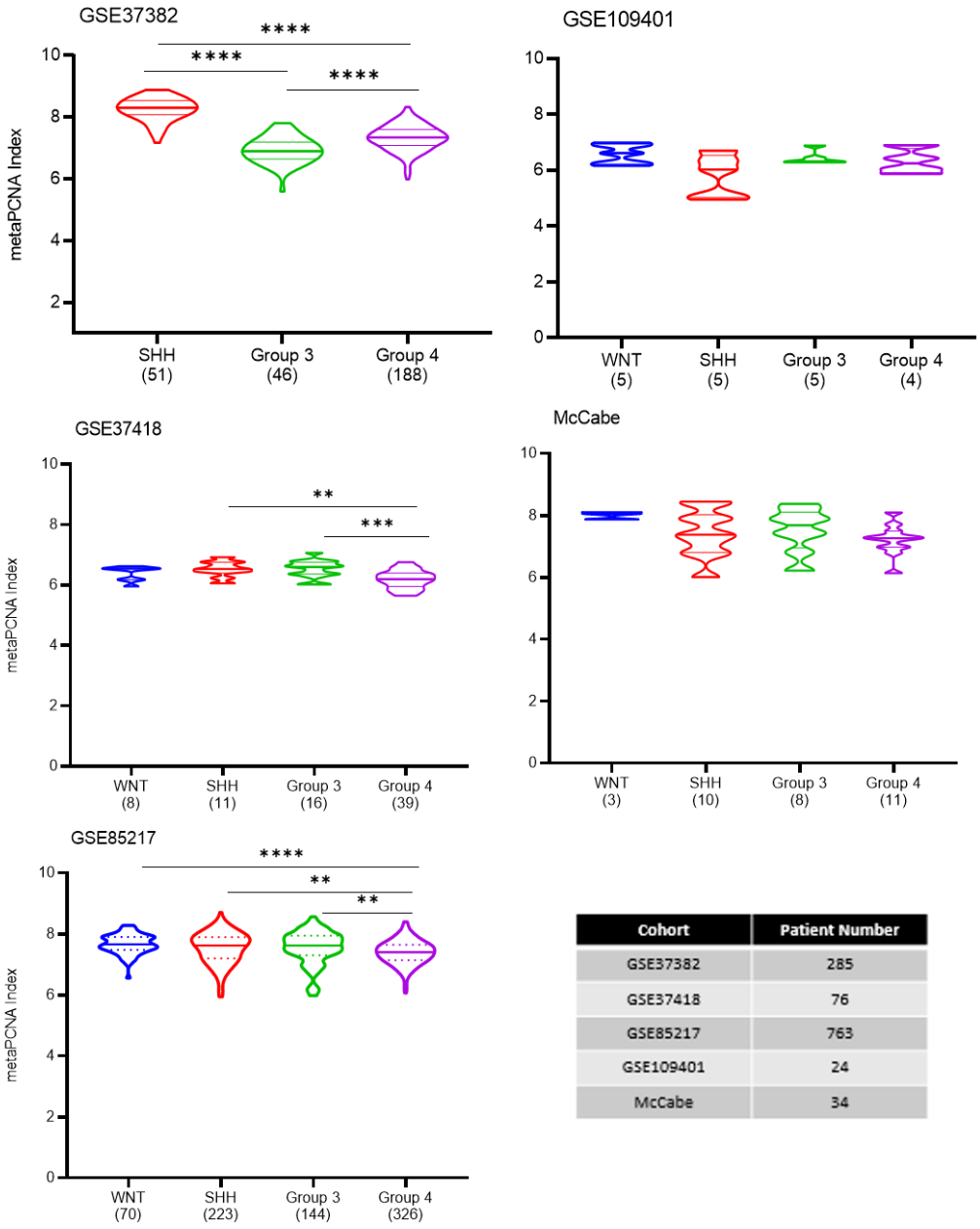

Cohort	Patient Number
GSE37382	285
GSE37418	76
GSE85217	763
GSE109401	24
McCabe	34

Figure 34: No consistent association between molecular subgroup (cohort classification) and meta-PCNA scores. *The distribution of meta-PCNA index scores for the four subgroups within the five patient cohorts. The central line of the violin plot indicates the median. No cross-cohort pattern in meta-PCNA index scores was observed. * p<0.05, ** p<0.01, *** P<0.001, **** p<0.0001 One-Way ANOVA.*

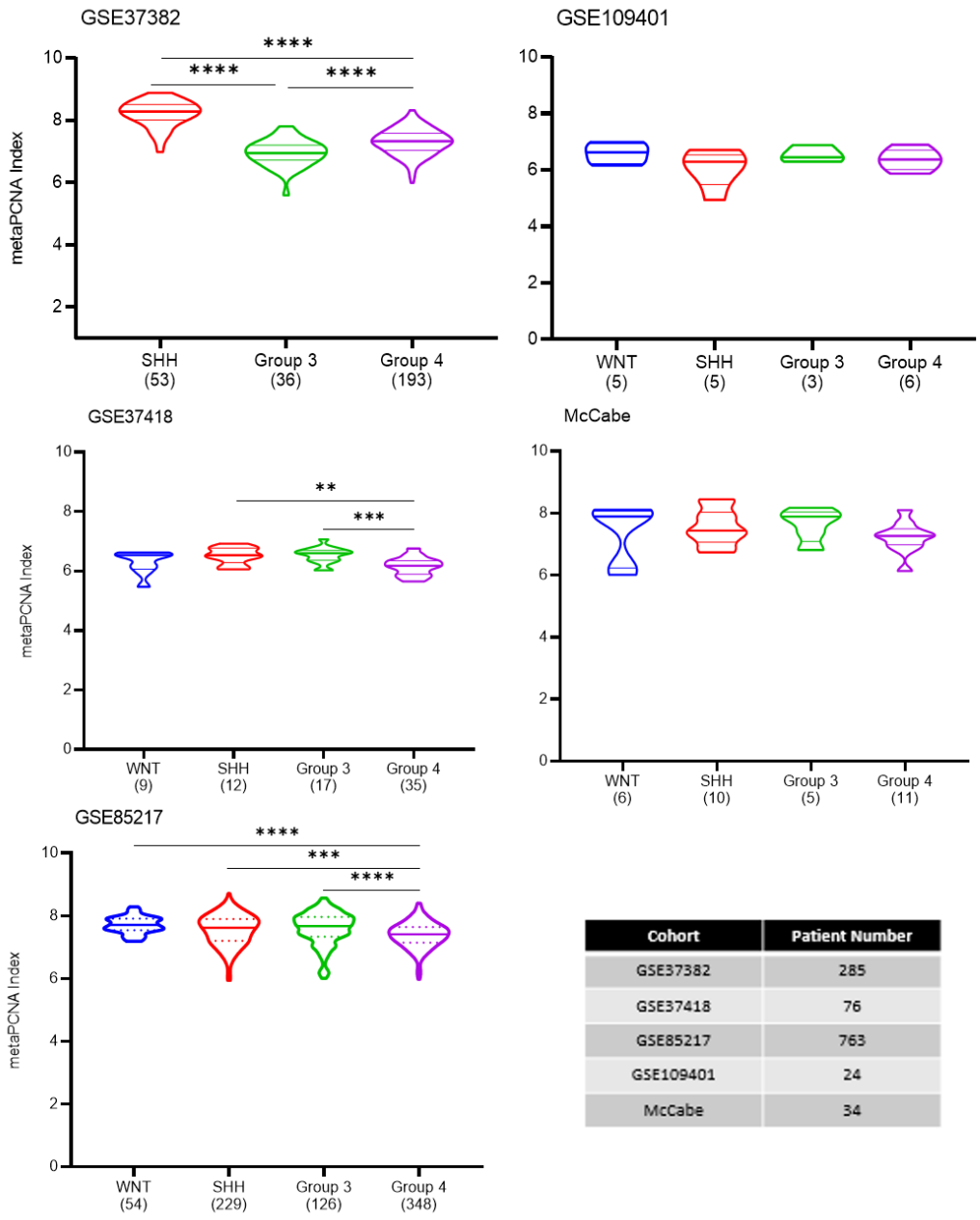

Cohort	Patient Number
GSE37382	285
GSE37418	76
GSE85217	763
GSE109401	24
McCabe	34

Figure 35: No consistent association between molecular subgroup (MM2S classification) and meta-PCNA scores. *The distribution of meta-PCNA index scores for the four subgroups within the five patient cohorts. The central line of the violin plot indicates the median. No cross-cohort pattern in meta-PCNA index scores was observed. * p<0.05, ** p<0.01, *** P<0.001, **** p<0.0001 One-Way ANOVA.*

In the two smallest cohorts (GSE109401, McCabe), no significant differences between mean mPI score and subgroup were found. In GSE37382, the SHH subgroup had the highest mPI scores, followed by Group 4 and Group 3 tumours. In GSE37418, the mPI score was significantly lower than that of SHH or Group 3 tumours, but did not differ from WNT and no difference was found between these other three subgroups. In GSE85217, Group 4 tumours

have significantly lower scores than the remaining three subgroups. Again, no difference between these subgroups was observed. As with the single gene expression data, no consistent patterns in subgroup gene expression was observed across the subgroups or cohorts.

3.4 Hypoxia

The presence of hypoxia in MBL tumours was investigated using gene expression markers and hypoxia gene signatures (Section 2.6).

3.4.1 Hypoxia assessed using gene/protein expression

The mRNA expression of CAIX, a widely used marker to detect the presence of hypoxia, was investigated in the patient cohorts (Figure 36 and Figure 37). There was no consistent pattern of differences in the level of CAIX mRNA expression across the MBL molecular subgroups, irrespective of the approach used to identify subgroups. However, three of the cohorts were small. In the two largest cohorts, CAIX expression was significantly higher in SHH tumours than in Group 3 or Group 4 subgroups. In GSE37382, CAIX expression was significantly higher for Group 4 tumours compared to Group 3. CAIX gene expression, stratified using the 75th percentile[548], was not found to be prognostic in GSE85217 (HR = 0.9, 95% CI = 0.62-1.3, p = 0.59; Figure 38).

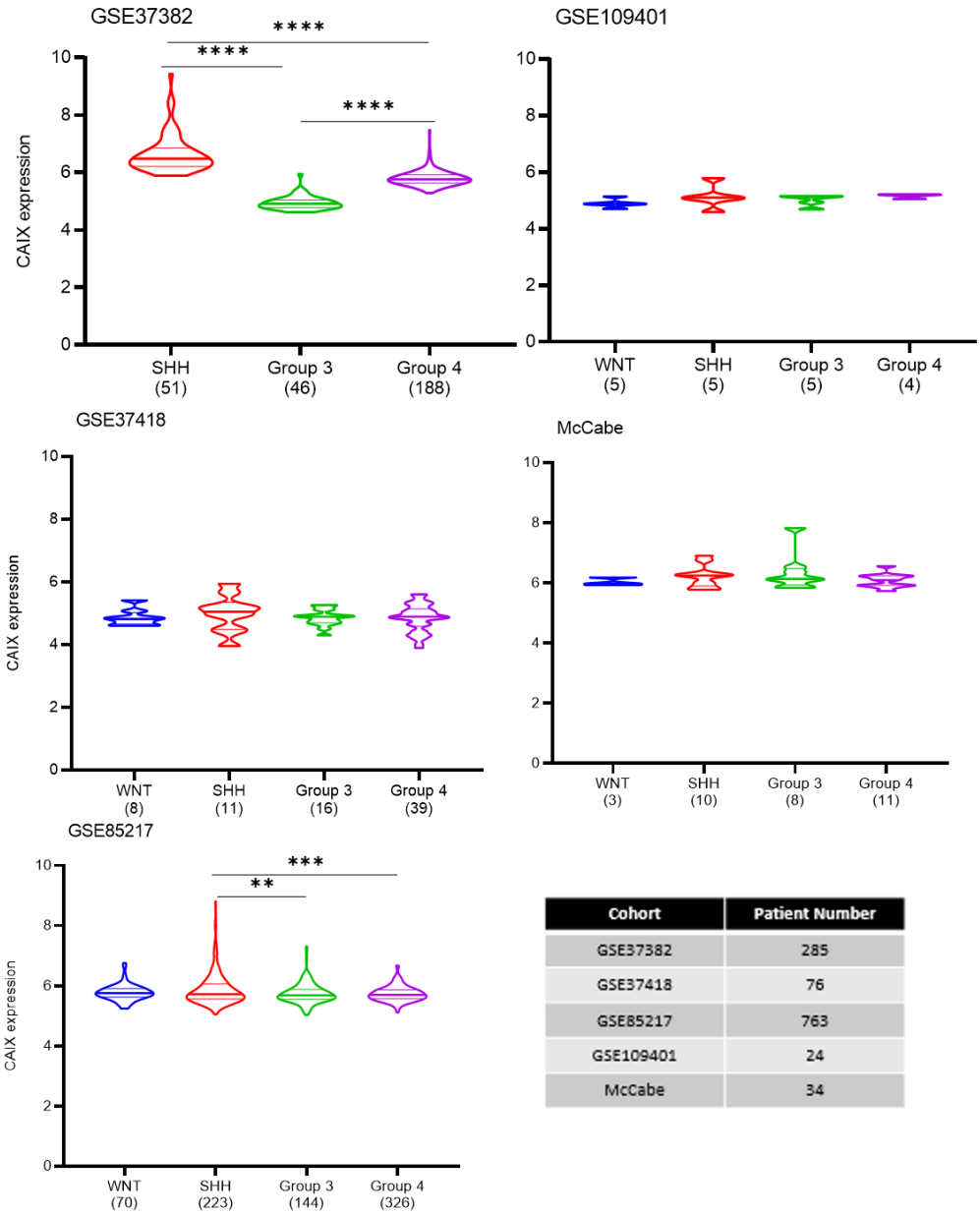

Cohort	Patient Number
GSE37382	285
GSE37418	76
GSE85217	763
GSE109401	24
McCabe	34

Figure 36: No consistent association between molecular subgroup (cohort classification) and CAIX mRNA expression. *The distribution of CAIX gene expression for the four subgroups within the five patient cohorts. Subgroup assignments were provided with the cohort data. The central line of the violin plot indicates the median. No cross-cohort pattern in CAIX expression and subgroups was observed. * p<0.05, ** p<0.01, *** P<0.001, **** p<0.0001 One-Way ANOVA.*

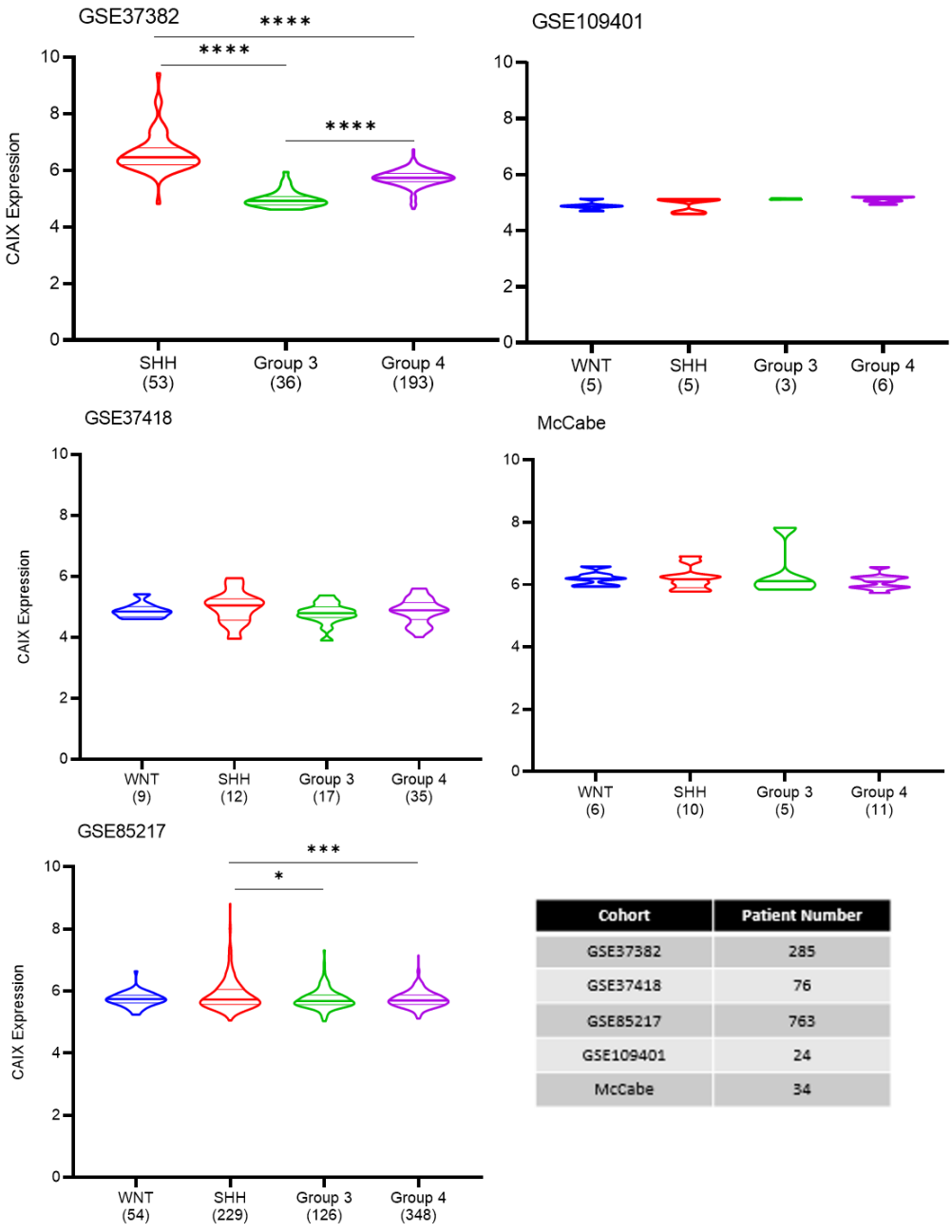

Cohort	Patient Number
GSE37382	285
GSE37418	76
GSE85217	763
GSE109401	24
McCabe	34

Figure 37: No consistent association between molecular subgroup (MM2S classification) and CAIX mRNA expression. *The distribution of CAIX expression for the four subgroups within the five patient cohorts. The central line of the violin plot indicates the median. No cross-cohort pattern in CAIX expression and subgroups was observed. * p<0.05, ** p<0.01, *** P<0.001, **** p<0.0001 One-Way ANOVA.*

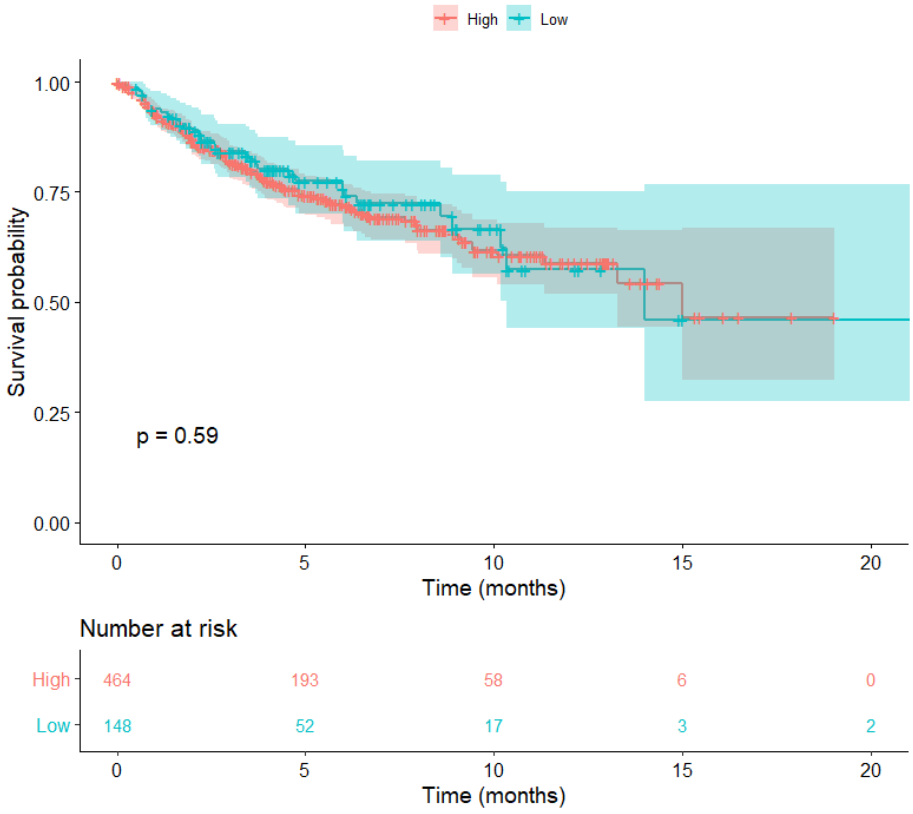

Figure 38: CAIX gene expression is not prognostic in the GSE85217 cohort. *The Kaplan-Meier curve for CAIX gene expression for GSE85217 when dichotomised by the 75th percentile gene expression. High CAIX expression did not indicate a significantly worse outcome than low CAIX expression. (HR 1.1, 95% CI 0.81-1.5, p=0.51).*

The gene expression of a second marker, GLUT1, had no association with subgroup status (Figure 39, Figure 40) and again, no pattern between subgroup status and GLUT1 expression was observed. In GSE37382, GLUT1 expression was significantly higher in SHH tumours than Group 3 or Group 4. In the other large cohort GSE85217 however, SHH tumours had significantly lower GLUT1 gene expression than Group 3 or Group 4 tumours. Additionally, in GSE85217 cohort GLUT1 expression was significantly higher in Group 3 tumours than Group 4 or WNT. The median cohort value was used to classify sample GLUT1 gene expression as high or low[549,550]. GLUT1 gene expression was not prognostic (HR = 0.98, 95% CI = 0.71-1.3, p=0.877; Figure 41).

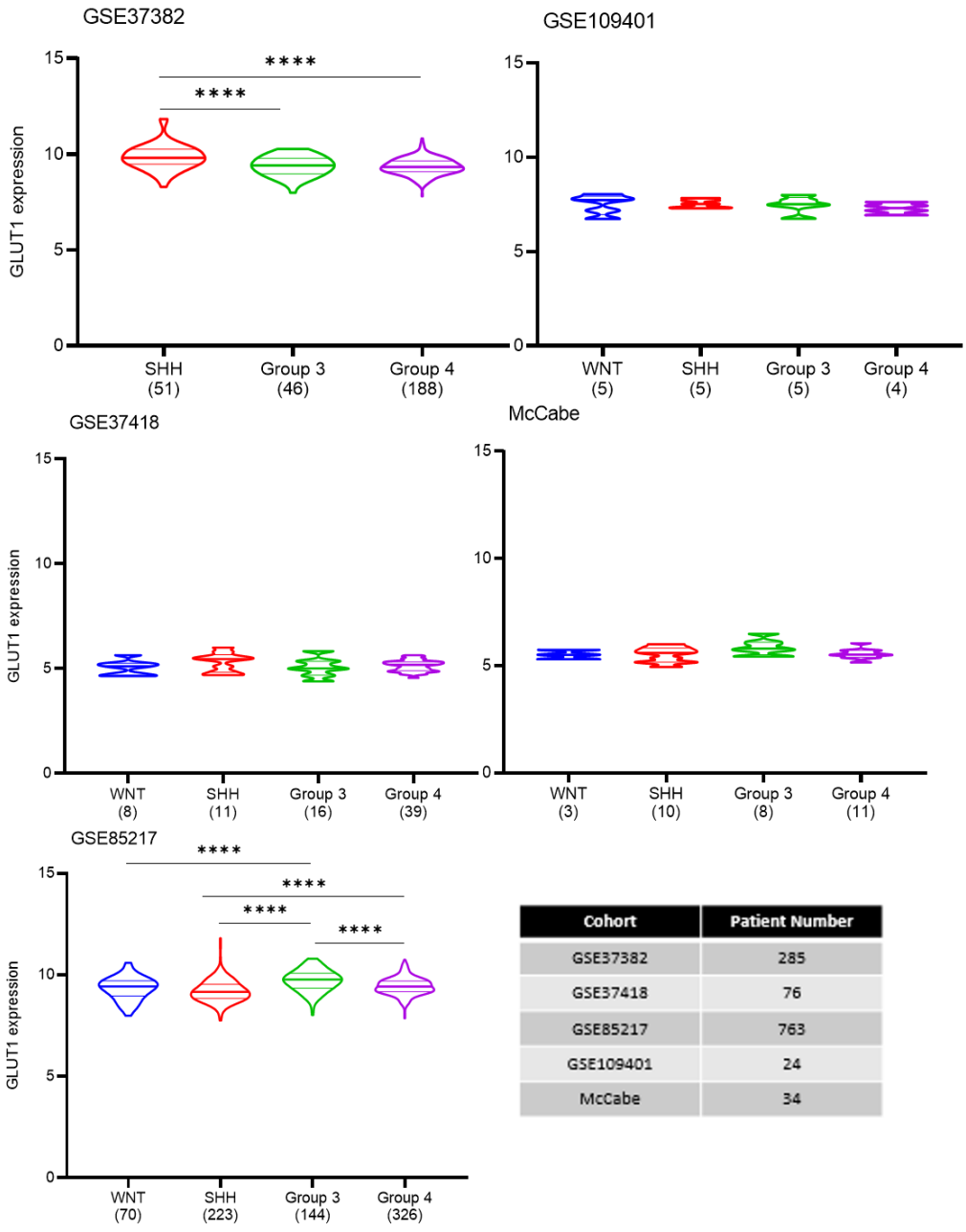

Cohort	Patient Number
GSE37382	285
GSE37418	76
GSE85217	763
GSE109401	24
McCabe	34

Figure 39: No consistent association between molecular subgroup (cohort classification) and GLUT1 expression. *The distribution of GLUT1 expression for the four subgroups within the five patient cohorts. The central line of the violin plot indicates the median. No cross-cohort pattern in GLUT1 expression and subgroups was observed. * p<0.05, ** p<0.01, *** P<0.001, **** p<0.0001 One-Way ANOVA.*

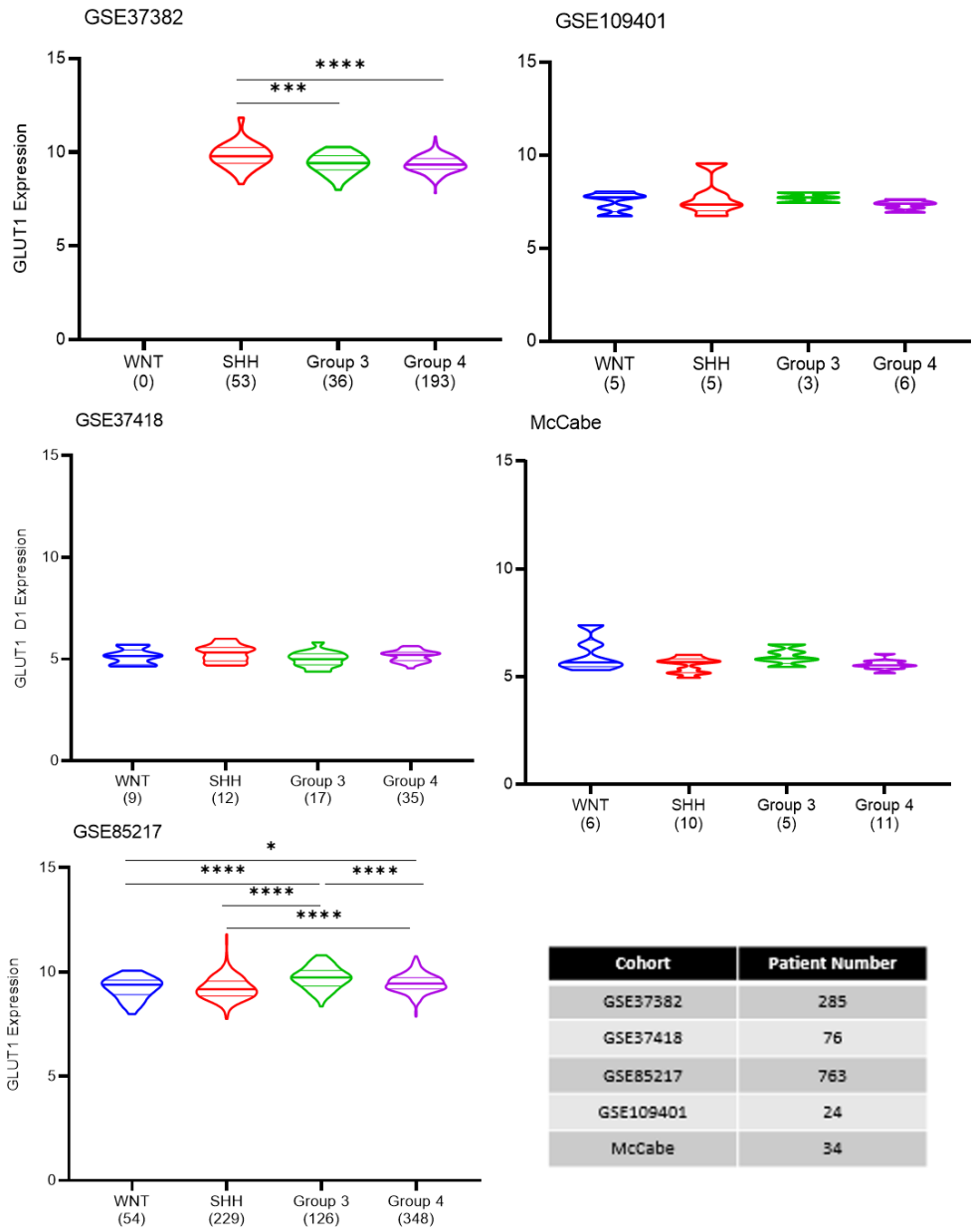

Cohort	Patient Number
GSE37382	285
GSE37418	76
GSE85217	763
GSE109401	24
McCabe	34

Figure 40: No consistent association between molecular subgroups (MM2S classification) and GLUT1 expression. *The distribution of GLUT1 expression for the four subgroups within the five patient cohorts. The central line of the violin plot indicates the median. No cross-cohort pattern in GLUT1 expression and subgroups was observed. * p<0.05, ** p<0.01, *** P<0.001, **** p<0.0001 One-Way ANOVA.*

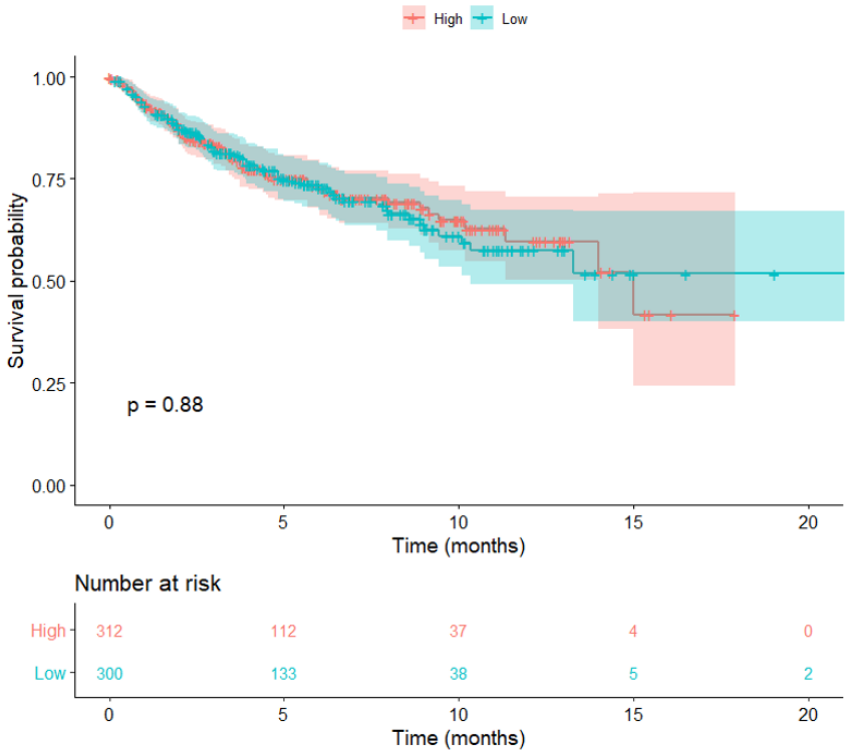

Figure 41: GLUT1 gene expression is not prognostic in the GSE85217 cohort. *The Kaplan-Meier curve for GLUT1 gene expression in GSE85217 compares survival outcomes for patients stratified by the median. High tumour GLUT1 expression did not indicate a significantly worse outcome than low GLUT1 expression (HR 0.98, 95% CI 0.71-1.3, p=0.877).*

3.4.2 Hypoxia gene expression signatures

There are no hypoxia signatures derived using MBL cell lines or patient samples. A literature search identified 12 published signatures (Table 10, Section 2.6.6) derived in a variety of cancer types that could be tested in the GSE85217 cohort, which had outcome data available. Table 19 summarises the results of the analysis, showing that of the 12 signatures used none were prognostic. Additionally, whether a patient sample was assigned to the high or low hypoxia group by a signature was not consistent across signatures.

Table 19: Hazard ratios and log-rank p values for hypoxia gene signatures in GSE85217

Source	Hypoxia	Patients	HR(95% CI)	Log-rank p
Yang , 2018 (Prostate)[1]	Low High	382 381	1.00 0.87 (0.63-1.20)	0.369
Yang, 2017 (Bladder)[1]	Low High	381 382	1.00 0.99 (0.72-1.30)	0.929
Tardón, 2020 (Glioblastoma)[2]	Cluster 1 Cluster 2	467 296	1.00 1.20 (0.86-1.60)	0.315
Eustace, 2013 (Head & Neck, Bladder)[1]	Low High	382 381	1.00 1.00 (0.73-1.40)	0.995
Sun, 2020 (Lung adenocarcinoma)[1]	Low High	381 382	1.00 0.81 (0.59-1.10)	0.201
Lin, 2020 (Glioma)[1]	Low High	381 382	1.00 1.20 (0.88-1.60)	0.261
Fardin, 2010 (Neuroblastoma)[2]	Cluster 1 Cluster 2	557 206	1.00 0.68 (0.45-1.10)	0.084
Buffa, 2010 (Metagene)[1]	Low High	381 382	1.00 0.84 (0.61-1.10)	0.263
Van Malenstein, 2010 (Hepatocellular)[1]	Low High	381 382	1.00 1.20 (0.88-1.60)	0.256
Wang, 2020 (Breast)[1]	Low High	382 381	1.00 1.00 (0.75-1.40)	0.837
Wang, 2020 (Glioblastoma)[1]	Low High	381 382	1.00 1.20 (0.87-1.60)	0.273

*Stratification criteria were 1-median, 2-k-means clustering. *values in bold were significant (p<0.05)*

The lowest p-value was achieved using the Fardin NBL signature[389], and therefore this signature was selected for use in multivariable analysis (Table 20, Table 21). NBL, like MBL, is an embryonal tumour from immature nerve cells (blasts)[551]. Only the variables that were significant in univariable analysis were included in the multivariable analysis. In univariable analysis the hypoxia signature had borderline prognostic significance, which was lost upon multivariable analysis, regardless of subgroup classification method.

Across the entire patient cohort, k-means clustering assigned 73% of samples to the 'high hypoxia' class using the Fardin signature. A similar proportion of 'high hypoxia' samples was found within each the four molecular subgroups - 67% in WNT, 77% in SHH, 69% in Group 3 and 74% in Group 4, suggesting the degree of hypoxia may be independent of subgroup status.

Table 20: Univariable and multivariable analyses for GSE85217 using the cohort subgroup classification

			Univariable		Multivariable	
Variable		n	HR (95% CI)	p-value	HR (95% CI)	p-value
Age Group	Infant	119	1.00			
	Child	499	0.82 (0.54-1.30)	0.371		
	Adult	111	0.56 (0.30-1.10)	0.072		
CAIX	Low	381	1.00			
	High	382	0.90 (0.66-1.20)	0.51		
Fardin	Cluster 1	557	1.00		1.00	
	Cluster 2	206	0.68 (0.45-1.10)	0.084	0.70 (0.44-1.10)	0.129
Gender	Female	247	1.00			
	Male	472	1.20 (0.83-1.60)	0.368		
	High	382	1.40 (1.00-1.90)	0.051		
Metastatic stage	M0	397	1.00		1.00	
	M+	176	1.60 (1.20-2.30)	**0.004**	1.50 (1.05-2.10)	**0.027**
Subgroup (Cohort)	WNT	70	1.00		1.00	
	SHH	223	5.30 (1.60-17.00)	**0.006**	4.50 (1.39-14.8)	**0.012**
	Group 3	144	10.9 (3.40-35.00)	**<0.001**	7.90 (2.46-25.7)	**<0.001**
	Group 4	326	6.00 (1.90-19.00)	**0.002**	4.20 (1.31-13.3)	**0.016**

**values in bold were significant (p<0.05)*

Table 21: Univariable and multivariable analyses for GSE85217 using the MM2S subgroup classification

			Univariable		Multivariable	
Variable		n	HR (95% CI)	p-value	HR (95% CI)	p-value
Age Group	Infant	119	1.00			
	Child	499	0.82 (0.54-1.30)	0.371		
	Adult	111	0.56 (0.30-1.10)	0.072		
CAIX	Low	381	1.00			
	High	382	0.90 (0.66-1.20)	0.51		
Fardin	Cluster 1	557	1.00		1.00	
	Cluster 2	206	0.68 (0.45-1.10)	0.084	0.68 (0.43-1.10)	0.106
Gender	Female	247	1.00			
	Male	472	1.20 (0.83-1.60)	0.368		
	High	382	1.40 (1.00-1.90)	0.051		
Metastatic stage	M0	397	1.00		1.00	
	M+	176	1.60 (1.20-2.30)	**0.004**	1.55 (1.09-2.20)	**0.015**
Subgroup (MM2S)	WNT	54	1.00		1.00	
	SHH	229	4.20 (1.30-13.00)	**0.018**	3.45 (1.06-11.3)	**0.04**
	Group 3	126	8.60 (2.70-28.00)	**<0.001**	6.07 (1.87-19.7)	**0.003**
	Group 4	348	5.00 (1.60-16.00)	**0.006**	3.33 (1.05-10.6)	**0.042**

**values in bold were significant (p<0.05)*

The Fardin[389] hypoxia signature uses k-means clustering of gene expression values to classify patients as high or low hypoxia tumours. K-means clustering divides *n* samples into *k* clusters. The number of clusters used to process the samples is defined either by prior knowledge of the dataset or by determination of the optimal number of clusters. Commonly, the optimal number of clusters is the value of k that minimises the dispersion between them. As the purpose of the gene signatures is to assign samples to high or low hypoxia groups, the publication and the above analysis used k=2. However, the optimal number of clusters for this cohort as determined using the Elbow method to minimise the sum-of-squares differences was four. This was also found to be the case for the other clustering based signature (Tardón[434]). Due to the nature of the k-means clustering algorithm, the output will always produce k clusters regardless of whether they actually exist in the data. Using k=2 when k=4 is optimal could produce two clusters that are amalgamations of the four 'true'

clusters. Using a greater than optimal k value would result in subdivisions of the 'true' clusters. In order to see if using the optimal number of clusters resulted in statistical significance, the clustering analysis was repeated with both the Fardin and Tardón signature gene sets and k=4 (Table 22). In the re-analysis, the Tardón signature was prognostic, however no significance was found with the Fardin signature. The PCA plots resulting from these two values of k are shown in Figure 42. For the Fardin hypoxia signature (Figure 42 A and C), the two clusters are more clearly separate groups than the four clusters, which matches with the survival analyses where k=2 produces a lower p-value. For the Tardón hypoxia signature (Figure 42 B and D) neither k value defined distinct clusters and it looks as if one single cluster was split into either 2 or 4 depending on the algorithm parameters. However, as the four clusters from the Tardón re-analysis represented the four molecular subgroups, which was not the case for the Fardin signature, this clustering may not be as arbitrary as it appears (Table 22).

Table 22: Univariable analysis for signatures using k-means clustering

				Univariable	
Signature	Cluster	Number	Major Subgroup	HR (95% CI)	p-value
Fardin	1	174	SHH (100%)	1.00	
	2	159	WNT (42%) Group 3 (55%)	1.10 (0.66-1.90)	0.685
	3	80	SHH (55%)	1.70 (0.92-3.00)	0.093
	4	350	Group 4 (85%)	1.40 (0.93-2.20)	0.102
Tardón	1	223	Group 3 (61%)	1.00	
	2	270	Group 4 (90%)	0.65 (0.45-0.93)	**0.018**
	3	201	SHH (97%)	0.56 (0.37-0.85)	**0.006**
	4	69	WNT (97%)	0.12 (0.036-0.37)	**<0.001**

**values in bold were significant (p<0.05)*

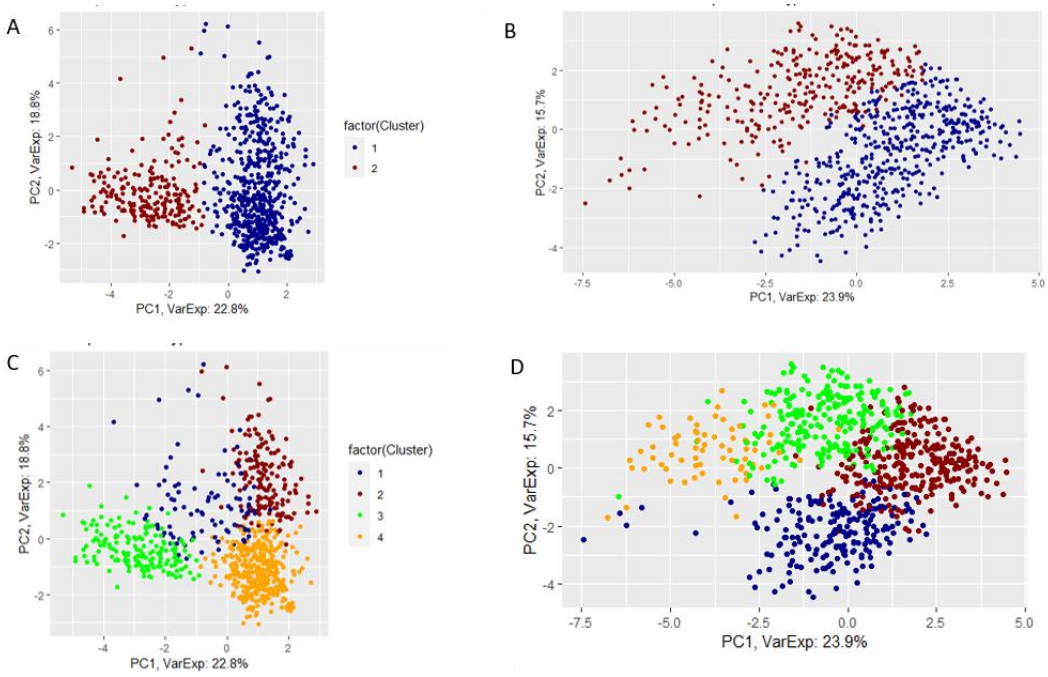

Figure 42: PCA plots of the k-means clustering results for two hypoxia signatures. *The Fardin (A, C) and Tardón hypoxia gene signatures were applied to the GSE85217 cohort. The k-means clustering algorithm was applied using k=2 (A, B), as reported in the literature and k=4 (B, D), which was determined to be the optimal number of clusters using the Elbow method to minimise the sum-of-squares error.*

In order to investigate whether the identification of the subgroups would occur at random, a thousand randomly selected sets of 36 genes were generated on three separate occasions. The resulting clusters were analysed to see if the same level of subgroup distinction occurred with the random selections, i.e., three clusters with >80% and a fourth cluster with >60% of a unique subgroup. In all three repeats, fewer than 5% of the randomly generated gene sets reached this level of subgroup distribution across the cohort, indicating that the identification of the subgroups by the Tardón signature was not by chance (Table 23).

Table 23: Number of repeats with a certain level of subgroup identification using randomly generated gene sets

	Repeat 1	Repeat 2	Repeat 3
3 clusters with >80% from one subgroup	6.0%	5.0%	7.2%
3 clusters with >80% from one subgroup & 1 cluster with >60% from one subgroup*	**3.1%**	**2.2%**	**3.1%**
4 clusters with >80% from one subgroup	**0.5%**	**0.3%**	**0.4%**

**as found with hypoxia signature. values in bold were significant (p<0.05)*

These results suggest the Tardón signature was able to separate out the four molecular subgroups either by identifying different expression levels of hypoxia-associated genes across the four molecular subgroups or by containing genes that are subgroup-specific but independent of tumour hypoxia status. The Tardón signature also separated the molecular subgroups in the second largest cohort, GSE37382. This cohort, which contained no WNT tumours, used the optimal k=3. Cluster 1 contained 57% SHH tumours, cluster 2 61% Group 3 tumours and cluster 3 contained 97% Group 4 tumours. As outcome data were unavailable, the prognostic significance of these clusters could not be determined. The remaining cohorts were too small to produce robust, reproducible clustering and therefore the signature could not be examined within these patients.

3.5 Migration

During the clonogenic assay work, it was observed that the colonies at higher radiation doses were more diffuse. It was hypothesised that radiation was increasing the rate of cell migration in the cell lines. The wound healing assay was used to investigate cell migration (2.7). The assay involves producing gaps in cell culture and measuring the speed of gap closure by measuring the gap width or gap area at selected time points. It is recommended that at least 100 measurements are taken per image to generate large data sets for robust analysis[552]. The gap width can be measured by the user manually drawing and measuring lines across the digital image using an image processing software such as ImageJ. This analysis method is here referred to as ‘Manual Measurements’. Manual Measurements restrict the number of images and time points that can realistically be carried out, as the process is labour intensive and time-consuming. In order to best utilise the high-throughput assay formats and time-lapse microscopy available in our laboratory and to minimise the time required and subjectivity in the analysis, an automated approach was investigated prior to completing the irradiation experiments. Only one software package was found that was compatible with the MBL cell lines, the MRI ImageJ Wound Healing Macro (‘MRI Macro’). The other software trialled, including T-Scratch[553], PyScratch[554] and the IncuCyte in-built analysis software[555], were unable to accurately detect the gap edges in the initial test images and so could not analyse experimental data. The MRI Macro is available to download and

works with the ImageJ software to analyse single and series of images. It uses a variance filter method to detect regions of an image containing cells, and measures the remaining area of the image (Figure 43). Several disadvantages of this software were noted, which may impact the precision and accuracy of the reported results. Firstly, the user is required to optimise several parameters for the software ('variance filter radius', 'threshold', 'radius open' and 'min. size'). There is little instruction available regarding what these parameters do or how best to optimise them, which results in trial-and-error optimisation required for each well during analysis. This technique not only increases the time required for analysis but also produces an inherent point of subjectivity and variability within the image analysis process. Secondly, a single image can report multiple area measurements if the gap is not detected as a single entity by the MRI Macro, so each image had to be inspected in order to allocate the correct gap area to the correct timepoint **(**Figure 43). Finally, the desired output metric was a gap closure rate, measured in μm/hour. As the MRI Macro reports gap area, further data analysis was required.

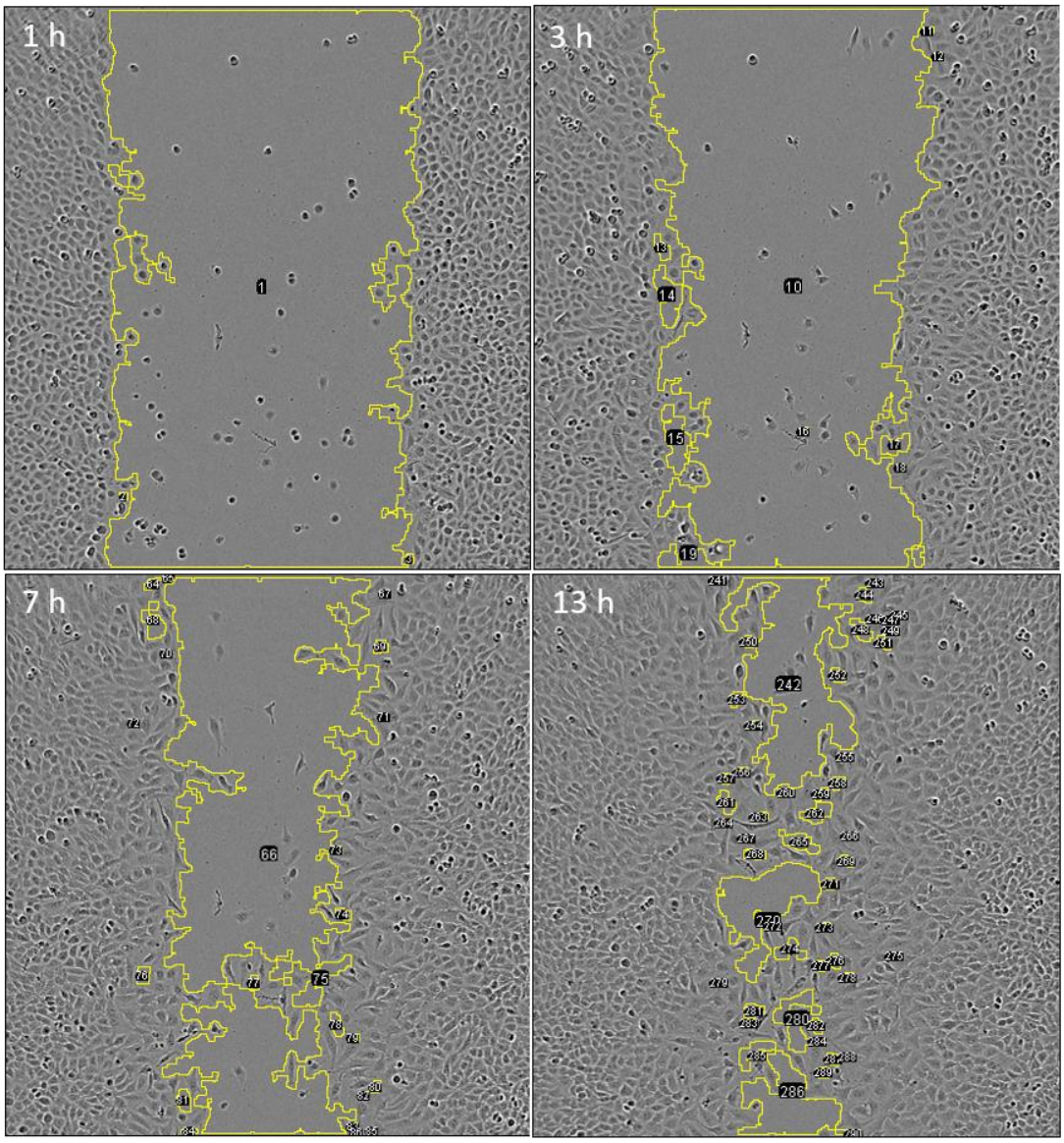

Figure 43: Representative images from the MRI Macro analysis showing multiple gap area measurements for a single image. *The MRI Macro measures the gap area within each image. During gap closure, the gap is not detected as a single entity, and so at later time points multiple gap areas are detected and reported. In the 1 h image, only a single gap is detected. At 3, 7 and 13 h, 10, 23 and 50 separate portions of the gap are detected. Each gap area is numbered on the image and in the macro-generated results sheet. The total gap area for each timepoint must be calculated by cross referencing the images with the output sheet and calculating the sum of all detected gaps within a single image, which is not done by the MRI Macro.*

In order to address these points, an image analysis program was written in-house using the Python programming language ('Python Code', Section 3.5.1). The performance of the Python Code was compared to both the Manual Measurements and the MRI Macro methods using a set of test wells (Section 3.5.2). Once the analysis method had been chosen, the

experimental parameters were optimised (Section 3.5.3). Specific experimental parameters investigated were the method of generating the gap (Ibidi Inserts vs EssenBio WoundMaker), cell seeding densities and serum concentrations during the experiment. The effect of irradiation on cell migration was then investigated in the panel of adherent cell lines (Section 3.5.4).

3.5.1 Python Code development

The analysis workflow for the Python Code is shown in Figure 44. The data generation and image processing steps are carried out by the user, then the processed images are imported by the Python Code, which then guides the user through the parameter determination step. Mask application, image analysis and data analysis are carried out automatically by the Python Code.

The raw data are time-lapse image series of each well taken using the IncuCyte Zoom (for representative image, see Figure 45A). The image processing step is carried out manually using ImageJ. First, a central portion of the gap was selected to exclude the far ends, which undergo gap closure horizontally and vertically (Figure 45B). The frequency distribution of number of pixel rows in processed images (Figure 45C) shows that cropped images were between 50 and 900 pixel rows in height. Images with <100 rows of pixels were excluded from further analysis. No further manual image processing is required.

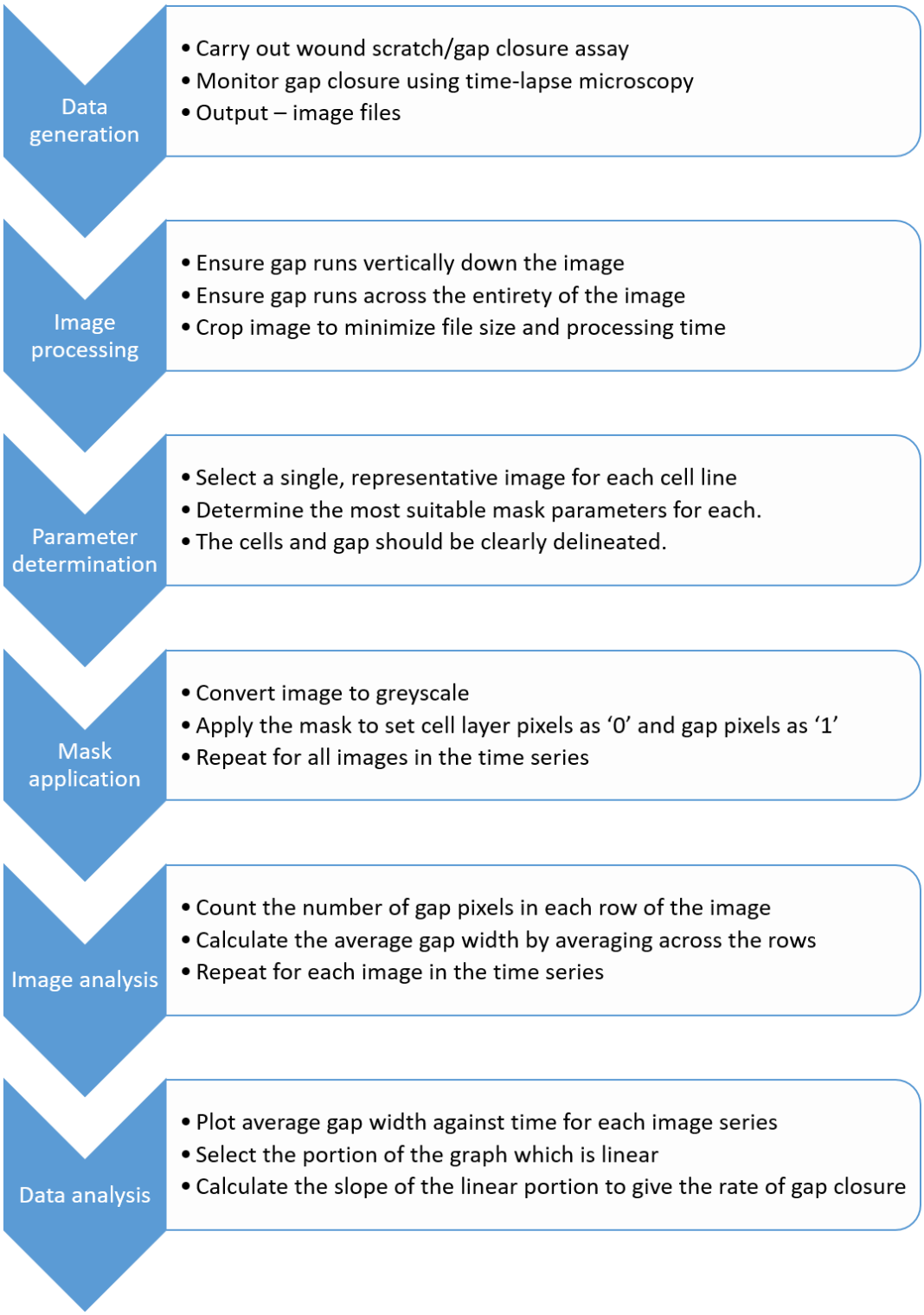

Figure 44: Overview of the Python analysis program ('Python Code') process for gap closure assay analysis.

The software allocates each pixel as belonging to the cell monolayer or to the gap based on the pixel intensity. The number of 'gap' pixels along each pixel row are counted. The distance covered by each pixel is a known characteristic of the objective used to capture the image, and is used to convert the number of 'gap' pixels into a measurement of distance. This process is repeated for each image within the time series. The software then plots and presents the gap width over time (Figure 46). Gap width decreases in a linear manner until the gap has almost completely closed, at which point the decrease plateaus off. The software allows the user to define where the linear portion begins and ends, then calculates and reports the gap closure rate by calculating the slope of the line over this portion of the graph.

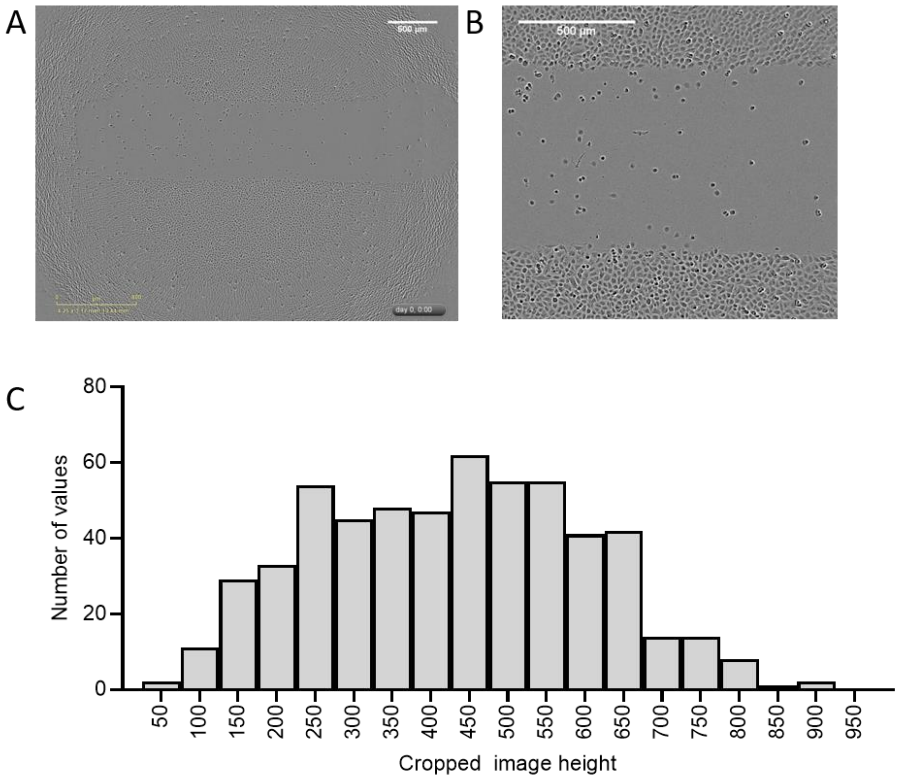

Figure 45: Representative images from the IncuCyte Zoom and frequency distribution of number of measurements taken for each well. *Raw (A) and processed (B) images for a gap closure assay are shown for ONS-76, 0 Gy at t=1 h post-scratch. The raw images taken in the migration experiment included the whole scratch (A). Images were then cropped to exclude the scratch edges (B). The cropped images were then processed by Manual Measurements, the MRI Macro or the Python Code analysis methods. In order to produce a statistically robust data set, a minimum of 100 measurements of gap width per image is recommended (applicable to Manual Measurements and Python Code methods only). The Python Code measures gap width along each row of pixels of an image. The frequency distribution of the number of measurements per image set across all experiments confirms most met this requirement (C). Images with fewer than 100 rows of pixels following manual processing were excluded from analysis.*

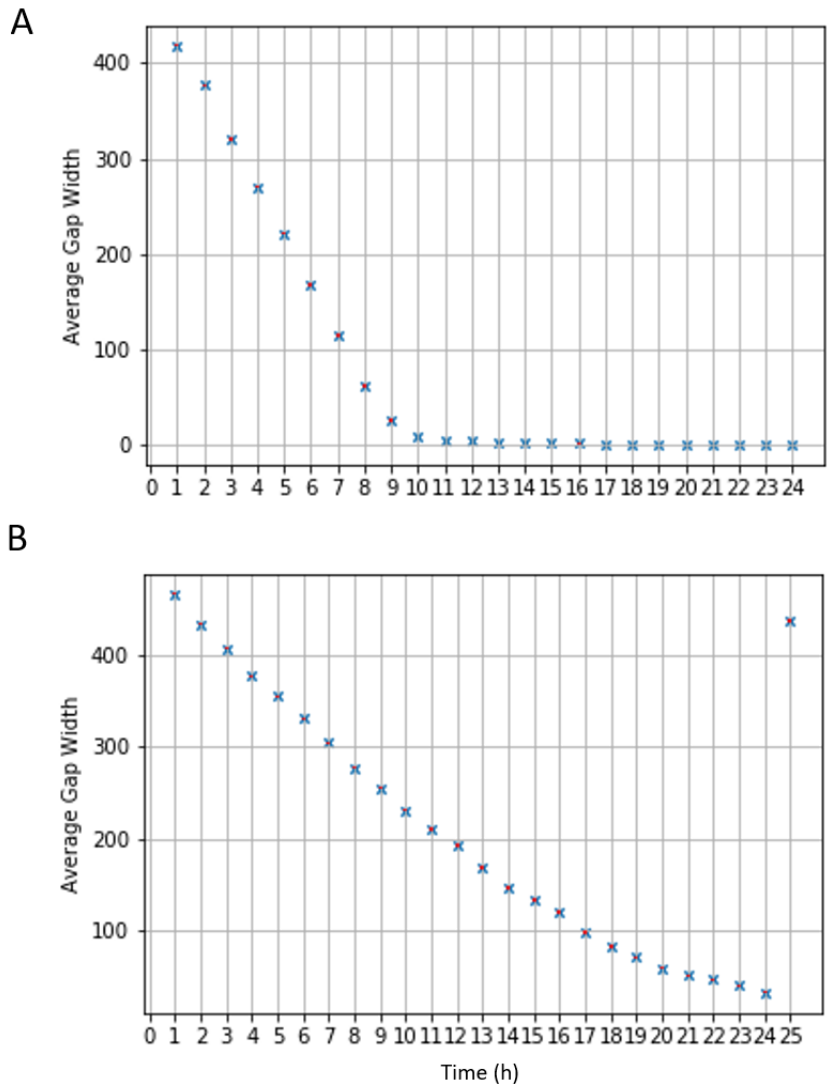

Figure 46: Example graphs produced by the Python Code for calculating gap closure rate. *Representative plots for the cell lines ONS-76 (A) and UW228-2 (B) after 0 Gy of radiation using the Ibidi insert gap creation method are shown. The analysis program plotted gap width against time, which is then displayed to the user who identifies the linear portion. The slope of the linear portion gives giving the gap closure rate. For ONS-76 the slope was calculated between the 2 h and 8 h time points. For UW228-2 the linear portion was selected between 1 h and 13 h.*

3.5.2 Evaluation of methods for gap closure analysis

The in-house analysis program (Python Code) was compared with the Manual Measurements and MRI Macro. This comparison was carried out on six test wells and two cell lines. ONS-76 and UW228-2 were selected to represent a simple and more challenging

analysis respectively due to the definition of the gap edge, which affects the ability of the automated software to accurately identify it (Figure 47).

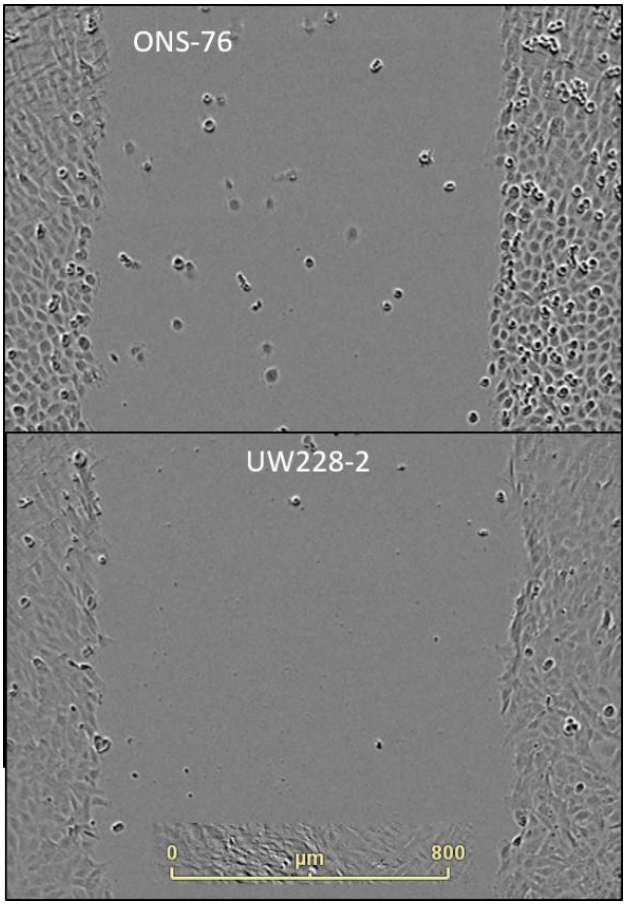

Figure 47: Representative cropped images of gaps for ONS-76 and UW228-2. *For evaluation of the analysis software, a cohort of sample data was established using three ONS-76 and three UW228-2 replicates from WoundMaker experiments. All six wells were unirradiated. A serum concentration of 1% FBS was used following irradiation to reduce the impact of cellular proliferation. Images were manually cropped in the same way for all three analysis methods. These cell lines were selected to test the analysis methods as they represent a well-defined gap edge (ONS-76) and a less-well defined gap edge (UW228-2).*

The first point of comparison was the time required for analysis, which is shown in Figure 48 as the analysis time taken per well (in minutes) and per image (in seconds). This distinction is made to account for the different numbers of images analysed by the automated methods compared to the manual methods. As expected, automated analysis methods were significantly faster than Manual Measurements, with the Python Code faster than the MRI Macro for both cell lines. The Python Code significantly reduced analysis time requirements compared to other available methods.

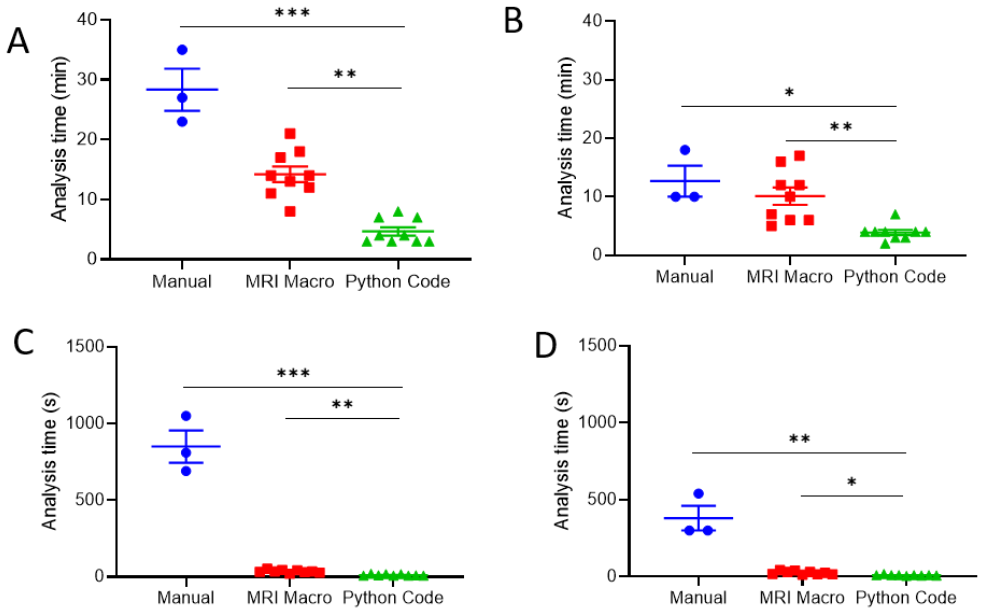

Figure 48: The time taken to analyse a single well or image using the three analysis methods. *Three individual wells for ONS-76 or UW228-2 were analysed and the analysis time taken was measured. Manual Measurements took the longest time per well for both ONS-76 (A) and UW228-2 (B). The Python Code required significantly less time to complete the analysis than the MRI Macro (One-way ANOVA followed by Kruskall-Wallis test). To account for the different number of images analysed, the analysis time per image was calculated for ONS-76 (C) and UW228-2 (D) cells. Manual Measurements took the longest time per image, with the Python Code faster per image than the MRI Macro. * p<0.05, ** p<0.01, *** p<0.00, One-Way ANOVA.*

The second point of comparison was how accurately the automated methods defined the gap edge compared to Manual Measurements. A single image was analysed with all three methods (Figure 49). The two automated methods returned suitable contouring when compared to the Manual Measurements. The MRI Macro was slightly more cautious at the gap edge, tending to apply a margin around cells into the gap. Debris located close to the gap edge was brought into the cell layer by both automated methods, but occurred less frequently with the Python Code.

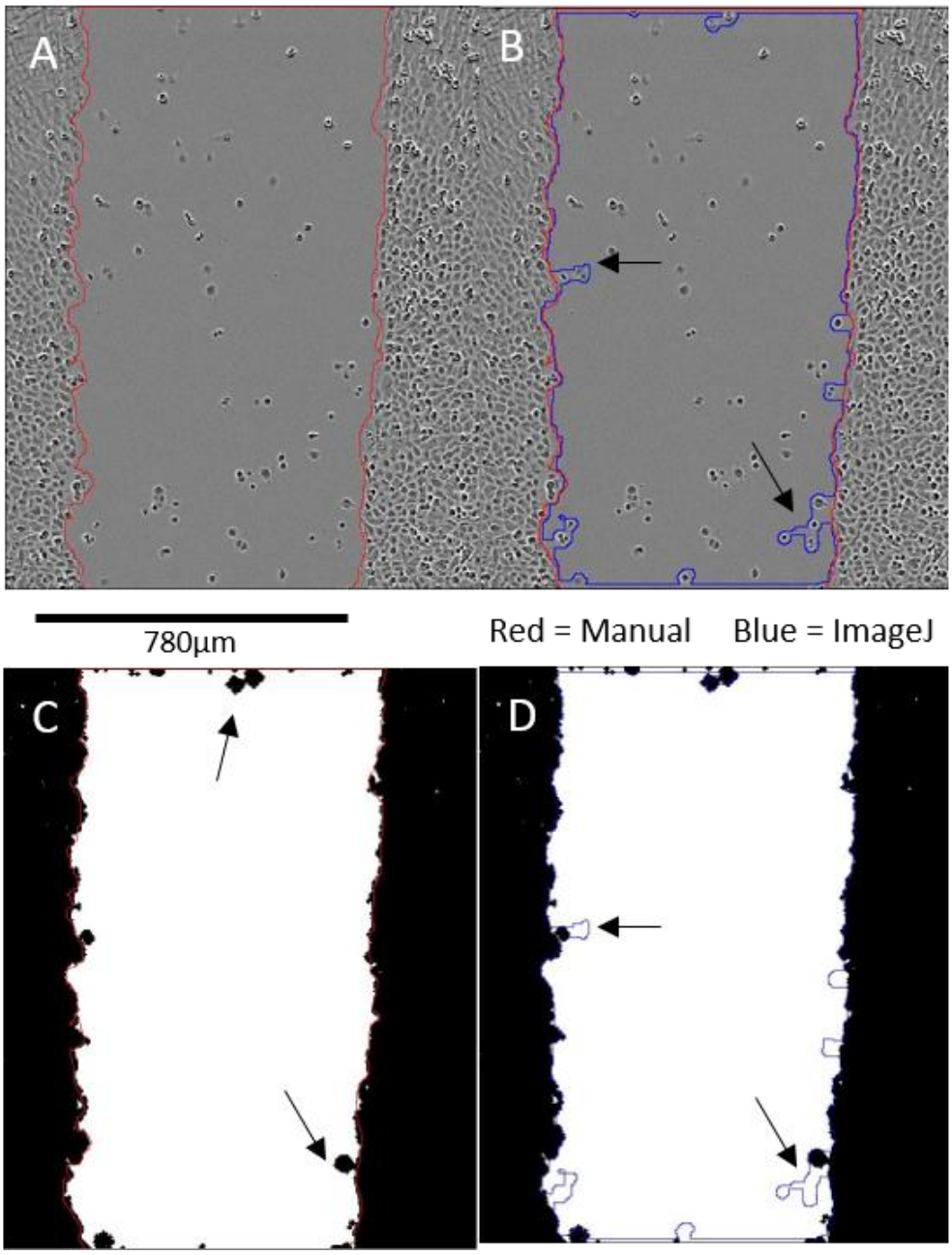

Figure 49: Comparison of the definition of the gap area between the three analysis methods. *A representative image of a gap created by the WoundMaker was processed using the three analysis methods. (A) Manual Measurements (red) only. (B) Manual Measurements (red) and MRI Macro (blue) overlays. (C) Manual Measurements (red) overlay on top of the Python Code image output (gap is shown in white). (D) MRI Macro (blue) overlay on top of the Python Code image output (gap is shown in white). Both the MRI Macro and the Python Code assigned debris located in the gap as part of the gap edge (highlighted in (B) and (C)). The MRI Macro analysis did so to a greater extent, with a larger margin than the Python Code (highlighted in (D)).*

The initial gap area for the six test wells was calculated for each method and normalised to the area reported by Manual Measurements (Figure 50). Automated analysis methods reported lower initial gap area for both of the cell lines. Although the decrease in gap area

was significant with the MRI Macro, the automated methods should be consistent across all time points and therefore the gap closure rate will be unaffected.

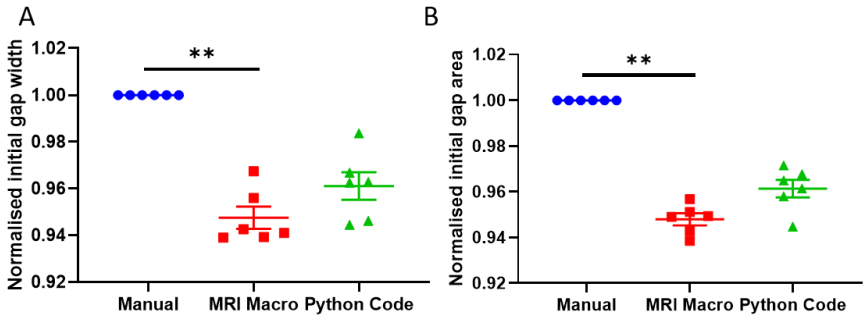

Figure 50: The initial gap area and width measured by the three analysis methods and normalised to the Manual Measurements. *Three individual wells for ONS-76 or UW228-2 were analysed on three separate occasions, and the average initial gap area (μm; A) or width (μm^2; B) was calculated from these analyses. To allow for all wells to be pooled, each well was normalised to the manually measured gap width/area. There was no difference in the measured initial gap area or width between the Manual Measurements and the Python Code. A significantly lower gap area and width was reported by the MRI Macro compared to the Manual Measurements. Each data point represents measurement of a single well. The y-axis scale does not start at 0 to better show differences in analysis methods. ** p<0.01, Friedman test.*

Figure 51 shows the gap width plotted against time for a single test well, with the gap width measured by the three analysis methods. Due to time requirements of Manual Measurements, data are only available for six hours of the experiment.

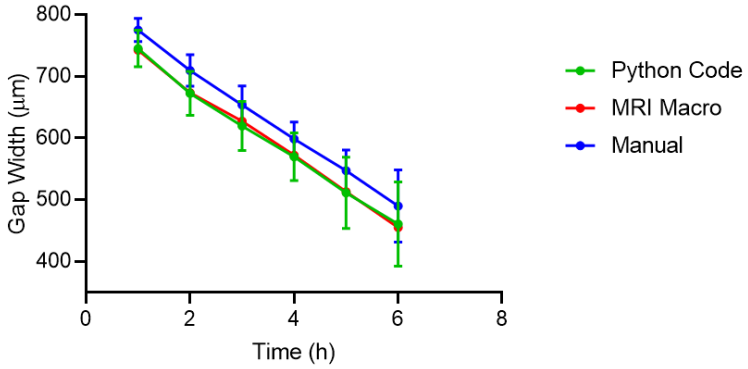

Figure 51: The change in gap width for a representative well using three analysis methods. *A single replicate well was analysed by the three analysis methods. The Manual Measurements and Python Code methods measure the gap width at various points along the image. Data points for these methods represent the mean ± SEM of the gap width measured along each pixel row within the image. The MRI Macro only outputs the gap area at each time point. Data points for this method represent the total gap area divided by the image height. Although the individual measurements are lower following automated analysis, the slope, representing the change in gap width over time is not altered by the analysis method used.*

For both automated analyses, the measured gap width was reduced compared to the manually measured gap width. Importantly, however, the slope is consistent across analysis methods. The slope is used to calculate the gap closure rate, therefore the slight decrease in reported gap width is acceptable.

A key comparison of the three methods is the gap closure rate. Figure 52 shows the calculated gap closure rate for the three wells per cell line from the three analysis methods. Manual Measurements were carried out on one occasion only, while the automated analyses were repeated three times, therefore nine data points are reported. For ONS-76, the gap closure rate was significantly higher when calculated using the Manual Measurements compared to either of the automated analysis methods. For UW228-2, the MRI Macro reported a gap closure rate that was significantly reduced compared to either of the other methods. No difference between the Manual Measurements and the Python Code methods was observed. ONS-76 cell lines have a much faster gap closure rate and close the gap within 10-12 h, while UW228-2 cells often had not completely closed the gap at the final 24 h time point. The differences may be because the Manual Measurements method uses only two time points to calculate rate of gap closure, unlike the automated analyses, which use the complete time-course data and the linear period of gap closure.

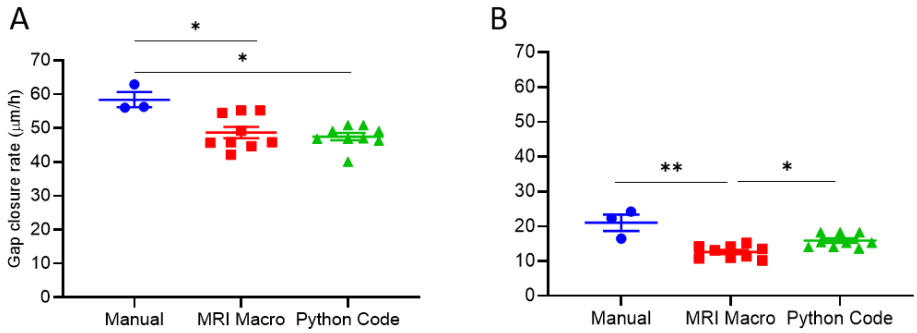

Figure 52: Gap closure rates generated using three different analysis methods. *Three wells of each of the two cell lines were analysed manually on one occasion and on three separate occasions using the automated analysis methods. The Manual Measurements reported rate of gap closure was higher than the rates calculated using the automated methods in both ONS-76 (A) and UW228-2 (B). As the Manual Measurements rate is calculated from two time points only, while the automated methods use multiple time points to generate a line of best fit and take the rate from the slope, it is not unexpected that the Manual Measurements method over-estimates the gap closure rate. * p<0.05, ** p<0.01, One-Way ANOVA.*

The use of automated methods is preferable if they reduce subjectivity within image analysis. Subjectivity is reduced by removing points where the user can influence the results. A few automated analyses programs have removed these points completely (e.g. PyScratch[554]). Our images could not be analysed with PyScratch because when the program did not correctly identify the scratches it was not possible for the user to correct the error. The MRI Macro and Python Code retain some user decision points when optimising image masking parameters. In the MRI Macro, these are the variance filter radius (VFR), the threshold, the radius open (RO) and the minimum size. In the Python Code, these are the upper and lower bounds of the mask and the number of iterations carried out. Analysis of the test wells was repeated three times at weekly intervals by the same user to assess intra-user variation. The user-defined parameters from each week are shown in Table 24.

Table 24: Parameters used for automated analysis for each well over the three weeks.

		MRI Macro				Python Code		
	Week	VFR	Threshold	RO	Minimum Size	UB	LB	Iterations
Well 2	1	1	50	4	1	0.46	0.54	2
	2	1	50	4	1	0.47	0.55	2
	3	1	25	3	1	0.46	0.55	2
Well 3	1	1	75	4	1	0.46	0.55	2
	2	2	50	4	1	0.45	0.54	2
	3	1	50	3	1	0.46	0.55	2
Well 4	1	1	75	4	1	0.46	0.55	2
	2	5	50	4	1	0.46	0.54	2
	3	1	40	3	1	0.44	0.55	2
Well 8	1	10	75	4	1	0.47	0.55	3
	2	3	25	4	1	0.47	0.55	3
	3	1	40	3	1	0.47	0.55	3
Well 9	1	10	75	4	1	0.46	0.54	3
	2	3	50	4	1	0.46	0.54	3
	3	1	40	3	1	0.47	0.55	3
Well 10	1	1	25	4	1	0.47	0.54	3
	2	2	20	4	1	0.47	0.53	2
	3	1	40	3	1	0.47	0.54	3

**VFR – variance filter radius; RO – radius open; UB – upper bound; LB – lower bound*

The parameters for the Python Code were more consistent both between weeks and between wells. The parameters for the MRI Macro varied not only between weeks but also within the wells of each cell line. While changes in the pixel intensity values used to define the mask by the Python Code did vary slightly, these variations did not alter the reported gap areas or gap widths (Figure 53). With regard to the gap closure rate output, the calculated rate remains consistent across the three week period, with the exception of one ONS-76 well (Figure 53C).

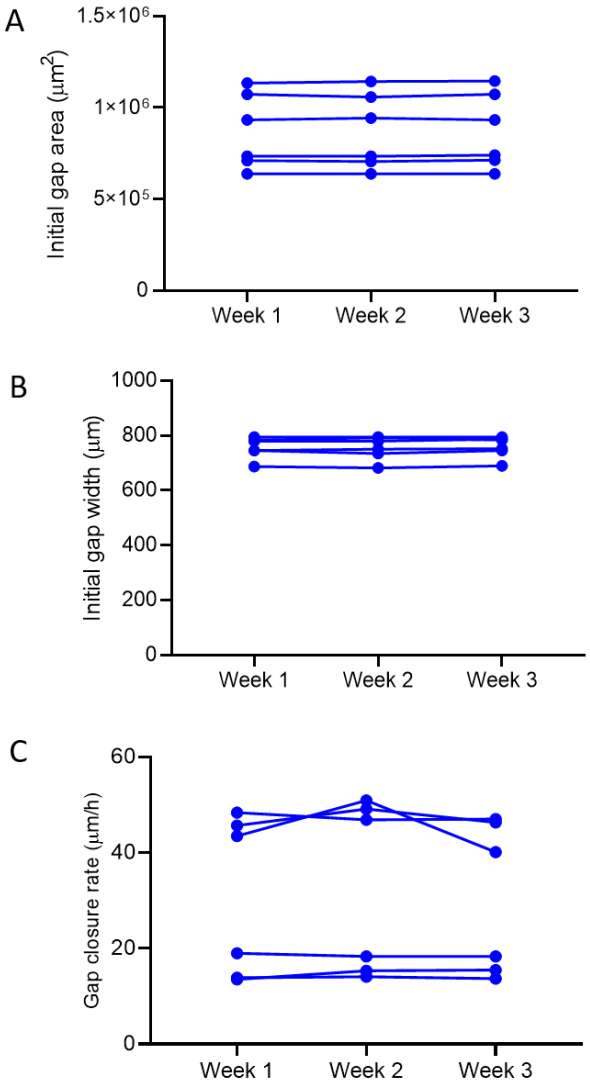

Figure 53: The intra-user variation over time when analysing gap closure experiments using the Python Code. *Three wells of each of the two cell lines were analysed on three separate occasions. The initial gap area and initial gap width measurements (A and B respectively) were calculated for each well across the three weeks of analysis. The gap closure rate (C) was calculated for all wells of UW228-2, which slight variation occurred in the analysis of one well of ONS-76.*

3.5.3 Migration assay method development

Two methods of gap creation were used in this work – the Ibidi inserts (Section 2.7.2) and the EssenBio WoundMaker (Section 2.7.1). The inserts use an occlusion technique to prevent cell adhesion and growth and produce a gap. The WoundMaker physically scrapes a line of cells off the culture surface. The method of generating the gap may contribute to the response of the cells and the nature of the gap closure. When comparing the results, the effect of gap creation method on gap closure rate was different between cells within our adherent cell line panel (Figure 54).

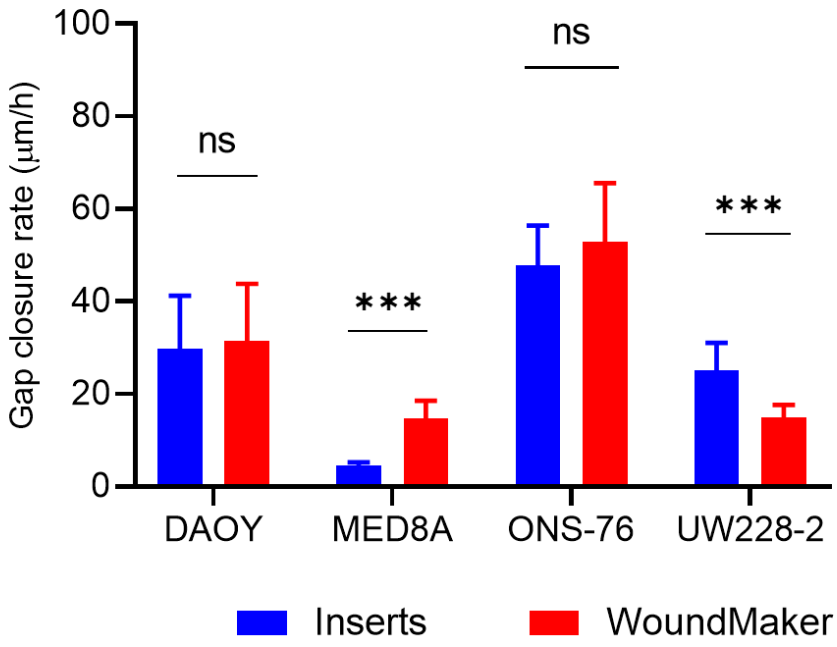

Figure 54: Gap creation method can affect gap closure rate. *Migration experiments using the Ibidi inserts or WoundMaker were carried out. Individual well results across multiple experiments were pooled and averaged. Data were generated using 1% serum concentration. For DAOY and ONS-76 the gap creation method did not affect the gap closure rate. For the MED8A cell line, gap closure was almost four times faster using the WoundMaker than the Ibidi inserts. For UW228-2 the opposite was observed, with the Ibidi inserts producing a faster gap closure rate. The mean ± SEM gap closure rate of ≥ 3 replicate wells is shown for each condition. *** p<0.001, t-test.*

The gap closure rate was unaffected by creation method for DAOY and ONS-76. In MED8A, the insert method resulted in a much slower gap closure rate. For UW228-2, the insert method resulted in a faster gap closure rate. As the gap creation method appeared to be an

influential factor in gap closure rate, comparisons were only made between experiments using the same methodology.

Figure 55 shows the results of seeding density optimisation tests using the two gap creation methods (Ibidi inserts and EssenBio WoundMaker). Both methods required a confluent monolayer of cells in which to create the gap. In order to confirm whether the number of cells used to create a confluent monolayer affected the rate of gap closure, two different seeding densities were used. For DAOY, ONS-76 and UW228-2 both seeding densities produced a confluent monolayer. For MED8A, only the higher seeding density produced a confluent monolayer, and this cell line was the only one to show a difference in gap closure rate depending on seeding density.

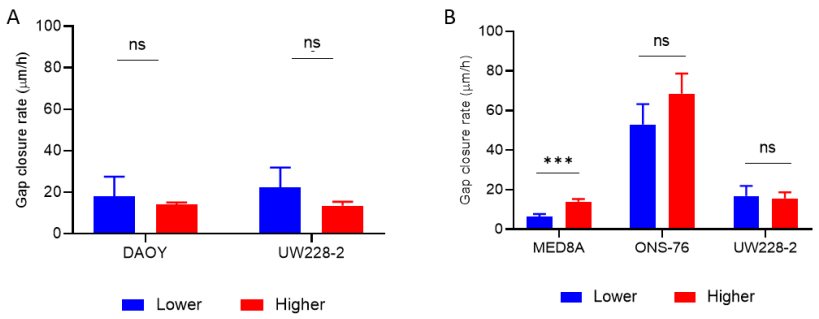

		Lower	Higher
Insert	DAOY	70,000	84,000
	UW228-2	70,000	84,000
WoundMaker	MED8A	40,000	50,000
	ONS-76	15,000	20,000
	UW228-2	15,000	20,000

Figure 55: The effect of seeding density on gap closure rate on the four cell lines using the two gap creation methods. *Migration experiments using the Ibidi inserts (A) or WoundMaker (B) were carried out using two seeding densities. The Ibidi insert data were generated over multiple experiments and calculated from individual well gap closure rates at 10% serum concentration. The WoundMaker data were generated from multiple wells over a single experiment at 1% serum concentration. In all experiments, DAOY, ONS-76 and UW228-2 cell seeding densities produced a confluent monolayer. For MED8A, only the higher seeding density (50,000 cells/well) produced a confluent monolayer, and this was the only cell line where a significant difference in gap closure rate was seen between seeding densities. The mean ± SEM gap closure rate of ≥ 3 replicate wells is shown for each condition. *** p<0.001, t-test.*

The gap closure may result from cells moving into the gap, or may result from cells proliferating into the gap. While cell proliferation can be pharmacologically inhibited, this runs the risk of interactions between the inhibiting drug and irradiation. A compromise is made by

using a confluent cell monolayer, which should reduce cell proliferation (although this is not certain, particularly with cancer cell lines which do not show contact inhibition) and minimising the time over which the experiment is conducted, to minimise the number of population doublings that can occur. Another measure is to reduce serum concentration, thus reducing the concentration of growth factors present within the medium. Figure 56 compares the gap closure rate calculated following experiments conducted using 1% or 10% serum concentration. For the cell lines MED8A and UW228-2, there was no significant change in gap closure rate when the serum concentration was reduced. For the cell lines DAOY and ONS-76, reducing the serum concentration significantly increased gap closure rate. These cell lines have shorter Tds than that of the unaffected cell lines, which may be why the serum concentration affects the gap closure rate.

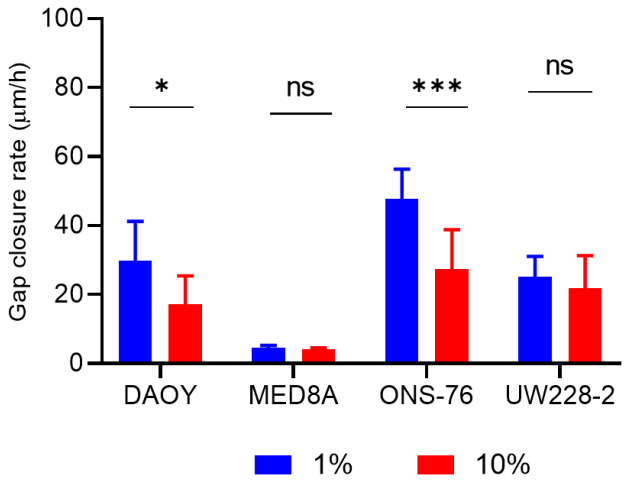

Figure 56: Serum concentration can affect gap closure rate. *Migration experiments using the Ibidi were carried out with the concentration of serum in the medium either kept at 10% throughout the experiment, or changed to 1% FBS at the time of irradiation. Individual well results across multiple experiments for 0 Gy were pooled and averaged. For MED8A and UW228-2, the serum concentration had no effect on the gap closure rate. For DAOY and ONS-6, reducing the serum concentration from 10% (red) to 1% (blue) significantly reduced the gap closure rate. These two cell lines have shorter population doubling times. Reducing the serum concentration in migration experiments is done with the aim of reducing the cell proliferation and differentiating between migration into the gap and proliferation into the gap. The doubling time of these two cell lines is short enough that affecting it would be observed over the 24 h experiment, whereas this is not the case for the other two cell lines. The mean ± SEM gap closure rate of ≥ 3 replicate wells is shown for each condition. * p<0.05, *** p<0.001, t-test.*

The first image that was practical to generate with time-lapse microscopy was 1 h post scratch, due to the equilibration of the microscope and plate once loaded in the incubator. At 1 h the gap has already begun to close therefore the initial gap width cannot be measured. If

the gap closure rate is affected by radiation, the amount of gap closure during the equilibration time would not be consistent across the radiation doses. To confirm that the initial gap width was unaffected by irradiation, samples were irradiated with 0, 2 or 8 Gy, incubated for 24 h then fixed using formalin immediately following gap creation (t=0 h) using the WoundMaker (Figure 57). The width of the gap created was consistent across all wells, and was not affected by irradiation dose.

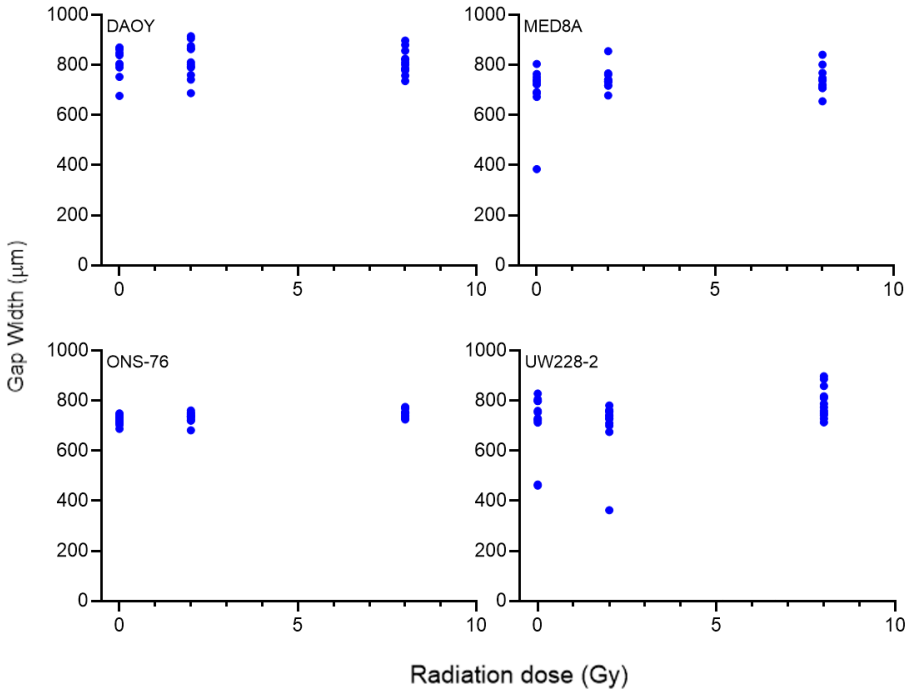

Figure 57: The initial gap width is not changed by irradiation. *A 96-well plate was irradiated with 0 Gy, 2 Gy or 8 Gy 24 h prior to the migration assay. Immediately after the scratch was made, the medium was removed and the cell monolayer was fixed with formalin. Fixed plates were scanned using an IncuCyte Zoom and images analysed in the same manner as for the time-lapse images. The initial gap width is shown. Increasing radiation dose had no effect on the size of the initial scratch created by the WoundMaker.*

Figure 58 shows the inter- and intra-assay variation for the gap closure experiments. Intra-assay variation for each of the four adherent cell lines was high with both the insert and WoundMaker methods. As the WoundMaker experiments were a 96-well plate format as opposed to the Inserts 12-well layout, a higher number of wells per assay could be carried out. For both gap creation methods, the inter-assay variation was found to be relatively high and was more obvious in the SHH cell lines, due to their faster rates of gap closure. Gap closure rates varied by as much as 50% between assays.

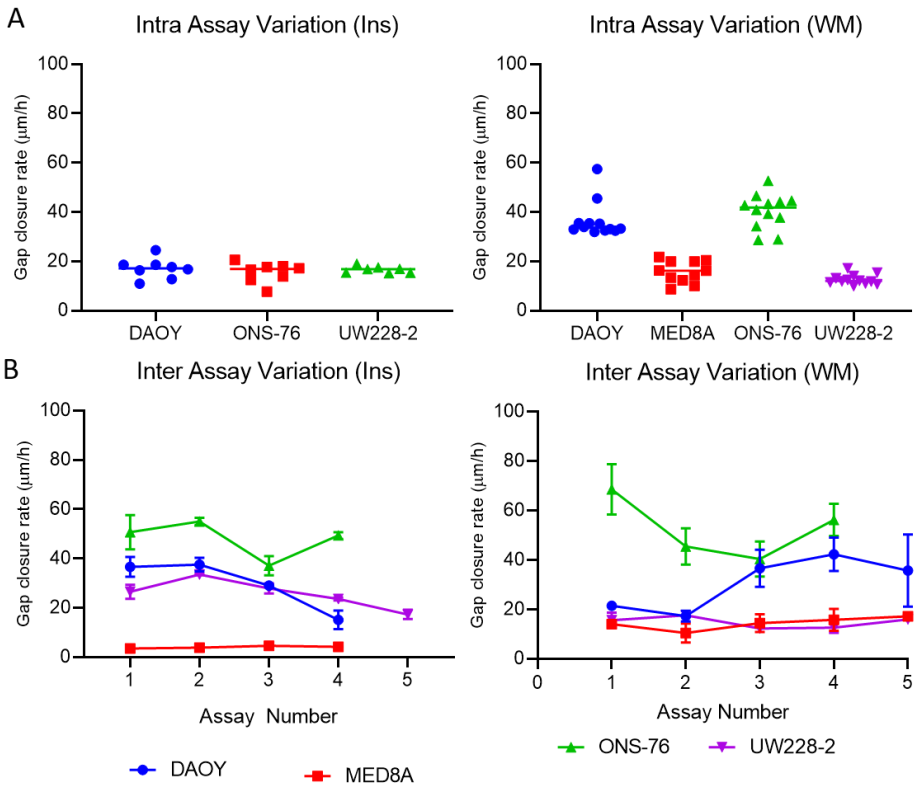

Figure 58: The intra- and inter-assay variation observed in gap closure rate experiments. *(A)The intra-assay variation calculated from either 8 inserts, Ins) or 12 (WoundMaker, WM) technical replicates at 0 Gy in a single experiment. (B) The inter-assay variation calculated from 0 Gy wells (n≥2) in each assay carried out with either the Insert or WoundMaker method.*

3.5.4 Migration assay results

The effect of radiation on migration was investigated with a series of gap closure experiments. Following the development worked described previously, a seeding density to produce a confluent monolayer and a 1% FBS concentration was used. Both methods of gap creation were included in the radiation work in case the method of gap creation (occlusion vs physical removal of cells) influenced the radiation response. Cells were irradiated 0 h, 24 h and 7 days prior to the generation of the gap, and gap closure rate was analysed using the Python Code.

When the irradiation was carried out immediately prior to the generation of the gap, no statistically significant changes in gap closure rates were observed for the cell lines MED8A and UW228-2 (Figure 59). No statistically significant changes were observed with the remaining cell lines using the Ibidi insert method. Following 8 Gy of irradiation, when DAOY

cells were removed with the WoundMaker, gap closure rate was significantly reduced compared to 0 Gy. For ONS-76 in the WoundMaker assay, gap closure rate was significantly increased following 8 Gy of irradiation compared to 0 Gy. There is a lack of context for this result, as, while the insert method allowed a complete data set to be generated for all four cell lines at all three doses, the WoundMaker dataset is limited to 8 Gy only. A high number of wells were excluded from analysis due to destruction of the cell monolayer and/or excessive debris blocking the image field.

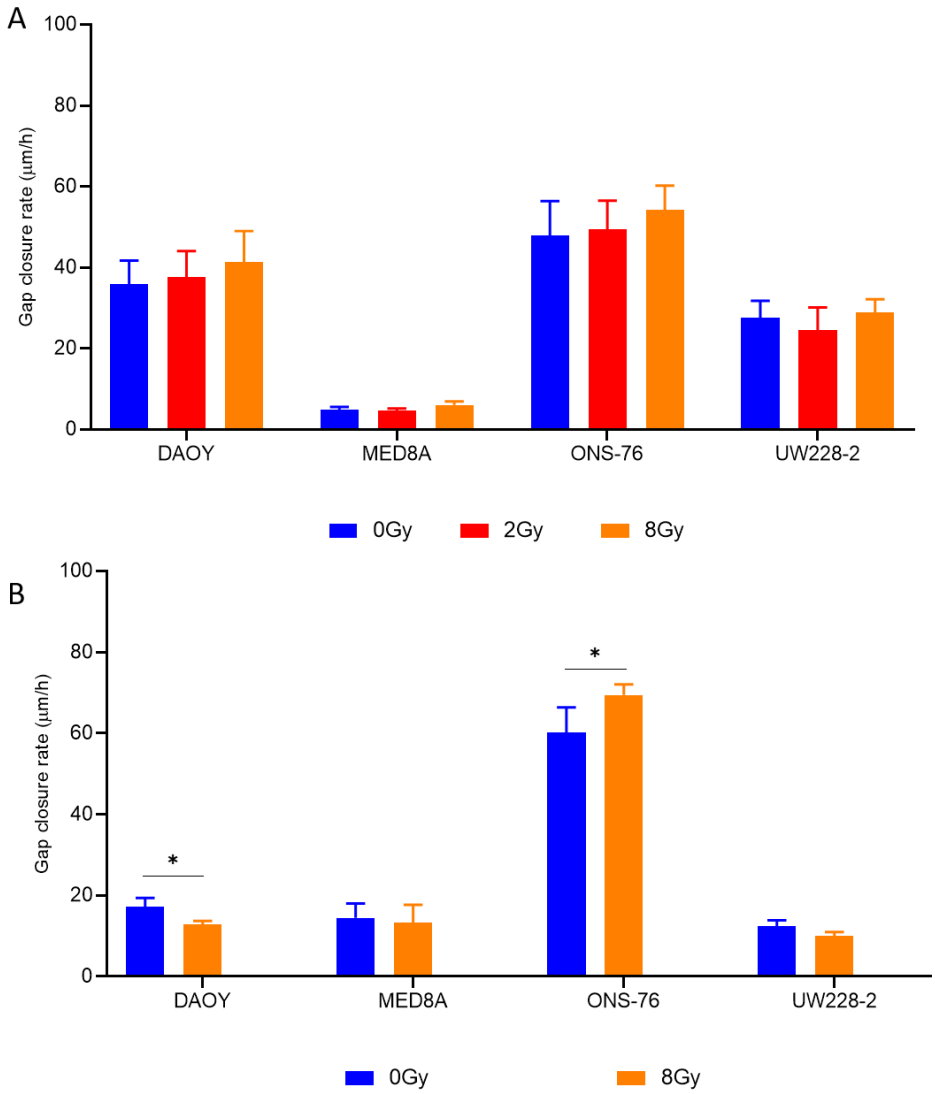

Figure 59: The effect of immediate radiation on gap closure in the four adherent cell lines. *Migration experiments using the Ibidi inserts (A) and WoundMaker (B) were carried out. Cells were irradiated 0 h prior to gap creation. When the Ibidi insert method was used immediately following irradiation, no effect of radiation on gap closure rate was observed in any of the cell lines. Immediate radiation experiments were limited when using the WoundMaker. A high number of well failures excluded all 2 Gy replicates from analysis. A slight radiation effect was observed between 0 Gy and 8 Gy in DAOY, with radiation reducing gap closure rate and in ONS-76, with radiation increasing gap closure rate. * p<0.05, Mann-Whitney U test.*

The complete insert data set indicates a general trend for dose-dependent increases in gap closure rate with irradiation, although this trend is not statistically significant. As there is little time for any cellular adaptation in response to irradiation in this experimental format, a lack of response is unsurprising. A 24 h delay in gap creation following irradiation was added (Figure 60). Also shown are the results from Ibidi insert experiments where gap creation was carried out 7 days after the cells were irradiated.

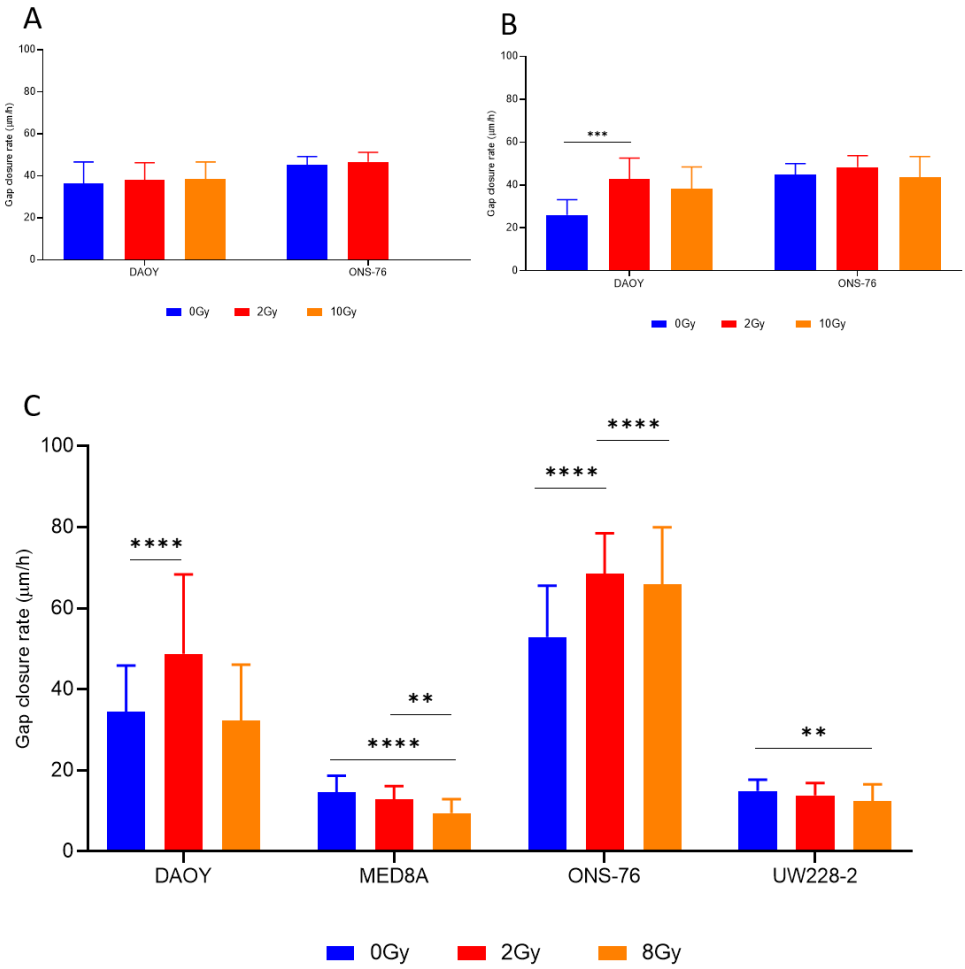

Figure 60: The effect of delayed radiation on gap closure rate following irradiation. *Migration experiments using the Ibidi Inserts or WoundMaker were carried out. Using the Ibidi insert method, cells were irradiated at either 24 h (A) or 7 days (B) prior to gap creation. Gap closure rate was increased for DAOY cells 7 days after 2 Gy of irradiation (Kruskall-Wallis test, p=0.0066). In MED8A and UW228-2 increasing radiation doses decreased gap closure rate. In DAOY and ONS-76, 2Gy caused an increase in gap closure rate, but increasing the dose to 8 Gy removed this effect. * p<0.05, ** p<0.01, *** p<0.001, Kruskall-Wallis test.*

As was seen with the immediate radiation, no change in gap closure rate was observed using the Ibidi inserts. Again, DAOY showed an exception, as a significant difference occurred at 7 days post irradiation, where 2 Gy increased gap closure rate compared to 0

Gy. This was in stark contrast to the results with the WoundMaker when a 24 h delay between irradiation and gap creation resulted in significant differences between control and irradiated cell gap closure for all four cell lines. For DAOY and ONS-76, gap closure rate was highest after 2 Gy of radiation. For MED8A and UW228-2, a dose-dependent decrease in gap closure rate was seen. These cell line groupings are not consistent with the molecular subgroups.

4. Discussion

4.1. Cell growth curves

4.1.1. The MBL cell line panel

The *in vitro* work of this project was conducted using a panel of established human cell lines as a model of MBL. The advantages of using established cell lines are that they are better characterised, have lower associated costs and are more readily available than primary cell cultures. There are well-established *in vitro* assays to measure parameters of interest such as radiosensitivity and cell migration in cell cultures. Our panel contained cells representing the SHH and Group 3 subgroups, but included no WNT or Group 4 subgroup cell lines. This is reflective of the entire collection of available MBL cell lines as, of the lines that have been subtyped, the majority are SHH or Group 3[556]. In fact, only one cell line has been described for each of the WNT[557] and Group 4[558] subgroups. The established cell lines are not reflective of the MBL patient population as all Group 3 cell lines are *MYC* amplified and 50% of SHH cell lines are *TP53* mutated, neither of which reflect the clinical situation[117]. Future work would involve expanding the cell line panel to include the WNT and Group 4 cell lines.

D283 and D425 are semi-adherent cell lines, which maintain relatively constant proportions of suspension and adherent cells. The semi-adherent phenotype excluded these cell lines from use within the standard clonogenic or gap closure assays and therefore their use in this thesis was restricted to the high-throughput assay only. The suspension cells within each culture grow as clusters suspended in the medium, while the adherent cells grow sparsely on the culture vessel surface forming clumps and colonies. Any influencing factors that determine the individual phenotypes of the cells within these lines have not been investigated, and both cell phenotypes are treated as a single culture in *in vitro* studies[559–563]. The results from the cell growth curves presented here demonstrate that external conditions such as hypoxia can alter the relative proportions of suspension/adherent cells within a culture. Under 0.1% oxygen, the proportion of D425 cells in suspension was significantly increased. If the change in cell phenotype is a reflection of underlying biological differences,

such as CD133-positivity, then these influencing factors warrant further investigation and characterisation.

The cell membrane protein CD133 was identified as a marker of haematopoietic stem cells[564] but has been used as a stem cell marker in colon cancer[565], Ewing's sarcoma[566], H&N cancer[567], HCC[568], melanoma[569], ovarian cancer[570], pancreatic cancer[571], prostate cancer[572] and brain tumours[573–575] including MBL[273,364,576–578]. CD133-positive (CD133+) cells are CSC-like and as such are more likely to form spheroids in culture[574,576,579], are more radioresistant[576,578–580] and, when high in human tumours, are associated with a worse overall survival[577]. MBL tumour tissue samples from Group 3 patients have the highest CD133 expression[577]. As shown in Table 25, the Group 3 cell lines within the panel also have much higher reported CD133-positivity. The published studies used antibodies against CD133 in flow cytometry protocols to calculate the percentage of CD133+ cells. These antibodies bind to different epitopes of the CD133 protein and these epitopes are subject to glycosylation modifications making them more or less available for binding under different conditions[581,582]. Additionally, using different antibodies on the same sample yields significantly different CD133+ percentages[583]. The variability in reported CD133 positivity across different studies using the same cell line, such as for DAOY or ONS-76, likely results from these differences in antibody specificity and expression of the target epitopes[584].

Table 25: The reported percentage of CD133+ of the medulloblastoma cell lines under normoxia

Cell Line	Subgroup	Phenotype	% CD133 positivity
DAOY	SHH[226]	Adherent	20.6[578] 5.0[501] 0.1[364]
ONS-76	SHH[226]	Adherent	54.5[501] 3.8[273]
UW228-2	SHH[226]	Adherent	1.0[501]
MED8A	Group 3[16]	Adherent	4.8[577]
D283	Group 3[506] Group 4[507]	Semi-adherent (90% suspension)	99.9[578] 90.6[364]
D425	Group 3[506]	Semi-adherent (50% suspension)	45.0[585] 39.1[577]

There is not only a much higher proportion of CD133+ cells within the semi-adherent cell lines compared to adherent cell lines, but also a similar proportion of CD133+ cells as suspension cells reported within these cell lines. As found in the cell growth experiments, over 90% of D283 cells were in suspension, within the range of 90-100% of CD133+ cells in this cell line. For D425, the cell growth experiments found 40-50% of D425 cells were in suspension, again corresponding to the published CD133+ proportions (40-45%). Hypoxic conditions increase the number of CD133+ cells[586–588]., and under hypoxia the proportion of suspension cells is increased for D425[589]. No hypoxia-induced increase was reported for the other semi-adherent cell line, D283, however this may be a result of the very high proportion of CD133+ cells found under normoxic conditions (99.9% in one report[578]) leaving little room for any increase in response to hypoxia.

It is hypothesised that the CD133+ cells within these cell lines make up the suspension population, while the CD133- cells are adherent. If this were the case, there would be implications for measuring the radiosensitivity of these cell lines. CD133+ cells are more radioresistant, and radiation increases the CD133+ proportion within glioma[580], GBM[574] and MBL[576–579] cell lines and in rectal tumours[590]. Cell lines with higher proportions of CD133-positivity would be expected to be more radioresistant and show a greater ability to repopulate a culture following irradiation as a result of the increased CSC-like proportion. This hypothesis would also explain why the radiosensitivity of these cell lines has been reported[270–274] as being less than either that predicted based on their assignment to the Group 3 subgroup or as presented here. Where studies used the clonogenic assay without adaptations for semi-adherent cell lines, the cell lines are more radiosensitive than would be expected. Based on this hypothesis these assays only measuring the radiosensitivity of the CD133-negative portion, which would be expected to be lower.

4.2. Radiosensitivity

The first objective was to investigate whether there were differences between MBL subgroups in radiosensitivity. The hypotheses and results are summarised in Figure 61. Radioresponsiveness is the extent to which a patient or tumour responds to radiotherapy treatment, and results from a combination of individual factors. One of these contributing factors is (intrinsic) radiosensitivity. The intrinsic radiosensitivity of a cell describes how susceptible a cell is to death following irradiation exposure. Cells that are more radiosensitive are more susceptible to death following irradiation, while those that are less radiosensitive (also referred to as more radioresistant) are less susceptible to death following irradiation. The intrinsic radiosensitivity of a cell can be measured *in vitro*, and correlates with observed clinical radioresponsiveness[151,152]. It was hypothesised that differences in clinical outcomes reflected differences in radioresponsiveness between the four molecular subgroups. The WNT subgroup would therefore be the most radioresponsive, followed by the SHH, Group 4 and Group 3 subgroups. Although radioresponsive tumours are, on average, more radiosensitive than those considered less radioresponsive, the molecular characteristics of the molecular subgroups lead to a different hypothesis. Activation of the WNT[92,111,209,212,213,215] and SHH[216–218,220–224] signalling pathways decreases radiosensitivity, and literature data indicated that SHH cell lines are less radiosensitive than Group 3 cell lines[270–274]. The radiosensitivity hypothesis was that the WNT and SHH subgroups would be relatively less radiosensitive than Groups 3 and 4, despite their better clinical outcomes.

The intrinsic radiosensitivity of MBL cell lines and patient samples was assessed. Intrinsic radiosensitivity was significantly associated with overall survival in MBL, and there was a significant difference between the molecular subgroups. Contrary to the radiosensitivity hypothesis of this study and published *in vitro* data, I found that SHH cell lines were more radiosensitive than Group 3. Similarly in patient samples, the SHH subgroup was the most radiosensitive, followed by the WNT, Group 3 and Group 4 subgroups. This finding is consistent with SHH/WNT molecular subtypes being more radioresponsive than Group 3 and 4.

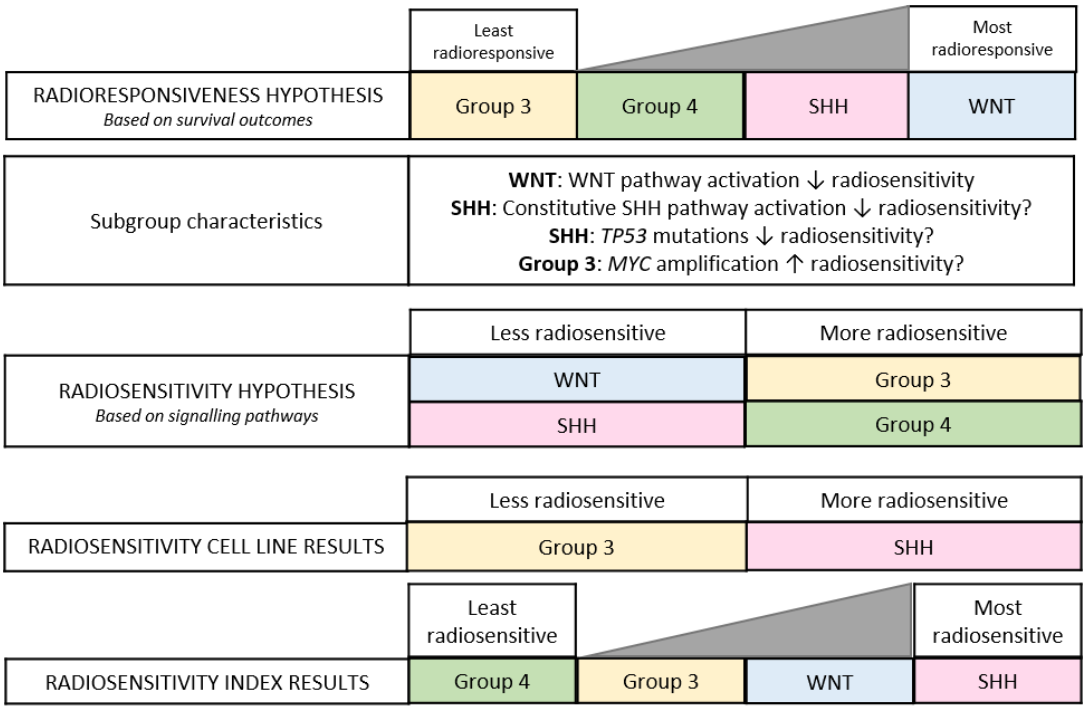

Figure 61: Summary of the radioresponsiveness and radiosensitivity work. *Based on the different survival outcomes, it was hypothesised that the radioresponsiveness rankings were, from most to least; WNT, SHH, Group 4 then Group 3. Observed radioresponsiveness is a result of several factors, one of which is intrinsic radiosensitivity which can be altered by the different subgroup characteristics. Based on these underlying features, it was hypothesised that the WNT and SHH subgroups would be less radiosensitive and the Group 3 and Group 4 subgroups would be more radiosensitive. Cell line work using a clonogenic assay and a high-throughput radiosensitivity assay found that the Group 3 cell lines were less radiosensitive than the SHH cell lines. Analysis of patient data using the radiosensitivity index found the least radiosensitive subgroup was Group 4 followed by Group 3, WNT and SHH. This ranking disagreed with the radiosensitivity hypothesis. There is better agreement with the radioresponsiveness hypothesis, as Groups 3 and 4 are less radiosensitive and less radioresponsive. Subgroup-specific radiosensitivity alone in part reflects the different clinical outcomes, but other contributing factors such as proliferation or tumour hypoxia might influence the radioresponsiveness.*

4.2.1. Clonogenic assay – method development

Following application of a clonogenic assay to the compatible (adherent) cell lines in the cell line panel, method development work of a soft agar colony formation assay was undertaken to adapt the protocol for the semi-adherent cell lines. The soft agar assay has previously been reported to have been applied to D283[512,591,592] and D425[591]. The soft agar colony formation assay uses layers of agar to hold individual cells in suspension where they can divide to form colonies. The cells are therefore not required to adhere to the culture vessel surface in order to be maintained as single cells. In a preliminary experiment, I found colonies were formed in this assay by D283 and D425, but they did not take up iodonitrotetrazolium violet (INT; a marker of viability). The lack of cell viability in the colonies

made it impossible to determine how many cells had survived irradiation (data not shown). An alternative assay, the high-throughput assay using CTG, was applied to the cell line panel[156,185]. The radiosensitivity of patient samples was then assessed using the RSI, a gene signature previously developed and validated within a range of cancers[170,171,207].

All four adherent cell lines formed colonies when seeded at low cell density in 6-well plates. Although the plating efficiencies were low (10-15%), the number of colonies seeded increased linearly with seeding density. The four adherent cell lines were therefore compatible with a clonogenic assay. While the irradiation set-up can influence the clonogenic assay results through parameters such as dose rate, temperature or pH changes and time required for irradiation[175,593,594], survival curves generated at the three sites used during the completion of this thesis were not significantly different, allowing data to be pooled. Although an automated colony counting set up was available, it was not able to accurately identify and count the MBL cell line colonies. The automated method produced higher colony counts than manual counts. This appears in contrast to previous comparative studies, where strong correlations between manual and automated counting methods are reported[595–597]. It should be noted, however, that these reports were conducted either by the automated method developers[595,597] or guided by them[596]. In a study where optimisation of the GelCount appears to have been carried out by a 'standard' user, similar to the setup here, the number of colonies reported by manual counting was significantly lower than the automated method[598]. Without the available expertise required for the GelCount software and in order to produce accurate colony counts and SFs across all cell lines, a manual counting method was used.

The Group 3 cell line MED8A required a higher medium FBS concentration (20%) in order to form colonies following irradiation. The SHH cell lines used complete medium which contained 10% FBS. FBS is required in cell culture medium as a source of nutrients, mammalian cell hormones, growth factors and attachment factors. The concentration of these different components can vary between batches and this is controlled by using a single FBS batch throughout a set of experiments. Increasing the FBS concentration in the

medium enhances colony formation in a dose-dependent manner until a plateau in response is reached[599]. For one of the SHH cell lines, ONS-76, FBS concentration did not significantly alter the PE suggesting for this cell line the plateau occurs before 10% FBS. Altering the concentration of FBS in the culture medium can affect cellular radiosensitivity, however this was only reported to be detectable in synchronised populations of cells[600]. In unsynchronised cell culture, changing the concentration of FBS had no effect on radiosensitivity[600]. In a synchronised population, the elongation of cell cycle phases due to low FBS concentration is maximised as all cells are in the same stage of the cell cycle. As different cell cycle phases are associated with more or less radiosensitivity, synchronised cell populations will show different radiosensitivities depending on the phase they are in during irradiation[143,322]. The work reported here used unsynchronised cells. The SHH cell line clonogenics were not repeated using the higher FBS concentration as the PE was not significantly altered and an unsynchronised population was used in all experiments.

4.2.2. Radiosensitivity measured using a clonogenic assay

There was no significant difference in radiosensitivity between the SHH and Group 3 subgroup adherent cell lines as measured in a clonogenic assay. As expected[451], the OER was between 2.5 and 3 for x-rays at 0.1% oxygen, showing that radiobiological hypoxia decreased radiosensitivity. Previously published data, although limited, reports SFs with these cell lines that do not consistently agree with our findings. For the SHH cell line DAOY the literature reports SF2 values of 0.40[271], 0.44[270] and 0.61[272], and my calculated SF2 of 0.42 was within the reported range. For the SHH cell line ONS-76 the literature reports SF2 values of 0.42[271] and 0.64[273] while my calculated SF2 was 0.54, again within the reported range. For the Group 3 cell line MED8A, there is a single published SF2 of 0.34[272], which is lower than my 0.89. Inter-assay variation of clonogenic assays, regardless of radiation parameters has been shown to be within the levels of precision recommended by the Food and Drug Administration (FDA)[593,601]. This documented consistency of results would suggest a different cause for the difference between the SFs from the literature and calculated here.

There are known problems with the reporting of clonogenic assays and the robustness of the assays – a literature analysis of clonogenics for CCLE cell lines found 30% of papers included only one biological repeat and 22% only one technical replicate[594]. Biological repeats are required to mitigate the influence of random biological variation between separate experiments[602]. Technical replicates are required to mitigate the influence of inter-experimental noise[602]. Both are required to provide confidence in the generated results[602]. For the literature data on MBL cell lines, all described completing three biological repeats, and the majority also contain three intra-assay technical replicates[127,270–274].

There are a number of concerns regarding the published data. First some studies used a clonogenic assay for semi-adherent cell lines without adapting the methodology[92,272]. Second, some studies did not perform or report appropriate statistical tests, e.g. using t-test for each dose point instead of an F-test to compare the whole curves[92,272,274]. Third, some did not generate sufficient data to extend a radiation survival curve to cover enough of the β component[92,274]. Fourth, data were not always fitted to an LQ model[92,272,274]. Finally, the time between seeding and irradiation, while consistent within each study, varied between studies with incubations reported as overnight[92], 24 h[274], 48 h[271] and four days[272]. In colon adenocarcinoma cells, the longer the interval between the sub-culture and irradiation of the experimental culture, the lower the SF2 value[603]. The published MBL data suggests the reverse for DAOY, where a four day incubation resulted in a higher SF2 value than 48 h (0.61[272] vs 0.44[270]), however a direct investigation is required to confirm this. Considering this incubation period may be a confounding factor, comparisons between cell lines generated using different experimental protocols must be carried out with caution.

The clonogenic assays used to produce the radiosensitivity data presented here for four adherent MBL cell lines used at least two technical replicates in at least three biological replicates (independent experiments) at each dose point of each cell line, matching the replicates for the reported data and providing confidence in the accuracy of the results. The survival curves were extended to cover multiple log cell-killing with a minimum of two log-kill under normoxia and the LQ equation was fit using two specialist programs, GraphPad Prism

and alpha_beta, providing confidence in the fit of the LQ equation. Clonogenic cell survival was also replicated in an independent high-throughput radiosensitivity assay conducted the following year, confirming reproducibility of the results. The results presented here are therefore considered to accurately represent the intrinsic radiosensitivity of the adherent MBL cell lines.

Statistical analysis of the survival curve for the adherent cell lines using an F-test showed no significant difference between the intrinsic radiosensitivity of the SHH and Group 3 subgroups. However, the subgroup comparisons are greatly limited by the use of only one cell line to represent Group 3. Subgroup specific differences in radiosensitivity may become more apparent combining methods such as SHH pathway inhibition or reporter assays, with a clonogenic assay.

The experimentally produced survival curves were also analysed using the in-house alpha_beta software. The alpha_beta software used Monte Carlo modelling to simulate 1000 experiments producing data matching the statistical parameters of the experimental data, generating 1000 pairs of LQ parameters, specifically the α and β values. Statistical analysis of these LQ parameters α and β using the alpha_beta software identified significant differences between the shapes of the survival curves under normoxia. Specifically, that there was no significant difference between the *TP53* mutant SHH cell lines DAOY and UW228-2, that the *TP53* WT SHH cell line ONS-76 was significantly different from these two SHH cell lines and that the Group 3 cell line MED8A was significantly different from all three SHH cell lines. The α value is a measure of radiosensitivity, and higher α values indicate the cells from which the curve is derived are more radiosensitive[178]. The simulated α values indicate that ONS-76 was the least radiosensitive cell line, and both DAOY and UW228-2 were the most radiosensitive cell lines. This is in agreement with the parameters calculated from the experimental survival curves themselves, where the α values were 0.078 Gy^{-1} for ONS-76, 0.086 Gy^{-1} for MED8A, 0.240 Gy^{-1} for UW228-2 and 0.280 Gy^{-1} for DAOY. However, the significant differences between the cell lines found in the alpha_beta analyses are, mainly, due to differences in the simulated β values. The β parameter describes the

quadratic component of the curve and higher β values reflect a greater curve, i.e. the cell survival falls more rapidly with increases in dose. Again, this is reflected in the experimental data, where ONS-76 and MED8A curves begin to curve away from the other two cell lines at higher radiation doses. This analysis therefore suggests that at lower doses the *TP53* WT cell lines ONS-76 and MED8A were less radiosensitive, but at higher doses the *TP53* mutant cell lines were less radiosensitive.

In the clonogenic assay and the subsequent alpha_beta analysis, although not in the high-throughput radiosensitivity assay, the SHH *TP53* mutant cell lines (DAOY, UW228-2) were less radiosensitive at higher doses than the SHH *TP53* WT cell line (ONS-76). These differences were detected as significant in the alpha_beta software analysis, where the simulated experiments emphasised them, but not from the experimental datasets (F-test). At lower doses, in the α portion of the curve, cell death results from single hit lethal DNA damage that cannot be repaired[176]. At higher doses, in the β portion, multiple-hit damage is the cause of cell death[176]. As multiple hits of DNA are required, there is space both temporally and spatially for p53-dependent processes[176]. In the *TP53* WT cells p53 is functioning normally to respond to DNA damage, resulting in cell death[241–243]. In the *TP53* mutant cells, the mutant p53 protein does not recognise and act on DNA damage, causing radioresistance[246,247,250]. These observations can be used to hypothesise that the *TP53* mutations may be enabling the DAOY and UW228-2 cell lines to survive otherwise lethal DNA damage, contributing to decreased radiosensitivity.

When the cell irradiations were carried out under hypoxia, the alpha_beta analysis showed no significant differences between the cell lines, in contrast to normoxia. As all four cell lines reported OERs of 2.5-3, the alpha_beta analysis suggests that not only does hypoxia decrease radiosensitivity for all cell lines (as expected) but that for two of the cell lines this occurs to a greater extent. Under normoxia, MED8A and ONS-76 were slightly though not significantly more radiosensitive than DAOY and UW228-2 at higher radiation doses. Under hypoxia, all four cell lines showed similar levels of radiosensitivity at all radiation doses used. If the relative radiosensitivity of only MED8A had been lost this could have been

hypothesised to be a result of hypoxia-induced SHH pathway activation[604,605] decreasing Group 3 radiosensitivity. For the SHH cell lines, the SHH pathway is already overactive under normoxic conditions, limiting the increase that can result under hypoxia. However, the difference between ONS-76 and the remaining SHH cell lines was also lost. Under hypoxic conditions, the *TP53* mutant cell lines (DAOY and UW228-2) no longer had a survival advantage over the *TP53* WT cell lines (ONS-76 and MED8A), indicating the *TP53* mutation status is important. Under hypoxia, *TP53* mutant but not WT cells showed a decrease in the fraction of cells in S-phase[606]. Cells in the S-phase of the cell cycle are more resistant, therefore under hypoxia *TP53* mutant cell lines contain a greater proportion of radiosensitive cells compared to normoxia than WT cell lines[143,322]. The *TP53* mutant cell lines would, in this way, be relatively more radiosensitive than the WT cell lines, and this has been shown using GBM cells[607].

Hypoxia can also influence the response of *TP53* WT cells to radiation, although this is not in a straightforward manner and appears to be cell line dependent. Hypoxic conditions can increase or decrease p53 protein in *TP53* WT melanoma[242], sarcoma[456] and NSCLC[608] cell lines. Altered p53 protein levels under hypoxia would contribute to altered radiosensitivity. In a study using three *TP53* WT sarcoma cell lines, cultures were pre-incubated in hypoxia before being irradiated under normoxic conditions[456]. Two of the three cell lines showed a decrease in radiosensitivity following the hypoxia pre-incubation which, as irradiation was not conducted under hypoxic conditions, could not be attributed to the oxygen fixation hypothesis[456]. The two sarcoma cell lines with decreased radiosensitivity also showed decreased p53 protein under hypoxia, subsequent suppression of irradiation-induced p53 activation and decreased protein expression of downstream pro-apoptotic proteins[456]. In cells not pre-incubated in normoxia, p53 was activated by irradiation and resulted in increased expression of the pro-apoptotic proteins[456]. In the sarcoma cell line where the pre-incubation did not alter radiosensitivity, hypoxia increased the p53 protein expression and there was no subsequent alteration in the p53 response to radiation[456]. Characterisation of the p53 protein expression in ONS-76 and MED8A following hypoxia pre-treatment would be expected to show a decrease of p53 protein and suppression of irradiation-induced p53

activation. The *TP53* mutant cell lines would be expected to show suppressed p53 activation following irradiation regardless of oxygen concentration due to these mutations. Therefore, not only would the *TP53* mutant cell lines be made relatively more radiosensitive under hypoxia but the *TP53* WT cell lines would also be relatively less radiosensitive. This would provide an explanation for the results of the alpha_beta analysis.

4.2.3. Radiosensitivity measured using a high-throughput assay

The high-throughput assay was established and used for five of the six MBL cell lines. This assay was found to be a suitable alternative to the gold standard clonogenic assay as (a) a screening tool for experimental conditions and cell lines or (b) as an alternative for non-clonogenic-compatible cell lines as long as a control that was clonogenic compatible was included to show the results were comparable.

The high-throughput assay used in the work presented here was based on parameters from the CCLE screen of 533 cell lines, on the basis that parameters used for such a wide number of cell lines would also be compatible with the MBL cell lines, particularly considering three of the cell lines in the MBL panel were included in the screen[156]. Two protocol adaptations were made, first increasing the incubation period between seeding and irradiation to 48 h in line with the clonogenic assay method used and second the medium removal step prior to the addition of the CTG reagent was excluded in our protocol. The medium removal step is not included in the CTG assay protocol itself and made the CCLE screen protocol incompatible with semi-adherent or suspension cell lines[609]. It was also decided to use a different output metric for the high-throughput assay results in this project. The CCLE screen reported re-scaled AUC values for each cell line. The AUC was calculated using the PF and log(dose) then multiplied by $7/\log_2 10$ to give a value between zero (completely radiosensitive) and seven (completely radioresistant)[156]. The paper does not explain why the AUC was re-scaled or how this scaling factor was generated, however the reasons may be inferred from context. Considering the doses used within the CCLE screen, the maximum raw AUC resulting from 100% cell survival at all dose points would be calculated as 3.32, the scaling factor appears to have been selected to convert this to a

whole number, 7, presumably for ease although why a scale between zero and seven was chosen is unclear. This scaling factor cannot therefore be applied to assays with different dose points, such as those used in this thesis.

The choice of the AUC as the output metric is explained in the previous publications, however the evidence provided is somewhat unconvincing[156,185]. During the method development on the MBL cell line panel, it was shown that the PF values from a high-throughput assay replicated the SF values from a clonogenic assay. In fact, in the supplementary material from the original high-throughput assay paper, survival curves can be generated for their cell line panel and these also show a good replication of the clonogenic survival curve by the high-throughput assay. Based on the information included within the main text of the publication, the authors decided to compare all doses tested across each assay for each cell line[156,185]. For example, the SF2 was compared to the PF10[156,185]. To demonstrate that the high-throughput assay replicates the clonogenic assay, this comparison does not seem logical as the SF and PF values need to be correlated at the same dose points only.

The AUC metric also contains some inherent flaws. The AUC was calculated using the trapezoidal method, where two neighbouring data points are joined by a straight line, and the area under this straight line calculated as the area of the trapezoid formed[156,185]. In the high-throughput and clonogenic assays, the neighbouring data points are produced from sequential dose points. The more dose points included in the assay the shorter the gap between the data points, producing a more arched and smoother curve. In the original papers, the clonogenic assays used 0, 2, 5 and 8 Gy while the high-throughput assay used 0, 1, 2, 3, 4, 5, 6, 8 and 10 Gy[156,185]. A comparison of AUC values calculated using the trapezoidal method is not, therefore, a fair comparison as the curve of the high-throughput assay will contain fewer assumptions between dose points. Additionally, the high-throughput assay extends to a higher dose than the clonogenic, 10 Gy vs 8 Gy. The AUC for the high-throughput assay will, at least theoretically, be larger. For the majority of cell lines the SF/PF at these high doses is likely to be small enough to make very little difference to the overall

AUC value, but for direct comparisons between the two assay methods this discrepancy is undesirable. Furthermore, the MBL work indicates that the high-throughput assay is less accurate at higher radiation doses and reports a higher cell survival than the clonogenic, another difference that would increase the AUC value but could only be detected by plotting and comparing the curves from both assays, not from the AUC values alone. The AUC of the high-throughput assay may therefore be artificially elevated compared to that of a clonogenic assay both due to increased number and extent of dose points and increased reported cell survival at higher doses.

The three cell lines used in the CCLE screen were DAOY, ONS-76 and D283 with reported AUC values of 1.08, 1.69 and 0.674 respectively[156]. For comparison, the reported AUC values from the CCLE screen have been converted back to raw AUC values by dividing by the scaling factor. ONS-76 could not be optimised in this work. The AUC values for DAOY and D283 calculated here were 0.98 and 1.14 respectively. The CCLE screen included a higher dose point than was done in this work, which, as discussed above, would necessarily increase the reported AUC values.

D283 is a semi-adherent cell line, which does not appear to have been taken into account in the CCLE screen and thus the radiosensitivity may not have been accurately determined[156]. D283 is not only reported as the most radiosensitive MBL cell line but also one of the most radiosensitive cell lines in the entire panel[156]. The CCLE screen method removes the medium from the wells prior to the addition of the CTG reagent. In a semi-adherent cell line such as D283, where up to 90% of the cells are in suspension, this step will remove a variable but significant proportion of the total cells from each well. Even though the medium is being removed from each well, the same number of cells will not be removed from each well and so the approach does not provide a compensatory control mechanism. As described above (Section 4.1.1), the proportion of suspension cells may be increased by irradiation and if this is the case then more cells could be removed from wells treated with higher radiation doses than from control wells. The reported number of cells in each well

would be reduced, indicating fewer cells had survived and indicating a greater radiosensitivity than is the case.

The cell line ONS-76 was included within the CCLE screen but could not be optimised during this project as the 0 Gy control plates showed saturated luminescence in every repeat experiment, despite reducing the seeding density to a minimum. The incubation period between irradiation and the CTG assay was 9 days as used in the previous screens. The 9 day incubation for the high-throughput assay was found to produce the most significantly similar AUC results to the clonogenic assay[185]. ONS-76 is the fastest growing cell line in the MBL panel, and requires the shortest incubation period in the clonogenic assay. Although the 9 day incubation period produced data in the CCLE screen, these results suggest that a reduced incubation period may be preferable. Subsequent uses of the high-throughput assay in the group have reduced the incubation time with some succession, using visual inspection for cell density to determine whether the assay should be terminated. The incubation period may need to be optimised for each cell line to account for different cell growth characteristics.

The difficultly in optimising the high-throughput assay for ONS-76 revealed an inherent limitation of this assay, an upper limit of detection. In the clonogenic assay, as the radiation dose increases the seeding density within the wells is increased to account for the subsequent decreased SF. The 0 Gy control wells are used to calculate the percentage of cells that would form colonies without radiation, and this is used to calculate the number of expected colonies in a well based on the number of cells seeded. Therefore, the increases in cell seeding density at higher radiation doses can be accounted for and a much higher seeding density can be used in an irradiated well than in a control well, allowing for very small SFs to be calculated. In the high-throughput assay, the PF is calculated by comparing the RLU at 0 Gy with the RLU at the dose point. There is no control for the number of cells seeded within a well, and so the number of cells seeded at the control and dose points must be the same. The assay is therefore limited, as higher doses require higher seeding densities to generate detectable luminescence, but using these higher seeding densities in the unirradiated control wells results in saturating the luminescence. The maximum number

of cells per well in the assay will be limited by the 0 Gy control, and the maximum number of cells per well will limit the maximum dose that can be used. This is reflected in the assay results –the high-throughput and clonogenic assays are in close agreement at lower doses but differences are observed at the higher dose points where the 0 Gy cells are reaching saturation with the number needed to produce a result at the dose point.

The high-throughput assay produced survival curves that did not significantly differ from the clonogenic assay results for each of the three cell lines used in both. The high-throughput assay was therefore applied to the semi-adherent cell lines as an assessment of radiosensitivity. The three Group 3 cell lines, D425, D283 and MED8A showed no significant difference in survival curves produced by the high-throughput assay. The cell line D283, which is reported as belonging to both the Group 3 and 4 subgroups, is slightly separated from the other two[16,117,506]. While the WNT and SHH subgroups are clearly defined separate entities in patients, Groups 3 and 4 show some overlap[95]. As shown previously and in the work here when the MM2S method was applied to confirm subgroup classifications, samples more frequently swap between these two groups than any other[95]. A recent paper with patient samples has reported the presence of an intermediate subgroup (Group 3/4) which is separate from the other two non-WNT, non-SHH subgroups[97]. This intermediate group contained tumours nominally clustered with Group 3 but containing genes belonging to both Group 3 and 4[97]. Group 3/4 has better survival outcomes than Group 3 or Group 4[97]. D283 may therefore be representing this subgroup, which would be predicted to be more radiosensitive than Group 3 based on the clinical outcomes.

The data presented here for the two SHH cell lines with previously published SF2 values are in agreement with the literature. The published SF2 values for DAOY are 0.40[271], 0.44[270] and 0.61[272]; here the SF2 was 0.42 and the PF2 was 0.36. The published SF2 values for ONS-76 were 0.42[271] and 0.64[273]; here the SF2 value was 0.54, with no PF2 values reported. For Group 3 however the published survival data indicates they are more radiosensitive than found in this work. The published SF2 values for D283 were 0.17[272] and 0.18[270]; here the PF2 value was 0.44. The published SF2 value for MED8A was 0.34[272]; here the SF2 was

0.89 and the PF2 was 0.52. No SF2 values have been reported for D425. The published SF2 values for D283 have the same issues as previously discussed, in that the clonogenic assay removes the medium prior to fixing and staining and D283, as a semi-adherent cell line, is not compatible with media removal steps. The reduced SF2 values in the literature can therefore be explained in this way. During method development of the clonogenic assay, certain adjustments were required for MED8A in order to optimise colony formation. Specifically, the FBS concentration for the incubation period was increased, and wash steps were removed from the fixing protocol. When the wash steps were included, MED8A colonies were washed off the plate meaning that the colonies counted after fixing did not represent the number of colonies that had formed. The literature methods do not mention such adaptations for the MED8A cell line, therefore the reported low SF2 values may be due to systematic errors, as for D283. The decreased radiosensitivity reported in this thesis is suggested to reflect the described methodological differences which provide a more accurate quantification of the cell radiosensitivity.

The agreement of the results from the clonogenic and high-throughput assays provides further confidence in the comparison of the clonogenic results across cell lines. While the SHH cell line clonogenic work used the standard complete medium FBS concentration of 10%, the Group 3 cell line work used 20%. As discussed previously, the FBS concentration may have an effect on PE and SF of cell lines and the different FBS concentrations may limit subgroup comparisons (Section 4.2.1). The high-throughput assay does not require surviving cells to form distinct, fixable colonies and so all cell lines were incubated in the same culture medium (complete medium containing 10% FBS). The MED8A survival curve produced from the high-throughput assay was not significantly different from that produced from the clonogenic assay, indicating that the FBS concentration used for each cell line was not significantly affecting the radiosensitivity of this cell line.

The high-throughput assay results were used in conjunction with the clonogenic assay results to compare the radiosensitivity of the subgroups. Overall, the *in vitro* work showed SHH cell lines were significantly more radiosensitive than the Group 3 cell lines. Clinically,

Group 3 tumours have worse overall survival than SHH, which would be a result of decreased radiosensitivity, considering radiotherapy protocols are not tailored to the molecular subgroups. Increased SHH pathway activity decreases radiosensitivity and, as increased pathway activity is a marker for the SHH subgroup[13,15,216–218,220–222], this subgroup may be expected to be less radiosensitive. In this case, inhibition of the SHH pathway would increase radiosensitivity and cell kill. Work in prostate cancer cells, which also have intrinsically increased SHH pathway signalling, showed that inhibiting the SHH pathway in these cell lines only increased radiosensitivity in cell lines where the pathway was indirectly activated by AR signalling[227–231]. In the cell lines where the pathway activation could not be explained through AR signalling, inhibition of SHH signalling had no effect on radiosensitivity[227]. If constitutive SHH pathway activation does not result in reduced radiosensitivity similar to that which occurs following acute pathway activation, SHH pathway inhibition would not result in radiosensitisation. What effect the overactive SHH pathway has cannot be determined from the results presented here as, while more radiosensitive than Group 3 cell lines, the SHH cell lines are radioresistant compared to non-MBL cell lines[151,152,155,156,160,593,610–635]. Future experiments are needed to test the effects of SHH pathway inhibition on radiosensitivity. Characterisation of the SHH pathway signalling with the MBL cell lines in parallel with the radiosensitivity work could provide a better understanding of how SHH signalling contributes to radiosensitivity and potentially suggest therapeutic targets to increase tumour radiosensitivity.

Proton irradiation causes a different extent of radiation damage to x-ray irradiation, and this is calculated as the RBE[134,135,137,276,299,300,306,307]. An RBE of 1.1 is generally accepted and used clinically however this value is controversial and a wide range of RBE values have been reported across cell lines. The high-throughput radiosensitivity assay was identified as a potential method for rapidly generating RBE values for a wide number of cell lines. Carrying out a screen of cell lines using clonogenic assays would be labour intensive and time consuming. Additionally, The Proton Research Room at the Christie hospital has some restrictions preventing the extensive use of clonogenics: limited facilities for re-seeding cells into the 6-well plates following irradiation; limited facilities for long-term incubation of 6-well

plates for colony formation; a horizontal beam requiring culture vessels to be positioned vertically during irradiation; and restriction of beam access time to outside of clinical working hours. The high-throughput assay addresses some of these issues: there is no re-seeding step therefore cell culture facilities are not required; fewer plates are required per experiment due to the 96-well plate format; there is a low media volume so the vertical position required does not cause media spillage; and the assay protocol can maximise the throughput as the plates can be prepared in advance and only the irradiation is required during the night-shift.

Initial proof-of-principle experiments were completed using two MBL cell lines that had already been used in the high-throughput assay, DAOY and MED8A. The proton data set represents a single experiment conducted on two cell lines. The small nature of this dataset means that interpretation must be limited and cautious, but it shows that proton radiation caused greater cell kill compared to x-rays. As part of the demonstration of the usefulness of the high-throughput assay an exploration of the RBE values for DAOY and MED8A was carried out, despite the single biological repeat for proton irradiation. The clinically used RBE value is 1.1, which appears to be applicable to DAOY where the RBE at 10% cell survival was reported as 1.06[127]. The RBE at 50%, 10% and 1% cell survival for DAOY was calculated 1.01, 1.08 and 1.16 respectively. No RBE value for MED8A has been published. The RBE at 50%, 10% and 1% cell survival for MED8A was 1.11, 1.34 and 1.36 respectively. Our small data set suggests that the Group 3 cell line showed a greater increase in cell kill following proton compared to x-ray irradiation compared to the SHH cell line. This preliminary work, if reproduced and found to be significant, could suggest subgroup specific differences in proton radiosensitivity of the subgroups not reported following x-ray irradiation.

The high-throughput assay uses the assumption that ATP production is not altered by irradiation. Further validation of the endpoint of the high-throughput assay would require a study of the long-term effect of a single radiation dose on ATP production to confirm this assumption. The incubation period of the high-throughput assay should also be investigated by repeating the initial published experiments extending the incubation time beyond 9 days

and comparing the incubation time required in the two radiosensitivity assays for each cell line to see if there is a correlation[156,185]. The *in vitro* subgroup comparison work would be expanded using cell lines representing the remaining two subgroups. Follow up work would target the SHH signalling pathway to characterise the response to radiation in the SHH and non-SHH subgroups.

4.2.4. Radiosensitivity measured using the radiosensitivity index

The RSI was prognostic within the MBL patient cohort GSE85217 demonstrating radiosensitivity is important in MBL and affects the probability of survival. RSI should only be prognostic in patients treated with radiotherapy. Treatment regimens were unknown for the patients within this cohort. Patients under three years of age, representing 13% of the GSE85217 cohort, are not routinely treated with radiotherapy, however patient age affects survival[20,21,55,56]. Additionally, the total radiotherapy dose prescribed is dependent upon standard- or high-risk status, either 23.4 Gy or 36.0/39.6 Gy respectively[30,32]. In order to minimise the number of assumptions made during analysis that could confound the results, and considering the majority of patients would have had some radiotherapy in their treatment regimen, the entire cohort was used in all survival analyses. Validation of the RSI within MBL requires additional analysis of another large patient cohort with detailed radiotherapy regimen information.

The cut-off point for the RSI to determine whether a sample was radiosensitive or radioresistant was the 25th percentile for each cohort. Across the five patient cohorts used in this study, the 25th percentile cut-off value showed a fairly wide range, from 0.4903 GSE37418 to 0.6824. The cohort with the lowest 25th percentile, GSE37418, also showed lower gene expression values across the entire dataset. The different cohorts were generated using different sample preparation and microarray methodologies. It is well established that technical differences between the microarrays result in different reported values and difficulty in comparing across platforms without certain adjustments[636–640]. While these adjustments can be used to combine individual cohorts into a single large cohort to interrogate this was not carried out for this project[640]. The five patient cohorts provided different meta-data, which would limit analysis of a merged cohort. For example, only

GSE85217 provided survival data and patient age was only available for GSE37382 and GSE85217. Using multiple cohorts also allowed for patterns of gene expression to be compared and contrasted.

Using the 25th percentile to distinguish between radiosensitive and radioresistant tumours classes 75% of all tumours as radioresistant. There was a different ratio of sensitive to resistant tumours within each of the four molecular subgroups, with 95% of Group 4 tumours, 73% of Group 3, 59% of WNT and 44% of SHH classed as radioresistant. The Group 4 subgroup contained more radioresistant tumours than expected, while the WNT and SHH subgroups contained fewer. As could be expected, the proportion of radioresistant tumours was reflected in the median RSI, where Group 4 tumours had the highest values (and therefore the least radiosensitive) in each of the cohorts followed by Group 3, WNT and SHH subgroups. This was in agreement with the cell line work, which reported SHH cell lines to be more radiosensitive than Group 3.

Patients with the most radioresistant tumours should have worse tumour control and overall survival following radiotherapy. The subgroup with the worst overall survival rates, Group 3[15,131], would be predicted, therefore, to contain the highest proportion of tumours classed as radioresistant by the RSI. Instead, Group 4, which has intermediate survival outcomes[15], contained the highest proportion (95%) while Group 3 contained the expected number of radioresistant tumours using a 25th percentile cut-off (73%). The reduced proportion of radioresistant tumours in Group 3 compared to Group 4 might be due to the major clinical characteristic of Group 3, *MYC* amplification. *MYC* amplification can increase radiosensitivity through increased DNA damage and subsequent apoptotic cell death[264]. As the contribution of *MYC* amplification to radiosensitivity is unclear, and higher levels of c-myc protein[266] or *MYC* amplification[267] have also been associated with radioresistance, further *in vitro* experimental work investigating irradiation-induced DNA damage in MBL cell lines is required to identify the contribution of *MBL* amplification to radiosensitivity.

As mentioned above, the 25th percentile cut-off point used with the RSI would be expected to class the majority (75%) of all tumours as radioresistant, however considering the 90% survival rates for the WNT subgroup[15,38,76,102,103,131,641] the majority of tumours within this subgroup were expected to be classed as radiosensitive. In fact, only 41% of WNT subgroup patients had radiosensitive tumours, and the SHH subgroup contained a larger proportion of radiosensitive tumours (56%). Overactive WNT signalling within this subgroup produces a leakier BBB compared to the other subgroup, and this directly affects chemosensitivity[106]. This inherent susceptibility to chemotherapy might counteract the relative radioresistance compared to the SHH subgroup and could explain the much improved survival outcomes in WNT tumours. Three active clinical trials remove or reduce the radiotherapy component of WNT subgroup treatment[41,43,44]. If the removal of radiotherapy from treatment does not significantly reduce the survival outcomes, this will provide evidence that radiosensitivity is not an important determinant of survival in this subgroup. If chemotherapy is producing most of the tumour control, it may be that differences in chemosensitivity are important.

In the MBL cell line panel, *in vitro* radiosensitivity assays showed that the SHH cell lines were more radiosensitive than the Group 3 cell lines. Cell lines representing the WNT and Group 4 subgroups were unavailable, and so the *in vitro* work is restricted to the SHH and Group 3 subgroups. The RSI of a patient sample is a predicted SF2 value for that tumour, if a primary cell culture was derived and used in the *in vitro* radiosensitivity assay. In the MBL patient cohorts which contain patients representing all four molecular subgroups, the RSI showed the SHH subgroup was more radiosensitive than Group 3, agreeing with the *in vitro* data. The RSI also showed that WNT subgroup samples were slightly less radiosensitive than SHH samples but much more radiosensitive than Group 3 samples. Group 4 patients had the highest RSI values, indicating this subgroup was the least radiosensitive.

The WNT and SHH subgroups are associated with overactive signalling pathways, and activation of either the WNT[92,111,212,213] or SHH[216–218,220–222] signalling pathway decreases radiosensitivity. It was hypothesised that these subgroups would be less radiosensitive. However, in comparison to MBL as a whole, the WNT and SHH subgroups are more

radiosensitive and it would appear then that the overactive signalling pathways are not contributing to radiosensitivity as predicted. As reflected by their generic names, molecular features of the Group 3 and Group 4 subgroups are still undefined. It is possible that these features are important in the relative radioresistance of Group 3 and Group 4 tumours. For example, Group 3 tumours contain a greater proportion of CSCs[577], which are intrinsically more radioresistant than non-CSCs. While intrinsic radiosensitivity is technically genetically determined and inherent to each individual cell, measurements of intrinsic radiosensitivity (clonogenic assay, high-throughput radiosensitivity assay and the RSI gene signature) quantify the intrinsic radiosensitivity of a population of cells. If that population of cells contains a greater proportion of more radioresistant cells, such as CSCs, then the intrinsic radiosensitivity of that cell population will be reduced. The observed radiosensitivity of Group 3 tumours would therefore be decreased and the WNT and SHH subgroups, which contain fewer radioresistant CSCs, would appear relatively radiosensitive. Alternatively, the constitutive activation of the WNT and SHH signalling pathways is acting differently than the temporary activation observed in *in vitro* experiments, either by having no effect or increasing radiosensitivity. Repetition of the *in vitro* radiosensitivity work using SHH pathway inhibitors would help quantify the contribution of the SHH signalling pathway to radiosensitivity and identify if the underlying overactive pathway contributes to the radiosensitivity of the SHH subgroup.

The RSI scores demonstrate a significant difference in radiosensitivity across the subgroups. This difference somewhat reflects clinical outcomes and hypothesised radioresponsiveness, and therefore could be clinically exploited in terms of personalising radiotherapy regimens between subgroups. Specifically, greater tumour control could result from higher radiotherapy doses for subgroups with lower intrinsic radiosensitivity (Groups 3 and 4), normal tissue tolerance permitting. For the WNT and SHH subgroups which are more radiosensitive, a reduction in radiation dose may produce the same level of tumour control but reduce side effect severity. The radiosensitivity rankings within MBL are inconsistent with the current understanding of the subgroup molecular biology, as the WNT and SHH groups have defined aberrant signalling pathways known to decrease radiosensitivity. However,

MBL as a single entity is a more radioresistant tumour type and these overactive pathways may contribute to this decreased radiosensitivity for the WNT and SHH subgroups. Evidence that constitutive WNT and SHH pathway activation d in these subgroups could be used to argue for a benefit of concurrent inhibition of these pathways during radiation treatment. However, the mechanism of action of radiation is complicated and involves multiple pathways.

DNA damage response (DDR) pathways affect radiosensitivity, and mutations that enhance or diminish the DDR following irradiation can decrease or increase radiosensitivity respectively. There have been no definitive connections between genes involved in DDR pathways and any particular MBL subgroup. The most well-known radiosensitivity associated gene is *ATM* (ataxia-telangiectasia mutated, encoding a DDR kinase[642]), however mutations in the *ATM* gene are not associated with MBL[643]. No significant differences in mutations of other genes within DNA repair pathways (specifically *MSH2*, *RAD50* and *NBN*) across the molecular subgroups were found in one patient cohort[644]. The authors noted germline mutations in the three genes were absent from all SHH tumours[644], however as this cohort contained only 102 patients with only 51 assigned to molecular subgroups[644] the numbers were not large enough to produce statistical significance. A second study found that, while germline mutations occurred in all four molecular subgroups, the SHH subgroup contained the highest number of *BRCA2* and *PALB2* mutations[645]. The *BRCA2* and *PALB2* genes encode proteins involved in the homologous recombination DNA repair pathway, and the mutations found in MBLs were indicative of homologous recombination repair deficiency[645]. Mutations in *MSH2*[646], *RAD50*[647], *NBN*[648] and *BRCA2*[649] can increase radiosensitivity. Although only a small percentage of SHH patients had these germline mutations[645], an impaired DDR within the SHH pathway could explain the relative radiosensitivity of this subgroup. Characterisation of the DDR in cell lines and the relative levels of germline mutations in DDR associated genes in patient samples would identify any subgroup-specific aberrations in the DDR.

The RSI was correlated with other clinical characteristics including gender, age and histology. Age and gender are known to influence radiosensitivity, but the influence of the molecular subgroups may also be contributing. For example, while males are less radiosensitive than females[650,651], male patients are also more likely to belong to the less radiosensitive Groups 3 and 4[13,97,101]. Radiosensitivity varies throughout life, and children and the elderly are more radiosensitive[651,652]. This is not fully reflected in the MBL patient cohorts, where children are less radiosensitive than adult or infant patients. The child age group contains fewer radiosensitive SHH tumours than any other subgroup[13,15,17,38,101,117,118], which would explain the relatively decreased radiosensitivity. Classic tumours were less radiosensitive than the remaining histological subtypes combined, however over 50% of the classic tumours in these cohorts belong to the least radiosensitive subgroup, Group 4.

Metastatic status, molecular subgroup and RSI were significantly correlated with survival in univariable analysis. Higher metastatic status and RSI scores were associated with worse overall survival. The WNT subgroup had the best overall survival, followed by the SHH, Group 4 and Group 3 subgroups. In multivariable analysis combining these three variables, only molecular subgroup and metastatic status remained significantly associated with survival. Again, higher metastatic status increased the risk of death, and the same pattern of survival was observed for the different subgroups. The RSI scores were no longer significantly associated with survival outcomes. Multivariable analysis models are influenced by the relationships between the variables, and these relationships can explain the loss of significance. A higher proportion of Group 3 patients were positive for metastases than the other molecular subgroups; both of these characteristics are associated with an increased risk of death so these variables are related and predict overall survival in the same way. The mean RSI score is significantly different between the molecular subgroups, however the subgroup with the worst risk of death does not contain the most radioresistant patients. The RSI score and subgroup status do not agree with respect to prediction of survival outcomes. When these two variables are included in the multivariable model the RSI score becomes less predictive of overall survival and loses significance. This confirms that, despite the

significant differences between the subgroups (SHH/WNT more radiosensitive than Group 3/Group 4), intrinsic radiosensitivity alone does not explain the different survival outcomes.

4.3. Proliferation

The second objective of this thesis was to investigate whether there were differences between MBL subgroups in proliferation. It was hypothesised that differences in proliferative capacity could contribute to survival outcomes, which could not be explained by the intrinsic radiosensitivity alone. Activation of the SHH signalling pathway[122,221,354–357] or *MYC* overexpression[358–362] increases proliferation, suggesting these subgroups would be more proliferative. The proliferative capacity of MBL was investigated using gene expression biomarkers and the meta-PCNA signature in the five patient cohorts. While cellular proliferation can be measured *in vitro* it is influenced by environmental factors such as cell culture medium[653,654], FBS batch[653], FBS concentration[518,653] and seeding density[518,654]. This thesis found that proliferation was not associated with survival, with no significant differences between the subgroups of MBL.

4.3.1. Gene expression markers of proliferation

Gene expression biomarkers are usually investigated in terms of their protein expression [314,328–330,334,335,338–342,402,404,405,407–412,416–426,655,656]. A central dogma of biology states that DNA is transcribed to RNA which is translated to protein, however post-translational modifications and protein turnover rates mean that there is not a direct correlation between mRNA and protein expression[657]. mRNA expression is at least weakly correlated with protein expression however, and increased mRNA expression is indicative of increased protein expression[658–662]. The biomarkers of proliferation investigated in this project were Ki67 and PCNA. The mRNA expression of Ki67 has been shown to correlate with the protein expression, and while this was not the case for PCNA, both PCNA protein and mRNA expression do correlate with clinical outcomes and characteristics[331,332,337,338].

In the MBL cohort GSE85217, neither Ki67 nor PCNA mRNA expression was significantly associated with overall survival. Detectable levels of mRNA were reported for both Ki67 and PCNA in contrast to non-cancerous brain tissue where Ki67 is not expressed and PCNA is only expressed at low levels[663,664]. Increased Ki67 and PCNA protein expression has been reported for PNET tumours including MBL previously, although no survival analysis was carried out[363]. Across all five patient cohorts, the expression patterns were not consistently altered between the molecular subgroups. The gene expression biomarkers indicate that proliferation is not significantly associated with overall survival in MBL, and there is no significant difference between the molecular subgroups.

4.3.2. Meta-PCNA index as a marker of proliferation

The meta-PCNA signature is a gene signature of proliferation. Gene signatures take into account a pattern of gene expression that is associated with a particular phenotype of interest. The meta-PCNA signature includes 131 genes whose expression is most up-regulated in accordance with the proliferation protein PCNA, reflecting a network of gene expression that is altered by a cell during proliferation. The median gene expression of this signature, the mPI, can be used to determine whether a cancer is proliferative-informative or not. A proliferative-informative cancer is one where the proliferation rate significantly affects survival outcomes, while non-proliferative-informative cancers show no effect of proliferation on survival outcomes[351]. The MBL cohort GSE85217 showed no significant relationship between the mPI score and the survival outcomes, classifying MBL as a non-proliferative-informative cancer. Non-proliferative informative cancers were those with the highest expression of proliferation markers, which agrees with the previous indication from single gene markers that proliferation was significantly increased in the MBL samples[351]. As a non-proliferative informative cancer the implication is that proliferation no longer contributes directly to the survival outcomes, instead other outcomes such as immune activation or metastasis do[351].

If the proliferative capacity of the tumours were acting to increase or decrease radioresponse, and using the assumption that the majority of patients are treated with

radiotherapy, then a difference in survival outcomes between tumours with different proliferative rates would be expected. By giving MBL the status of non-proliferative informative cancer, proliferation is not contributing to survival outcomes and therefore is also not significantly contributing to radioresponsiveness.

As for the single gene biomarkers, the mPI showed no consistent differences between molecular subgroups. Considering that proliferation is not associated with the risk of death in MBL, that the survival outcomes do not show differences in proliferation markers in accordance with their different survival outcomes is not surprising. Activation of the WNT and SHH signalling pathways increases cellular proliferation[115,122,221,352–357] and so the constitutive activation within the subgroups may be expected to also increase cellular proliferation. Instead, no significant differences are seen within these subgroups. *In vitro* studies using established cell lines and pathway inhibitors would demonstrate whether there is a contribution of these signalling pathways to proliferation. As for radiosensitivity, it is possible that the constitutively active pathways have a different influence on proliferation than the acute activation used in drug or transfection studies, or that Group 3 and 4 subgroups have underlying molecular aberrations that also increase proliferation.

A large patient cohort with clinical outcomes, molecular subgroup status, mRNA expression data and tumour biopsy samples could be used to confirm the results presented here. The single gene expression marker results could be confirmed using both mRNA and protein expression studies within such a cohort to demonstrate the correlation between the two metrics and confirm the findings across the disease as a whole and the molecular subgroups.

4.4. Hypoxia

The third objective of this thesis was to investigate whether there were differences between MBL subgroups in the extent of tumour hypoxia. It was hypothesised that lower tumour hypoxia could contribute to the survival outcomes that were not explained by intrinsic radiosensitivity alone. The subgroups with higher than expected radiosensitivity, SHH and Group 3 were predicted to be more hypoxic than those with lower than expected

radiosensitivity, WNT and Group 4. Work carried out for this thesis showed no relationship between the degree of tumour hypoxia and patient outcome, and was inconclusive with regards to the extent of hypoxia between molecular subgroups but suggested that WNT tumours were the most hypoxic.

While MBLs will contain regions of hypoxia because they are solid tumours[457–459], only two studies report on markers of tumour hypoxia[106,460]. The first study using a small cohort (n=35, 28 MBL and 7 PNET) reported approximately 25% of tumours contained some level of CAIX staining[460]. While the number of samples with strong (>30% CAIX-positive cells, n=1), moderate (10-30% CAIX-positive cells, n=6) and weak (<10% CAIX-positive cells, n=2) can be deduced, which tumours were MBL and which were PNET cannot. This study was carried out prior to the consensus on the molecular subgroups and therefore does not report on subgroup status and MBL. The second used the hypoxia biomarker GLUT1 and showed lower expression of this biomarker within the WNT subgroup compared to the other three subgroups as part of an investigation demonstrating WNT tumour vasculature was the most extensive[106]. This study used two patient cohorts with a total of 98 patients comprising 10WNT, 24 SHH, 22 Group 3 and 32 Group 4 patients, and confirmed downregulation of the expression of Slc2a1, the GLUT1 gene in mice[106]. Although not included in the study, the lower level of GLUT1 staining reported within the WNT subgroup may imply there are lower levels of hypoxia within this subgroup.

Tumour hypoxia was investigated using gene expression biomarkers and hypoxia gene expression signatures in the five patient cohorts. Hypoxia is a feature of the tumour microenvironment, and while it can be reproduced *in vitro* in cell lines this cannot provide information regarding the hypoxia status of the original tumours. The patient cohorts were investigated with regard to gene expression biomarkers and signatures to detect the presence of hypoxia with the tumours. Tumour hypoxia was not associated with survival in MBL. A difference between tumour hypoxia across the molecular subgroups was identified with one hypoxia gene signature (Group 3 being the most hypoxic followed by Group 4, SHH

and WNT), suggesting subgroup-specific differences in tumour hypoxia contribute to the different overall survival rates.

4.4.1. Hypoxia assessed using gene/protein expression

The mRNA expression of two single gene markers of hypoxia, CAIX and GLUT1 was investigated in this study. Neither marker was significantly linked to survival outcomes or showed consistent differences between the subgroups. This finding contrasts with the previous report mentioned above, where the WNT subgroup was shown to have lower GLUT1 protein expression than the remaining three molecular subgroups[106]. The mRNA and protein expression levels have been correlated for both of these markers[406,413]. CAIX mRNA expression is enhanced within the normal cerebellum, the brain region where MBLs originate, and therefore may not be a suitable hypoxia marker within this region[30,665]. GLUT1 has low expression across all brain regions, potentially making it more suitable within this context[666].

4.4.2. Hypoxia gene expression signatures

Hypoxia signatures can be developed using patient data where both the mRNA and hypoxia status of the tumour are available, or using *in vitro* cell line data, where cells are cultured under a variety of oxygen concentrations and gene expression differences between the two compared. There are no hypoxia gene expression signatures derived using MBL samples. Specialist bioinformatics knowledge is required to develop a robust and reproducible gene signature using the most appropriate models. For hypoxia gene signatures to be applied to patients and inform treatment decisions, validation in clinical cohorts is required however a lack of validation of hypoxia gene signatures has been highlighted as a barrier to their widespread clinical use[385,667]. Hypoxia gene signatures are rarely validated in cancer types outside of those that they were developed in, and when this validation is carried out it generally shows that the signatures are not applicable to all cancer types[389].

A literature search identified 21 hypoxia gene signatures across a range of cancer types and 12 of these were applied to the MBL patient cohorts. The signatures derived in brain cancers[388,434,435] and NBL[389] were included as these were expected to show the greatest overlap with MBL based on tumour location and cells of origin respectively[388,389,434,435]. Signatures which generated a hypoxia score and classified samples as low or high hypoxia based on the median cohort score were included[388,390,391,427,436,438,440]. Signatures which required alternative analysis[431,433,437,439] or for the results to be compared with previously assessed data[432,437,441] were excluded. Where multiple signatures were identified from a single cancer type, such as for prostate or breast, only one was applied to the MBL patient data. Across the 12 signatures, none were prognostic within MBL.

All but two of the 12 applied signatures used the median hypoxia signature score to classify patients as high or low hypoxia. The only available data for MBL reported only 25% of samples stained positive for CAIX, suggesting significant hypoxia is present in 25% of tumours[460]. Although the cohort size of this study was small and also included PNET tumours, it suggests a median cut-off value might be suboptimal. The two remaining signatures used k-means clustering based on the gene expression signature data to assign samples to the high or low hypoxia groups. The Tardón GBM signature reported 40% of patients in the high hypoxia group, while the Fardin NBL signature reported 70% of patients as high hypoxia. Although neither signature was prognostic, the fact that the samples were not divided equally between the two groups further suggests that the median score is not a suitable cut-off. Using the 25th percentile as a cut-off in the applied signatures reduced the p-value in the majority of cohorts, although none reached statistical significance. A larger sample cohort should be used to confirm the expected proportion of MBL tumours containing regions of hypoxia, providing evidence for a re-assessment of the cut-off point.

It was anticipated that gene signatures derived in carcinomas would be least transferable to MBL, while those derived in glioma or GBM would be most prognostic. This was found not to be the case, and the gene signature that produced groupings with the lowest p-value was the Fardin NBL signature[389]. NBL and MBL share some similarities that are not present with gliomas that may contribute to this. NBL and MBL are embryonal tumours originating from

blast cells in the peripheral and central nervous systems respectively[30,668]. Along with their embryonic nature, both are more common in early childhood[73]. Gliomas and GBMs originate from glial cells and are more frequent in adults[669]. NBL and MBL also share similar histology[73]. Cancers with more similar histology have a similar levels of hypoxia[441], and histological features can be used to assess tumour hypoxia[670,671]. Cancers of a similar histology would appear to share certain gene markers of hypoxia. Across the 21 hypoxia gene signatures identified in the literature search, 50% of genes found in more than one signature were only found in signatures derived from carcinomas. Half of these carcinoma-only genes were equally represented in multiple cancer types, i.e. were found in an equal number of signatures for at least two cancer types. This may explain why the NBL was more applicable to the MBL cohort than the other brain cancer hypoxia gene expression signatures.

It could be expected that, based on the potential links between histology and hypoxia, the levels of hypoxia would vary across the histological subgroups. The four histological subgroups were not well represented across the GSE85217 cohort, with only 18 MBEN compared to 387 classic tumours. Two of the histological subgroups, DN and MBEN, did not contain enough events to allow survival analysis[672]. A relationship between histological subgroup and hypoxia could not be investigated. Future investigations of hypoxia and MBL would benefit from details regarding both the molecular and histological subgroups of each sample.

As no signature proved to be prognostic, the multivariable analysis was carried out using the classification produced by the Fardin signature. The other variables included in the analysis were metastatic status, subgroup status and RSI, which were found to significantly contribute to survival in univariable analysis. The multivariable analysis only found metastatic status and subgroup status to be significant predictors of survival.

For the two applied signatures which used k-means clustering, Fardin NBL[389] and Tardón GBM[434], both the reported and optimal values of k were used in the algorithm, k=2 and k=4

respectively. When the optimal k=4 was used in the Tardón signature, the resulting four clusters represented the four molecular subgroups. This gene signature was derived using GBM cell lines and validated in glioma and GBM cohorts. It seems unlikely that it is also a gene expression signature for the MBL molecular subgroups, especially considering the 36 genes within the Tardón signature have no known associated with any of the molecular subgroups. This finding was replicated in the second largest patient cohort but not in the smaller cohorts. It was also demonstrated that this clustering into the subgroups was not occurring by chance as it was not seen when random sets of 36 genes were used. This result suggests that the different molecular subgroups have different gene expression levels of hypoxia-associated genes.

Survival outcomes of the four Tardón signature clusters, where the cluster with the worst survival outcomes is deemed the most hypoxic, showed that the WNT subgroup is the least hypoxic, followed by SHH, Group 4 and Group 3. However, as the clusters are so representative of the molecular subgroups and this survival follows the clinical patterns for the molecular subgroups, confirmation using CAIX or GLUT1 staining of samples with known subgroup affiliations should be carried out. GLUT1 staining previously reported the WNT subgroup to have the lowest protein expression than the other molecular subgroups, which is in agreement with the Tardón signature analysis[106]. The WNT subgroup was also reported to have more vascularity, which would indicate a better blood supply, and hence better oxygen supply, to the tumour[106]. If this pattern of hypoxia across the subgroups is correct, then the contribution of hypoxia could explain the different radioresponsiveness across the molecular subgroups.

The work presented here is inconclusive, presenting neither a difference nor a similarity in hypoxia between the molecular subgroups. While neither of the gene expression biomarkers were prognostic within MBL, single gene markers are not reliable[400] and, depending on the study, can be prognostic or not prognostic in the same cancer type. For example, CAIX staining in H&N patient cohorts was prognostic in one study and not in another[402,408,409]. None of the applied gene signatures were prognostic, but as they were not derived using MBL samples and, because hypoxia gene signatures are on the whole not transferable, the

signatures may not be compatible with MBL[389]. To address this, a MBL specific hypoxia gene expression signature would need to be developed and validated. A MBL specific gene signature would then enable a more thorough investigation of subgroup-specific differences in hypoxia status, to confirm that the level of hypoxia within the tumours is significantly contributing to the radioresponsiveness. Subgroup-specific differences in tumour hypoxia could be exploited by including hypoxia-targeted therapies such as CON or nimorazole in subgroups with higher levels of hypoxia. As tumours should be routinely assigned to molecular subgroups prior to treatment, this approach would be easy to implement and not require any additional profiling, such as with a hypoxia gene expression signature.

4.5. Cell migration

The fourth objective of this thesis was to investigate whether there were differences between MBL subgroups in cell migration. Group 3 tumours are more aggressive and more likely to be metastatic[131] than SHH tumours. Metastasis involves many cell processes including migration but also degradation of the ECM, EMT and invasion. *In vitro* migration rate can be an indicator of metastatic potential, therefore the clinical features of Group 3 tumours suggest Group 3 cell lines would be more migratory. However, the gap closure assay used in this thesis measured cellular migration only, and the activation of the SHH signalling pathway clearly increases cellular migration in a range of cell lines[123,125,130,488–495]. It was hypothesised, therefore, that the activation of the SHH signalling pathway in SHH subgroup cell lines would result in a higher baseline rate of cell migration in the gap closure assays compared to the Group 3 cell line. It was also predicted that radiation would increase the rate of cell migration. An *in vitro* migration assay, the gap closure assay, was optimised to assess cellular migration in the MBL cell line panel. The work found that the SHH cell lines had a higher baseline rate of gap closure, but that gap closure rate was highly cell line dependent. Irradiation-induced effects on gap closure rate were observed for all cell lines, however these were also cell line dependent and appeared independent of subgroup status.

4.5.1. Python code development

The gap closure assay, where the closure of a gap in a cell monolayer is measured over time, is widely used in the literature to measure migration [224,243,471,472,476,481]. Gap closure can be measured and reported as gap width at different time points, gap area at different time points and the gap closure rate. For measurements of gap width the Nature protocol recommends taking at least 100 measurements per time point[552], although this has not been reported in any of the publications reviewed during this project[224,243,471,472,476,481]. In fact, the accurate measurement of gap width or area and subsequent calculation of gap closure rate is rarely reported.

As part of the gap closure assay optimisation, an automated analysis method was sought to provide non-subjective and rapid analysis. Several programs were available but none were found to be suitable. The companion software for the IncuCyte Zoom live-cell imaging system, which was used to capture images during the experiments, was not compatible with other experimental parameters including the culture vessel. This software also reported the relative wound density rather than the gap width as recommended in the Nature protocol[552]. The TScratch[673] and PyScratch[554] programs were unable to accurately differentiate the cell monolayer from the gap region. The parameters of the image analysis algorithms for these two programs were not under user control, and therefore could not be adjusted to optimise image analysis for the MBL cell lines. The most suitable, pre-existing program was a macro for the ImageJ software, 'MRI Wound Healing'[674]. This software does allow the user to alter the image analysis algorithm parameters, however the optimisation of these for each well was time-consuming and some subjectivity still remained. The macro also reported gap area rather than gap width.

An alternative automated analysis method that could fulfil all the analysis requirements was devised using the Python programming language. These requirements were: compatible and adaptable for a wide range of cell lines; quick analysis of large time-lapse microscopy datasets; at least 100 measurements of gap width for each image; produced documentation of the experimental and analysis parameters along with the analysed images; and would

calculate the gap closure rate for each well. In order for the program to be compatible with a wide range of cell lines, the parameters for the image analysis process were user-controlled. A separate function was written into the program to provide quick optimisation of these parameters for each cell line.

4.5.2. Evaluation of methods for gap closure analysis

Comparison experiments demonstrated that the in-house python program was as accurate at analysing images as the 'gold standard' manual measurements. Direct comparisons between analysis methods for gap closure assays are rare within the literature, even in papers describing a new analysis software. The TScratch software carries out comparisons between TScratch and manual analysis, showing no difference in the reported gap area of identical data sets by these two methods[673]. No further comparisons, such as time required for analysis, delineation of gap edge or reproducibility of the analysis over time were reported[673]. The more recently published PyScratch software compares between PyScratch and the MRI Macro, but no manual analysis was carried out[554]. There was no significant difference between the normalised gap area or gap closure rate reported by the two methods for the same dataset[554]. In this thesis, the MRI Macro reported significantly reduced gap width and area measurements compared to the manual measurements. While the PyScratch software was not able to be used with the MBL datasets, it may be anticipated that PyScratch would also report reduced gap area compared to manual measurements.

There are many metrics that can be generated by the gap closure assay including the gap width over time, the gap area over time and gap closure rate[675]. Both TScratch[673] and PyScratch[554] report the gap area over time, and compare this metric to the chosen alternative analysis methods. Gap closure rate removes subjectivity, is independent of the initial gap size and does not require complete gap closure[675] and therefore was selected for use. The gap closure rate should only be measured during the linear portion of gap closure as gap closure rate can decrease over time in some cell lines[676]. The largest difference between the manual measurements method and the Python code for the MBL data was the gap closure rate. The calculation of the gap closure rate is where the manual measurements

method is weakest as the rate is calculated between the first image of the assay and a later time point[552,675]. While this later time point is user selected, the Nature protocols recommends selecting just before the gap is completely closed under the conditions that produce the fastest gap closure[552]. As gap closure rate decreased over time[676], in the wells where gap closure is fastest, this recommendation will include part of the non-linear portion of gap closure. The gap closure rate produced by the Python code is therefore more comparable across wells and conditions.

4.5.3. Migration assay method development

A review of the gap closure assay highlighted a lack of standardisation across publications with regards to the method of gap creation, culture parameters during the assay and quantification of gap closure[675]. The development of the Python code provided confidence in the gap width being accurately and reproducibly quantified. Further method development work was undertaken in order to identify the most suitable method of gap creation and culture parameters.

Two methods of gap creation were investigated, using Ibidi inserts which physically prevent the cell monolayer from forming in a region of the culture surface and using the EssenBio WoundMaker which physically scratches a section of a cell monolayer from the culture surface. A barrier method such as the Ibidi inserts provide increased gap reproducibility and cause minimal damage to both the culture surface and the remaining cell monolayer[675,677]. The Ibidi inserts are claimed to prevent the removal of gap surface ECM residues, vessel surface damage, cell damage and the initiation of signalling from necrotic or apoptotic cells, all of which can result from a physical scratch[678]. However, cells can adhere to the inserts prior to removal, and the removal of the inserts can cause jagged edges when these adhered cells are also removed[675]. Often, these advantages are in reference to a low-throughput scratch method, such as using a pipette tip or spatula, in order to create the scratch. Each well is individually scratched, and the inevitable variation in pressure and extent of cell damage contribute to the reproducibility issues of this assay[677]. There are gap edge effects with scratch-based assays as well, as the cells at the gap edge neighbour those

sheared off the surface and may also sustain some cell damage[675]. The WoundMaker was designed to produce a scratch in every well of a 96-well plate using a consistent and even pressure, thus removing the problems of gap reproducibility and cell/vessel damage[679]. The two methods of gap creation are relevant to different *in vivo* biological processes involving cell migration. The barrier method is more representative of collective cell migration where there has been no physical stimulus, as occurs in metastasis, while a scratch may be more representative of processes such as wound healing in response to a physical stimulus[677]. There are many complex processes and signalling events during cancer metastasis. The gap closure assay is an attempt to model a single process in a 2D cell monolayer containing a single cell type and is perhaps so far removed from the *in vivo* situation that the nuance of gap creation method is inconsequential. Considering a stimulus is required to induce cellular migration[463], it may be that a physical scratch is required within the gap closure assay in order to induce the migration process. Both methods had potentially equal value and so both were initially investigated in the four adherent cell lines.

The method of gap creation had a significant difference on gap closure rate within two of the cell lines. A small number of studies have also shown that gap creation method can affect gap closure rate. In studies comparing a damaging method, such as a physical scratch, to a non-damaging method, the scratch produced faster gap closure. For example, comparing a scratch made with a pipette tip to a gap from selectively applied trypsin, the physical scratch induced faster gap closure[680]. Barrier methods using custom-made inserts repeatedly resulted in slower gap closure than physical scratches[681,682]. When an agarose strip was used to create a physical barrier to cell growth, no difference from a pipette tip generated scratch was reported[683]. However, this study compared the percentage of the initial gap width at each time point[683]. If gap closure rate is constant within a cell line at the same time after the gap is created, during the assay the distance travelled over a time period will be the same in each well. However, in wells where the initial gap width was larger this will account for a smaller percentage change of the initial gap width. Neither the agarose strip nor the pipette scratch methods are likely to produce uniform gaps between wells, therefore producing a variety of initial gap widths across the assay. The lack of difference between the

methods in this study may be a result of the analysis method rather than a true similarity between the two. In contrast, no difference was seen when both methods caused cellular damage while the gap was created – for example using a pipette tip or a magnet to scratch cells from the surface[682] or comparing a pipette tip and ultraviolet light to remove the cells[684]

For MED8A the physical damage of the WoundMaker induces the cells to close the gap faster. For UW228-2 cells, the physical damage slowed gap closure. From the data available, it is not possible to identify why these two cell lines produced the opposite responses, whether this is a biological response or a result of the methodologies, or why the remaining two cell lines showed no effect of gap closure method. A potential biological explanation would be that the scratch increases SHH signalling in the Group 3 cell line but not in the SHH cell lines, where the pathway is already overactive, inducing migration and faster gap closure in this cell line. Alternatively, the WoundMaker may damage the culture vessel in a manner that prevents gap closure of the better adhered UW228-2 cell line but not of the MED8A cell line which is much less well-adhered to the vessel surface. As neither gap creation method was able to be selected over the other, both were used in the irradiation experiments.

The gap closure assay measures the closure of the gap as a surrogate for cellular migration[675]. While the gap closure may be due to cells moving into the gap through cellular migration, the proliferation of cells within the monolayer will also act to close the gap[675]. Cellular proliferation can be inhibited or minimised during the gap closure assay to control for this, the most common methods are reducing the FBS concentration in the medium or pharmacological inhibition using actinomycin C or mitomycin C[675,685,686]. The pharmacological inhibition of proliferation can result in off-target effects such as increased apoptosis which can influence the assay results[675,685,686]. While a reduced FBS concentration can also cause toxic cellular effects, it had been established previously within the group that the MBL cell line panel could survive well in 0.1% FBS concentrations for at least 48 h with no significant increases in apoptosis. The serum starvation method using the higher concentration of 1% was therefore selected for use in this project.

Decreasing the serum concentration from 10% to 1% FBS increased gap closure rate in DAOY and ONS-76. The lower FBS concentration was expected to reduce proliferation and therefore reduce the contribution of proliferation to gap closure and gap closure rate. The opposite was observed. It has been previously shown using time-lapse microscopy and individual cell tracking that MBL cell lines do not undergo mitosis and migrate at the same time[687]. While this may suggest that cells which divide more frequently spend more time not moving, no correlation was found between the number of divisions and the total distance migrated across the cell lines[687]. A reduced FBS concentration elongates the phases of the cell cycle[600] and thus prolongs the time a cell spends outside of mitosis. The 1% FBS concentration would therefore mean that the cells spend a greater proportion of the 24 h period of the assay moving compared to 10% FBS, which could result in an increased gap closure rate. Alternatively, the reduced FBS concentration induced a more migratory phenotype, as reduced FBS concentrations have been found to induce EMT *in vitro*[688,689]. As the altered gap closure rate was only observed in two cell lines this would suggest that the different cell lines were responding differently to the low FBS concentration. However, the two cell lines showing increased gap closure with decreased FBS were the faster growing of the panel, with doubling times of 16 h for DAOY and 12 h for ONS-76. This would provide an explanation for the different responses of the cell lines as DAOY and ONS-76 cells are unable to migrate due to mitosis more frequently than MED8A or UW228-2 cells. Profiling of EMT protein marker expression under low FBS conditions would be required to completely rule out the induction of a migratory phenotype.

4.5.4. Migration assay results

Under control conditions, the SHH cell lines showed faster gap closure than the Group 3 cell line. The SHH signalling pathway increases cellular migration, and in the SHH subgroup this pathway is constitutively activated[13,15]. Two of the SHH cell lines, DAOY and ONS-76, have been used in a gap closure assay previously, however the published results showed that DAOY[243,502] was faster than ONS-76[502] while the opposite is reported here. The MBL cell line panel only contains one Group 3 cell line, MED8A. MED8A showed a very slow gap closure

rate, which was unexpected considering Group 3 tumours are more likely to be metastatic on presentation[131]. This observation may be due to experimental limitations rather than an accurate reflection of the metastatic potential of MED8A. This cell line does not form a confluent monolayer especially readily and required a very high seeding density in the gap closure assay, twice that of the SHH cell lines. Additionally, the MED8A cells only weakly adhere to the culture vessel surface which would impede their ability to migrate as this process requires adhesions to the culture surface[463]. Coating of the vessel surface to improve adhesion or use of an alternative migration assay, such as the transwell assay, may be more suited to this cell line and provide a more accurate measure of cell migration.

For UW228-2 and MED8A, the control gap closure rates remained fairly consistent between the insert and WoundMaker assays and across the different time points. These cells were not used in the longer-term Ibidi insert assays as they did not form confluent monolayers when re-seeded into the inserts following a 24 h or seven day incubation. For ONS-76 the control gap closure rates are also consistent, however for DAOY cells the control gap closure rate for the seven day insert assay is lower than in the other assays. A significant difference is reported between the 0 Gy and 2 Gy results in this assay. As the 0 Gy control flasks did not have any growth delay or cell death as a result of radiation treatment, these flasks had a higher cell density for longer periods of time during this seven day delay. These stressful conditions could explain the reduced gap closure rate in these samples, and the reduced gap closure rate in the control accounts for the significantly increased 2 Gy gap closure rate.

Biological changes following irradiation take hours-days to manifest, and this is likely to be the case for irradiation-induced migration changes. In the work presented here, monitoring gap closure immediately following irradiation produced no significant changes in gap closure using the Ibidi insert method. A delay between irradiation and gap creation of either 24 h or 7 days also produced no differences in the gap closure rate, with the exception of DAOY, discussed above. In the WoundMaker assay, immediately following irradiation changes were observed for two cell lines at the highest radiation dose, 8 Gy, only. For DAOY cells, the gap

closure was decreased. This decrease in gap closure may be a result of cell death following the high radiation exposure preventing cells from being able to migrate into the gap.

The Ibidi insert method resulted in the same gap closure rate regardless of radiation dose for the four cell lines, while the WoundMaker method resulted in significant irradiation-induced changes. The stimulus of a physical scratch may be required for irradiation-induced changes to cell migration to be observed in the *in vitro* gap closure assay. The majority of irradiation studies were carried out using the transwell migration assay, most of which reported no change in migration following irradiation[470,473,474,480]. The majority of wound healing assays from the literature, which use the physical scratch method of gap creation, report irradiation-induced increases in migration[243,471,472,476]. If the scratch is required as a stimulus in these assays, this may explain the contradictory results from different assay protocols. If there is a requirement of a physical scratch to produce altered migration in response to irradiation, this would make the *in vitro* migration assay further removed from the *in vivo* situation. However, radiation increases cell migration, invasion and metastasis *in vivo*[466–469], therefore the ability to mimic these could make the scratch-based assay more valuable.

When a 24 h delay between irradiation and gap creation was included, significant alterations to gap closure rate were found for all four adherent cell lines. There was a dose-dependent increase in gap closure in ONS-76, a dose-dependent decrease in gap closure in MED8A and UW228-2 and an increase following 2 Gy but no change following 8 Gy for DAOY. Our results for the Group 3 cell lines MED8A, of a decreased gap closure rate following irradiation suggesting a decrease in cell migration following irradiation, are in agreement with the results from a previously reported transwell assay[503]. DAOY has been reported as having decreased cell migration in the gap closure assay following a 7 Gy dose[504]. At 8 Gy, this project also found a decrease in gap closure rate both immediately following irradiation and at 24 h, although the latter was not significant. The previously reported gap closure assay included a single dose of 7 Gy and does not report either a delay between irradiation and gap creation[504], therefore this assay is most similar to the immediate irradiation method

described here. No publication has reported the effect of irradiation on the ONS-76 or UW228-2 cell lines.

The delayed irradiation results using the WoundMaker method divides the cells into two groups, however these are not split by subgroup. The most obvious difference between the cell lines that show increased gap closure and those that show decreased gap closure is doubling time. DAOY and ONS-76, whose gap closure is increased following irradiation, are faster growing cells than UW228-2 and MED8A. The interplay between proliferation and migration would appear more influential to the radiation response than the subgroup status and associated underlying biological differences. Expansion of the work to investigate EMT markers within cells, both before and after irradiation, and patient samples would further confirm this if no subgroup-specific expression patterns were observed. An invasion assay using Matrigel to simulate the ECM could be used to quantify the semi-adherent as well as the adherent cell lines, and investigate literature reports of increased invasion following irradiation in MBL cell lines[504]. Unless a link with the subgroups is demonstrated, repetition of the gap closure assay work with SHH pathway inhibitors is only necessary to confirm that the faster gap closure in SHH cell lines is a result of the overactive pathway in this subgroup.

4.6. Conclusions

The overall aim of this thesis was to identify factors that might lead to differences in the radioresponsiveness of the four MBL molecular subgroups and could potentially be used in the future to personalise treatments. The radioresponsiveness of a tumour describes the extent of clinical response to radiotherapy. The different molecular subgroups of MBL have significantly different survival outcomes[14,75–77], which could reflect differences in radioresponsiveness. Three factors which significantly contribute to radioresponse are intrinsic radiosensitivity, proliferative capacity and tumour hypoxia and these have been investigated in MBL cell lines and patient samples.

Despite the small number of cell lines available to study, the work presented in this thesis showed for the first time that the molecular subgroups of MBL have significantly different

intrinsic radiosensitivities *in vitro*. In cell line work, Group 3 cell lines were less radiosensitive than SHH cell lines, and within the SHH subgroup *TP53* mutant cell lines were less radiosensitive than the *TP53* WT cell line. Findings *in vivo* were broadly similar with Group 3 being less radiosensitive than the SHH subgroup in patient cohorts. However, in the clinical cohorts Group 4 tumours, which have intermediate survival outcomes, were the least radiosensitive MBL subgroup suggesting that radiosensitivity alone cannot explain the different clinical outcomes of MBL. Given the differences found *in vitro* and that the RSI was prognostic in univariable analysis, further study would be worthwhile in more cell lines and cohorts. This future work needs to consider radiosensitivity alongside other factors that might be important such as the number of CSCs.

The preliminary proton irradiation work represents the first use of the high-throughput radiosensitivity assay to generate RBE values for MBL cell lines representing different molecular subgroups. Previously, proton and x-ray comparisons using MBL cell lines have been done using a single cell line. The Group 3 cell line MED8A had higher RBE values than the SHH cell line. If confirmed by completion of the biological replicates for all six MBL cell lines in our panel, this finding would indicate that Group 3 tumours would receive greater benefit from PBT.

As radiotherapy is a significant, contributing factor to overall survival in MBL[7–10,55], other factors must influence the radioresponse. MBL was classified as a non-proliferative-informative cancer, indicating that proliferation does not significantly contribute to survival outcomes. The proliferative capacity as measured by single gene expression markers and a proliferation gene signature was not shown not to be significantly different between the MBL molecular subgroups. Therefore, the conclusion from this thesis is that proliferative capacity is unlikely to be contributing to a different radioresponse across the subgroups.
The final contributing factor to radioresponse investigated in this project was tumour hypoxia. The hypoxia biomarkers applied to the MBL patient cohorts were not prognostic and no significant difference in expression was found across the molecular subgroups. From the work carried out for this thesis, it is not possible to draw any conclusion for a role of hypoxia

in subgroup-specific radioresponsiveness in MBL. However, the gene signature work generated some evidence for different levels of hypoxia across MBL subgroups and these different levels of hypoxia help to explain the different survival outcomes across the molecular subgroups. Development of a hypoxia gene signature for MBL and IHC staining of subgrouped tumour samples for hypoxia biomarkers is required to confirm these findings.

An investigation into *in vitro* cellular migration using a gap closure assay found that the SHH cell lines tested showed faster baseline gap closure than the Group 3 cell line, but additional cell lines are required to confirm this is a subgroup-specific difference. Treatment with irradiation did induce dose-dependent changes across the cell line panel, but this was not associated with subgroup status in our cell line panel. The interaction of irradiation and metastasis-related processes in MBL is worth further study to confirm irradiation-induced changes in patient samples and identify potential underlying causes.

This thesis investigated whether subgroup-specific differences in radioresponsiveness affect clinical outcomes in MBL. It provides evidence that two factors which influence radioresponsiveness, intrinsic radiosensitivity and extent of tumour hypoxia, show subgroup-specific differences. Intrinsic radiosensitivity was prognostic in MBL, however subgroup-specific radiosensitivities do not reflect subgroup survival outcomes. Tumour hypoxia was not prognostic in MBL, however subgroup-specific differences were identified which did reflect survival outcomes. The different levels of tumour hypoxia may mitigate the intrinsic radiosensitivity, resulting in the observed radioresponses of the subgroups. In conclusion, subgroup-specific differences in intrinsic radiosensitivity and level of hypoxia are found within MBL and the resulting subgroup-specific radioresponsiveness may contribute to clinical outcomes.

5. References

1. Cancer Research UK. Cancer mortality statistics | Cancer Research UK. Available at: https://www.cancerresearchuk.org/health-professional/cancer-statistics/mortality. (Accessed: 31st May 2021)
2. Cancer Research UK. Cancer risk statistics | Cancer Research UK. Available at: https://www.cancerresearchuk.org/health-professional/cancer-statistics/risk. (Accessed: 31st May 2021)
3. Cancer Research UK. Cancer survival for common cancers | Cancer Research UK. Available at: https://www.cancerresearchuk.org/health-professional/cancer-statistics/survival/common-cancers-compared. (Accessed: 31st May 2021)
4. Quaresma, M., Coleman, M. P. & Rachet, B. 40-year trends in an index of survival for all cancers combined and survival adjusted for age and sex for each cancer in England and Wales, 1971-2011: A population-based study. *Lancet* **385**, 1206–1218 (2015).
5. Cancer Research UK. Children's cancer statistics | Cancer Research UK. Available at: https://www.cancerresearchuk.org/health-professional/cancer-statistics/childrens-cancers. (Accessed: 31st May 2021)
6. Cancer Research UK. Children's cancers survival statistics | Cancer Research UK. Available at: https://www.cancerresearchuk.org/health-professional/cancer-statistics/childrens-cancers/survival. (Accessed: 31st May 2021)
7. Kun, L. E., Mulhern, R. K. & Crisco, J. J. Quality of life in children treated for brain tumors. Intellectual, emotional, and academic function. *J Neurosurg* **58**, 1–6 (1983).
8. Duffner, P. K., Cohen, M. E. & Thomas, P. Late Effects of Treatment on the Intelligence of Children with Posterior Fossa Tumors. *Cancer* **51**, 233–237 (1983).
9. Spiegler, B. J., Bouffet, E., Greenberg, M. L., Rutka, J. T. & Mabbott, D. J. Change in Neurocognitive Functioning After Treatment With Cranial Radiation in Childhood. *J. Clin. Oncol.* **22**, 706–713 (2004).
10. Grau, C. & Overgaard, J. Postirradiation sensorineural hearing loss: A common but ignored late radiation complication. *Int. J. Radiat. Oncol. Biol. Phys.* **36**, 515–517 (1996).
11. Duffner, P. K., Cohen, M. E., Thomas, P. R. M. & Lansky, S. B. The Long-Term Effects of Cranial Irradiation on the Central Nervous System. *Cancer* **56**, 1841–1846 (1985).
12. Laughton, S. J. *et al.* Endocrine Outcomes for Children With Embryonal Brain Tumors After Risk-Adapted Craniospinal and Conformal Primary-Site Irradiation and High-Dose Chemotherapy With Stem-Cell Rescue on the SJMB-96 Trial. *J. Clin. Oncol.* **26**, 1112–1118 (2008).
13. Northcott, P. A. *et al.* Medulloblastoma Comprises Four Distinct Molecular Variants. *J. Clin. Oncol.* **29**, 1408–1414 (2011).
14. Kool, M. *et al.* Integrated Genomics Identifies Five Medulloblastoma Subtypes with Distinct Genetic Profiles, Pathway Signatures and Clinicopathological Features. *PLoS One* **3**, e3088 (2008).
15. Kool, M. *et al.* Molecular subgroups of medulloblastoma: an international meta-analysis of transcriptome, genetic aberrations, and clinical data of WNT, SHH, Group 3, and Group 4 medulloblastomas. *Acta Neuropathol.* **123**, 473–484 (2012).
16. Northcott, P. A. *et al.* Subgroup specific structural variation across 1,000 medulloblastoma genomes. *Nature* **488**, 49–56 (2012).
17. Remke, M. *et al.* Adult Medulloblastoma Comprises Three Major Molecular Variants. *J. Clin. Oncol.* **29**, 2717–2723 (2011).
18. Taylor, M. D. *et al.* Molecular subgroups of medulloblastoma: The current consensus. *Acta Neuropathol.* **123**, 465–472 (2012).
19. Baskar, R., Lee, K. A., Yeo, R. & Yeoh, K. W. Cancer and Radiation Therapy: Current Advances and Future Directions. *International Journal of Medical Sciences* **9**, 193–199 (2012).
20. Merchant, T. E. Clinical controversies : Pediatric tumors. *Semin Radiat Oncol* **23**, 97–108 (2013).
21. Michiels, E., Schouten-van Meeteren, A., Doz, F., Janssens, G. & Van Dalen, E.

Chemotherapy for children with medulloblastoma (Review). *Cochrane Database of Systematic Reviews* (2015). doi:10.1002/14651858.CD006678.pub2.www.cochranelibrary.com
22. First cancer patient in England ready for proton beam therapy. Available at: https://www.christie.nhs.uk/about-us/news-at-the-christie/latest-news-stories/first-cancer-patient-in-england-to-receive-proton-beam-therapy-set-for-treatment. (Accessed: 31st May 2021)
23. Medulloblastoma - American Brain Tumor Association. Available at: https://www.abta.org/tumor_types/medulloblastoma/. (Accessed: 12th October 2016)
24. The Royal Marsden NHS Foundation Trust. Medulloblastoma/PNET | The Royal Marsden NHS Foundation Trust. Available at: https://www.royalmarsden.nhs.uk/your-care/cancer-types/paediatric-cancers/medulloblastomapnet. (Accessed: 31st May 2021)
25. Dolecek, T. A., Propp, J. M., Stroup, N. E. & Kruchko, C. CBTRUS Statistical Report : Primary Brain and Central Nervous System Tumors Diagnosed in the United States in 2005-2009. *Neuro. Oncol.* **14**, v1–v49 (2012).
26. Ellison, D. Classifying the medulloblastoma: Insights from morphology and molecular genetics. *Neuropathology and Applied Neurobiology* **28**, 257–282 (2002).
27. Evans, D. G. R., Farndon, P. A., Burnell, L. D., Rao Gattamaneni, H. & Birch, J. M. The incidence of Gorlin syndrome in 173 consecutive cases of medulloblastoma. *Br. J. Cancer* **64**, 959–961 (1991).
28. Cancer Research UK. Medulloblastoma | Children's brain tumours | Cancer Research UK. Available at: https://www.cancerresearchuk.org/about-cancer/childrens-cancer/brain-tumours/types/medulloblastoma. (Accessed: 31st May 2021)
29. NCI. Medulloblastoma Diagnosis and Treatment - National Cancer Institute. Available at: https://www.cancer.gov/rare-brain-spine-tumor/tumors/medulloblastoma. (Accessed: 31st May 2021)
30. The Royal College of Radiologists. *Radiotherapy dose fractionation*. *Radiology dose fractionation* (Clinical Oncology, 2019). doi:10.1259/0007-1285-48-575-960-a
31. Menyhárt, O., Giangaspero, F. & Gyorffy, B. Molecular markers and potential therapeutic targets in non-WNT/non-SHH (group 3 and group 4) medulloblastomas. *J. Hematol. Oncol.* **12**, 1–17 (2019).
32. Thompson, E. M., Ashley, D. & Landi, D. Current medulloblastoma subgroup specific clinical trials. *Transl. Pediatr.* **9**, 157–162 (2020).
33. BMJ. BMJ Best Practice - Medulloblastoma Diagnostic Investigations. (2016). Available at: http://bestpractice.bmj.com/best-practice/monograph/733/diagnosis/tests.html. (Accessed: 14th November 2016)
34. Yock, T. I. *et al.* Quality of life outcomes in proton and photon treated pediatric brain tumor survivors. *Radiother. Oncol.* **113**, 89–94 (2014).
35. Gottardo, N. G. *et al.* Medulloblastoma Down Under 2013: a report from the third annual meeting of the International Medulloblastoma Working Group. *Acta Neuropathol.* **127**, 189–201 (2014).
36. Menyhárt, O. & Győrffy, B. Molecular stratifications, biomarker candidates and new therapeutic options in current medulloblastoma treatment approaches. *Cancer Metastasis Rev.* (2020). doi:10.1007/s10555-020-09854-1
37. Packer, R. J. *et al.* Phase III Study of Craniospinal Radiation Therapy Followed by Adjuvant Chemotherapy for Newly Diagnosed Average-Risk Medulloblastoma. *J. Clin. Oncol.* **24**, 4202–4208 (2006).
38. Gajjar, A. *et al.* Risk-adapted craniospinal radiotherapy followed by high-dose chemotherapy and stem-cell rescue in children with newly diagnosed medulloblastoma (St Jude Medulloblastoma-96): long-term results from a prospective, multicentre trial. *Lancet Oncol.* **7**, 813–820 (2006).
39. Search of: medulloblastoma - List Results - ClinicalTrials.gov. Available at: https://clinicaltrials.gov/ct2/results?cond=medulloblastoma&term=&cntry=&state=&city=&dist=. (Accessed: 25th June 2021)
40. Search of: subgroup AND Molecular | Medulloblastoma - List Results - ClinicalTrials.gov. Available at: https://clinicaltrials.gov/ct2/results?term=subgroup+AND+Molecular&cond=Medulloblastoma. (Accessed: 25th June 2021)

41. ClinicalTrials.gov. A Clinical and Molecular Risk-Directed Therapy for Newly Diagnosed Medulloblastoma. *ClinicalTrials.gov* 1–20 (2017). Available at: https://clinicaltrials.gov/ct2/show/NCT01878617. (Accessed: 24th November 2016)
42. Study Assessing the Feasibility of a Surgery and Chemotherapy-Only in Children With Wnt Positive Medulloblastoma - ClinicalTrials.gov. Available at: https://clinicaltrials.gov/ct2/show/NCT02212574?cond=Medulloblastoma&draw=2&rank=5. (Accessed: 20th July 2017)
43. Reduced Craniospinal Radiation Therapy and Chemotherapy in Treating Younger Patients With Newly Diagnosed WNT-Driven Medulloblastoma - ClinicalTrials.gov. Available at: https://clinicaltrials.gov/ct2/show/NCT02724579?cond=Medulloblastoma&draw=2&rank=12. (Accessed: 20th July 2017)
44. Focal Radiotherapy Plus Low Dose Craniospinal Irradiation Followed by Adjuvant Chemotherapy in WNT Medulloblastoma. - Full Text View - ClinicalTrials.gov. Available at: https://clinicaltrials.gov/ct2/show/NCT04474964?cond=Medulloblastoma&draw=2&rank=8. (Accessed: 1st June 2021)
45. Doyle, T. A Clinical and Molecular Risk-Directed Therapy for Newly Diagnosed Medulloblastoma - Full Text View - ClinicalTrials.gov. 1–20 (2017).
46. ClinicalTrials.gov & Pharmaceuticals, N. A Phase II Study of Oral LDE225 in Patients With Hedge-Hog (Hh)-Pathway Activated Relapsed Medulloblastoma (MB). *ClinicalTrials.gov [Internet]* Available at: https://clinicaltrials.gov/ct2/show/NCT01708174?cond=Medulloblastoma&draw=2&rank=15. (Accessed: 6th January 2017)
47. Study of Vismodegib in Combination With Temozolomide Versus Temozolmide Alone in Patients With Medulloblastomas With an Activation of the Sonic Hedgehog Pathway - Clinicaltrials.gov. Available at: https://clinicaltrials.gov/ct2/show/NCT01601184?cond=medulloblastoma&draw=2&rank=18.
48. Personalized Risk-Adapted Therapy in Post-Pubertal Patients With Newly-Diagnosed Medulloblastoma - Full Text View - ClinicalTrials.gov. Available at: https://clinicaltrials.gov/ct2/show/NCT04402073?cond=Medulloblastoma&draw=2&rank=7. (Accessed: 1st June 2021)
49. Vismodegib in Treating Patients With Recurrent or Refractory Medulloblastoma - Full Text View - ClinicalTrials.gov. Available at: https://clinicaltrials.gov/ct2/show/NCT00939484?cond=Medulloblastoma&draw=2&rank=21. (Accessed: 1st June 2021)
50. SJDAWN: St. Jude Children's Research Hospital Phase 1 Study Evaluating Molecularly-Driven Doublet Therapies for Children and Young Adults With Recurrent Brain Tumors - Full Text View - ClinicalTrials.gov. Available at: https://clinicaltrials.gov/ct2/show/NCT03434262?cond=Medulloblastoma&draw=2&rank=83. (Accessed: 1st June 2021)
51. HeadStart4: Newly Diagnosed Children (<10 y/o) With Medulloblastoma and Other CNS Embryonal Tumors - Full Text View - ClinicalTrials.gov. Available at: https://clinicaltrials.gov/ct2/show/NCT02875314?cond=Medulloblastoma&draw=2&rank=32. (Accessed: 1st June 2021)
52. Girardi, F., Allemani, C. & Coleman, M. P. Worldwide Trends in Survival From Common Childhood Brain Tumors: A Systematic Review. *J. Glob. Oncol.* (2019). doi:10.1200/JGO.19.00140
53. Cancer.net. Medulloblastoma - Childhood: Statistics. Available at: http://www.cancer.net/cancer-types/medulloblastoma-childhood/statistics. (Accessed: 11th May 2020)
54. Wahba, H., Abu-Hegazy, M., Wasel, Y., Ismail, E. & Zidan, A. S. Adjuvant chemotherapy after reduced craniospinal irradiation dose in children with average-risk medulloblastoma: A 5-year follow-up study. *JBUON* **18**, 425–429 (2013).
55. Narayan, V. *et al.* Medulloblastoma: Distinctive Histo-Molecular Correlation with Clinical Profile, Radiologic Characteristics, and Surgical Outcome. *Pediatr. Neurosurg.* **54**, 329–340 (2019).
56. Shih, D. J. H. *et al.* Cytogenetic Prognostication Within Medulloblastoma Subgroups.

J. Clin. Oncol. **32**, 886–896 (2014).
57. Ris, M. D., Packer, R., Goldwein, J., Jones-Wallace, D. & Boyett, J. M. Intellectual Outcome After Reduced-Dose Radiation Therapy Plus Adjuvant Chemotherapy for Medulloblastoma : A Children's Cancer Group Study. *J. Clin. Oncol.* **19**, 3470–3476 (2001).
58. Szentes, A. *et al.* Cognitive deficits and psychopathological symptoms among children with medulloblastoma. *Eur. J. Cancer Care (Engl).* e12912 (2018). doi:10.1111/ecc.12912
59. Helseth, E., Due-Tønnessen, B., Wesenberg, F., Lote, K. & Lundar, T. Posterior fossa medulloblastoma in children and young adults (0-19 years): survival and performance. *Child's Nerv. Syst.* **15**, 451–456 (1999).
60. Heikens, J. *et al.* Long-term Neuro-endocrine Sequelae After Treatment for Childhood Medulloblastoma. *Eur. J. Cancer* **34**, 1592–1597 (1998).
61. Paulino, A. C. Hypothyroidism in children with medulloblastoma: a comparison of 3600 and 2340 cGy craniospinal radiotherapy. *Int. J. Radiat. Oncol. Biol. Phys.* **53**, 543–547 (2002).
62. Chin, D. *et al.* Thyroid Dysfunction as a Late Effect in Survivors of Pediatric Medulloblastoma/Primitive Neuroectodermal Tumors: A Comparison of Hyperfractionated versus Conventional Radiotherapy. *Cancer* **80**, 798–804 (1997).
63. Jimenez, R. B. *et al.* Proton Radiation Therapy for Pediatric Medulloblastoma and Supratentorial Primitive Neuroectodermal Tumors: Outcomes for Very Young Children Treated With Upfront Chemotherapy. *Int. J. Radiat. Oncol. Biol. Phys.* **87**, 120–126 (2013).
64. Fossati, P., Ricardi, U. & Orecchia, R. Pediatric medulloblastoma: Toxicity of current treatment and potential role of protontherapy. *Cancer Treat. Rev.* **35**, 79–96 (2009).
65. Xu, W., Janss, A. & Moshang, T. Adult Height and Adult Sitting Height in Childhood Medulloblastoma Survivors. *J. Clin. Endocrinol. Metab.* **88**, 4677–4681 (2003).
66. Gurney, J. G. *et al.* Endocrine and cardovascular late effects among adult survivors of childhood brain tumors. *Cancer* **97**, 663–672 (2003).
67. Armstrong, G. T. Long-term survivors of childhood central nervous system malignancies: The experience of the Childhood Cancer Survivor Study. *Eur. J. Paediatr. Neurol.* **14**, 298–303 (2010).
68. Eberhart, C. G. *et al.* Histopathologic Grading of Medulloblastomas: A Pediatric Oncology Group study. *Cancer* **94**, 552–560 (2002).
69. Louis, D. N. *et al.* The 2007 WHO Classification of Tumours of the Central Nervous System. *Acta Neuropathol.* **114**, 97–109 (2007).
70. Massimino, M. *et al.* Histological variants of medulloblastoma are the most powerful clinical prognostic indicators. *Pediatr. Blood Cancer* **60**, 210–216 (2013).
71. Orr, B. A. Pathology, diagnostics, and classification of medulloblastoma. *Brain Pathology* **30**, 664–678 (2020).
72. Borowska, A. & Jóźwiak, J. Medulloblastoma: molecular pathways and histopathological classification. *Arch. Med. Sci.* **12**, 659–666 (2016).
73. Wippold II, F. J. & Perry, A. Neuropathology for the Neuroradiologist: Rosettes and Pseudorosettes. *American Journal of Neuroradiology* **27**, 488–492 (2006).
74. Louis, D. N. *et al.* The 2016 World Health Organization Classification of Tumors of the Central Nervous System: a summary. *Acta Neuropathol.* **131**, 803–820 (2016).
75. Kameda-Smith, M. M. Pediatric medulloblastoma in the molecular era: what are the surgical implications? *Cancer Metastasis Rev.* (2020). doi:10.1007/s10555-020-09865-y
76. Ellison, D. W. *et al.* Medulloblastoma: clinicopathological correlates of SHH, WNT, and non-SHH/WNT molecular subgroups. *Acta Neuropathol.* **121**, 381–396 (2011).
77. Gibson, P. *et al.* Subtypes of medulloblastoma have distinct developmental origins. *Nature* **468**, 1095–1099 (2010).
78. Northcott, P. A. *et al.* Rapid, reliable, and reproducible molecular sub-grouping of clinical medulloblastoma samples. *Acta Neuropathol.* **123**, 615–626 (2012).
79. Thompson, M. C. *et al.* Genomics Identifies Medulloblastoma Subgroups That Are Enriched For Specific Genetic Alterations. *J. Clin. Oncol.* **24**, 1924–1931 (2006).
80. Kaur, K. *et al.* Integrating Molecular Subclassification of Medulloblastomas into Routine Clinical Practice: A Simplified Approach. *Brain Pathol.* **26**, 334–343 (2016).

81. Schwalbe, E. C. *et al.* DNA methylation profiling of medulloblastoma allows robust sub-classification and improved outcome prediction using formalin-fixed biopsies. *Acta Neuropathol.* **125**, 359–371 (2013).
82. Northcott, P. A., Korshunov, A., Pfister, S. M. & Taylor, M. D. The clinical implications of medulloblastoma subgroups. *Nat. Rev. Neurol.* **8**, 340–351 (2012).
83. Schwalbe, E. C. *et al.* Rapid diagnosis of medulloblastoma molecular subgroups. *Clin. Cancer Res.* **17**, 1883–1894 (2011).
84. Min, H. S., Lee, J. Y., Kim, S.-K. & Park, S.-H. Genetic Grouping of Medulloblastomas by Representative Markers in Pathologic Diagnosis. *Transl. Oncol.* **6**, 265–272 (2013).
85. Woolman, M. *et al.* Rapid determination of medulloblastoma subgroup affiliation with mass spectrometry using a handheld picosecond infrared laser desorption probe. *Chem. Sci.* **8**, 6508–6519 (2017).
86. Iv, M. *et al.* MR Imaging-Based Radiomic Signatures of Distinct Molecular Subgroups of Medulloblastoma. *Am. J. Neuroradiol.* **40**, 154–161 (2019).
87. Mata-Mbemba, D. *et al.* MRI Characteristics of Primary Tumors and Metastatic Lesions in Molecular Subgroups of Pediatric Medulloblastoma: A Single-Center Study. *Am. J. Neuroradiol.* **39**, 949–955 (2018).
88. Frappaz, D. *et al.* Are molecular subgroups of medulloblastomas really prognostic? *Curr. Opin. Neurol.* **31**, 747–751 (2018).
89. Brosh, R. & Rotter, V. When mutants gain new powers: news from the mutant p53 field. *Nat Rev Cancer* **9**, 701–713 (2009).
90. Lindsey, J. C. *et al.* TP53 Mutations in Favorable-Risk Wnt/Wingless-Subtype Medulloblastomas. *J. Clin. Oncol.* **29**, 344–346 (2011).
91. Zhukova, N. *et al.* Subgroup-Specific Prognostic Implications of TP53 Mutation in Medulloblastoma. *J. Clin. Oncol.* **31**, 2927–2935 (2013).
92. Zhukova, N. *et al.* WNT activation by lithium abrogates TP53 mutation associated radiation resistance in medulloblastoma. *Acta Neuropathol. Commun.* **2**, (2014).
93. Cho, Y.-J. J. *et al.* Integrative Genomic Analysis of Medulloblastoma Identifies a Molecular Subgroup That Drives Poor Clinical Outcome. *J. Clin. Oncol.* **29**, 1424–1430 (2011).
94. Schwalbe, E. C. *et al.* Novel molecular subgroups for clinical classification and outcome prediction in childhood medulloblastoma: a cohort study. *Lancet Oncol.* **18**, 958–971 (2017).
95. Cavalli, F. M. G. *et al.* Intertumoral Heterogeneity within Medulloblastoma Subgroups. *Cancer Cell* **31**, 737–754 (2017).
96. Archer, T. C. *et al.* Proteomics, Post-translational Modifications, and Integrative Analyses Reveal Molecular Heterogeneity within Medulloblastoma Subgroups. *Cancer Cell* **34**, 396–410 (2018).
97. Łastowska, M. *et al.* Medulloblastoma with transitional features between Group 3 and Group 4 is associated with good prognosis. *J. Neurooncol.* **138**, 231–240 (2018).
98. Castillo-Rodríguez, R. A., Dávila-Borja, V. M. & Juárez-Méndez, S. Data mining of pediatric medulloblastoma microarray expression reveals a novel potential subdivision of the Group 4 molecular subgroup. *Oncol. Lett.* **15**, 6241–6250 (2018).
99. Sharma, T. *et al.* Second-generation molecular subgrouping of medulloblastoma: an international meta-analysis of Group 3 and Group 4 subtypes. *Acta Neuropathol.* **138**, 309–326 (2019).
100. Northcott, P. A. *et al.* Medulloblastomics: the end of the beginning. *Nat. Rev. Cancer* **12**, 818–834 (2012).
101. Juraschka, K. & Taylor, M. D. Medulloblastoma in the age of molecular subgroups: a review. *J. Neurosurg. Pediatr.* **24**, 353–363 (2019).
102. Ellison, D. W. *et al.* β-Catenin Status Predicts a Favorable Outcome in Childhood Medulloblastoma: The United Kingdom Children's Cancer Study Group Brain Tumour Committee. *J. Clin. Oncol.* **23**, 7951–7957 (2005).
103. Ramaswamy, V. *et al.* Medulloblastoma subgroup-specific outcomes in irradiated children: who are the true high-risk patients? *Neuro. Oncol.* **0**, 1–7 (2015).
104. Clifford, S. C. *et al.* Wnt/Wingless Pathway Activation and Chromosome 6 Loss Characterize a Distinct Molecular Sub-Group of Medulloblastomas Associated with a Favorable Prognosis. *Cell Cycle* **5**, 2666–2670 (2006).

105. Pugh, T. J. *et al.* Medulloblastoma exome sequencing uncovers subtype-specific somatic mutations. *Nature* **488**, 106–110 (2012).
106. Phoenix, T. N. *et al.* Medulloblastoma Genotype Dictates Blood Brain Barrier Phenotype. *Cancer Cell* **29**, 508–522 (2016).
107. Logan, C. Y. & Nusse, R. The Wnt Signaling Pathway in Development and Disease. *Annu. Rev. Cell Dev. Biol.* **20**, 781–810 (2004).
108. Ikeda, S. *et al.* Axin, a negative regulator of the Wnt signaling pathway, forms a complex with GSK-3β and β-catenin and promotes GSK-3β-dependent phosphorylation of β-catenin. *EMBO J.* **17**, 1371–1384 (1998).
109. Cong, F., Schweizer, L., Chamorro, M. & Varmus, H. Requirement for a Nuclear Function of β-Catenin in Wnt Signaling. *Mol. Cell. Biol.* **23**, 8462–8470 (2003).
110. Schweizer, L. & Varmus, H. Wnt/Wingless signaling through β-catenin requires the function of both LRP/Arrow and frizzled classes of receptors. *BMC Cell Biol.* **4**, 4 (2003).
111. Yang, Y., Zhou, H., Zhang, G. & Xue, X. Targeting the canonical Wnt/β-catenin pathway in cancer radioresistance: Updates on the molecular mechanisms. *J Can Res Ther* **15**, 272–277 (2019).
112. Huse, J. T. & Holland, E. C. Targeting brain cancer: advances in the molecular pathology of malignant glioma and medulloblastoma. *Nat. Rev. Cancer* **10**, 319–331 (2010).
113. Shtutman, M. *et al.* The cyclin D1 gene is a target of the β-catenin/LEF-1 pathway. *Proc. Natl. Acad. Sci. U. S. A.* **96**, 5522–5527 (1999).
114. He, T.-C. C. *et al.* Identification of c-MYC as a Target of the APC Pathway. *Science (80-.).* **281**, 1509–1512 (1998).
115. Li, Y., Gao, Q., Yin, G., Ding, X. & Hao, J. WNT/β-Catenin-Signaling Pathway Stimulates the Proliferation of Cultured Adult Human Sertoli Cells via Upregulation of C-myc Expression. *Reprod. Sci.* **19**, 1232–1240 (2012).
116. Roussel, M. F. & Robinson, G. W. Role of MYC in Medulloblastoma. *Cold Spring Harb Perspect Med* a014308 (2013). doi:10.1101/cshperspect.a014308
117. Ivanov, D. P., Coyle, B., Walker, D. A. & Grabowska, A. M. In vitro models of medulloblastoma: Choosing the right tool for the job. *J. Biotechnol.* **236**, 10–25 (2016).
118. Al-Halabi, H. *et al.* Preponderance of sonic hedgehog pathway activation characterizes adult medulloblastoma. *Acta Neuropathol.* **121**, 229–239 (2011).
119. Raffel, C. *et al.* Sporadic Medulloblastomas Contain PTCH Mutations. *Cancer Res.* **57**, 842–845 (1997).
120. Skowron, P., Ramaswamy, V. & Taylor, M. D. Genetic and Molecular Alterations Across Medulloblastoma Subgroups. *J Mol Med* **93**, 1333–1338 (2015).
121. Giroux-Leprieur, E., Costantini, A., Ding, V. W. & He, B. Hedgehog Signaling in Lung Cancer: From Oncogenesis to Cancer Treatment Resistance. *Int. J. Mol. Sci.* **19**, 1–17 (2018).
122. Giroux Leprieur, E. *et al.* Sonic Hedgehog Pathway Activation Is Associated With Resistance to Platinum-Based Chemotherapy in Advanced Non-Small-Cell Lung Carcinoma. *Clin. Lung Cancer* **17**, 301–308 (2016).
123. Riaz, S. K., Ke, Y., Wang, F., Kayani, M. A. & Malik, M. F. A. Influence of SHH/GLI1 axis on EMT mediated migration and invasion of breast cancer cells. *Sci. Rep.* **9**, 1–13 (2019).
124. Maréchal, R. *et al.* Sonic Hedgehog and Gli1 Expression Predict Outcome in Resected Pancreatic Adenocarcinoma. *Clin. Cancer Res.* **21**, 1215–1224 (2015).
125. Chen, J. S. *et al.* Sonic hedgehog signaling pathway induces cell migration and invasion through focal adhesion kinase/AKT signaling-mediated activation of matrix metalloproteinase (MMP)-2 and MMP-9 in liver cancer. *Carcinogenesis* **34**, 10–19 (2013).
126. Shahi, M. H. *et al.* Regulation of sonic hedgehog-GLI1 downstream target genes PTCH1, Cyclin D2, Plakoglobin, PAX6 and NKX2.2 and their epigenetic status in medulloblastoma and astrocytoma. *BMC Cancer* **10**, (2010).
127. Konings, K. *et al.* The Combination of Particle Irradiation With the Hedgehog Inhibitor GANT61 Differently Modulates the Radiosensitivity and Migration of Cancer Cells Compared to X-Ray Irradiation. *Front. Oncol.* **9**, (2019).

128. Riobo-Del Galdo, N., Lara Montero, Á. & Wertheimer, E. Role of Hedgehog Signaling in Breast Cancer: Pathogenesis and Therapeutics. *Cells* **8**, 375 (2019).
129. Bailey, J. M., Mohr, A. M. & Hollingsworth, M. A. Sonic hedgehog paracrine signaling regulates metastasis and lymphangiogenesis in pancreatic cancer. *Oncogene* **28**, 3513–3525 (2009).
130. Zhang, H. *et al.* Aberrant Activation Of Hedgehog Signalling Promotes Cell Migration And Invasion Via Matrix Metalloproteinase-7 In Ovarian Cancer Cells. *J. Cancer* **10**, 990–1003 (2019).
131. Ramaswamy, V. *et al.* Risk stratification of childhood medulloblastoma in the molecular era: The Current Consensus. *Acta Neuropathol.* **131**, 821–831 (2016).
132. Yeo, K. K. *et al.* Prognostic significance of molecular subgroups of medulloblastoma in young children receiving irradiation-sparing regimens. *J. Neurooncol.* **145**, 375–383 (2019).
133. Armoogum, K. S. & Thorp, N. Dosimetric Comparison and Potential for Improved Clinical Outcomes of Paediatric CNS Patients Treated with Protons or IMRT. *Cancers (Basel).* **7**, 706–722 (2015).
134. Morse, K. F. & Wolfe, C. M. Radiobiology. in *Radiation Therapy for Skin Cancer* (eds. Jr Cognetta, A. B. & Mendenhall, W. M.) 9–16 (Springer, 2013).
135. Gerelchuluun, A. *et al.* The Major DNA Repair Pathway after Both Proton and Carbon-Ion Radiation is NHEJ, but the HR Pathway is More Relevant in Carbon Ions. *Radiat. Res.* **183**, 345–356 (2015).
136. Boss, M.-K., Bristow, R. & Dewhirst, M. W. Linking the History of Radiation Biology to the Hallmarks of Cancer. *Radiat. Res.* **181**, 561–577 (2014).
137. Wenz, F., Pasciuti, K. & Herskind, C. Radiobiology. in *Targeted Intraoperative Radiotherapy In Oncology* (eds. Keshtgar, M., Pigott, K. & Wenz, F.) 45–52 (Springer Berlin Heidelberg, 2014).
138. Barcellos-Hoff, M. H., Park, C. & Wright, E. G. Radiation and the microenvironment - tumorigenesis and therapy. *Nat. Rev. Cancer* **5**, 867–875 (2005).
139. Baskar, R., Dai, J., Wenlong, N., Yeo, R. & Yeoh, K.-W. Biological response of cancer cells to radiation treatment. *Front. Mol. Biosci.* **1**, 24 (2014).
140. Willers, H., Dahm-Daphi, J. & Powell, S. N. Repair of radiation damage to DNA. *Br. J. Cancer* **90**, 1297–1301 (2004).
141. Bentzen, S. M. Preventing or reducing late side effects of radiation therapy: radiobiology meets molecular pathology. *Nat. Rev. Cancer* **6**, 702–713 (2006).
142. Barnett, G. C. *et al.* Normal tissue reactions to radiotherapy: towards tailoring treatment dose by genotype. *Nat. Rev. Cancer* **9**, 134–142 (2009).
143. Beyzadeoglu, M., Gokhan, O. & Ebruli, C. *Basic Radiation Oncology*. *Springer Heidelberg* (2010).
144. Withers, H. R. The Four R's of Radiotherapy. in **5**, 241–271 (Elsevier, 1975).
145. Steel, G. G., Mcmillan, T. J. & Peacock, J. H. The 5Rs of Radiobiology. *Int. J. Radiat. Biol.* **56**, 1045–1048 (1989).
146. Hayabuchi, N. Radiocurable Tumors and Non-Radiocurable Tumors. *JMAJ* **47**, 79–83 (2004).
147. Griñán-Lisón, C. *et al.* miRNAs as radio-response biomarkers for breast cancer stem cells. *Mol. Oncol.* **14**, 556–570 (2020).
148. Agency, I. A. E. *Predictive assays and their role in selection of radiation as the therapeutic modality*. (2002).
149. Kerns, S. L., Ostrer, H. & Rosenstein, B. S. Radiogenomics: Using Genetics to Identify Cancer Patients at Risk for Development of Adverse Effects Following Radiotherapy. *Cancer Discovery* **4**, 155–165 (2014).
150. Bentzen, S. M. Potential clinical impact of normal-tissue intrinsic radiosensitivity testing. *Radiotherapy and Oncology* **43**, 121–131 (1997).
151. Fertil, B. & Malaise, E. P. Inherent cellular radiosensitivity as a basic concept for human tumor radiotherapy. *Int. J. Radiat. Oncol. Biol. Phys.* **7**, 621–629 (1981).
152. Deacon, J., Peckham, M. J. & Steel, G. G. The radioresponsiveness of human tumours and the initial slope of the cell survival curve. *Radiother. Oncol.* **2**, 317–323 (1984).
153. West, C. M. L. *et al.* The intrinsic radiosensitivity of normal and tumour cells. *Int. J. Radiat. Biol.* **73**, 409–413 (1998).

154. Girinsky, T. *et al.* In vitro parameters and treatment outcome in head and neck cancers treated with surgery and/or radiation: Cell characterization and correlations with local control and overall survival. *Int. J. Radiat. Oncol. Biol. Phys.* **30**, 789–794 (1994).
155. Kiltie, A. E. *et al.* A correlation between residual DNA double-strand breaks and clonogenic measurements of radiosensitivity in fibroblasts from preradiotherapy cervix cancer patients. *Int. J. Radiat. Oncol. Biol. Phys.* **39**, 1137–1144 (1997).
156. Yard, B. D. *et al.* A genetic basis for the variation in the vulnerability of cancer to DNA damage. *Nat. Commun.* **7**, (2016).
157. Deschavanne, P. J. & Fertil, B. A review of human cell radiosensitivity in vitro. *International Journal of Radiation Oncology Biology Physics* **34**, 251–266 (1996).
158. West, C. M. L., Davidson, S. E., Roberts, S. A. & Hunter, R. D. The independence of intrinsic radiosensitivity as a prognostic factor for patient response to radiotherapy of carcinoma of the cervix. *Br. J. Cancer* **76**, 1184–1190 (1997).
159. Björk-Eriksson, T., West, C., Karlsson, E. & Mercke, C. Tumor radiosensitivity (SF2) is a prognostic factor for local control in head and neck cancers. *Int. J. Radiat. Oncol. Biol. Phys.* **46**, 13–19 (2000).
160. West, C. M. L., Davidson, S. E., Roberts, S. A. & Hunter, R. D. Intrinsic radiosensitivity and prediction of patient response to radiotherapy for carcinoma of the cervix. *Br J Cancer* **68**, 819–823 (1993).
161. Ramsay, J., Ward, R. & Bleehen, N. M. Radiosensitivity testing of human malignant gliomas. *Int. J. Radiat. Oncol. Biol. Phys.* **24**, 675–680 (1992).
162. Greve, B. *et al.* Evaluation of Different Biomarkers to Predict Individual Radiosensitivity in an Inter-Laboratory Comparison-Lessons for Future Studies. *PLoS One* **7**, e47185 (2012).
163. Vaughan, A. T. M., Anderson, P., Wallace, D., Beaney, R. P. & Lynch, T. H. Local control of T2/3 transitional cell carcinoma of bladder is correlated to differences in DNA supercoiling: evidence for two discrete tumor populations. *Cancer Res.* **53**, (1993).
164. Choudhury, A. *et al.* MRE11 Expression Is Predictive of Cause-Specific Survival following Radical Radiotherapy for Muscle-Invasive Bladder Cancer. *Cancer Res.* **70**, 7017–7026 (2010).
165. Laurberg, J. R. *et al.* Expression of TIP60 (tat-interactive protein) and MRE11 (meiotic recombination 11 homolog) predict treatment-specific outcome of localised invasive bladder cancer. *BJU Int.* **110**, (2012).
166. Teo, M. T. W. *et al.* Next-generation sequencing identifies germline MRE11A variants as markers of radiotherapy outcomes in muscle-invasive bladder cancer. *Ann. Oncol.* **25**, 877–883 (2014).
167. Gurung, P. M. S. *et al.* Loss of expression of the tumour suppressor gene AIMP3 predicts survival following radiotherapy in muscle-invasive bladder cancer. *Int. J. Cancer* **136**, 709–720 (2015).
168. Berlin, A. *et al.* NBN gain is predictive for adverse outcome following image guided radiotherapy for localized prostate cancer. *Oncotarget* **5**, 11081–11090 (2014).
169. Noordermeer, S. M. *et al.* Expression of the BRCA1 complex member BRE predicts disease free survival in breast cancer. *Breast Cancer Res. Treat.* **135**, 125–133 (2012).
170. Torres-Roca, J. F. *et al.* RSI: A Novel Biomarker Predicts RT Therapeutic Benefit in Breast Cancer. in *International Journal of Radiation Oncology*Biology*Physics* **81**, S62 (Elsevier BV, 2011).
171. Eschrich, S. A. *et al.* A Gene Expression Model of Intrinsic Tumor Radiosensitivity: Prediction of Response and Prognosis After Chemoradiation. *Int. J. Radiat. Oncol. Biol. Phys.* **75**, 489–496 (2009).
172. Eschrich, S. A. *et al.* Validation of a Radiosensitivity Molecular Signature in Breast Cancer. *Clin. Cancer Res.* **18**, 5134–5143 (2012).
173. Tramm, T. *et al.* Development and Validation of a Gene Profile Predicting Benefit of Postmastectomy Radiotherapy in Patients with High-Risk Breast Cancer: A Study of Gene Expression in the DBCG82bc cohort. *Clin. Cancer Res.* **20**, 5272–5280 (2014).
174. Weichselbaum, R. R. *et al.* An interferon-related gene signature for DNA damage resistance is a predictive marker for chemotherapy and radiation for breast cancer.

PNAS **105**, 18490–18495 (2008).
175. Franken, N. a P., Rodermond, H. M., Stap, J., Haveman, J. & van Bree, C. Clonogenic assay of cells in vitro. *Nat. Protoc.* **1**, 2315–2319 (2006).
176. Brenner, D. J. The Linear-Quadratic Model Is an Appropriate Methodology for Determining Isoeffective Doses at Large Doses Per Fraction. *Semin. Radiat. Oncol.* **18**, 234–239 (2008).
177. McMahon, S. J. & Prise, K. M. Mechanistic modelling of radiation responses. *Cancers* **11**, (2019).
178. van Leeuwen, C. M. *et al.* The alfa and beta of tumours: A review of parameters of the linear-quadratic model, derived from clinical radiotherapy studies. *Radiation Oncology* **13**, (2018).
179. McMahon, S. J. The linear quadratic model: usage, interpretation and challenges. *Phys. Med. Biol.* **64**, 01TR01 (2019).
180. Williams, M. V., Denekamp, J. & Fowler, J. F. A review of α/β ratios for experimental tumors: Implications for clinical studies of altered fractionation. *Int. J. Radiat. Oncol. Biol. Phys.* **11**, 87–96 (1985).
181. Brenner, D. J., Sachs, R. K., Peters, L. J., Withers, H. R. & Hall, E. J. We forget at our peril the lessons built into the α/β model. *International Journal of Radiation Oncology Biology Physics* **82**, 1312–1314 (2012).
182. Brenner, D. J. *et al.* Direct evidence that prostate tumors show high sensitivity to fractionation (low α/β ratio) similar to late-responding normal tissue. *Int J Radiat. Oncol. Biol Phys* **52**, 6–13 (2002).
183. Owen, J. R. *et al.* Effect of radiotherapy fraction size on tumour control in patients with early-stage breast cancer after local tumour excision: long-term results of a randomised trial. *Lancet Oncol.* **7**, 467–471 (2006).
184. Puck, T. T. & Marcus, P. I. Action of x-rays on mammalian cells. *J. Exp. Med.* **103**, 653–666 (1956).
185. Abazeed, M. E. *et al.* Integrative radiogenomic profiling of squamous cell lung cancer. *Cancer Res.* **73**, 6289–6298 (2013).
186. Crouch, S. P. M., Kozlowski, R., Slater, K. J. & Fletcher, J. The use of ATP bioluminescence as a measure of cell proliferation and cytotoxicity. *J. Immunol. Methods* **160**, 81–88 (1993).
187. Riss, T. L. *et al.* Cell Viability Assays. in *Assay Guidance Manual* (Eli Lilly & Company and the National Center for Advancing Translational Sciences, 2004).
188. Posimo, J. M. *et al.* Viability Assays for Cells in Culture. *J. Vis. Exp.* **83**, 50645 (2014).
189. Ohshima, Y., Tsukimoto, M., Harada, H. & Kojima, S. Involvement of connexin43 hemichannel in ATP release after γ-irradiation. *J. Radiat. Res.* **53**, 551–557 (2012).
190. Lu, C. L. *et al.* Tumor Cells Switch to Mitochondrial Oxidative Phosphorylation under Radiation via mTOR-Mediated Hexokinase II Inhibition - A Warburg-Reversing Effect. *PLoS One* **10**, e0121046 (2015).
191. Ohshima, Y. *et al.* γ-Irradiation induces P2X(7) receptor-dependent ATP release from B16 melanoma cells. *Biochim. Biophys. Acta* **1800**, 40–46 (2010).
192. Kim, E. J., Lee, M., Kim, D. Y., Kim, K. Il & Yi, J. Y. Mechanisms of Energy Metabolism in Skeletal Muscle Mitochondria Following Radiation Exposure. *Cells* **8**, 950 (2019).
193. Bhatt, A. N. *et al.* Transient elevation of glycolysis confers radio-resistance by facilitating DNA repair in cells. *BMC Cancer* **15**, 335 (2015).
194. Baselet, B. *et al.* Rosiglitazone Protects Endothelial Cells From Irradiation-Induced Mitochondrial Dysfunction. *Front. Pharmacol.* **11**, 268 (2020).
195. Cantini, L. *et al.* Classification of gene signatures for their information value and functional redundancy. *npj Syst. Biol. Appl.* **8**, (2018).
196. Naylor, S. Biomarkers: current perspectives and future prospects. *Expert Review of Molecular Diagnostics* **3**, 525–529 (2003).
197. FDA-NIH Biomarker Working Group. Understanding Prognostic versus Predictive Biomarkers. in *BEST (Biomarkers, EndpointS and other Tools)* (Food and Drug Administration (US), 2016).
198. Torres-Roca, J. F. A molecular assay of tumor radiosensitivity: A roadmap towards biology-based personalized radiation therapy. *Per. Med.* **9**, 547–557 (2012).

199. Mohammadi, H. *et al.* Using the Radiosensitivity Index (RSI) to Predict Pelvic Failure in Endometrial Cancer Treated With Adjuvant Radiation Therapy. *Int. J. Radiat. Oncol. Biol. Phys.* **106**, 496–502 (2020).
200. Strom, T. *et al.* Regional Radiation Therapy Impacts Outcome for Node-Positive Cutaneous Melanoma. *J. Natl. Compr. Cancer Netw.* **15**, 473–482 (2017).
201. Strom, T. *et al.* Radiosensitivity index predicts for survival with adjuvant radiation in resectable pancreatic cancer. *Radiother. Oncol.* **117**, 159–164 (2015).
202. Ahmed, K. A. *et al.* The radiosensitivity index predicts for overall survival in glioblastoma. *Oncotarget* **6**, 34414–34422 (2015).
203. Ahmed, K. A. *et al.* Differences Between Colon Cancer Primaries and Metastases Using a Molecular Assay for Tumor Radiation Sensitivity Suggest Implications for Potential Oligometastatic SBRT Patient Selection. *Int. J. Radiat. Oncol. Biol. Phys.* **92**, 837–842 (2015).
204. Strom, T. *et al.* Tumour radiosensitivity is associated with immune activation in solid tumours. *Eur. J. Cancer* **84**, 304–314 (2017).
205. Ahmed, K. A. *et al.* The radiosensitivity of brain metastases based upon primary histology utilizing a multigene index of tumor radiosensitivity. *Neuro. Oncol.* **19**, 1145–1146 (2017).
206. Yuan, Z. *et al.* Intrinsic radiosensitivity, genomic-based radiation dose and patterns of failure of penile cancer in response to adjuvant radiation therapy. *Reports Pract. Oncol. Radiother.* **24**, 593–599 (2019).
207. Torres-Roca, J. F. *et al.* Integration of a Radiosensitivity Molecular Signature into the Assessment of Local Recurrence Risk in Breast Cancer. *Int. J. Radiat. Oncol. Biol. Phys.* **93**, 631–638 (2015).
208. Ahmed, K. A. *et al.* Radiosensitivity of Lung Metastases by Primary Histology and Implications for Stereotactic Body Radiation Therapy Using the Genomically Adjusted Radiation Dose. *J. Thorac. Oncol.* **13**, 1121–1127 (2018).
209. Zhao, Y. *et al.* Wnt signaling induces radioresistance through upregulating HMGB1 in esophageal squamous cell carcinoma. *Cell Death Dis.* **9**, 433 (2018).
210. Wang, Y. *et al.* High Canonical Wnt/β-Catenin Activity Sensitizes Murine Hematopoietic Stem and Progenitor Cells to DNA Damage. *Stem Cell Rev. Reports* **16**, 212–221 (2020).
211. Tian, D., Shi, Y., Chen, D., Liu, Q. & Fan, F. The Wnt inhibitor LGK-974 enhances radiosensitivity of HepG2 cells by modulating Nrf2 signaling. *Int. J. Oncol.* **51**, 545–554 (2017).
212. Emons, G. *et al.* Chemoradiotherapy resistance in colorectal cancer cells is mediated by Wnt/β-catenin signaling. *Mol. Cancer Res.* **15**, 1481–1490 (2017).
213. He, H. *et al.* Overexpression of β-Catenin decreases the radiosensitivity of human nasopharyngeal carcinoma CNE-2 cells. *Cell. Physiol. Biochem.* **50**, 1929–1944 (2018).
214. Kim, Y. *et al.* Wnt activation is implicated in glioblastoma radioresistance. *Lab. Investig.* **92**, 466–473 (2012).
215. Guo, X. *et al.* Long noncoding RNA HOTAIR knockdown inhibits autophagy and epithelial–mesenchymal transition through the Wnt signaling pathway in radioresistant human cervical cancer HeLa cells. *J. Cell. Physiol.* **234**, 3478–3489 (2019).
216. Gonnissen, A., Isebaert, S., McKee, C. M., Muschel, R. J. & Haustermans, K. The effect of metformin and GANT61 combinations on the radiosensitivity of prostate cancer cells. *Int. J. Mol. Sci.* **18**, 399 (2017).
217. Tsai, C. L. *et al.* Sonic Hedgehog inhibition as a strategy to augment radiosensitivity of hepatocellular carcinoma. *J. Gastroenterol. Hepatol.* **30**, 1317–1324 (2015).
218. Chiang, M. F. *et al.* Modulation of Sonic hedgehog signaling and WW domain containing oxidoreductase WOX1 expression enhances radiosensitivity of human glioblastoma cells. *Exp. Biol. Med.* **240**, 392–399 (2015).
219. Ma, J. *et al.* Sonic Hedgehog Signaling Pathway Supports Cancer Cell Growth during Cancer Radiotherapy. *PLoS One* **8**, e65032 (2013).
220. Chen, Y. J. *et al.* Sonic Hedgehog signaling protects human hepatocellular carcinoma cells against ionizing radiation in an autocrine manner. *Int. J. Radiat. Oncol. Biol. Phys.* **80**, 851–859 (2011).

221. Sims-Mourtada, J. *et al.* Hedgehog: An attribute to tumor regrowth after chemoradiotherapy and a target to improve radiation response. *Clin. Cancer Res.* **12**, 6565–6572 (2006).
222. Zeng, J. *et al.* Hedgehog pathway inhibition radiosensitizes non-small cell lung cancers. *Int. J. Radiat. Oncol. Biol. Phys.* **86**, 143–149 (2013).
223. Yao, F. *et al.* Primary impact of Gli1 on radioresistance in esophageal cancer. *Oncol. Lett.* **18**, 4825–4833 (2019).
224. Qu, W., Li, D., Wang, Y., Wu, Q. & Hao, D. Activation of sonic hedgehog signaling is associated with human osteosarcoma cells radioresistance characterized by increased proliferation, migration, and invasion. *Med. Sci. Monit.* **24**, 3764–3771 (2018).
225. Arnhold, V., Boos, J. & Lanvers-Kaminsky, C. Targeting hedgehog signaling pathway in pediatric tumors: In vitro evaluation of SMO and GLI inhibitors. *Cancer Chemother. Pharmacol.* **77**, 495–505 (2016).
226. Triscott, J. *et al.* Personalizing the Treatment of Pediatric Medulloblastoma: Polo-like Kinase 1 as a Molecular Target in High-Risk Children. *Cancer Res.* **73**, 6734–6744 (2013).
227. Gonnissen, A. *et al.* The hedgehog inhibitor GANT61 sensitizes prostate cancer cells to ionizing radiation both in vitro and in vivo. *Oncotarget* **7**, 84286–84298 (2016).
228. Karhadkar, S. S. *et al.* Hedgehog signalling in prostate regeneration, neoplasia and metastasis. *Nature* **431**, 707–712 (2004).
229. Zhang, X. *et al.* Shh overexpression is correlated with GRP78 and AR expression in primary prostate cancer: Clinicopathological features and outcomes in a Chinese cohort. *Cancer Manag. Res.* **12**, 1569–1578 (2020).
230. Niyaz, M., Khan, M. S. & Mudassar, S. Hedgehog Signaling: An Achilles' Heel in Cancer. *Translational Oncology* **12**, 1334–1344 (2019).
231. Sheng, T. *et al.* Activation of the hedgehog pathway in advanced prostate cancer. *Mol. Cancer* **3**, (2004).
232. Li, N. *et al.* Non-canonical activation of hedgehog in prostate cancer cells mediated by the interaction of transcriptionally active androgen receptor proteins with Gli3. *Oncogene* **37**, 2313–2325 (2018).
233. Hollstein, M., Sidransky, D., Vogelstein, B. & Harris, C. C. p53 mutations in human cancers. *Science (80-.).* **253**, 49–53 (1991).
234. Kruse, J. P. & Gu, W. Modes of p53 Regulation. *Cell* **137**, 609–622 (2009).
235. Shaw, P. *et al.* Induction of apoptosis by wild-type p53 in a human colon tumor-derived cell line. *Proc. Natl. Acad. Sci. U. S. A.* **89**, 4495–4499 (1992).
236. Zhan, Q. Gadd45a, a p53- and BRCA1-regulated stress protein, in cellular response to DNA damage. *Mutation Research* **569**, 133–143 (2005).
237. Yoon, T. *et al.* Tumor-prone phenotype of the DDB2-deficient mice. *Oncogene* **24**, 469–478 (2005).
238. Kuerbitz, S. J., Plunkett, B. S., Walsh, W. V & Kastan, M. B. Wild-type p53 is a cell cycle checkpoint determinant following irradiation. *Proc. Natl. Acad. Sci. U. S. A.* **89**, 7491–7495 (1992).
239. El-Deiry, W. S. *et al.* WAF1, a potential mediator of p53 tumor suppression. *Cell* **75**, 817–825 (1993).
240. Vousden, K. H. Outcomes of p53 activation - spoilt for choice. *J. Cell Sci.* **119**, 5015–5020 (2006).
241. Turesson, I. *et al.* Biological Response to Radiation Therapy. *Acta Oncol* **42**, 92–106 (2003).
242. Danielsen, T. *et al.* No association between radiosensitivity and TP53 status, G1 arrest or protein levels of p53, myc, ras or raf in human melanoma lines. *Int. J. Radiat. Biol.* **75**, 1149–1160 (1999).
243. Asuthkar, S. *et al.* Gadd45a sensitizes medulloblastoma cells to irradiation and suppresses MMP-9-mediated EMT. *Neuro. Oncol.* **13**, 1059–1073 (2011).
244. Good, J. S. & Harrington, K. J. The hallmarks of cancer and the radiation oncologist: Updating the 5Rs of radiobiology. *Clin. Oncol.* **25**, 569–577 (2013).
245. Matsui, Y., Tsuchida, Y. & Keng, P. C. Effects of p53 mutations on cellular sensitivity to ionizing radiation. *Am. J. Clin. Oncol. Cancer Clin. Trials* **24**, 486–490 (2001).
246. Lee, J. M. & Bernstein, A. P53 Mutations Increase Resistance To Ionizing Radiation.

Proc. Natl Acad Sci. USA **90**, 5742–5746 (1993).
247. Cheng, G. *et al.* The tumor suppressor, p53, contributes to radiosensitivity of lung cancer cells by regulating autophagy and apoptosis. *Cancer Biother. Radiopharm.* **28**, 153–159 (2013).
248. Spiegelberg, D. *et al.* The MDM2/MDMX-p53 antagonist PM2 radiosensitizes wild-type p53 tumors. *Cancer Res.* **78**, (2018).
249. Brachman, D. G. *et al.* p53 Mutation Does Not Correlate with Radiosensitivity in 24 Head and Neck Cancer Cell Lines. *Cancer Res.* **53**, 3667–3669 (1993).
250. Okaichi, K. *et al.* Variations in Sensitivity to Ionizing Radiation in Relation to p53 Mutation Point. *Anticancer Res.* **28**, 2687–2690 (2008).
251. Beroukhim, R. *et al.* The landscape of somatic copy-number alteration across human cancers. *Nature* **463**, 899–905 (2010).
252. Ciriello, G. *et al.* Emerging landscape of oncogenic signatures across human cancers. *Nat. Genet.* **45**, 1127–1133 (2013).
253. Zack, T. I. *et al.* Pan-cancer patterns of somatic copy number alteration. *Nat. Genet.* **45**, 1134–1140 (2013).
254. Balko, J. M. *et al.* Molecular profiling of the residual disease of triple-negative breast cancers after neoadjuvant chemotherapy identifies actionable therapeutic targets. *Cancer Discov.* **4**, 232–245 (2014).
255. Bell, D. *et al.* Integrated genomic analyses of ovarian carcinoma. *Nature* **474**, 609–615 (2011).
256. Witkiewicz, A. K. *et al.* Whole-exome sequencing of pancreatic cancer defines genetic diversity and therapeutic targets. *Nat. Commun.* **6**, (2015).
257. Escot, C. *et al.* Genetic alteration of the c-myc protooncogene (MYC) in human primary breast carcinomas. *Proc. Natl. Acad. Sci. U. S. A.* **83**, 4834–4838 (1986).
258. Sicklick, J. K. *et al.* Dysregulation of the Hedgehog pathway in human hepatocarcinogenesis. *Carcinogenesis* **27**, 748–757 (2006).
259. Zeller, K. I., Jegga, A. G., Aronow, B. J., O'Donnell, K. A. & Dang, C. V. An integrated database of genes responsive to the Myc oncogenic transcription factor: identification of direct genomic targets. *Genome Biol.* **4**, (2003).
260. Dang, C. V. c-Myc target genes involved in cell growth, apoptosis, and metabolism. *Mol. Cell. Biol.* **19**, 1–11 (1999).
261. von Bueren, A. O. *et al.* c-MYC expression sensitizes medulloblastoma cells to radio- and chemotherapy and has no impact on response in medulloblastoma patients. *BMC Cancer* **11**, 74 (2011).
262. Mao, A. *et al.* MicroRNA-449a enhances radiosensitivity by downregulation of c-Myc in prostate cancer cells. *Sci. Rep.* **6**, 27346 (2016).
263. Fan, Y., Jia, X., Xie, T., Zhu, L. & He, F. Radiosensitizing effects of c-myc gene knockdown-induced G2/M phase arrest by intrinsic stimuli via the mitochondrial signaling pathway. *Oncol. Rep.* **44**, 2669–2677 (2020).
264. Karlsson, A. *et al.* Defective double-strand DNA break repair and chromosomal translocations by MYC overexpression. *Proc. Natl. Acad. Sci. U. S. A.* **100**, 9974–9979 (2003).
265. Rygaard, K., Slebos, R. J. C. & Spang-Thomsen, M. Radiosensitivity of small-cell lung cancer xenografts compared with activity of c-myc, N-myc, L-myc, c-raf-1 and K-ras proto-oncogenes. *Int. J. Cancer* **49**, 279–284 (1991).
266. Sheridan, M. T., O'Dwyer, T., Seymour, C. B. & Mothersill, C. E. Potential indicators of radiosensitivity in squamous cell carcinoma of the head and neck. *Radiat. Oncol. Investig.* **5**, 180–186 (1997).
267. Wade, M. A. *et al.* C-MYC is a radiosensitive locus in human breast cells. *Oncogene* **34**, 4985–4994 (2015).
268. Zhang, J. *et al.* Knockdown of c-Myc activates Fas-mediated apoptosis and sensitizes A549 cells to radiation. *Oncol. Rep.* **38**, 2471–2479 (2017).
269. Weichselbaum, R. R., Nove, J. & Little, J. B. X-ray sensitivity of human tumor cells in vitro. *Int J Radiat. Oncol. Biol Phys* **6**, 437–440 (1980).
270. Powell, S., McMillan, T. J. & Steel, G. In vitro radiosensitivity of human medulloblastoma cell lines. *J. Neurooncol.* **15**, 91–92 (1993).
271. Whiteway, S. L. *et al.* Inhibition of cyclin-dependent kinase 6 suppresses cell proliferation and enhances radiation sensitivity in medulloblastoma cells. *J.*

Neurooncol. **111**, 113–121 (2013).
272. Patties, I., Kortmann, R.-D., Menzel, F. & Glasow, A. Enhanced inhibition of clonogenic survival of human medulloblastoma cells by multimodal treatment with ionizing irradiation, epigenetic modifiers, and differentiation-inducing drugs. *J. Exp. Clin. Cancer Res.* **35**, 94 (2016).
273. Sun, L. *et al.* In vitro stemness characterization of radio-resistant clones isolated from a medulloblastoma cell line ONS-76. *J. Radiat. Res.* **54**, 61–69 (2013).
274. Chetty, C., Dontula, R., Gujrati, M., Dinh, D. H. & Lakka, S. S. Blockade of SOX4 mediated DNA repair by SPARC enhances radioresponse in medulloblastoma. *Cancer Lett* **323**, 188–198 (2012).
275. Turesson, I., Johansson, K.-A. & Mattsson, S. The Potential of Proton and Light Ion Beams in Radiotherapy. *Acta Oncol. (Madr).* **42**, 107–114 (2003).
276. Zhang, X. *et al.* Therapy resistant cancer stem cells have differing sensitivity to photon versus proton beam radiation. *J Thorac Oncol* **8**, 1484–1491 (2013).
277. Wilson, R. R. Radiological use of fast protons. *Radiology* **47**, 487–491 (1946).
278. Arjomandy, B. Proton therapy advancement. *J. Prot. Ther.* **1**, 115 (2015).
279. Durante, M. & Paganetti, H. Nuclear physics in particle therapy: a review. *Rep. Prog. Phys.* **79**, 096702 (2016).
280. Bhide, S. & Nutting, C. Recent advances in radiotherapy. *BMC Med.* **8**, 25 (2010).
281. Bush, D. A. *et al.* Partial Breast Radiation Therapy With Proton Beam: 5-Year Results With Cosmetic Outcomes. *Int. J. Radiat. Oncol. Biol. Phys.* **90**, 501–505 (2014).
282. Archambeau, J., Slater, J., Slater, J. & Tangeman, R. Role for proton beam irradiation in treatment of pediatric CNS malignancies. *Int. J. Radiat. Oncol. Biol. Phys.* **22**, 287–294 (1992).
283. PTCOG. Facilities In Operation. (2016). Available at: https://www.ptcog.ch/index.php/facilities-in-operation. (Accessed: 6th December 2016)
284. Bush, D. A. *et al.* Hypofractionated Proton Beam Radiotherapy for Stage I Lung Cancer. *Chest* **126**, 1198–1203 (2004).
285. Curran Jr, W. J. *et al.* Sequential vs Concurrent Chemoradiation for Stage III Non-Small Cell Lung Cancer: Randomized Phase III Trial RTOG 9410. *J. Natl. Cancer Inst.* **103**, 1452–1460 (2011).
286. Chang, J. Y. *et al.* Phase II Study of High-Dose Proton Therapy with Concurrent Chemotherapy for Unresectable Stage III Non-Small Cell Lung Cancer. *Cancer* **117**, 4707–4713 (2011).
287. Yock, T. I. *et al.* Long-term toxic effects of proton radiotherapy for paediatric medulloblastoma: A phase 2 single-arm study. *Lancet Oncol.* **17**, 287–298 (2016).
288. Lin, S. H. *et al.* Proton Beam Therapy and Concurrent Chemotherapy for Esophageal Cancer. *Int. J. Radiat. Oncol. Biol. Phys.* **83**, e345–e351 (2012).
289. DeLaney, T. F. *et al.* Phase II Study of High-Dose Photon/Proton Radiotherapy in the Management of Spine Sarcomas. *Int. J. Radiat. Oncol. Biol. Phys.* **74**, 732–739 (2009).
290. Allen, A. M. *et al.* An evidence based review of proton beam therapy: The report of ASTRO's emerging technology committee. *Radiother. Oncol.* **103**, 8–11 (2012).
291. Trikalinos, T. A., Terasawa, T., Ip, S., Raman, G. & Lau, J. *Particle Beam Radiation Therapies for Cancer. Technical Brief No. 1.* (Rockville, MD: Agency for Healthcare Research and Quality, 2009).
292. Laprie, A. *et al.* Paediatric brain tumours: A review of radiotherapy, state of the art and challenges for the future regarding protontherapy and carbontherapy. *Cancer/Radiotherapie* **19**, 775–789 (2015).
293. Leroy, R., Benahmed, N., Hulstaert, F., Van Damme, N. & De Ruysscher, D. Proton Therapy in Children: A Systematic Review of Clinical Effectiveness in 15 Pediatric Cancers. *Int. J. Radiat. Oncol. Biol. Phys.* **95**, 267–278 (2016).
294. Lundkvist, J., Ekman, M., Ericsson, S. R., Jönsson, B. & Glimelius, B. Cost-Effectiveness of Proton Radiation in the Treatment of Childhood Medulloblastoma. *Cancer* **103**, 793–801 (2005).
295. Howell, R. M. *et al.* Comparison of therapeutic dosimetric data from passively scattered proton and photon craniospinal irradiations for medulloblastoma. *Radiat. Oncol.* **7**, 116 (2012).

296. St. Clair, W. H. *et al.* Advantage of protons compared to conventional X-ray or IMRT in the treatment of a pediatric patient with medulloblastoma. *Int. J. Radiat. Oncol. Biol. Phys.* **58**, 727–734 (2004).
297. Johnstone, P. A. S., McMullen, K. P., Buchsbaum, J. C., Douglas, J. G. & Helft, P. Pediatric CSI: Are Protons the Only Ethical Approach? *Int. J. Radiat. Oncol. Biol. Phys.* **87**, 228–230 (2013).
298. Proton Beam Radiotherapy for Medulloblastoma and Pineoblastoma - Full Text View - ClinicalTrials.gov. Available at: https://clinicaltrials.gov/ct2/show/NCT01063114?cond=Medulloblastoma&draw=2&rank=40. (Accessed: 1st June 2021)
299. Hall, E. J. *Radiobiology for the Radiologist*. (JB Lippincott, 1988).
300. Paganetti, H. Relative biological effectiveness (RBE) values for proton beam therapy. Variations as a function of biological endpoint, dose, and linear energy transfer. *Phys Med Biol* **59**, R419–R472 (2014).
301. Goitein, M. & Cox, J. D. Should Randomized Clinical Trials Be Required for Proton Radiotherapy? *J. Clin. Oncol.* **26**, 175–176 (2008).
302. Paganetti, H. Significance and Implementation of RBE Variations in Proton Beam Therapy. *Technol. Cancer Res. Treat.* **2**, 413–426 (2003).
303. Liu, Q. *et al.* Lung Cancer Cell Line Screen Links Fanconi Anemia/BRCA Pathway Defects to Increased Relative Biological Effectiveness of Proton Radiation. *Int. J. Radiat. Oncol. Biol. Phys.* **91**, 1081–1089 (2015).
304. Iwata, H. *et al.* Spot Scanning and Passive Scattering Proton Therapy: Relative Biological Effectiveness and Oxygen Enhancement Ratio in Cultured Cells. *Int. J. Radiat. Oncol. Biol. Phys.* **95**, 95–102 (2016).
305. Jones, B., Wilson, P., Nagano, A., Fenwick, J. & McKenna, G. Dilemmas concerning dose distribution and the influence of relative biological effect in proton beam therapy of medulloblastoma. *Br. J. Radiol.* **85**, e912–e918 (2012).
306. Alan Mitteer Jr, R. *et al.* Proton beam radiation induces DNA damage and cell apoptosis in glioma stem cells through reactive oxygen species. *Sci. Rep.* **5**, 13961 (2015).
307. Fontana, A. O. *et al.* Differential DNA repair pathway choice in cancer cells after proton- and photon-irradiation. *Radiother. Oncol.* **116**, 374–380 (2015).
308. Golias, C. H., Charalabopoulos, A. & Charalabopoulos, K. Cell proliferation and cell cycle control: a mini review. *Int. J. Clin. Pract.* **58**, 1134–1141 (2004).
309. Hanahan, D. & Weinberg, R. A. Hallmarks of Cancer: The Next Generation. *Cell* **144**, 646–674 (2011).
310. Jaros, E. *et al.* Prognostic implications of p53 protein, epidermal growth factor receptor, and Ki-67 labelling in brain tumours. *Br. J. Cancer* **66**, 373–385 (1992).
311. Gilbertson, R. J. *et al.* Mitotic percentage index: A new prognostic factor for childhood medulloblastoma. *Eur. J. Cancer Part A* **33**, 609–615 (1997).
312. De Azambuja, E. *et al.* Ki-67 as prognostic marker in early breast cancer: A meta-analysis of published studies involving 12 155 patients. *Br. J. Cancer* **96**, 1504–1513 (2007).
313. Tsuji, M., Kojima, K., Murakami, Y., Kanayama, H. & Kagawa, S. Prognostic value of Ki-67 antigen and p53 protein in urinary bladder cancer: Immunohistochemical analysis of radical cystectomy specimens. *Br. J. Urol.* **79**, 367–372 (1997).
314. Klöppel, G. & La Rosa, S. Ki67 labeling index: assessment and prognostic role in gastroenteropancreatic neuroendocrine neoplasms. *Virchows Archiv* **472**, 341–349 (2018).
315. Martin, B. *et al.* Ki-67 expression and patients survival in lung cancer: Systematic review of the literature with meta-analysis. *British Journal of Cancer* **91**, 2018–2025 (2004).
316. Ciancio, N. *et al.* Prognostic value of p53 and Ki67 expression in fiberoptic bronchial biopsies of patients with non small cell lung cancer. *Multidiscip. Respir. Med.* **7**, 29 (2012).
317. Bolger, B. S. *et al.* Prediction of radiotherapy response of cervical carcinoma through measurement of proliferation rate. *Br. J. Cancer* **74**, 1223–1226 (1996).
318. Corvò, R. *et al.* Evidence of cell kinetics as predictive factor of response to radiotherapy alone or chemoradiotherapy in patients with advanced head and neck

cancer. *Int. J. Radiat. Oncol. Biol. Phys.* **47**, 57–63 (2000).
319. Bartee, L., Shriner, W. & Creech, C. The Eukaryotic Cell Cycle. in *Principles of Biology* (Open Oregon Educational Resources).
320. Goranov, A. I. *et al.* The rate of cell growth is governed by cell cycle stage. *Genes Dev.* **23**, 1408–1422 (2009).
321. Cooper, G. M. The Eukaryotic Cell Cycle. in *The Cell* (Sinauer Associates, 2000).
322. Sinclair, W. K. & Morton, R. A. X-Ray and Ultraviolet Sensitivity of Synchronized Chinese Hamster Cells at Various Stages of the Cell Cycle. *Biophys. J.* **5**, 1–25 (1965).
323. Barnum, K. J. & O'Connell, M. J. Cell cycle regulation by checkpoints. *Methods Mol. Biol.* **1170**, 29–40 (2014).
324. Kastan, M. B. & Bartek, J. Cell-cycle checkpoints and cancer. *Nature* **432**, 316–323 (2004).
325. Wojtowicz, J. M. & Kee, N. BrdU assay for neurogenesis in rodents. *Nat. Protoc.* **1**, 1399–1405 (2006).
326. Prusoff, W. Synthesis and biological activities of iododeoxyuridine, an analog of thymidine. *Biochim Biophys Acta* **32**, 295–296 (1959).
327. Muskhelishvili, L., Latendresse, J. R., Kodell, R. L. & Henderson, E. B. Evaluation of Cell Proliferation in Rat Tissues with BrdU, PCNA, Ki-67(MIB-5) Immunohistochemistry and in Situ Hybridization for Histone mRNA. *J. Histochem. Cytochem.* **51**, 1681–1688 (2003).
328. Ishibashi, N. *et al.* Correlation between the Ki-67 proliferation index and response to radiation therapy in small cell lung cancer. *Radiat. Oncol.* **12**, 16 (2017).
329. Juríková, M., Danihel, Ľ., Polák, Š. & Varga, I. Ki67, PCNA, and MCM proteins: Markers of proliferation in the diagnosis of breast cancer. *Acta Histochemica* **118**, 544–552 (2016).
330. Gerdes, J., Schwab, U., Lemke, H. & Stein, H. Production of a mouse monoclonal antibody reactive with a human nuclear antigen associated with cell proliferation. *Int. J. Cancer* **31**, 13–20 (1983).
331. Yamamoto, S. *et al.* Clinical relevance of Ki67 gene expression analysis using formalin-fixed paraffin-embedded breast cancer specimens. *Breast Cancer* **20**, 262–270 (2013).
332. Sinn, H.-P. *et al.* Comparison of immunohistochemistry with PCR for assessment of ER, PR, and Ki-67 and prediction of pathological complete response in breast cancer. doi:10.1186/s12885-017-3111-1
333. Sobecki, M. *et al.* The cell proliferation antigen Ki-67 organises heterochromatin. *Elife* **5**, (2016).
334. Qiu, X. *et al.* Correlation analysis between expression of PCNA, Ki-67 and COX-2 and X-ray features in mammography in breast cancer. *Oncol. Lett.* **14**, 2912–2918 (2017).
335. Okuno, Y., Nishimura, Y., Kashu, I., Ono, K. & Hiraoka, M. Prognostic values of proliferating cell nuclear antigen (PCNA) and Ki-67 for radiotherapy of oesophageal squamous cell carcinomas. *Br. Joumal Cancer* **80**, 387–395 (1999).
336. Manohar, K. & Acharya, N. Characterization of proliferating cell nuclear antigen (PCNA) from pathogenic yeast Candida albicans and its functional analyses in S. Cerevisiae. *BMC Microbiol.* **15**, 257 (2015).
337. Chen, G. *et al.* Discordant protein and mRNA expression in lung adenocarcinomas. *Mol. Cell. Proteomics* **1**, 304–313 (2002).
338. Ye, X. *et al.* Clinical significance of high expression of proliferating cell nuclear antigen in non-small cell lung cancer. *Medicine (Baltimore).* **99**, e19755 (2020).
339. Wang, X. *et al.* Elevated expression of cancer-associated proliferating cell nuclear antigen in high-grade prostatic intraepithelial neoplasia and prostate cancer. *Prostate* **71**, 748–754 (2011).
340. Fan, J., Zhou, X., Huang, J., Wang, X. & Che, G. Prognostic roles of PCNA expressions in non-small cell lung cancer: a meta-analysis. *Int J Clin Exp Med* **9**, 5655–5665 (2016).
341. Isozaki, H. *et al.* The Significance of Proliferating Cell Nuclear Antigen (PCNA) Expression in Cancer of the Ampulla of Vater in Terms of Prognosis. *Jpn J Surg* **24**, 494–499 (1994).

342. Schönborn, I., Minguillon, C., Möhner, M. & Ebeling, K. PCNA as a potential prognostic marker in breast cancer. *The Breast* **3**, 97–102 (1994).
343. Yin, S. *et al.* Prognostic value and clinicopathological significance of proliferating cell nuclear antigen expression in gastric cancer: A systematic review and meta-analysis. *Onco. Targets. Ther.* **10**, 319–327 (2017).
344. Wang, X. *et al.* The prognostic value of PCNA expression in patients with osteosarcoma. *Medicine (United States)* **96**, (2017).
345. Murad, H., Alghamian, Y., Aljapawe, A. & Madania, A. Effects of ionizing radiation on the viability and proliferative behavior of the human glioblastoma T98G cell line. *BMC Res. Notes* **11**, 330 (2018).
346. Begg, A. C. The clinical status of Tpot as a predictor? or why no tempest in the Tpot! *International Journal of Radiation Oncology, Biology, Physics* **32**, 1539–1541 (1995).
347. Begga, A. C. *et al.* The value of pretreatment cell kinetic parameters as predictors for radiotherapy outcome in head and neck cancer: A multicenter analysis. *Radiother. Oncol.* **50**, 13–23 (1999).
348. Lara, P. C. *et al.* The role of Ki67 proliferation assessment in predicting local control in bladder cancer patients treated by radical radiation therapy. *Radiother. Oncol.* **49**, 163–167 (1998).
349. Freudlsperger, C., Freier, K., Hoffmann, J. & Engel, M. Ki-67 expression predicts radiosensitivity in oral squamous cell carcinoma. *Int. J. Oral Maxillofac. Surg.* **41**, 965–969 (2012).
350. Venet, D., Dumont, J. E. & Detours, V. Most random gene expression signatures are significantly associated with breast cancer outcome. *PLoS Comput. Biol.* **7**, (2011).
351. Ramaker, R. C. *et al.* RNA sequencing-based cell proliferation analysis across 19 cancers identifies a subset of proliferation-informative cancers with a common survival signature. *Oncotarget* **8**, 38668–38681 (2017).
352. Wang, B. M. & Li, N. Effect of the Wnt/β-catenin signaling pathway on apoptosis, migration, and invasion of transplanted hepatocellular carcinoma cells after transcatheter arterial chemoembolization in rats. *J. Cell. Biochem.* **119**, 4050–4060 (2018).
353. Salaroli, R. *et al.* Wnt activation affects proliferation, invasiveness and radiosensitivity in medulloblastoma. *J. Neurooncol.* **121**, 119–127 (2015).
354. Stecca, B. & Ruiz i Altaba, A. A GLI1-p53 inhibitory loop controls neural stem cell and tumour cell numbers. *EMBO J.* **28**, 663–676 (2009).
355. Kitagawa, K. *et al.* Possible correlation of sonic hedgehog signaling with epithelial–mesenchymal transition in muscle-invasive bladder cancer progression. *J. Cancer Res. Clin. Oncol.* **145**, 2261–2271 (2019).
356. Chen, Y. & Zhu, W. Knockdown of the Sonic Hedgehog (SHH) Gene Inhibits Proliferation of Hep3B and SMMC-7721 Hepatocellular Carcinoma Cells via the PI3K/Akt/PCK1 Signaling Pathway. *Med. Sci. Monit.* **25**, 6023–6033 (2019).
357. Dormoy, V. *et al.* The sonic hedgehog signaling pathway is reactivated in human renal cell carcinoma and plays orchestral role in tumor growth. *Mol. Cancer* **8**, 1–16 (2009).
358. Felsher, D. W. & Bishop, J. M. Transient excess of MYC activity can elicit genomic instability and tumorigenesis. *Proc. Natl. Acad. Sci. U. S. A.* **96**, 3940–3944 (1999).
359. Melnik, S. *et al.* Impact of c-MYC expression on proliferation, differentiation, and risk of neoplastic transformation of human mesenchymal stromal cells. *Stem Cell Res. Ther.* **10**, (2019).
360. Wang, F. *et al.* Morusin inhibits cell proliferation and tumor growth by downregulating c-Myc in human gastric cancer. *Oncotarget* **8**, 57187–57200 (2017).
361. Kim, T. *et al.* MYC-repressed long noncoding RNAs antagonize MYC-induced cell proliferation and cell cycle progression. *Oncotarget* **6**, 18780–18789 (2015).
362. Feng, W. *et al.* Myc is a prognostic biomarker and potential therapeutic target in osteosarcoma. *Ther. Adv. Med. Oncol.* **12**, (2020).
363. Schouten-van Meeteren, A. *et al.* Features of proliferation and in vitro drug resistance in central primitive neuro-ectodermal tumors. *Neuropathol. Appl. Neurobiol.* **28**, 200–209 (2002).
364. Casciati, A. *et al.* Human medulloblastoma cell lines: Investigating on cancer stem cell-like phenotype. *Cancers (Basel).* **12**, (2020).

365. Tatum, J. L. Hypoxia: Importance in tumor biology, noninvasive measurement by imaging, and value of its measurement in the management of cancer therapy. *Int. J. Radiat. Biol.* **82**, 699–757 (2006).
366. Bertout, J. A., Patel, S. A. & Simon, M. C. The impact of O2 availability on human cancer. *Nat. Rev. Cancer* **8**, 967–975 (2008).
367. Begg, K. & Tavassoli, M. Inside the hypoxic tumour: reprogramming of the DDR and radioresistance. *Off. J. Cell Death Differ. Assoc.* **6**, 1234567890 (2020).
368. Hamanaka, R. B. & Chandel, N. S. Targeting glucose metabolism for cancer therapy. *J. Exp. Med.* **209**, 211–215 (2012).
369. Bristow, R. G. & Hill, R. P. Hypoxia, DNA repair and genetic instability. *Nat. Rev. Cancer* **8**, 180–192 (2008).
370. Meng, A. X. *et al.* Hypoxia down-regulates DNA double strand break repair gene expression in prostate cancer cells. *Radiother. Oncol.* **76**, 168–176 (2005).
371. Rampling, R., Cruickshank, G., Lewis, A. D., Fitzsimmons, S. A. & Workman, P. Direct measurement of pO2 distribution and bioreductive enzymes in human malignant brain tumors. *Int. J. Radiat. Oncol. Biol. Phys.* **29**, 427–431 (1994).
372. Brizel, D. M., Sibley, G. S., Prosnitz, L. R., Scher, R. L. & Dewhirst, M. W. Tumor hypoxia adversely affects the prognosis of carcinoma of the head and neck. *Int. J. Radiat. Oncol.* **38**, 285–289 (1997).
373. Höckel, M. *et al.* Association between Tumor Hypoxia and Malignant Progression in Advanced Cancer of the Uterine Cervix. *Cancer Res.* **56**, (1996).
374. Brizel, D. M. *et al.* Tumor Oxygenation Predicts for the Likelihood of Distant Metastases in Human Soft Tissue Sarcoma. *Cancer Res.* **56**, 941–943 (1996).
375. Lalonde, E. *et al.* Tumour genomic and microenvironmental heterogeneity for integrated prediction of 5-year biochemical recurrence of prostate cancer: A retrospective cohort study. *Lancet Oncol.* **15**, 1521–1532 (2014).
376. Milosevic, M. *et al.* Tumor hypoxia predicts biochemical failure following radiotherapy for clinically localized prostate cancer. *Clin. Cancer Res.* **18**, 2108–2114 (2012).
377. Höckel, M., Vorndran, B., Schienger, K., Baßmann, E. & Knapstein, P. G. Tumor oxygenation: A new predictive parameter in locally advanced cancer of the uterine cervix. *Gynecol. Oncol.* **51**, 141–149 (1993).
378. Ward, C. *et al.* Carbonic anhydrase IX (CAIX), cancer, and radiation responsiveness. *Metabolites* **8**, (2018).
379. Semenzas, G. L., Roth, P. H., Fang, H.-M. & Wang, G. L. Transcriptional regulation of genes encoding glycolytic enzymes by hypoxia-inducible factor 1. *J Biol Chem* **269**, 23757–23763 (1994).
380. Mingyuan, X. *et al.* Hypoxia-inducible factor-1α activates transforming growth factor-β1/Smad signaling and increases collagen deposition in dermal fibroblasts. *Oncotarget* **9**, 3188–3197 (2018).
381. Forsythe, J. A. *et al.* Activation of vascular endothelial growth factor gene transcription by hypoxia-inducible factor 1. *Mol. Cell. Biol.* **16**, 4604–4613 (1996).
382. Ben-Yosef, Y., Lahat, N., Shapiro, S., Bitterman, H. & Miller, A. Regulation of endothelial matrix metalloproteinase-2 by hypoxia/reoxygenation. *Circ. Res.* **90**, 784–791 (2002).
383. Li, Y. Y. & Zheng, Y. L. Hypoxia promotes invasion of retinoblastoma cells in vitro by upregulating HIF-1α/MMP9 signaling pathway. *Eur. Rev. Med. Pharmacol. Sci.* **21**, 5361–5369 (2017).
384. Vaupel, P., Höckel, M. & Mayer, A. Detection and characterization of tumor hypoxia using pO2 histography. *Antioxidants and Redox Signaling* **9**, 1221–1235 (2007).
385. Yang, L. J. & West, C. M. L. Hypoxia gene expression signatures as predictive biomarkers for personalising radiotherapy. *British Journal of Radiology* **92**, (2019).
386. Van Malenstein, H. *et al.* A seven-gene set associated with chronic hypoxia of prognostic importance in hepatocellular carcinoma. *Clin. Cancer Res.* **16**, 4278–4288 (2010).
387. Buffa, F. M., Harris, A. L., West, C. M. & Miller, C. J. Large meta-analysis of multiple cancers reveals a common, compact and highly prognostic hypoxia metagene. *Br. J. Cancer* **102**, 428–435 (2010).
388. Wang, Z. *et al.* A novel hypoxic tumor microenvironment signature for predicting the survival, progression, immune responsiveness and chemoresistance of glioblastoma:

A multi-omic study. *Aging (Albany. NY).* **12**, 17038–17061 (2020).
389. Fardin, P. *et al.* A biology-driven approach identifies the hypoxia gene signature as a predictor of the outcome of neuroblastoma patients. *Mol. Cancer* **9**, 185 (2010).
390. Winter, S. C. *et al.* Relation of a hypoxia metagene derived from head and neck cancer to prognosis of multiple cancers. *Cancer Res.* **67**, 3441–3449 (2007).
391. Yang, L. *et al.* A gene signature for selecting benefit from hypoxia modification of radiotherapy for high-risk bladder cancer patients. *Clin. Cancer Res.* **23**, 4761–4768 (2017).
392. Overgaard, J. *et al.* A randomized double-blind phase III study of nimorazole as a hypoxic radiosensitizer of primary radiotherapy in supraglottic larynx and pharynx carcinoma. Results of the Danish Head and Neck Cancer Study (DAHANCA) Protocol 5-85. *Radiother. Oncol.* **46**, 135–146 (1998).
393. Overgaard, J. Hypoxic modification of radiotherapy in squamous cell carcinoma of the head and neck - A systematic review and meta-analysis. *Radiotherapy and Oncology* **100**, 22–32 (2011).
394. Hoskin, P. J., Rojas, A. M., Bentzen, S. M. & Saunders, M. I. Radiotherapy with concurrent carbogen and nicotinamide in bladder carcinoma. *J. Clin. Oncol.* **28**, 4912–4918 (2010).
395. Kjellen, E., Joiner, M. C., Collier, J. M., Johns, H. & Rojas, A. A therapeutic benefit from combining normobaric carbogen or oxygen with nicotinamide in fractionated X-ray treatments. *Radiother. Oncol.* **22**, 81–91 (1991).
396. Bennett, M. H., Feldmeier, J., Smee, R. & Milross, C. Hyperbaric oxygenation for tumour sensitisation to radiotherapy. *Cochrane Database of Systematic Reviews* (2012). doi:10.1002/14651858.CD005007.pub3
397. Falk, S. J., Ward, R. & Bleehen, N. M. The influence of carbogen breathing on tumour tissue oxygenation in man evaluated by computerised pO2 histography. *Br. J. Cancer* **66**, 919–924 (1992).
398. Jackson, L. *East and North Hertfordshire NHS Trust Radiotherapy with carbogen and nicotinamide*. (2021).
399. Olive, P. L., Banáth, J. P. & Aquino-Parsons, C. Measuring Hypoxia in Solid Tumours&Is There a Gold Standard? *Acta Oncol. (Madr).* **40**, 917–923 (2001).
400. Le, Q. T. & Courter, D. Clinical biomarkers for hypoxia targeting. *Cancer and Metastasis Reviews* **27**, 351–362 (2008).
401. Peerlings, J. *et al.* Hypoxia and hypoxia response-associated molecular markers in esophageal cancer: A systematic review. *Methods* **130**, 51–62 (2017).
402. Hui, E. P. *et al.* Coexpression of Hypoxia-inducible Factors 1 and 2, Carbonic Anhydrase IX, and Vascular Endothelial Growth Factor in Nasopharyngeal Carcinoma and Relationship to Survival. *Clin. Cancer Res.* **8**, 2595–2604 (2002).
403. Vleugel, M. M. *et al.* Differential prognostic impact of hypoxia induced and diffuse HIF-1α expression in invasive breast cancer. *J. Clin. Pathol.* **58**, 172–177 (2005).
404. Trastour, C. *et al.* HIF-1α and CA IX staining in invasive breast carcinomas: Prognosis and treatment outcome. *Int. J. Cancer* **120**, 1451–1458 (2007).
405. Kim, S. J. *et al.* Expression of HIF-1α, CA IX, VEGF, and MMP-9 in surgically resected non-small cell lung cancer. *Lung Cancer* **49**, 325–335 (2005).
406. Eckert, A. W. *et al.* Investigation of the prognostic role of carbonic anhydrase 9 (CAIX) of the cellular mRNA/protein level or soluble CAIX protein in patients with oral squamous cell carcinoma. *Int. J. Mol. Sci.* **20**, 375 (2019).
407. Brennan, D. J. *et al.* CA IX is an independent prognostic marker in premenopausal breast cancer patients with one to three positive lymph nodes and a putative marker of radiation resistance. *Clin. Cancer Res.* **12**, 6421–6431 (2006).
408. Koukourakis, M. I. *et al.* Endogenous markers of two separate hypoxia response pathways (hypoxia inducible factor 2 alpha and carbonic anhydrase 9) are associated with radiotherapy failure in head and neck cancer patients recruited in the CHART randomized trial. *J. Clin. Oncol.* **24**, 727–735 (2006).
409. Koukourakis, M. I. *et al.* Hypoxia-regulated Carbonic Anhydrase-9 (CA9) Relates to Poor Vascularization and Resistance of Squamous Cell Head and Neck Cancer to Chemoradiotherapy. *Clin. Cancer Res.* **7**, 3399–3403 (2001).
410. Loncaster, J. A. *et al.* Carbonic Anhydrase (CA IX) Expression, a Potential New Intrinsic Marker of Hypoxia: Correlations with Tumor Oxygen Measurements and

Prognosis in Locally Advanced Carcinoma of the Cervix. *Cancer Res.* **61**, 6394–6399 (2001).
411. Hedley, D. *et al.* Carbonic Anhydrase IX Expression, Hypoxia, and Prognosis in Patients with Uterine Cervical Carcinomas. *Clin. Cancer Res.* **9**, 5666–5674 (2003).
412. Wook Kim, B. *et al.* Prognostic assessment of hypoxia and metabolic markers in cervical cancer using automated digital image analysis of immunohistochemistry. *J. Transl.* **11**, 185 (2013).
413. Hao, L. S. *et al.* Correlation and expression analysis of hypoxia-inducible factor 1α, glucose transporter 1 and lactate dehydrogenase 5 in human gastric cancer. *Oncol. Lett.* **18**, 1431–1441 (2019).
414. Pardridges, W. M., Boado, R. J. & Farrell, C. R. Brain-type glucose transporter (GLUT-1) is selectively localized to the blood-brain barrier. Studies with quantitative western blotting and in situ hybridization. *J. Biol. Chem.* **265**, 18035–18040 (1990).
415. Boado, R. J. & Pardridge, W. M. The brain-type glucose transporter mRNA is specifically expressed at the blood-brain barrier. *Biochem. Biophys. Res. Commun.* **166**, 174–179 (1990).
416. Kunkel, M. *et al.* Overexpression of Glut-1 and increased glucose metabolism in tumors are associated with a poor prognosis in patients with oral squamous cell carcinoma. *Cancer* **97**, 1015–1024 (2003).
417. Cho, H., Lee, Y. S., Kim, J., Chung, J.-Y. & Kim, J.-H. Cancer Investigation Overexpression of Glucose Transporter-1 (GLUT-1) Predicts Poor Prognosis in Epithelial Ovarian Cancer Overexpression of Glucose Transporter-1 (GLUT-1) Predicts Poor Prognosis in Epithelial Ovarian Cancer. *Cancer Invest.* **31**, 607–615 (2013).
418. Sung, J.-Y., Kim, G. Y., Lim, S.-J., Park, Y.-K. & Kim, Y. W. Expression of the GLUT1 glucose transporter and p53 in carcinomas of the pancreatobiliary tract | Elsevier Enhanced Reader. *Pathol Res Pr.* **206**, 24–29 (2010).
419. Cooper, R. *et al.* Glucose transporter-1 (GLUT-1): a potential marker of prognosis in rectal carcinoma? *Br. J. Cancer* **89**, 870–876 (2003).
420. Chen, B. *et al.* miR-22 as a prognostic factor targets glucose transporter protein type 1 in breast cancer. *Cancer Lett* **356**, 410–417 (2015).
421. Kaira, K. *et al.* Biological Correlation of 18F-FDG Uptake on PET in Pulmonary Neuroendocrine Tumors. *Anticancer Res.* **33**, 4219–4228 (2013).
422. Basturk, O. *et al.* GLUT-1 Expression in Pancreatic Neoplasia: Implications in Pathogenesis, Diagnosis, and Prognosis. *Pancreas* **40**, 187–192 (2011).
423. Airley, R. *et al.* Glucose Transporter Glut-1 Expression Correlates with Tumor Hypoxia and Predicts Metastasis-free Survival in Advanced Carcinoma of the Cervix. *Clin. Cancer Res.* **7**, 928–934 (2001).
424. Wang, J. *et al.* Glucose transporter GLUT1 expression and clinical outcome in solid tumors: A systematic review and meta-analysis. *Oncotarget* **8**, 16875–16886 (2017).
425. Yu, M. *et al.* The prognostic value of GLUT1 in cancers: A systematic review and meta-analysis. *Oncotarget* **8**, 43356–43367 (2017).
426. Zhang, B., Xie, Z. & Li, B. The clinicopathologic impacts and prognostic significance of GLUT1 expression in patients with lung cancer: A meta-analysis. *Gene* **689**, 76–83 (2019).
427. Wang, J. *et al.* Development and validation of a hypoxia-related prognostic signature for breast cancer. *Oncol. Lett.* **20**, 1906–1914 (2020).
428. Seigneuric, R. *et al.* Impact of supervised gene signatures of early hypoxia on patient survival. *Radiother. Oncol.* **83**, 374–382 (2007).
429. Hu, Z. *et al.* A compact VEGF signature associated with distant metastases and poor outcomes. *BMC Med.* **7**, 9 (2009).
430. Ghazoui, Z. *et al.* Close and stable relationship between proliferation and a hypoxia metagene in aromatase inhibitor-treated ER-positive breast cancer. *Clin. Cancer Res.* **17**, 3005–3012 (2011).
431. Halle, C. *et al.* Hypoxia-induced gene expression in chemoradioresistant cervical cancer revealed by dynamic contrast-enhanced MRI. *Cancer Res.* **72**, 5285–5295 (2012).
432. Fjeldbo, C. S. *et al.* Integrative analysis of DCE-MRI and gene expression profiles in construction of a gene classifier for assessment of hypoxia-related risk of

chemoradiotherapy failure in cervical cancer. *Clin. Cancer Res.* **22**, 4067–4076 (2016).
433. Dekervel, J. *et al.* Hypoxia-driven gene expression is an independent prognostic factor in stage II and III colon cancer patients. *Clin. Cancer Res.* **20**, 2159–2168 (2014).
434. Tardón, M. C. *et al.* An experimentally defined hypoxia gene signature in glioblastoma and its modulation by metformin. *Biology (Basel).* **9**, 1–17 (2020).
435. Lin, W. *et al.* Characterization of Hypoxia Signature to Evaluate the Tumor Immune Microenvironment and Predict Prognosis in Glioma Groups. *Front. Oncol.* **10**, 796 (2020).
436. Eustace, A. *et al.* A 26-gene hypoxia signature predicts benefit from hypoxia-modifying therapy in laryngeal cancer but not bladder cancer. *Clin. Cancer Res.* **19**, 4879–4888 (2013).
437. Toustrup, K. *et al.* Development of a hypoxia gene expression classifier with predictive impact for hypoxic modification of radiotherapy in head and neck cancer. *Cancer Res.* **71**, 5923–5931 (2011).
438. Sun, J. *et al.* Development and validation of a hypoxia-related gene signature to predict overall survival in early-stage lung adenocarcinoma patients. *Ther. Adv. Med. Oncol.* **12**, 1–14 (2020).
439. Ragnum, H. B. *et al.* The tumour hypoxia marker pimonidazole reflects a transcriptional programme associated with aggressive prostate cancer. *Br. J. Cancer* **112**, 382–390 (2015).
440. Yang, L. *et al.* Development and Validation of a 28-gene Hypoxia-related Prognostic Signature for Localized Prostate Cancer. *EBioMedicine* **31**, 182–189 (2018).
441. Yang, L. *et al.* Validation of a hypoxia related gene signature in multiple soft tissue sarcoma cohorts. *Oncotarget* **9**, 3946–3955 (2018).
442. Abou Khouzam, R. *et al.* Integrating tumor hypoxic stress in novel and more adaptable strategies for cancer immunotherapy. *Seminars in Cancer Biology* **65**, 140–154 (2020).
443. Yaromina, A. *et al.* Radiobiological hypoxia, histological parameters of tumour microenvironment and local tumour control after fractionated irradiation. *Radiother. Oncol.* **96**, 116–122 (2010).
444. Horsman, M., Wouters, B., Joiner, M. & Overgaard, J. The oxygen effect and fractionated radiotherapy. in *Basic Clinical Radiobiology* (ed. Steel, G.) 207–216 (Hodder Arnold, 2009).
445. Churchill-Davidson, I., Sanger, C. & Thomlinson, R. H. High-pressure oxygen and radiotherapy. *Lancet* **265**, 1091–1095 (1955).
446. Nordsmark, M. *et al.* Prognostic value of tumor oxygenation in 397 head and neck tumors after primary radiation therapy. An international multi-center study. *Radiother. Oncol.* **77**, 18–24 (2005).
447. Nordsmark, M., Overgaard, M. & Overgaard, J. Pretreatment oxygenation predicts radiation response in advanced squamous cell carcinoma of the head and neck. *Radiother. Oncol.* **41**, 31–9 (1996).
448. Fyles, A. *et al.* Tumor hypoxia has independent predictor impact only in patients with node-negative cervix cancer. *J. Clin. Oncol.* **20**, 680–687 (2002).
449. Wenzl, T. & Wilkens, J. J. Modelling of the oxygen enhancement ratio for ion beam radiation therapy. *Phys. Med. Biol.* **56**, 3251–3268 (2011).
450. Tinganelli, W. *et al.* Influence of acute hypoxia and radiation quality on cell survival. *J. Radiat. Res.* **54**, i23–i30 (2013).
451. Hall, E. J. The Oxygen Effect and Reoxygenation. in *Radiobiology for the Radiologist* 137–160 (Lippencott, 1988).
452. Pajonk, F., Vlashi, E. & McBride, W. H. Radiation Resistance of Cancer Stem Cells: The 4 R's of Radiobiology Revisited. *Stem Cells* **28**, 639–648 (2010).
453. Thomlinson, R. H. & Gray, L. H. The histological structure of some human lung cancers and the possible implications for radiotherapy. *Br. J. Cancer* **9**, 539–549 (1955).
454. Powers, W. E. & Tolmach, L. J. Demonstration of an Anoxic Component in a Mouse Tumor-Cell Population by in Vivo Assay of Survival Following Irradiation. *Radiology* **83**, 328–336 (1964).

455. Ma, N.-Y., Tinganelli, W., Maier, A., Durante, M. & Kraft-Weyrather, W. Influence of chronic hypoxia and radiation quality on cell survival. *J. Radiat. Res.* **54**, i13–i22 (2013).
456. Zhang, L., Subarsky, P. & Hill, R. P. Hypoxia-regulated p53 and its effect on radiosensitivity in cancer cells. *Int. J. Radiat. Biol.* **83**, 443–456 (2007).
457. Tian, J. *et al.* The Antiproliferative and Colony-suppressive Activities of STAT3 Inhibitors in Human Cancer Cells Is Compromised Under Hypoxic Conditions. *Anticancer Res.* **37**, 547–553 (2017).
458. Valencia-Cervantes, J. *et al.* Hypoxia increases chemoresistance in human medulloblastoma DAOY cells via hypoxia-inducible factor 1α-mediated downregulation of the CYP2B6, CYP3A4 and CYP3A5 enzymes and inhibition of cell proliferation. *Oncol. Rep.* **41**, 178–190 (2019).
459. Cowman, S., Fan, Y. N., Pizer, B. & Sée, V. Decrease of Nibrin expression in chronic hypoxia is associated with hypoxia-induced chemoresistance in some brain tumour cells. *BMC Cancer* **19**, 1–16 (2019).
460. Nordfors, K. *et al.* The tumour-associated carbonic anhydrases CA II, CA IX and CA XII in a group of medulloblastomas and supratentorial primitive neuroectodermal tumours: An association of CA IX with poor prognosis. *BMC Cancer* **10**, 1–10 (2010).
461. Pantazi, P., Carollo, E., Carter, D. R. F. & Brooks, S. A. A practical toolkit to study aspects of the metastatic cascade in vitro. *Acta Histochemica* **122**, 151654 (2020).
462. Iglesias, P. A. & Levchenko, A. Modeling the Cell's Guidance System. *Sci. Signal.* **2002**, (2002).
463. Horwitz, R. & Webb, D. Cell Migration. *Curr. Biol.* **13**, 720–730 (2016).
464. Justus, C. R., Leffler, N., Ruiz-Echevarria, M. & Yang, L. V. In vitro Cell Migration and Invasion Assays. *J. Vis. Exp.* 1–8 (2014). doi:10.3791/51046
465. Frixen, U. H. *et al.* E-cadherin-mediated cell-cell adhesion prevents invasiveness of human carcinoma cells. *J. Cell Biol.* **113**, 173–185 (1991).
466. Moncharmont, C. *et al.* Radiation-enhanced cell migration/invasion process: A review. *Crit. Rev. Oncol. Hematol.* **92**, 133–142 (2014).
467. Camphausen, K. *et al.* Radiation Therapy to a Primary Tumor Accelerates Metastatic Growth in Mice. *Cancer Res.* **61**, 2207–2211 (2001).
468. Chou, C. H. *et al.* MMP-9 from sublethally irradiated tumor promotes Lewis lung carcinoma cell invasiveness and pulmonary metastasis. *Oncogene* **31**, 458–468 (2012).
469. Biswas, S. *et al.* Inhibition of TGF-β with neutralizing antibodies prevents radiation-induced acceleration of metastatic cancer progression. *J. Clin. Invest.* **117**, 1305–1313 (2007).
470. Young, A. G. H. & Bennewith, K. L. Ionizing Radiation Enhances Breast Tumor Cell Migration *In Vitro*. *Radiat. Res.* **188**, RR14738.1 (2017).
471. De Bacco, F. *et al.* Induction of MET by ionizing radiation and its role in radioresistance and invasive growth of cancer. *J. Natl. Cancer Inst.* **103**, 645–661 (2011).
472. Kawamoto, A. *et al.* Radiation induces epithelial-mesenchymal transition in colorectal cancer cells. *Oncol. Rep.* **27**, 51–57 (2012).
473. Wild-Bode, C., Weller, M., Rimner, A., Dichgans, J. & Wick, W. Sublethal Irradiation Promotes Migration and Invasiveness of Glioma Cells: Implications for Radiotherapy of Human Glioblastoma. *Cancer Res.* **61**, 2744–2750 (2001).
474. Rieken, S. *et al.* Carbon ion irradiation inhibits glioma cell migration through downregulation of integrin expression. *Int. J. Radiat. Oncol. Biol. Phys.* **83**, 394–399 (2012).
475. Fehlauer, F., Muench, M., Richter, E. & Rades, D. The inhibition of proliferation and migration of glioma spheroids exposed to temozolomide is less than additive if combined with irradiation. *Oncol. Rep.* **17**, 941–945 (2007).
476. Pickhard, A. C. *et al.* Inhibition of radiation induced migration of human head and neck squamous cell carcinoma cells by blocking of EGF receptor pathways. *BMC Cancer* **11**, 388 (2011).
477. Beck, C. *et al.* The kallikrein-kinin-system in head and neck squamous cell carcinoma (HNSCC) and its role in tumour survival, invasion, migration and response to radiotherapy. *Oral Oncol.* **48**, 1208–1219 (2012).

478. Ogata, T. *et al.* Particle irradiation suppresses metastatic potential of cancer cells. *Cancer Res.* **65**, 113–20 (2005).
479. Cheng, J. C. H., Chou, C. H., Kuo, M. L. & Hsieh, C. Y. Radiation-enhanced hepatocellular carcinoma cell invasion with MMP-9 expression through PI3K/Akt/NF-κB signal transduction pathway. *Oncogene* **25**, 7009–7018 (2006).
480. Akino, Y. *et al.* Carbon-Ion Beam Irradiation Effectively Suppresses Migration and Invasion of Human Non-Small-Cell Lung Cancer Cells. *Int. J. Radiat. Oncol. Biol. Phys.* **75**, 475–481 (2009).
481. Narang, H., Kumar, A., Bhat, N., Pandey, B. N. & Ghosh, A. Effect of proton and gamma irradiation on human lung carcinoma cells: Gene expression, cell cycle, cell death, epithelial-mesenchymal transition and cancer-stem cell trait as biological end points. *Mutat. Res. - Fundam. Mol. Mech. Mutagen.* **780**, 35–46 (2015).
482. Qian, L.-W. *et al.* Radiation-induced Increase in Invasive Potential of Human Pancreatic Cancer Cells and Its Blockade by a Matrix Metalloproteinase Inhibitor, CGS27023. *Clin. Cancer Res.* **8**, 1223–1227 (2002).
483. Ganji, P. N. *et al.* siRNA-mediated Downregulation of MMP-9 and uPAR in Combination with Radiation Induces G2/M Cell Cycle Arrest in Medulloblastoma. *Mol Cancer Res* **9**, 51–66 (2011).
484. Lechapt-Zalcman, E. *et al.* Transforming growth factor-1 increases airway wound repair via MMP-2 upregulation: a new pathway for epithelial wound repair? *Am J Physiol Lung Cell Mol Physiol* **290**, 1277–1282 (2006).
485. Mcguire, J. K., Li, Q. & Parks, W. C. Matrilysin (Matrix Metalloproteinase-7) Mediates E-Cadherin Ectodomain Shedding in Injured Lung Epithelium. *Am. J. Pathol.* **162**, (2003).
486. Webb, A. H. *et al.* Inhibition of MMP-2 and MMP-9 decreases cellular migration, and angiogenesis in in vitro models of retinoblastoma. doi:10.1186/s12885-017-3418-y
487. Asuthkar, S., Gogineni, V. R., Rao, J. S. & Velpula, K. K. Nuclear Translocation of Hand-1 Acts as a Molecular Switch to Regulate Vascular Radiosensitivity in Medulloblastoma Tumors: The Protein uPAR Is a Cytoplasmic Sequestration Factor for Hand-1. *Mol. Cancer Ther.* **13**, 1309–1322 (2014).
488. Yang, B., Miao, S. & Li, Y. SCUBE2 inhibits the proliferation, migration and invasion of human non-small cell lung cancer cells through regulation of the sonic hedgehog signaling pathway. *Gene* **672**, 143–149 (2018).
489. Jiang, L. *et al.* Gli promotes tumor progression through regulating epithelial-mesenchymal transition in non-small-cell lung cancer. *J. Cardiothorac. Surg.* **15**, 1–8 (2020).
490. Li, H. *et al.* Gli promotes epithelial-mesenchymal transition in human lung adenocarcinomas. *Oncotarget* **7**, 80415–80425 (2016).
491. Yoo, Y. A. *et al.* Sonic hedgehog pathway promotes metastasis and lymphangiogenesis via activation of Akt, EMT, and MMP-9 pathway in gastric cancer. *Cancer Res.* **71**, 7061–7070 (2011).
492. Wang, Y. H. *et al.* BRD4 induces cell migration and invasion in HCC cells through MMP-2 and MMP-9 activation mediated by the Sonic hedgehog signaling pathway. *Oncol. Lett.* **10**, 2227–2232 (2015).
493. Chang, L. *et al.* Activation of sonic hedgehog signaling enhances cell migration and invasion by induction of matrix metalloproteinase-2 and -9 via the phosphoinositide-3 kinase/AKT signaling pathway in glioblastoma. *Mol. Med. Rep.* **12**, 6702–6710 (2015).
494. Peng, W. X. *et al.* Smoothened regulates migration of fibroblast-like synoviocytes in rheumatoid arthritis Via activation of rho GTPase signaling. *Front. Immunol.* **8**, 1–9 (2017).
495. Zhang, Z. *et al.* Suppressor of fused (Sufu) promotes epithelial-mesenchymal transition (EMT) in cervical squamous cell carcinoma. *Oncotarget* **8**, 114226–114238 (2017).
496. Feldmann, G. *et al.* Blockade of hedgehog signaling inhibits pancreatic cancer invasion and metastases: A new paradigm for combination therapy in solid cancers. *Cancer Res.* **67**, 2187–2196 (2007).
497. Cowling, V. H. & Cole, M. D. E-cadherin repression contributes to c-Myc-induced epithelial cell transformation. *Oncogene* **26**, 3582–3586 (2007).

498. Xu, X.-H., Zhang, S.-J., Hu, Q.-B., Song, X.-Y. & Pan, W. Effects of microRNA-494 on proliferation, migration, invasion, and apoptosis of medulloblastoma cells by mediating *c-myc* through the p38 MAPK signaling pathway. *J. Cell. Biochem.* (2018). doi:10.1002/jcb.27559
499. Zhang, C., Xu, B., Lu, S., Zhao, Y. & Liu, P. HN1 contributes to migration, invasion, and tumorigenesis of breast cancer by enhancing MYC activity. *Mol. Cancer* **16**, (2017).
500. Ranger, A., McDonald, W., Moore, E. & DelMaestro, R. The invasiveness of five medulloblastoma cell lines in collagen gels. *J Neurooncol* **96**, 181–189 (2010).
501. Zanini, C. *et al.* Medullospheres from DAOY, UW228 and ONS-76 Cells: Increased Stem Cell Population and Proteomic Modifications. *PLoS One* **8**, (2013).
502. Bonfim-Silva, R. *et al.* Biological characterization of the UW402, UW473, ONS-76 and DAOY pediatric medulloblastoma cell lines. *Cytotechnology* **3**, (2019).
503. Rieken, S. *et al.* Radiation-induced motility alterations in medulloblastoma cells. *J. Radiat. Res.* **56**, 430–436 (2015).
504. Nalla, A. K. *et al.* Suppression of uPAR Retards Radiation-Induced Invasion and Migration Mediated by Integrin β1/FAK Signaling in Medulloblastoma. *PLoS One* **5**, e13006 (2010).
505. Reid, Y., Storts, D., Riss, T. & Minor, L. Authentication of Human Cell Lines by STR DNA Profiling Analysis. in *Assay Guidance Manual [Internet]* (eds. Sittampalam, G. et al.) (Eli Lilly & Company and the National Center for Advancing Translational Sciences, 2013).
506. Weeraratne, S. D. *et al.* Pleiotropic effects of miR-183~96~182 converge to regulate cell survival, proliferation and migration in medulloblastoma. *Acta Neuropathol.* **123**, 539–552 (2012).
507. Snuderl, M. *et al.* Targeting Placental Growth Factor/Neuropilin 1 Pathway Inhibits Growth and Spread of Medulloblastoma. *Cell* **152**, 1065–1076 (2013).
508. Kunkele, A. *et al.* Pharmacological activation of the p53 pathway by nutlin-3 exerts anti-tumoral effects in medulloblastomas. *Neuro. Oncol.* **14**, 859–869 (2012).
509. Saylors, R. L. *et al.* Infrequent p53 Gene Mutations in Medulloblastomas. *Cancer Res.* **51**, 4721–4723 (1991).
510. Ghassemifar, S. & Mendrysa, S. M. MDM2 antagonism by nutlin-3 induces death in human medulloblastoma cells. *Neurosci. Lett.* **513**, 106–110 (2012).
511. Langdon, J. A. *et al.* Combined Genome-Wide Allelotyping and Copy Number Analysis Identify Frequent Genetic Losses Without Copy Number Reduction in Medulloblastoma. *Genes, Chromosom. Cancer* **45**, 47–60 (2006).
512. Friedman, H. S. *et al.* Establishment and Characterization of the Human Medulloblastoma Cell Line and Transplantable Xenograft D283 Med. *J. Neuropathol. Exp. Neurol.* **44**, 592–605 (1985).
513. Lacroix, J. *et al.* Oncolytic effects of parvovirus H-1 in medulloblastoma are associated with repression of master regulators of early neurogenesis. *Int. J. Cancer* **134**, 703–716 (2014).
514. Bigner, S. H., Friedman, H. S., Vogelstein, B., Oakes, W. J. & Bigner, D. D. Amplification of the c-myc Gene in Human Medulloblastoma Cell Lines and Xenografts. *Cancer Res.* **50**, 2347–2350 (1990).
515. Jacobsen, P., Jenkyn, D. J. & Papadimitriou, J. M. Establishment of a Human Medulloblastoma Cell Line and Its Heterotransplantation into Nude Mice. *J. Neuropathol. Exp. Neurol.* **44**, 472–485 (1985).
516. Yamada, M. *et al.* Establishment and biological characterization of human medulloblastoma cell lines. *No To Shinkei* **41**, 695–702 (1989).
517. Keles, G. E. *et al.* Establishment and characterization of four human medulloblastoma-derived cell lines. *Oncol. Res.* **7**, 493–503 (1995).
518. Geraghty, R. J. *et al.* Guidelines for the use of cell lines in biomedical research. *Br. J. Cancer* **111**, 1021–1046 (2014).
519. Gautier, L., Cope, L., Bolstad, B. M. & Irizarry, R. A. affy - analysis of Affymetrix GeneChip data at the probe level. *Bioinformatics* **20**, 307–315 (2004).
520. McDonald, J. affycoretools: Functions useful for those doing repetitive analyses with Affymetrix GeneChips. R Package version 1.62.0 (2020).
521. Pages, H., Carlson, M., Falcon, S. & Li, N. AnnotationDbi: Manipulation of SQLite-

based annotations in Bioconductor. R package version 1.52.0 (2020).
522. Huber, W. *et al.* Orchestrating high-throughput genomic analysis with Bioconductor. *Nat. Methods* **12**, 115–121 (2015).
523. Wickman, H., François, R., Henry, L. & Muller, K. dlpyr: A Grammar of Data Manipulation. (2021).
524. Davis, S. & Meltzer, P. GEOquery: a bridge between the Gene Expression Ombinbus (GEO) and Bioconductor. *Bioinformatics* **14**, 1846–1847 (2007).
525. Wickham, H. ggplot2: Elegant Graphics for Data Analysis. Springer-Verlag New York (2016).
526. Warnes, G. gplots: Various R Programming Tools for Plotting Data. (2020).
527. Carlson, M. hgu133plus2.db: Affymetrix Human Genome U133 Plus 2.0 Array annotation data (chip hgu133plus2). R package version 3.2.3 (2016).
528. Project, T. hgu133plus2cdf: hgu133plus2cdf. R package version 2.18.0 (2015).
529. MacDonald, J. hugene11sttranscriptcluster.db: Affymetrix hugene11 annotation data (chip hugene11sttranscriptcluster). R package version 8.7.0 (2017).
530. MacDonald, J. hugene20sttranscriptcluster.db: Affymetrix hugene20 annotation data (chip hugene20sttranscriptcluster). R package version 8.7.0 (2017).
531. Bengtsson, H. matrixStats: Functions that Apply to Rows and Columns of Matrices (and to Vectors). (2021).
532. Gendoo, D. M. A. D. & Haibe-Kains, B. MM2S: personalized diagnosis of medulloblastoma patients and model systems. *Source Code Biol. Med.* **11**, 6 (2016).
533. Carvalho, B. S. & Irizarry, R. A. A framework for oligonucleotide microarray preprocessing. *Bioinformatics* **26**, 2363–2367 (2010).
534. Kolde, R. pheatmap: Pretty Heatmaps. (2019).
535. Wickham, H. stringr: Simple, Consistent Wrappers for Common String Operations. (2019).
536. Kassambara, A. survminer: Drawing Survival Curves using 'ggplot2'. (2020).
537. Therneau, T. A Package for Survival Analysis in R. R package version 3.2-7 (2020).
538. Ooms, J. writexl: Export Data Frames to Excel 'xlsx' Format.
539. Robinson, G. *et al.* Novel mutations target distinct subgroups of medulloblastoma. *Nature* **488**, 43–48 (2012).
540. Morfouace, M. *et al.* ABCG2 transporter expression impacts group 3 medulloblastoma response to chemotherapy. *Cancer Res.* **75**, 3879–3889 (2015).
541. Robinson, M. D. & Speed, T. P. A comparison of affymetrix gene expression arrays. *BMC Bioinformatics* **8**, 449 (2007).
542. Rivero-Hinojosa, S. *et al.* Proteomic analysis of Medulloblastoma reveals functional biology with translational potential. *Acta Neuropathol. Commun.* **6**, (2018).
543. Data Sheets: Human Gene 2.0 and 2.1 Arrays ST Arrays. Available at: https://www.thermofisher.com/document-connect/document-connect.html?url=https%3A%2F%2Fassets.thermofisher.com%2FTFS-Assets%2FLSG%2Fbrochures%2Fhugene_2_st_datasheet.pdf&title=RGF0YSBTaGVldHM6IEh1bWFuIEdlbmUgMi4wIGFuZCAyLjEgQXJyYXlzIFNUIEFycmF5cw==. (Accessed: 14th January 2021)
544. Ramaswamy, V. & Taylor, M. D. Bioinformatic Strategies for the Genomic and Epigenomic Characterization of Brain Tumors. *Methods Mol. Biol.* **1869**, 37–56 (2019).
545. Affymetrix. Affymetrix ® Human, Mouse, and Rat Gene 1.1 ST Array Strips provide whole-transcript coverage in a convenient four-array strip format.
546. Milde-Langosch, K. *et al.* Validity of the proliferation markers Ki67, TOP2A, and RacGAP1 in molecular subgroups of breast cancer. *Breast Cancer Res. Treat.* **137**, 57–67 (2013).
547. Assays and annotation - The Human Protein Atlas. Available at: https://www.proteinatlas.org/about/assays+annotation#tcga_survival. (Accessed: 11th May 2021)
548. Ivanova, L. *et al.* Prognostic relevance of carbonic anhydrase IX expression is distinct in various subtypes of breast cancer and its silencing suppresses self-renewal capacity of breast cancer cells. *Cancer Chemother. Pharmacol.* **75**, 235–246 (2015).
549. Zeng, K., Ju, G., Wang, H. & Huang, J. GLUT1/3/4 as novel biomarkers for the prognosis of human breast cancer. *Transl. Cancer Res.* **9**, 2363–2377 (2020).

550. Starska, K. *et al.* Gene and protein expression of glucose transporter 1 and glucose transporter 3 in human laryngeal cancer—the relationship with regulatory hypoxia-inducible factor-1α expression, tumor invasiveness, and patient prognosis. *Tumor Biol.* **36**, 2309–2321 (2015).
551. Davidoff, A. M. Neuroblastoma. *Semin. Pediatr. Surg.* **21**, 2–14 (2012).
552. Liang, C. C., Park, A. Y. & Guan, J. L. In vitro scratch assay: A convenient and inexpensive method for analysis of cell migration in vitro. *Nat. Protoc.* **2**, 329–333 (2007).
553. De Ieso, M. L. & Pei, J. V. An accurate and cost-effective alternative method for measuring cell migration with the circular wound closure assay. *Bioscience Reports* **38**, (2018).
554. Garcia-Fossa, F., Gaal, V. & de Jesus, M. B. PyScratch: An ease of use tool for analysis of scratch assays. *Comput. Methods Programs Biomed.* **193**, 105476 (2020).
555. Incucyte® Scratch Wound Analysis Software Module (Cat. No. 9600-0012) - Incucyte® Software | Automated Analysis of Live-Cell Images. Available at: https://www.essenbioscience.com/en/products/software/cell-player-cell-migration-software-module/. (Accessed: 2nd June 2021)
556. Wenger, S. L. *et al.* Comparison of Established Cell Lines at Different Passages by Karyotype and Comparative Genomic Hybridization. *Biosci. Rep.* **24**, 631–639 (2004).
557. Othman, R. T. *et al.* Overcoming multiple drug resistance mechanisms in medulloblastoma. *Acta Neuropathol. Commun.* **2**, 57 (2014).
558. Xu, J. *et al.* Disseminated medulloblastoma in a child with germline BRCA2 6174delT mutation and without Fanconi anemia. *Front. Oncol.* **5**, 27 (2015).
559. Morrison, L. C. *et al.* Deconstruction of Medulloblastoma Cellular Heterogeneity Reveals Differences between the Most Highly Invasive and Self-Renewing Phenotypes. *Neoplasia* **15**, 384–398 (2013).
560. Rostomily, R. C. *et al.* Expression of Neurogenic Basic Helix-Loop-Helix Genes in Primitive Neuroectodermal Tumours. *Cancer Res.* **57**, 3526–3531 (1997).
561. Siu, I.-M., Lal, A., Blankenship, J. R., Aldosari, N. & Riggins, G. J. c-Myc Promoter Activation in Medulloblastoma. *Cancer Res.* **63**, 4773–4776 (2003).
562. Lindsey, J. C. *et al.* Identification of tumour-specific epigenetic events in medulloblastoma development by hypermethylation profiling. *Carcinogenesis* **25**, 661–668 (2004).
563. Bai, R. *et al.* Evaluation of retinoic acid therapy for OTX2-positive medulloblastomas. *Neuro. Oncol.* **12**, 655–663 (2010).
564. Yin, A. H. *et al.* AC133, a Novel Marker for Human Hematopoietic Stem and Progenitor Cells. *Blood* **90**, 5002–5012 (1997).
565. Todaro, M. *et al.* Colon Cancer Stem Cells Dictate Tumor Growth and Resist Cell Death by Production of Interleukin-4. *Cell Stem Cell* **1**, 389–402 (2007).
566. Suvà, M. L. *et al.* Identification of cancer stem cells in Ewing's sarcoma. *Cancer Res.* **69**, 1776–1781 (2009).
567. Chiou, S. H. *et al.* Positive correlations of Oct-4 and Nanog in oral cancer stem-like cells and high-grade oral squamous cell carcinoma. *Clin. Cancer Res.* **14**, 4085–4095 (2008).
568. Ma, S., Lee, T. K., Zheng, B. J., Chan, K. W. & Guan, X. Y. CD133+ HCC cancer stem cells confer chemoresistance by preferential expression of the Akt/PKB survival pathway. *Oncogene* **27**, 1749–1758 (2008).
569. Quintana, E. *et al.* Efficient tumour formation by single human melanoma cells. *Nature* **456**, 593–598 (2008).
570. Baba, T. *et al.* Epigenetic regulation of CD133 and tumorigenicity of CD133+ ovarian cancer cells. *Oncogene* **28**, 209–218 (2009).
571. Hermann, P. C. *et al.* Distinct Populations of Cancer Stem Cells Determine Tumor Growth and Metastatic Activity in Human Pancreatic Cancer. *Cell Stem Cell* **1**, 313–323 (2007).
572. Dubrovska, A. *et al.* The role of PTEN/Akt/PI3K signaling in the maintenance and viability of prostate cancer stem-like cell populations. *Proc. Natl. Acad. Sci. U. S. A.* **106**, 268–273 (2009).

573. Uchida, N. *et al.* Direct isolation of human central nervous system stem cells. *Proc. Natl. Acad. Sci. U. S. A.* **97**, 14720–14725 (2000).
574. Beier, D. *et al.* CD133+ and CD133- glioblastoma-derived cancer stem cells show differential growth characteristics and molecular profiles. *Cancer Res.* **67**, 4010–4015 (2007).
575. Singh, S. K. *et al.* Identification of a Cancer Stem Cell in Human Brain Tumors. *Cancer Res.* **63**, 5821–5828 (2003).
576. Chen, K.-H. *et al.* Celecoxib enhances radiosensitivity in medulloblastoma-derived CD133-positive cells. *Child's Nerv. Syst.* **26**, 1605–1612 (2010).
577. Garg, N. *et al.* CD133+ brain tumor-initiating cells are dependent on STAT3 signaling to drive medulloblastoma recurrence. *Oncogene* **36**, 606–617 (2017).
578. Blazek, E. R., Foutch, J. L. & Maki, G. Daoy medulloblastoma cells that express CD133 are radioresistant relative to CD133- cells, and the CD133+ sector is enlarged by hypoxia. *Int. J. Radiat. Oncol. Biol. Phys.* **67**, 1–5 (2007).
579. Lu, K.-H. *et al.* Evaluation of radiotherapy effect in resveratrol-treated medulloblastoma cancer stem-like cells. *Child's Nerv. Syst.* **25**, 543–550 (2009).
580. Bao, S. *et al.* Glioma stem cells promote radioresistance by preferential activation of the DNA damage response. *Nature* **444**, 756–760 (2006).
581. Kemper, K. *et al.* The AC133 Epitope, but not the CD133 Protein, Is Lost upon Cancer Stem Cell Differentiation. *Cancer Res.* **70**, 719–729 (2010).
582. Bidlingmaier, S., Zhu, X. & Liu, B. The utility and limitations of glycosylated human CD133 epitopes in defining cancer stem cells. *J. Mol. Med. (Berl).* **86**, 1025 (2008).
583. Hermansen, S. K., Christensen, K. G., Jensen, S. S. & Kristensen, B. W. Inconsistent Immunohistochemical Expression Patterns of Four Different CD133 Antibody Clones in Glioblastoma. *J. Histochem. Cytochem.* **59**, 391 (2011).
584. Glumac, P. M. & LeBeau, A. M. The role of CD133 in cancer: a concise review. *Clin. Transl. Med.* **7**, 18 (2018).
585. Williams, A. P. *et al.* UAB30, A Novel Rexinoid Agonist, Decreases Stemness In Group 3 Medulloblastoma Human Cell Line Xenografts. *Transl. Oncol.* **12**, 1364–1374 (2019).
586. Platet, N. *et al.* Influence of oxygen tension on CD133 phenotype in human glioma cell cultures. *Cancer Lett.* **258**, 286–290 (2007).
587. Soeda, A. *et al.* Hypoxia promotes expansion of the CD133-positive glioma stem cells through activation of HIF-1α. *Oncogene* **28**, 3949–3959 (2009).
588. McCord, A. M. *et al.* Physiologic oxygen concentration enhances the stem-like properties of CD133+ human glioblastoma cells in vitro. *Mol. Cancer Res.* **7**, 489–497 (2009).
589. Friedman, G. K. *et al.* Pediatric medulloblastoma xenografts including molecular subgroup 3 and CD133+ and CD15+ cells are sensitive to killing by oncolytic herpes simplex viruses. *Neuro. Oncol.* **18**, 227–235 (2016).
590. Kawamoto, A. *et al.* Clinical significance of radiation-induced CD133 expression in residual rectal cancer cells after chemoradiotherapy. *Exp. Ther. Med.* **3**, 403–409 (2012).
591. Damodar Reddy, C. *et al.* Anticancer effects of fenretinide in human medulloblastoma. *Cancer Lett.* **231**, 262–269 (2006).
592. Spina, R. *et al.* Critical role of zinc finger protein 521 in the control of growth, clonogenicity and tumorigenic potential of medulloblastoma cells. *Oncotarget* **4**, 1280–92 (2013).
593. Nuryadi, E., Permata, T. B. M., Komatsu, S., Oike, T. & Nakano, T. Inter-assay precision of clonogenic assays for radiosensitivity in cancer cell line A549. *Oncotarget* **9**, 13706–13712 (2018).
594. Oike, T. *et al.* Reporting of methodologies used for clonogenic assays to determine radiosensitivity. *J. Radiat. Res.* **61**, 828–831 (2020).
595. Wouters, A. *et al.* Counting clonogenic assays from normoxic and anoxic irradiation experiments manually or by using densitometric software. *Phys. Med. Biol.* **55**, N167 (2010).
596. Dahle, J., Kakar, M., Steen, H. B. & Kaalhus, O. Automated counting of mammalian cell colonies by means of a flat bed scanner and image processing. *Cytom. Part A* **60A**, 182–188 (2004).

597. Siragusa, M., Dall'Olio, S., Fredericia, P. M., Jensen, M. & Groesser, T. Cell colony counter called CoCoNut. *PLoS One* **13**, e0205823 (2018).
598. Kumar Maurya, D. ColonyCountJ: A User-Friendly Image J Add-on Program for Quantification of Different Colony Parameters in Clonogenic Assay. (2017). doi:10.4172/2161-0495.1000358
599. Lee, S.-H. *et al.* The Effect of Fetal Bovine Serum (FBS) on Efficacy of Cellular Reprogramming for Induced Pluripotent Stem Cell (iPSC) Generation. *Cell Transplant.* **25**, 1025–1042 (2016).
600. Serum Concentration: Effects on Cycle and X-ray Sensitivity of Mammalian Cells on JSTOR. Available at: https://www-jstor-org.manchester.idm.oclc.org/stable/1717267?sid=primo&seq=2#metadata_info_tab_contents. (Accessed: 21st June 2021)
601. Brix, N. *et al.* The clonogenic assay: robustness of plating efficiency-based analysis is strongly compromised by cellular cooperation. *Radiat. Oncol.* **15**, 1–12 (2020).
602. Blainey, P., Krzywinski, M. & Altman, N. Points of significance: Replication. *Nature Methods* **11**, 879–880 (2014).
603. West, C. M. L., Keng, P. C. & Sutherland, R. M. Growth phase related variation in the radiation sensitivity of human colon adenocarcinoma cells. *Int. J. Radiat. Oncol.* **14**, 1213–1219 (1988).
604. Zhou, J. *et al.* Reciprocal regulation of hypoxia-inducible factor 2α and GLI1 expression associated with the radioresistance of renal cell carcinoma. *Int. J. Radiat. Oncol. Biol. Phys.* **90**, 942–951 (2014).
605. Bijlsma, M. F. *et al.* Hypoxia induces a hedgehog response mediated by HIF-1α. *J. Cell. Mol. Med.* **13**, 2053–2060 (2009).
606. Zölzer, F. *et al.* Increased radiosensitivity with chronic hypoxia in four human tumor cell lines. *Int. J. Radiat. Oncol.* **54**, 910–920 (2002).
607. Yount, G. L. *et al.* Cell cycle synchrony unmasks the influence of p53 function on radiosensitivity of human glioblastoma cells. *Cancer Res.* **56**, 500–506 (1996).
608. Leszczynska, K. B. *et al.* Hypoxia-induced p53 modulates both apoptosis and radiosensitivity via AKT. *J. Clin. Invest.* **125**, 2385–2398 (2015).
609. CellTiter-Glo® Luminescent Cell Viability Assay Protocol. Available at: https://www.promega.co.uk/resources/protocols/technical-bulletins/0/celltiter-glo-luminescent-cell-viability-assay-protocol/. (Accessed: 16th May 2021)
610. Gordon Steel, G. *et al.* The dose-rate effect in human tumour cells. *Radiotherapy and Oncology* **9**, 299–310 (1987).
611. Makurat, S., Spisz, P., Kozak, W., Rak, J. & Zdrowowicz, M. 5-iodo-4-thio-2′-deoxyuridine as a sensitizer of X-ray induced cancer cell killing. *Int. J. Mol. Sci.* **20**, 1308 (2019).
612. Mehta, M. *et al.* Regorafenib sensitizes human breast cancer cells to radiation by inhibiting multiple kinases and inducing DNA damage. *Int. J. Radiat. Biol.* **2**, 1–12 (2020).
613. Rouhani, M., Goliaei, B., Khodagholi, F. & Nikoofar, A. Lithium increases radiosensitivity by abrogating DNA repair in breast cancer spheroid culture. *Arch. Iran. Med.* **17**, 352–360 (2014).
614. Bjork-Eriksson, T. *et al.* The in vitro radiosensitivity of human head and neck cancers. *Br. Joumal Cancer* 2371–2375 (1998).
615. Sheridan, M. T. & West, C. M. L. Ability to undergo apoptosis does not correlate with the intrinsic radiosensitivity (SF2) of human cervix tumor cell lines. *Int. J. Radiat. Oncol. Biol. Phys.* **50**, 503–509 (2001).
616. Hall, J. S. *et al.* Investigation of radiosensitivity gene signatures in cancer cell lines. *PLoS One* **9**, e86329 (2014).
617. Tam, K. F. *et al.* Potential application of the ATP cell viability assay in the measurement of intrinsic radiosensitivity in cervical cancer. *Gynecol. Oncol.* **96**, 765–770 (2005).
618. Björk-Eriksson, T., West, C., Karlsson, E. & Mercke, C. Discrimination of human tumor radioresponsiveness using low-dose rate irradiation. *Int. J. Radiat. Oncol. Biol. Phys.* **42**, 1147–1153 (1998).
619. Kelland, L. R. & Steel, G. G. Differences in radiation response among human cervix carcinoma cell lines. *Radiother. Oncol.* **13**, 225–232 (1988).

620. West, C. M. L., Davidson, S. E., Burt, P. A. & Hunter, R. D. The intrinsic radiosensitivity of cervical carcinoma: correlations with clinical data. *Int. J. Radiat. Oncol. Biol. Phys.* **31**, 841–846 (1995).
621. Allalunis-Turner, M. J. *et al.* Inherent radio sensitivity testing of tumor biopsies obtained from patients with carcinoma of the cervix or endometrium. *Radiother. Oncol.* **22**, 201–205 (1991).
622. Dunne, A. L. *et al.* Relationship between clonogenic radiosensitivity, radiation-induced apoptosis and DNA damage/repair in human colon cancer cells. *Br. J. Cancer* **89**, 2277–2283 (2003).
623. Challeton, C. *et al.* Characterization and radiosensitivity at high or low dose rate of four cell lines derived from human thyroid tumors. *Int. J. Radiat. Oncol. Biol. Phys.* **37**, 163–169 (1997).
624. Fehlauer, F. *et al.* Additive cytotoxic effect of cisplatin and X-irradiation on human glioma cell cultures derived from biopsy-tissue. *J. Cancer Res. Clin. Oncol.* **126**, 711–716 (2000).
625. Petersen, C., Petersen, S., Milas, L., Lang, F. F. & Tofilon, P. J. Enhancement of Intrinsic Tumor Cell Radiosensitivity Induced by a Selective Cyclooxygenase-2 Inhibitor. *Clin. Cancer Res.* **6**, 2513–2520 (2000).
626. Stausbøl-Grøn, B. *et al.* In vitro radiosensitivity of tumour cells and fibroblasts derived from head and neck carcinomas: Mutual relationship and correlation with clinical data. *Br. J. Cancer* **79**, 1074–1084 (1999).
627. Stausbøl-Grøn, B. & Overgaard, J. Relationship between tumour cell in vitro radiosensitivity and clinical outcome after curative radiotherapy for squamous cell carcinoma of the head and neck. *Radiother. Oncol.* **50**, 47–55 (1999).
628. Patties, I., Jahns, J., Hildebrandt, G., Kortmann, R.-D. & Glasow, A. Additive Effects of 5-Aza-2'-deoxycytidine and Irradiation on Clonogenic Survival of Human Medulloblastoma Cell Lines. *Strahlentherapie und Onkol.* **185**, 331–338 (2009).
629. Leonard, J. H., Ramsay, J. R., Kearsley, J. H. & Birrell, G. W. Radiation sensitivity of Merkel cell carcinoma cell lines. *Int. J. Radiat. Oncol. Biol. Phys.* **32**, 1401–1407 (1995).
630. Slotman, B. J., Karim, A. B. M. F. & Rao, B. R. Ovarian cancer: radiation sensitivity in vitro. *Radiother. Oncol.* **19**, 323–327 (1990).
631. Kelland, L. R., Bingle, L., Edwards, S. & Steel, G. G. High intrinsic radiosensitivity of a newly established and characterised human embryonal rhabdomyosarcoma cell line. *Br. J. Cancer* **59**, 160–164 (1989).
632. Joan Allalunis-Turner, M., Barron, G. M., Day, R. S., Fulton, D. S. & Urtasun, R. C. Radiosensitivity testing of human primary brain tumor specimens. *Int J Radiat. Oncol. Biol Phys* **23**, 339–343 (1992).
633. Eschrich, S. *et al.* Systems Biology Modeling of the Radiation Sensitivity Network: A Biomarker Discovery Platform. *Int. J. Radiat. Oncol. Biol. Phys.* **75**, 497–505 (2009).
634. McMillan, T. J. & Holmes, A. The isolation and partial characterization of a radiation-sensitive clone of a human bladder carcinoma cell line. *Radiat. Res.* **128**, 301–305 (1991).
635. Bodgi, L. *et al.* Assessing radiosensitivity of bladder cancer in vitro: A 2D vs. 3D approach. *Front. Oncol.* **9**, 153 (2019).
636. Maouche, S. *et al.* Performance comparison of two microarray platforms to assess differential gene expression in human monocyte and macrophage cells. (2008). doi:10.1186/1471-2164-9-302
637. Kothapalli, R., Yoder, S. J., Mane, S. & Loughran, T. P. Microarray result: How accurate are they? *BMC Bioinformatics* **3**, 1–10 (2002).
638. Kuo, W. P., Jenssen, T. K., Butte, A. J., Ohno-Machado, L. & Kohane, I. S. Analysis of matched mRNA measurements from two different microarray technologies. *Bioinformatics* **18**, 405–412 (2002).
639. Tan, P. K. *et al.* Evaluation of gene expression measurements from commercial microarray platforms. *Nucleic Acids Res.* **31**, 5676–5684 (2003).
640. Parmigiani, G., Garrett-Mayer, E. S., Anbazhagan, R. & Gabrielson, E. A Cross-Study Comparison of Gene Expression Studies for the Molecular Classification of Lung Cancer. *Clin. Cancer Res.* **10**, 2922–2927 (2004).
641. Gajjar, A. J. & Robinson, G. W. Medulloblastoma - translating discoveries from the

bench to the bedside. *Nat. Rev. Clin. Oncol.* **11**, 714–722 (2014).
642. Maréchal, A. & Zou, L. DNA Damage Sensing by the ATM and ATR Kinases. *Cold Spring Harb. Perspect. Biol.* **5**, (2013).
643. Liberzon, E. *et al.* ATM gene mutations are not involved in medulloblastoma in children. *Cancer Genet. Cytogenet.* **146**, 167–169 (2003).
644. Trubicka, J. *et al.* The germline variants in DNA repair genes in pediatric medulloblastoma: a challenge for current therapeutic strategies. *BMC Cancer* **17**, (2017).
645. SM, W. *et al.* Spectrum and prevalence of genetic predisposition in medulloblastoma: a retrospective genetic study and prospective validation in a clinical trial cohort. *Lancet. Oncol.* **19**, 785–798 (2018).
646. Franchitto, A. *et al.* The mammalian mismatch repair protein MSH2 is required for correct MRE11 and RAD51 relocalization and for efficient cell cycle arrest induced by ionizing radiation in G2 phase. *Oncogene* **22**, 2110–2120 (2003).
647. Chang, L. *et al.* Targeting Rad50 sensitizes human nasopharyngeal carcinoma cells to radiotherapy. (2016). doi:10.1186/s12885-016-2190-8
648. Schröder-Heurich, B. *et al.* Functional deficiency of NBN, the Nijmegen breakage syndrome protein, in a p.R215W mutant breast cancer cell line. *BMC Cancer* **14**, 434 (2014).
649. Baert, A. *et al.* Analysis of chromosomal radiosensitivity of healthy BRCA2 mutation carriers and non-carriers in BRCA families with the G2 micronucleus assay. *Oncol. Rep.* **37**, 1379 (2017).
650. Alsbeih, G. *et al.* Gender bias in individual radiosensitivity and the association with genetic polymorphic variations. *Radiother. Oncol.* **119**, 236–243 (2016).
651. International Commission on Radiological Protection. *Annals of the ICRP Published on behalf of the International Commission on Radiological Protection*. (2007).
652. Kato, K., Kuwabara, M. & Kashiwakura, I. The Influence of Gender-and Age-related Differences in the Radiosensitivity of Hematopoietic Progenitor Cells Detected in Steady-state Human Peripheral Blood. *J. Radiat. Res* **52**, 293–299 (2011).
653. Yao, T. & Asayama, Y. Animal-cell culture media: History, characteristics, and current issues. *Reproductive Medicine and Biology* **16**, 99–117 (2017).
654. Hirsch, C. & Schildknecht, S. In vitro research reproducibility: Keeping up high standards. *Frontiers in Pharmacology* **10**, 1484 (2019).
655. Giatromanolaki, A. *et al.* Expression of Hypoxia-inducible Carbonic Anhydrase-9 Relates to Angiogenic Pathways and Independently to Poor Outcome in Non-Small Cell Lung Cancer. *Cancer Res.* **61**, 7992–7998 (2001).
656. Deng, Y., Zou, J., Deng, T. & Liu, J. Clinicopathological and prognostic significance of GLUT1 in breast cancer A meta-analysis. *Medicine (United States)* **97**, (2018).
657. Greenbaum, D., Colangelo, C., Williams, K. & Gerstein, M. Comparing protein abundance and mRNA expression levels on a genomic scale. *Genome Biol.* **4**, 117 (2003).
658. Edfors, F. *et al.* Gene-specific correlation of RNA and protein levels in human cells and tissues . *Mol. Syst. Biol.* **12**, 883 (2016).
659. Griffin, T. J. *et al.* Complementary profiling of gene expression at the transcriptome and proteome levels in Saccharomyces cerevisiae. *Mol. Cell. Proteomics* **1**, 323–333 (2002).
660. Guo, Y. *et al.* How is mRNA expression predictive for protein expression? A correlation study on human circulating monocytes. *Acta Biochim. Biophys. Sin. (Shanghai).* **40**, 426–436 (2008).
661. Koussounadis, A., Langdon, S. P., Um, I. H., Harrison, D. J. & Smith, V. A. Relationship between differentially expressed mRNA and mRNA-protein correlations in a xenograft model system OPEN. *Nat. Publ. Gr.* (2015). doi:10.1038/srep10775
662. Gry, M. *et al.* Correlations between RNA and protein expression profiles in 23 human cell lines. (2009). doi:10.1186/1471-2164-10-365
663. MKI67 protein expression summary - The Human Protein Atlas. Available at: https://www.proteinatlas.org/ENSG00000148773-MKI67. (Accessed: 23rd June 2021)
664. PCNA protein expression summary - The Human Protein Atlas. Available at: https://www.proteinatlas.org/ENSG00000132646-PCNA. (Accessed: 23rd June 2021)
665. CA9 protein expression summary - The Human Protein Atlas. Available at:

https://www.proteinatlas.org/ENSG00000107159-CA9. (Accessed: 23rd June 2021)
666. SLC2A1 protein expression summary - The Human Protein Atlas. Available at: https://www.proteinatlas.org/ENSG00000117394-SLC2A1. (Accessed: 23rd June 2021)
667. Thiruthaneeswaran, N. *et al.* Lost in application: Measuring hypoxia for radiotherapy optimisation. *Eur. J. Cancer* **148**, 260–276 (2021).
668. Johnsen, J. I., Kogner, P., Albihn, A. & Henriksson, M. A. Embryonal neural tumours and cell death. *Apoptosis* **14**, 424–438 (2009).
669. Zong, H., Verhaak, R. G. W. & Canolk, P. The cellular origin for malignant glioma and prospects for clinical advancements. *Expert Review of Molecular Diagnostics* **12**, 383–394 (2012).
670. Chi, J. T. *et al.* Gene expression programs in response to hypoxia: Cell type specificity and prognostic significance in human cancers. *PLoS Med.* **3**, 395–409 (2006).
671. Sundstrom, A., Grabocka, E., Bar-Sagi, D. & Mishra, B. Histological image processing features induce a quantitative characterization of chronic tumor hypoxia. *PLoS One* **11**, e0153623 (2016).
672. Peduzzi, P., Concato, J., Feinstein, A. R. & Holford, T. R. Importance of events per independent variable in proportional hazards regression analysis II. Accuracy and precision of regression estimates. *J. Clin. Epidemiol.* **48**, 1503–1510 (1995).
673. Gebäck, T., Schulz, M. M. P., Koumoutsakos, P. & Detmar, M. TScratch: A novel and simple software tool for automated analysis of monolayer wound healing assays. *Biotechniques* **46**, 265–274 (2009).
674. MontpellierResourcesImagerie. MRI Wound Healing Tool.
675. Jonkman, J. E. N. *et al.* An introduction to the wound healing assay using live-cell microscopy. *Cell Adhesion and Migration* **8**, 440–451 (2014).
676. Kauanova, S., Urazbayev, A. & Vorobjev, I. The Frequent Sampling of Wound Scratch Assay Reveals the “Opportunity” Window for Quantitative Evaluation of Cell Motility-Impeding Drugs. *Front. Cell Dev. Biol.* **9**, 391 (2021).
677. Riahi, R., Yang, Y., Zhang, D. D. & Wong, P. K. Advances in wound-healing assays for probing collective cell migration. *Journal of Laboratory Automation* **17**, 59–65 (2012).
678. Wound Healing and Migration Assays | Gap Creation Methods | ibidi. Available at: https://ibidi.com/content/282-creating-the-gap. (Accessed: 24th June 2021)
679. Cell Migration and Invasion in Scratch Wound Assays - Incucyte® Live-Cell Assays and Applications | Quantify Cell Proliferation. Available at: https://www.essenbioscience.com/en/applications/live-cell-assays/scratch-wound-cell-migration-invasion/. (Accessed: 24th June 2021)
680. Meer, A. D. van der, Vermeul, K., Poot, A. A., Feijen, J. & Vermes, I. A microfluidic wound-healing assay for quantifying endothelial cell migration. *https://doi.org/10.1152/ajpheart.00933.2009* **298**, 719–725 (2010).
681. Horssen, R. van, Galjart, N., Rens, J. A. P., Eggermont, A. M. M. & Hagen, T. L. M. ten. Differential effects of matrix and growth factors on endothelial and fibroblast motility: Application of a modified cell migration assay. *J. Cell. Biochem.* **99**, 1536–1552 (2006).
682. Fenu, M. *et al.* A novel magnet-based scratch method for standardisation of wound-healing assays. *Sci. Reports 2019 91* **9**, 1–9 (2019).
683. Block, E. R., Matela, A. R., SundarRaj, N., Iszkula, E. R. & Klarlund, J. K. Wounding Induces Motility in Sheets of Corneal Epithelial Cells through Loss of Spatial Constraints: role of heparin-binding epidermal growth factor-like growth factor signaling. *J. Biol. Chem.* **279**, 24307–24312 (2004).
684. Wu, S.-Y., Sun, Y.-S., Cheng, K.-C. & Lo, K.-Y. A Wound-Healing Assay Based on Ultraviolet Light Ablation. *SLAS Technol.* **22**, 36–43 (2017).
685. Reinhart-King, C. A. Chapter 3 Endothelial Cell Adhesion and Migration. *Methods in Enzymology* **443**, 45–64 (2008).
686. ibidi Application Guide. doi:10.1016/j
687. Corcoran, A. & Del Maestro, R. F. Testing the ‘Go or Grow’ Hypothesis in Human Medulloblastoma Cell Lines in Two and Three Dimension. *Neurosurgery* **53**, 174–185 (2003).

688. Wang, W., Dong, L., Zhao, B., Lu, J. & Zhao, Y. E-cadherin is downregulated by microenvironmental changes in pancreatic cancer and induces EMT. *Oncol. Rep.* **40**, 1641–1649 (2018).
689. Novoa-Herran, S., Umaña-Perez, A., Canals, F. & Sanchez-Gomez, M. Serum depletion induces changes in protein expression in the trophoblast-derived cell line HTR-8/SVneo. *Cell. Mol. Biol. Lett.* **21**, 1–19 (2016).

6. Appendix 1

A literature search was conducted for studies reporting radiosensitivity as measured by the methods used in this thesis. Journal articles reporting results from a clonogenic assay, the high-throughput radiosensitivity assay or application of the RSI gene signature.

PubMed searches were conducted using the following terms: ‘radiosensitivity index’, ‘RSI’, and ‘clonogenic assay + surviving fraction’. The search for ‘radiosensitivity index’ produced 26 results. The search for ‘RSI’ produced 1860 results, but filtering to those published after the gene signature (2010), those published in English, specific to the cancer research field and restricting to journal articles only reduced this number to 136. The search for ‘clonogenic assay’ alone produced 2893 results, and so the ‘surviving fraction’ term was added. The search for ‘clonogenic assay + surviving fraction’ produced 116 results.

Additionally PubMed searches were carried out to identify papers that cited the original paper describing the high-throughput assay method[1] or the initial papers reporting on the RSI[2–5].

SF2 was selected as the parameter produced by the clonogenic assay. SF2 values were only included if they were stated within the paper and were not determined or estimated from figures containing surviving curves. The reported metric for the high-throughput radiosensitivity assay was the AUC. RSI values for individual patients within a cohort are rarely reported, instead the median RSI with the reported error and cohort size are included here.

Blank lines have been added in order to keep the cancer type results together.

Cancer type/site	Sample	SF2	AUC	Median RSI (error, n)
Ampullar of Vater carcinoma	SNU478		2.83[6]	
	SNU869		4.11[6]	
	Patient cohort			0.299 (0.250-0.428, 16)[7]
Astrocytoma	BECKER		3.23[6]	
	CCFSTTG1		4.72[6]	
	GMS10		4.00[6]	
	GOS3		4.13[6]	
	SF268	0.45[3]	2.68[6]	
	SNB19	0.43[3]		
	SW1088		4.75[6]	
	TM31		2.89[6]	
	U118MG		3.12[6]	
	Patient-derived	0.51[8] 0.17[8] 0.43[8]		
Bladder	5637		2.47[6]	
	647V		3.37[6]	
	BC3C		3.36[6]	
	HT1197		4.45[6]	
	HT1376		5.228[6]	
	J82		3.198[6]	
	JMSU1		2.792[6]	
	KMBC2		4.126[6]	
	KU1919		3.503[6]	
	MGH-U1	0.72[9] 0.52[10]		
	RT112	0.73[11]	3.04[6]	
	RT4	0.54[12]	2.94[6]	
	SCABER		1.88[6]	
	SW1710		3.31[6]	
	T24	0.38[12]	2.37[6]	
	TCCSUP		3.54[6]	
	UBLC1		2.91[6]	
	UMUC1		3.35[6]	
	UMUC3	0.36[12]	3.23[6]	
	VMCUB1		4.41[6]	
	WX67	0.09[11]		
	Patient cohort			0.438 (0.312-0.509, 193)[7]
Burkitt lymphoma	P3HR-1	0.18[13] 0.17[10]		
Cholangiocarcinoma	HUH28		3.88[6]	
	SNU245		4.15[6]	
Colorectal	WIDR	0.62[14]		
	Patient-derived	0.48[15]		
Ewings sarcoma	A673		1.39[6]	
	MHHES1		1.64[6]	
	SKES1		1.84[6]	
	SKNMC		2.09[6]	
Follicular adenoma	Patient-derived	0.27[16] 0.39[16]		
Gallbladder	SNU308		5.42[6]	
Leukaemia	CCRFCEM	0.19[3]		
	HL60	0.32[3]		
	MOLT4	0.05[3]		
Glioma	H4		3.16[6]	
	U373	0.71[21]		
	Patient-derived	0.72[21] 0.61[21]		
	Patient cohort			0.576 (0.522-0.645, 174)[7]

Cancer type/site	Sample	SF2	AUC	Median RSI (error, n)
Breast	AU565		3.78[6]	
	BT20		3.49[6]	
	BT474		5.32[6]	
	BT549	0.63[3]	3.05[6]	
	CAL148		1.01[6]	
	CAL51		2.65[6]	
	CAMA1		3.95[6]	
	EFM192A		5.35[6]	
	HCC1419		6.19[6]	
	HCC1428		2.87[6]	
	HCC1569		3.27[6]	
	HCC1806		3.78[6]	
	HCC1937		4.70[6]	
	HCC1954		2.57[6]	
	HCC202		4.84[6]	
	HCC38		2.68[6]	
	HMC18		0.76[6]	
	HS578T	0.79[3]		
	HX99	0.55[11]		
	MCF7	0.58[3] 0.98[17] 0.30[10]	3.21[6]	
	MDAM B231	0.82[3]		
	MDAM B435	0.18[3]		
	MDAMB157		3.07[6]	
	MDAMB231	0.66[18]	2.62[6]	
	MDAMB361		4.79[6]	
	MDAMB415		3.52[6]	
	MDAMB453		5.50[6]	
	MDAMB468		3.62[6]	
	SF539	0.82[3]	3.39[6]	
	SKCO1		1.61[6]	
	SUM159PT	0.88[18]		
	T47D	0.69[19] 0.52[3]	4.17[6]	
	ZR751		4.61[6]	
	ZR7530		5.46[6]	
	Patient-derived	0.24[15]		
	Patient cohort			0.51 (0.13-0.75, 285)[20] 0.38 (0.05-0.68, 545)[20] 0.4 (0.22-0.65, 58)[20] 0.41 (0.08-0.61, 98)[20] 0.408 (0.330-0.480, 82)[7] 0.388 (0.31-0.475, 2487)[7] 0.419 (0.336-0.483, 427)[7]
Lung	CHAGOK1		3.38[6]	
	HCC1195		2.28[6]	
	HCC366		2.22[6]	
	NCIH292		5.28[6]	
	NCIH727		4.46[6]	
Hilar cholangiocarcinoma	SNU1196		2.35[6]	
Primary signet-ring cell carcinoma	Patient cohort			0.422 (0.342-0.507, 11)[7]
Lymphoma	Patient-derived	0.30[15]		

Cancer type/site	Sample	SF2	AUC	Median RSI (error, n)
Cervical	808	0.33[23]		
	Boku	0.41[23]		
	C33A	0.53[24] 0.25[23] 0.55[22]		
	C41	0.72[14] 0.63[22] 0.27[24]		
	Caski	0.66[24] 0.47[23] 0.75[14] 0.92[22]		
	HCSC1	0.32[23]		
	HeLa	0.70[24] 0.41[23] 0.53[22] 0.27[13] 0.52[13] 0.46[13]		
	HeLaS3-1	0.46[13]		
	HeLaS3	0.52[13] 0.50[13] 0.42[13] 0.54[13] 0.47[13] 0.43[13] 0.26[13] 0.75[13] 0.36[13] 0.31[13] 0.27[13] 0.48[13]		
	HT3	0.35[23] 0.77[14] 0.36[22]		
	HX151c	0.23[25]		
	HX155c	0.45[25]		
	HX156	0.59[11]		
	HX156c	0.56[25]		
	HX160c	0.33[25]		
	HX171c	0.60[25]		
	Me180	0.35[23] 0.38[14] 0.36[22]		
	MS751	0.47[23] 0.85[14] 0.79[22]		
	NHIK3025	0.48[13] 0.58[10]		
	SiHa	0.67[24] 0.75[23] 0.51[14] 0.73[22]		
	SKGI	0.27[23]		
	SKGII	0.31[23]		
	SKGIIIa	0.37[23]		
	SW756	0.42[23]		
	SZC	0.42[13] 0.44[10]		
	Patient cohort			0.347 (0.278-0.453, 17)[7] 0.314 (0.268-0.393, 32)[7]

Cancer type/site	Sample	SF2	AUC	Median RSI (error, n)
Cervical Cont.	Patient-derived	0.43[26] 0.43[26] 0.48[26] 0.48[26] 0.21[27] 0.18[27] 0.32[27] 0.15[27] 0.19[27] 0.18[27] 0.18[27] 0.21[27] 0.29[27] 0.29[28] 0.43[29] 0.44[15]		
Endometrial	AN3CA		2.53[6]	
	EFE184		4.85[6]	
	ESS1		2.36[6]	
	HEC108		2.79[6]	
	HEC151		1.44[6]	
	HEC1A		2.55[6]	
	HEC1B		2.88[6]	
	HEC251		1.03[6]	
	HEC265		1.66[6]	
	HEC50B		1.72[6]	
	HEC59		2.80[6]	
	HEC6		1.90[6]	
	Ishikawa (Heraklio) 02 ER		1.32[6]	
	JHUEM1		1.50[6]	
	JHUEM2		1.18[6]	
	JHUEM3		4.40[6]	
	KLE		2.72[6]	
	MFE296		2.04[6]	
	MFE319		3.07[6]	
	RL952		1.22[6]	
	SNGM		1.18[6]	
	SNU1077		3.26[6]	
	SNU685		3.22[6]	
	Patient-derived	0.30[28]		
	Patient cohort			0.42 (0.321-0.485, 554)[7] 0.462 (0.385-0.489, 30)[7] 0.42 (0.11-0.7, 204)[30] 0.533 (0.417-0.595, 27)[7] 0.461 (0.373-0.572, 14)[7] 0.337 (0.310-0.458, 12)[7]
Medulloblastoma	D283MED	0.42[36]	1.42[6]	
	Daoy	0.53[36]	2.27[6]	
	MED8A	0.36[36]		
	ONS76		3.56[6]	
	TX14	0.28[13] 0.31[10]		
	TX7	0.28[13] 0.35[10]		
Myeloma	7	0.08[10]		
	9	0.24[10]		
Merkel cell carcinoma	MCC13	0.23[38]		
	MCC14/1	0.38[38]		
	MCC14/2	0.45[38]		
	MCC15	0.21[38]		

Cancer type/site	Sample	SF2	AUC	Median RSI (error, n)
Colon	C2BBE1		2.97[6]	
	CL11		2.59[6]	
	CL34		3.36[6]	
	COLO205	0.69[3]		
	COLO320		1.90[6]	
	COLO678		3.68[6]	
	CW2		1.51[6]	
	DLD1	0.75[10]	2.36[6]	
	GP2D		1.94[6]	
	HCC-2998	0.44[3]		
	HCC56		3.11[6]	
	HCT8	0.60[10] 0.57[13]		
	HCT116	0.38[3]		
	HCT15	0.4[3]	0.85[6]	
	HT115		2.60[6]	
	HT29	0.79[3] 0.72[31] 0.55[10] 0.56[13]	5.48[6]	
	HT55		2.81[6]	
	HX18	0.14[10] 0.14[13]		
	KM12	0.42[3]		
	LOVO	0.45[10] 0.40[13]	1.53[6]	
	LS1034		4.01[6]	
	LS123		3.87[6]	
	LS180		1.43[6]	
	LS411N		3.40[6]	
	LS513		2.26[6]	
	NCIH508		4.15[6]	
	RCM1		3.64[6]	
	RKO		3.15[6]	
	SKBR3		3.32[6]	
	SNU1033		5.26[6]	
	SNU175		2.19[6]	
	SNU283		3.18[6]	
	SNU407		1.73[6]	
	SNU503		5.85[6]	
	SNU61		3.48[6]	
	SNU81		2.66[6]	
	SNUC2A		1.73[6]	
	SNUC4		2.21[6]	
	SNUC5		1.58[6]	
	SW1116		4.12[6]	
	SW1417		4.26[6]	
	SW1463		3.09[6]	
	SW403		2.39[6]	
	SW48	0.14[31]	1.43[6]	
	SW480	0.69[31]	5.66[6]	
	SW620	0.62[3]		
	SW707	0.50[31]		
	SW837		5.49[6]	
	SW948		3.19[6]	
	T84		1.67[6]	
	Patient cohort			0.42 (-, 1362)[32] 0.421 (0.279-0.47, 1304)[7] 0.462 (0.311-0.473, 15)[7]

Cancer type/site	Sample	SF2	AUC	Median RSI (error, n)
Glioblastoma	42MGBA		3.38[6]	
	8MGBA		2.63[6]	
	A2	0.44[13]		
	A3	0.72[13]		
	A7	0.72[13]		
	A172		2.75[6]	
	AM38		5.30[6]	
	DBTRG05MG		1.97[6]	
	DKMG		3.12[6]	
	GAMG		5.24[6]	
	GB1		1.79[6]	
	KALS1		4.00[6]	
	KNS42		3.91[6]	
	KNS60		3.35[6]	
	KNS81		3.80[6]	
	LN18		2.72[6]	
	LN229		3.78[6]	
	M059K		4.31[6]	
	SF126		3.15[6]	
	SF295		2.43[6]	
	SNB75	0.55[3]	3.81[6]	
	SNU1105		4.99[6]	
	SNU466		4.54[6]	
	T98G		3.61[6]	
	TX13	0.31[13]		
	U251MG	0.57[3] 0.61[33]	3.59[6]	
	U87MG		3.11[6]	
	YH13		3.76[6]	
	YKG1		1.71[6]	
	Patient-derived	0.46[8] 0.52[8] 0.87[8] 0.17[8] 0.02[8] 0.68[8] 0.60[8] 0.19[8] 0.35[8] 0.18[8] 0.34[8] 0.30[8] 0.02[8] 0.51[8] 0.36[8] 0.19[8] 0.63[8] 0.24[8]		

Cancer type/site	Sample	SF2	AUC	Median RSI (error, n)
Head and neck	A253		1.37[6]	
	BICR16		3.48[6]	
	BICR18		3.68[6]	
	BICR22		1.31[6]	
	BICR31		3.59[6]	
	BICR56		3.43[6]	
	BICR6		1.71[6]	
	DETROIT562		2.48[6]	
	FADU		3.76[6]	
	HSC2		4.91[6]	
	HSC3		1.83[6]	
	HSC4		4.24[6]	
	PECAPJ15		2.61[6]	
	PECAPJ34CLONEC12		2.43[6]	
	PECAPJ49		2.81[6]	
	SCC25		2.11[6]	
	SCC9		2.42[6]	
	SNU1041		2.86[6]	
	SNU1066		2.23[6]	
	SNU1214		2.61[6]	
	SNU46		4.23[6]	
	SNU899		3.26[6]	
	YD10B		5.35[6]	
	YD15		3.93[6]	
	YD38		3.91[6]	
	YD8		4.91[6]	
	Patient-derived (all SF2)	0.19[34], 0.23[34], 0.24[34], 0.24[35], 0.25[34], 0.25[34], 0.27[35], 0.30[35], 0.30[34], 0.32[35], 0.33[35], 0.34[34], 0.35[35], 0.35[35], 0.36[34], 0.36[35], 0.37[35], 0.38[35], 0.38[34], 0.38[35], 0.38[35], 0.39[35], 0.39[35], 0.40[35], 0.40[35], 0.41[34], 0.41[34], 0.41[35], 0.41[35], 0.42[35], 0.42[35], 0.42[35], 0.43[34], 0.43[35], 0.44[35], 0.45[35], 0.45[35], 0.46[35], 0.46[35], 0.46[35], 0.46[34], 0.47[35], 0.48[34], 0.48[15], 0.48[35], 0.49[35], 0.49[35], 0.50[34], 0.50[34], 0.50[34], 0.50[34], 0.50[34], 0.50[34], 0.51[35], 0.51[35], 0.51[35], 0.52[35], 0.52[35], 0.56[35], 0.56[34], 0.56[34], 0.56[35], 0.57[35], 0.57[35], 0.58[35], 0.59[34], 0.59[34], 0.60[35], 0.60[35], 0.61[35], 0.65[35], 0.66[35], 0.67[35], 0.67[35], 0.67[34], 0.67[34], 0.68[35], 0.69[34], 0.70[35], 0.72[34], 0.73[35], 0.75[34], 0.75[34], 0.75[35], 0.75[35], 0.76[35], 0.77[35], 0.77[35], 0.78[34], 0.79[35], 0.87[34], 0.93[34], 0.94[35], 0.96[35], 1.00[34], 1.00[34], 1.00[34], 1.00[34], 1.00[34]		
	Patient cohort			0.394 (0.311-0.476, 95)[7]
Mesothelioma	ACCMESO1		3.24[6]	
	DM3		1.78[6]	
	ISTMES1		2.94[6]	
	JL1		5.24[6]	
	MPP89		3.35[6]	
	NCIH2052		2.61[6]	
	NCIH2452		3.10[6]	
	Patient cohort			0.481 (0.393-0.596, 12)[7]
Oligodendroglioma	HS683		5.62[6]	
	Patient-derived	0.48[8]		
Neonatal keratinocytes	Patient-derived	0.46[39]		
Papillary carcinomas	Patient-derived	0.39[16] 0.42[16]		
Penile carcinoma	Patient cohort			0.482 (0.215-0.682, 25)[40]

Cancer type/site	Sample	SF2	AUC	Median RSI (error, n)
Kidney/Renal	7860	0.66[3]		
	769P		3.12[6]	
	786O		3.78[6]	
	A498	0.61[3]	2.68[6]	
	ACHN	0.72[3]	0.99[6]	
	CAKI1	0.37[3]	3.37[6]	
	CAKI2		4.94[6]	
	CAL54		2.75[6]	
	KMRC1		4.43[6]	
	KMRC2		2.78[6]	
	KMRC3		2.90[6]	
	OSRC2		4.42[6]	
	RCC10RGB		5.66[6]	
	SN12C	0.62[3]		
	SNU1272		4.64[6]	
	TUHR10TKB		3.67[6]	
	UO31	0.62[3]	1.45[6]	
	VMRCRCW		1.65[6]	
	VMRCRCZ		2.88[6]	
	Patient cohort			0.422 (0.322-0.482, 716)[7] 0.301 (0.201-0.414, 34)[7]
Liver	HEP3B217		3.10[6]	
	HEPG2		5.22[6]	
	HLF		1.93[6]	
	HUH1		5.05[6]	
	JHH1		4.35[6]	
	JHH2		4.73[6]	
	JHH4		3.04[6]	
	JHH5		2.17[6]	
	JHH6		3.38[6]	
	LI7		3.90[6]	
	PLCPRF5		4.39[6]	
	SKHEP1		2.51[6]	
	SNU182		3.65[6]	
	SNU387		3.53[6]	
	SNU398		2.74[6]	
	SNU423		3.17[6]	
	SNU449		3.26[6]	
	SNU475		5.49[6]	
	SNU761		4.59[6]	
	SNU886		2.86[6]	
	Patient cohort			0.253 (0.177-0.330, 48)[7]
Lung large cell	HCC1438		3.91[6]	
	HOP92	0.43[3]	3.61[6]	
	HX147	0.82[11]		
	IALM		3.11[6]	
	LC1SQSF		3.62[6]	
	LCLC103H		4.14[6]	
	LCLC97TM1		1.90[6]	
	LU99		2.85[6]	
	NCIH1915		2.84[6]	
	NCIH661		4.68[6]	
	NCIH810		1.26[6]	
	T3M10		3.07[6]	
	Patient cohort			0.341 (0.274-0.410, 42)[7]
lung carcinoid tumour	Patient cohort			0.458 (0.425-0.492, 79)[7]
lung carcinoma	Patient cohort			0.427 (0.317-0.489, 102)[7] 0.45 (0.310-0.525, 63)[7]

Cancer type/site	Sample	SF2	AUC	Median RSI (error, n)
Lung adenocarcinoma	CALU3		1.78[6]	
	COLO699		2.80[6]	
	CORL105		3.50[6]	
	EKVX	0.70[3]	6.21[6]	
	HCC1833		3.87[6]	
	HCC2108		2.35[6]	
	HCC2279		2.90[6]	
	HCC4006		2.88[6]	
	HCC44		4.41[6]	
	HCC78		1.86[6]	
	HCC827		2.62[6]	
	HOP62	0.16[3]	1.78[6]	
	HX144	0.30[11]		
	HX148	0.55[11]		
	MORCPR		4.27[6]	
	NCIH1355		3.89[6]	
	NCIH1373		3.23[6]	
	NCIH1395		5.05[6]	
	NCIH1563		3.47[6]	
	NCIH1573		3.56[6]	
	NCIH1623		3.81[6]	
	NCIH1650		1.63[6]	
	NCIH1651		1.63[6]	
	NCIH1666		4.38[6]	
	NCIH1703		2.43[6]	
	NCIH1755		3.91[6]	
	NCIH1781		1.03[6]	
	NCIH1792		3.14[6]	
	NCIH2087		3.31[6]	
	NCIH2122		1.51[6]	
	NCIH2228		2.97[6]	
	NCIH2291		3.69[6]	
	NCIH2342		3.96[6]	
	NCIH2405		3.34[6]	
	NCIH322		4.88[6]	
	NCIH358		2.39[6]	
	NCIH650		4.62[6]	
	NCIH747		3.16[6]	
	RERFLCAD1		4.26[6]	
	RERFLCAD2		3.91[6]	
	SKLU1		3.61[6]	
	VMRCLCD		2.32[6]	
	Patient cohort			0.374 (0.303-0.47, 1165)[7]
Neuroblastoma	CHP212		1.83[6]	
	HX138	0.11[11] 0.11[10]		
	HX142	0.13[11]		
	HX143	0.08[11]		
	IMR32		0.63[6]	
	KPNSI9S		1.48[6]	
	MHHNB11		0.55[6]	
	NB1	0.34[14] 0.15[10]	0.77[6]	
	SKNAS		3.79[6]	
	SKNFI		3.41[6]	
	SKNSH		1.66[6]	
	LAN-1	0.37[10]		
Rhabdoid	G401		1.21[6]	
	G402		0.81[6]	

Cancer type/site	Sample	SF2	AUC	Median RSI (error, n)
Lung small cell carcinoma	COLO668		1.55[6]	
	DMS114		2.86[6]	
	DMS53		3.42[6]	
	HX33	0.20[10] 0.28[13]		
	H187	0.14[10]		
	H209	0.22[10]		
	H249	0.15[10]		
	H69	0.27[10]		
	H146	0.10[10]		
	LX1	0.18[10]		
	NCIH1048		1.24[6]	
	NCIH1339		3.24[6]	
	NCIH1341		3.34[6]	
	NCIH196		3.81[6]	
	NCIH211		0.70[6]	
	NCIH2196		4.21[6]	
	NCIH2286		2.00[6]	
	NCIH446		1.02[6]	
	NCIH69		2.18[6]	
	NCIH841		2.30[6]	
	SHP77		2.94[6]	
	SW1271		3.23[6]	
	Patient cohort			0.347 (0.287-0.458, 582)[7] 0.449 (0.341-0.516, 35)[7]
	Patient-derived	0.21[37] 0.41[37] 0.28[37] 0.73[37] 0.28[37] 0.43[37] 0.22[37] 0.18[37] 0.31[37] 0.27[37] 0.31[37] 0.26[37] 0.17[37] 0.48[37] 0.38[37]		
Osteosarcoma	G292CLONEA141B1		2.19[6]	
	HOS		2.54[6]	
	MG63		2.09[6]	
	SAOS2		1.39[6]	
	SJSA1		2.62[6]	
	U2OS		2.76[6]	
	TX4	0.37[13]		
Normal	Patient-derived	0.14[38] 0.18[38] 0.13[38] 0.20[38] 0.17[38] 0.25[35] 0.27[35] 0.028[27] 0.033[27]		
	lymphoblast	0.13[38]		
Rectal adenocarcinoma	HRT18	0.54[13] 0.53[10]		
	Patient cohort			0.438 (0.290-0.495, 20)[7] 0.462 (0.319-0.514, 113)[7]

Cancer type/site	Sample	SF2	AUC	Median RSI (error, n)
Lung squamous cell carcinoma	CALU1		3.95[6]	
	EBC1		3.33[6]	
	EPLC272H		3.94[6]	
	HARA		3.52[6]	
	HC12	0.41[11]		
	HCC15		2.06[6]	
	HCC1588		2.85[6]	
	HCC95		4.28[6]	
	HX149	0.26[11]		
	KNS62		3.63[6]	
	LK2		2.26[6]	
	LOUNH91		2.77[6]	
	LUDLU1		4.12[6]	
	NCIH1869		5.52[6]	
	NCIH2170		2.11[6]	
	NCIH226		3.52[6]	
	NCIH520		2.14[6]	
	RERFLCAI		2.39[6]	
	SKMES1		2.67[6]	
	SQ1		1.92[6]	
	SW1573		4.15[6]	
Prostate	22RV1		2.14[6]	
	DU145	0.52[3] 0.7[41]	3.32[6]	
	HX32	0.34[14]		
	PC3	0.48[3] 0.52[41]	2.41[6]	
	VCAP		4.79[6]	
	Patient cohort			0.403 (0.333-0.465, 186)[7]
Rhabdomyosarcoma	A204		1.96[6]	
	HS729		2.94[6]	
	HX170c	0.26[44]		
	KYM1		2.22[6]	
	RD		2.38[6]	
	RH18		2.27[6]	
	RH30		1.62[6]	
	RH41		0.84[6]	
	TE125T		2.03[6]	
	TE617T		1.40[6]	
Sarcoma	CAL78		3.70[6]	
	GCT		2.10[6]	
	HS819T		2.58[6]	
	Patient cohort			0.552 (0.401-0.631, 102)[7]
Soft tissue sarcoma	MESSA		1.50[6]	
	SKLMS1		2.41[6]	
	SKUT1		1.76[6]	
Testicular teratoma	GCT27	0.40[11]		

Cancer type/site	Sample	SF2	AUC	Median RSI (error, n)
Non-small-cell lung cancer	A549	0.80[42] 0.74[42] 0.65[42] 0.70[42] 0.64[42] 0.72[42] 0.87[42] 0.76[42] 0.72[42] 0.60[42] 0.63[42] 0.87[42] 0.49[42] 0.75[42] 0.87[42] 0.69[42] 0.65[42] 0.90[42] 0.47[42] 0.58[42] 0.61[3]		
	CAL12T		2.87[6]	
	H460	0.84[3]		
	HCC1171		3.12[6]	
	HCC2935		4.02[6]	
	NCIH1299		5.33[6]	
	NCIH1435		3.92[6]	
	NCIH1568		2.66[6]	
	NCIH1793		4.23[6]	
	NCIH1838		2.42[6]	
	NCIH1944		2.12[6]	
	NCIH1975		2.50[6]	
	NCIH2030		2.59[6]	
	NCIH2110		3.54[6]	
	NCIH23	0.086[3]	0.94[6]	
	NCIH522		2.67[6]	
	NCIH838		3.63[6]	
	PC14		2.15[6]	
	RERFLCMS		3.50[6]	
Thyroid	8505C		3.47[6]	
	BCPAP		2.95[6]	
	BHT101		1.56[6]	
	CGTHW1		2.92[6]	
	FTC133		2.78[6]	
	FTC238		5.62[6]	
	ML1		2.91[6]	
	SW579		2.95[6]	
	TT2609C02		2.68[6]	
	Patient cohort			0.524 (0.509-0.543, 28)[7]

Cancer type/site	Sample	SF2	AUC	Median RSI (error, n)
Melanoma	A101D		4.68[6]	
	A2058	0.57[38]	2.82[6]	
	Be211	0.39[13]		
	C32		4.40[6]	
	CJM		3.27[6]	
	COLO679		4.32[6]	
	COLO783		2.50[6]	
	COLO800		3.13[6]	
	COLO829		3.49[6]	
	HMCB		3.42[6]	
	HMV	0.57[13]		
	HS294T		1.74[6]	
	HS839T		4.11[6]	
	HS888T		3.91[6]	
	HS895T		3.23[6]	
	HS934T		2.66[6]	
	HS944T		2.13[6]	
	HT144		1.28[6]	
	HX118	0.43[11]		
	HX34	0.47[11], 0.54[13]		
	IGR1		3.87[6]	
	IGR37		5.06[6]	
	IGR39		4.40[6]	
	IPC298		3.12[6]	
	K029AX		3.82[6]	
	LeCa (39-4)	0.61[13]		
	LOXIMVI	0.68[3]		
	M14	0.42[3]		
	Ma111	0.52[13]		
	MALME3M	0.80[3]		
	MDAMB435S		4.19[6]	
	MELHO		2.60[6]	
	MEWO	0.22[13]	2.72[6]	
	MM96L	0.56[38]		
	Na11	0.51[13]		
	RVH421		3.56[6]	
	SKMEL	0.55[14]		
	SKMEL2	0.66[3]	1.95[6]	
	SKMEL24		3.25[6]	
	SKMEL28	0.74[3]	5.70[6]	
	SKMEL3		4.34[6]	
	SKMEL30		3.93[6]	
	SKMEL5	0.72[3]	3.73[6]	
	UACC257	0.48[3]		
	UACC62	0.52[3]		
	WM115		3.91[6]	
	WM1799		3.23[6]	
	WM2664		4.36[6]	
	WM793		2.12[6]	
	WM88		2.47[6]	
	WM983B		3.07[6]	
	Patient cohort			0.423 (0.337-0.502, 31)[7] 0.494 (0.399-0.553, 115)[7] 0.481 (0.117-0.71, 410)[43]

Cancer type/site	Sample	SF2	AUC	Median RSI (error, n)
Oesophagus	COLO680N		3.19[6]	
	ECGI10		2.58[6]	
	KYSE140		3.38[6]	
	KYSE150		3.07[6]	
	KYSE180		3.62[6]	
	KYSE30		1.49[6]	
	KYSE410		4.65[6]	
	KYSE450		4.68[6]	
	KYSE510		5.06[6]	
	KYSE520		3.54[6]	
	KYSE70		3.90[6]	
	OE19		3.54[6]	
	OE21		2.84[6]	
	OE33		1.53[6]	
	TE1		2.48[6]	
	TE10		3.37[6]	
	TE11		2.50[6]	
	TE14		3.66[6]	
	TE15		2.76[6]	
	TE4		2.66[6]	
	TE6		3.32[6]	
	TE8		2.88[6]	
	TE9		2.23[6]	
	Patient cohort			0.364 (0.265-0.470, 53)[7]
Stomach	AGS		1.26[6]	
	ECC12		2.45[6]	
	HS746T		4.46[6]	
	IM95		2.66[6]	
	KATOIII		2.74[6]	
	KE39		4.16[6]	
	LMSU		3.71[6]	
	MKN45		3.80[6]	
	MKN7		2.48[6]	
	MKN74		3.01[6]	
	NCIN87		2.05[6]	
	NUGC3		2.12[6]	
	NUGC4		2.87[6]	
	OCUM1		3.51[6]	
	SH10TC		3.50[6]	
	SNU216		2.32[6]	
	SNU601		0.87[6]	
	SNU668		2.96[6]	
	SNU719		3.63[6]	
	Patient cohort			0.38 (0.282-0.456, 53)[7] 0.462 (0.401-0.517, 31)[7]

Cancer type/site	Sample	SF2	AUC	Median RSI (error, n)
Ovarian	A2780	0.24[14]	0.94[6]	
	CAOV3		2.24[6]	
	COV318		2.27[6]	
	COV362		3.82[6]	
	COV434		1.84[6]	
	COV644		5.11[6]	
	EFO21		3.39[6]	
	EFO27		1.71[6]	
	ES2		3.31[6]	
	FUOV1		3.5[6]	
	HEYA8		0.75[6]	
	HOC8	0.45[14]		
	IGROV1		2.21[6]	
	JHOC5		1.72[6]	
	JHOM1		4.72[6]	
	JHOS2		3.24[6]	
	KURAMOCHI		4.86[6]	
	MCAS		2.62[6]	
	NIHOVCAR3		2.53[6]	
	OAW42	0.69[14]	3.58[6]	
	OC314		1.70[6]	
	ONCODG1		3.20[6]	
	OV 1225	0.07[45]		
	OV 166	0.13[45]		
	OV B09	0.38[45]		
	OV56		2.84[6]	
	OV7		3.62[6]	
	OV90		3.02[6]	
	OVC NOVA	0.22[45]		
	OVCAR3	0.55[3]		
	OVCAR4	0.29[3]	1.48[6]	
	OVCAR5	0.41[3]	2.63[6]	
	OVCAR8	0.60[3]	2.50[6]	
	OVISE		3.45[6]	
	OVK18		1.21[6]	
	OVKATE		0.70[6]	
	OVMANA		3.81[6]	
	OVSAHO		4.03[6]	
	OVTOKO		3.27[6]	
	RMUGS		4.61[6]	
	SKOV3	0.90[3]	3.64[6]	
	SNU119		2.43[6]	
	SNU840		2.28[6]	
	TOV112D		3.70[6]	
	TOV21G		0.95[6]	
	TYKNU		3.69[6]	
	Patient cohort			0.411 (0.275-0.484, 253)[7]

Cancer type/site	Sample	SF2	AUC	Median RSI (error, n)
Pancreas	ASPC1		3.05[6]	
	BXPC3		2.26[6]	
	CAPAN1		3.56[6]	
	CAPAN2		1.612[6]	
	CFPAC1		2.85[6]	
	DANG		4.04[6]	
	HPAFII		3.37[6]	
	HS766T		5.09[6]	
	HUPT3		3.23[6]	
	HUPT4		3.12[6]	
	HX32K	0.34[11] 0.22[13] 0.22[10]		
	HX58	0.25[11] 0.33[14]		
	KP2		2.25[6]	
	KP3		3.67[6]	
	L33		4.08[6]	
	MIAPACA2		2.96[6]	
	PANC0203		3.53[6]	
	PANC0327		2.75[6]	
	PANC0403		3.28[6]	
	PANC0504		5.16[6]	
	PANC0813		3.14[6]	
	PANC1005		3.62[6]	
	PATU8902		3.64[6]	
	PATU8988S		4.35[6]	
	PATU8988T		4.52[6]	
	PK1		4.01[6]	
	PK45H		5.30[6]	
	PK59		2.33[6]	
	PSN1		1.52[6]	
	QGP1		2.92[6]	
	SU8686		2.50[6]	
	SW1990		3.71[6]	
	TCCPAN2		2.92[6]	
	Patient cohort			0.44 (0.397-0.492, 278)[7] 0.475 (0.425-0.527, 53)[7]

Appendix 1 - References

1. Abazeed, M. E. *et al.* Integrative radiogenomic profiling of squamous cell lung cancer. *Cancer Res.* **73**, 6289–6298 (2013).
2. Torres-Roca, J. F. *et al.* RSI: A Novel Biomarker Predicts RT Therapeutic Benefit in Breast Cancer. in *International Journal of Radiation Oncology*Biology*Physics* **81**, S62 (Elsevier BV, 2011).
3. Eschrich, S. *et al.* Systems Biology Modeling of the Radiation Sensitivity Network: A Biomarker Discovery Platform. *Int. J. Radiat. Oncol. Biol. Phys.* **75**, 497–505 (2009).
4. Eschrich, S. A. *et al.* Validation of a Radiosensitivity Molecular Signature in Breast Cancer. *Clin. Cancer Res.* **18**, 5134–5143 (2012).
5. Eschrich, S. A. *et al.* A Gene Expression Model of Intrinsic Tumor Radiosensitivity: Prediction of Response and Prognosis After Chemoradiation. *Int. J. Radiat. Oncol. Biol. Phys.* **75**, 489–496 (2009).
6. Yard, B. D. *et al.* A genetic basis for the variation in the vulnerability of cancer to DNA damage. *Nat. Commun.* **7**, (2016).
7. Strom, T. *et al.* Tumour radiosensitivity is associated with immune activation in solid tumours. *Eur. J. Cancer* **84**, 304–314 (2017).
8. Joan Allalunis-Turner, M., Barron, G. M., Day, R. S., Fulton, D. S. & Urtasun, R. C. Radiosensitivity testing of human primary brain tumor specimens. *Int J Radiat. Oncol.*

Biol Phys **23**, 339–343 (1992).
9. McMillan, T. J. & Holmes, A. The isolation and partial characterization of a radiation-sensitive clone of a human bladder carcinoma cell line. *Radiat. Res.* **128**, 301–305 (1991).
10. Deacon, J., Peckham, M. J. & Steel, G. G. The radioresponsiveness of human tumours and the initial slope of the cell survival curve. *Radiother. Oncol.* **2**, 317–323 (1984).
11. Gordon Steel, G. *et al.* The dose-rate effect in human tumour cells. *Radiotherapy and Oncology* **9**, 299–310 (1987).
12. Bodgi, L. *et al.* Assessing radiosensitivity of bladder cancer in vitro: A 2D vs. 3D approach. *Front. Oncol.* **9**, 153 (2019).
13. Fertil, B. & Malaise, E. P. Inherent cellular radiosensitivity as a basic concept for human tumor radiotherapy. *Int. J. Radiat. Oncol. Biol. Phys.* **7**, 621–629 (1981).
14. Björk-Eriksson, T., West, C., Karlsson, E. & Mercke, C. Discrimination of human tumor radioresponsiveness using low-dose rate irradiation. *Int. J. Radiat. Oncol. Biol. Phys.* **42**, 1147–1153 (1998).
15. Bjork-Eriksson, T. *et al.* The in vitro radiosensitivity of human head and neck cancers. *Br. Joumal Cancer* 2371–2375 (1998).
16. Challeton, C. *et al.* Characterization and radiosensitivity at high or low dose rate of four cell lines derived from human thyroid tumors. *Int. J. Radiat. Oncol. Biol. Phys.* **37**, 163–169 (1997).
17. Makurat, S., Spisz, P., Kozak, W., Rak, J. & Zdrowowicz, M. 5-iodo-4-thio-2′-deoxyuridine as a sensitizer of X-ray induced cancer cell killing. *Int. J. Mol. Sci.* **20**, 1308 (2019).
18. Mehta, M. *et al.* Regorafenib sensitizes human breast cancer cells to radiation by inhibiting multiple kinases and inducing DNA damage. *Int. J. Radiat. Biol.* **2**, 1–12 (2020).
19. Rouhani, M., Goliaei, B., Khodagholi, F. & Nikoofar, A. Lithium increases radiosensitivity by abrogating DNA repair in breast cancer spheroid culture. *Arch. Iran. Med.* **17**, 352–360 (2014).
20. Ahmed, K. A. *et al.* Utilizing the genomically adjusted radiation dose (GARD) to personalize adjuvant radiotherapy in triple negative breast cancer management. *EBioMedicine* **47**, 163–169 (2019).
21. Fehlauer, F. *et al.* Additive cytotoxic effect of cisplatin and X-irradiation on human glioma cell cultures derived from biopsy-tissue. *J. Cancer Res. Clin. Oncol.* **126**, 711–716 (2000).
22. Sheridan, M. T. & West, C. M. L. Ability to undergo apoptosis does not correlate with the intrinsic radiosensitivity (SF2) of human cervix tumor cell lines. *Int. J. Radiat. Oncol. Biol. Phys.* **50**, 503–509 (2001).
23. Hall, J. S. *et al.* Investigation of radiosensitivity gene signatures in cancer cell lines. *PLoS One* **9**, e86329 (2014).
24. Tam, K. F. *et al.* Potential application of the ATP cell viability assay in the measurement of intrinsic radiosensitivity in cervical cancer. *Gynecol. Oncol.* **96**, 765–770 (2005).
25. Kelland, L. R. & Steel, G. G. Differences in radiation response among human cervix carcinoma cell lines. *Radiother. Oncol.* **13**, 225–232 (1988).
26. West, C. M. L., Davidson, S. E., Burt, P. A. & Hunter, R. D. The intrinsic radiosensitivity of cervical carcinoma: correlations with clinical data. *Int. J. Radiat. Oncol. Biol. Phys.* **31**, 841–846 (1995).
27. Kiltie, A. E. *et al.* A correlation between residual DNA double-strand breaks and clonogenic measurements of radiosensitivity in fibroblasts from preradiotherapy cervix cancer patients. *Int. J. Radiat. Oncol. Biol. Phys.* **39**, 1137–1144 (1997).
28. Allalunis-Turner, M. J. *et al.* Inherent radio sensitivity testing of tumor biopsies obtained from patients with carcinoma of the cervix or endometrium. *Radiother. Oncol.* **22**, 201–205 (1991).
29. West, C. M. L., Davidson, S. E., Roberts, S. A. & Hunter, R. D. Intrinsic radiosensitivity and prediction of patient response to radiotherapy for carcinoma of the cervix. *Br J Cancer* **68**, 819–823 (1993).
30. Mohammadi, H. *et al.* Using the Radiosensitivity Index (RSI) to Predict Pelvic Failure

in Endometrial Cancer Treated With Adjuvant Radiation Therapy. *Int. J. Radiat. Oncol. Biol. Phys.* **106**, 496–502 (2020).
31. Dunne, A. L. *et al.* Relationship between clonogenic radiosensitivity, radiation-induced apoptosis and DNA damage/repair in human colon cancer cells. *Br. J. Cancer* **89**, 2277–2283 (2003).
32. Ahmed, K. A. *et al.* Differences Between Colon Cancer Primaries and Metastases Using a Molecular Assay for Tumor Radiation Sensitivity Suggest Implications for Potential Oligometastatic SBRT Patient Selection. *Int. J. Radiat. Oncol. Biol. Phys.* **92**, 837–842 (2015).
33. Petersen, C., Petersen, S., Milas, L., Lang, F. F. & Tofilon, P. J. Enhancement of Intrinsic Tumor Cell Radiosensitivity Induced by a Selective Cyclooxygenase-2 Inhibitor. *Clin. Cancer Res.* **6**, 2513–2520 (2000).
34. Stausbøl-Grøn, B. & Overgaard, J. Relationship between tumour cell in vitro radiosensitivity and clinical outcome after curative radiotherapy for squamous cell carcinoma of the head and neck. *Radiother. Oncol.* **50**, 47–55 (1999).
35. Stausbøl-Grøn, B. *et al.* In vitro radiosensitivity of tumour cells and fibroblasts derived from head and neck carcinomas: Mutual relationship and correlation with clinical data. *Br. J. Cancer* **79**, 1074–1084 (1999).
36. Patties, I., Jahns, J., Hildebrandt, G., Kortmann, R.-D. & Glasow, A. Additive Effects of 5-Aza-2'-deoxycytidine and Irradiation on Clonogenic Survival of Human Medulloblastoma Cell Lines. *Strahlentherapie und Onkol.* **185**, 331–338 (2009).
37. Krarup, M., Poulsen, H. S. & Spang-Thomsen, M. Cellular radiosensitivity of small-cell lung cancer cell lines. *Int. J. Radiat. Oncol. Biol. Phys.* **38**, 191–196 (1997).
38. Leonard, J. H., Ramsay, J. R., Kearsley, J. H. & Birrell, G. W. Radiation sensitivity of Merkel cell carcinoma cell lines. *Int. J. Radiat. Oncol. Biol. Phys.* **32**, 1401–1407 (1995).
39. Slonina, D., Hoinkis, C. & Dorr, W. Effect of Keratinocyte Growth Factor on Radiation Survival and Colony Size of Human Epidermal Keratinocytes In Vitro on JSTOR. *Radiat. Res.* **156**, 761–766 (2001).
40. Yuan, Z. *et al.* Intrinsic radiosensitivity, genomic-based radiation dose and patterns of failure of penile cancer in response to adjuvant radiation therapy. *Reports Pract. Oncol. Radiother.* **24**, 593–599 (2019).
41. Brooks, C. *et al.* Preclinical evaluation of sunitinib, a multi-tyrosine kinase inhibitor, as a radiosensitizer for human prostate cancer. *Radiat. Oncol.* **7**, 154 (2012).
42. Nuryadi, E., Permata, T. B. M., Komatsu, S., Oike, T. & Nakano, T. Inter-assay precision of clonogenic assays for radiosensitivity in cancer cell line A549. *Oncotarget* **9**, 13706–13712 (2018).
43. Strom, T. *et al.* Regional Radiation Therapy Impacts Outcome for Node-Positive Cutaneous Melanoma. *J. Natl. Compr. Cancer Netw.* **15**, 473–482 (2017).
44. Kelland, L. R., Bingle, L., Edwards, S. & Steel, G. G. High intrinsic radiosensitivity of a newly established and characterised human embryonal rhabdomyosarcoma cell line. *Br. J. Cancer* **59**, 160–164 (1989).
45. Slotman, B. J., Karim, A. B. M. F. & Rao, B. R. Ovarian cancer: radiation sensitivity in vitro. *Radiother. Oncol.* **19**, 323–327 (1990).

7. Appendix 2 – the meta-PCNA gene signature

The 131 genes in the meta-PCNA gene signature, listed alphabetically.

Gene Name	Symbol	Ensembl ID
ADAM metallopeptidase with thrombospondin type 1 motif 13	ADAMTS13	ENSG00000160323
Alpha haemoglobin stabilizing protein	AHSP	ENSG00000169877
5'-aminolevulinate synthase 2	ALAS2	ENSG00000158578
Apolipoprotein B mRNA editing enzyme catalytic subunit 3B	APOBEC3B	ENSG00000179750
AT-rich interaction domain 3A	ARID3A	ENSG00000116017
Anti-silencing function 1B histone chaperone	ASF1B	ENSG00000105011
Aurora kinase A	AURKA	ENSG0000087586
Aurora kinase B	AURKB	ENSG00000178999
Baculoviral IAP repeat containing 5	BIRC5	ENSG00000089685
Bisphosphoglycerate mutase	BPGM	ENSG00000172331
BUB1 mitotic checkpoint serine/threonine kinase B	BUB1B	ENSG00000156970
Cyclin A2	CCNA2	ENSG00000145386
Cyclin B1	CCNB1	ENSG00000134057
Cyclin B2	CCNB2	ENSG00000157456
Cell division cycle 20	CDC20	ENSG00000117399
Cell division cycle 45	CDC45	ENSG0000093009
Cell division cycle associated 3	CDCA3	ENSG00000111665
Cell division cycle associated 4	CDCA4	ENSG00000170779
Cell division cycle associated 8	CDCA8	ENSG00000134690
Cyclin dependent kinase 1	CDK1	ENSG00000170312
Cyclin dependent kinase inhibitor 3	CDKN3	ENSG00000100526
Chromatin licensing and DNA replication factor 1	CDT1	ENSG00000167513
Centromere protein A	CENPA	ENSG00000115163
Centromere protein U	CENPU	ENSG00000151725
Chromatin assembly factor 1 subunit A	CHAF1A	ENSG00000167670
Chemokine like factor	CKLF	ENSG00000217555
CDC28 protein kinase regulatory subunit 1B	CKS1B	ENSG00000173207
CDC28 protein kinase regulatory subunit 2	CKS2	ENSG00000123975
DExD-box helicase 39A	DDX39A	ENSG00000123136
DNAJ heat shock protein family member C9	DNAJC9	ENSG00000213551
Denticleless E3 ubiquitin protein ligase homolog	DTL	ENSG00000143476
Erythrocyte membrane protein band 4.2	EPB42	ENSG00000166947
Extra spindle pole bodies like 1, separase	ESPL1	ENSG00000135476
F-box protein 5	FBXO5	ENSG00000112029
F-box protein 7	FBXO7	ENSG00000100225
Ferrochelatase	FECH	ENSG00000066926
Flap structure-specific endonuclease 1	FEN1	ENSG00000168496
Forkhead box M1	FOXM1	ENSG00000111206
GATA binding protein 1	GATA1	ENSG00000102145
GINS complex subunit 1	GINS1	ENSG00000101003
GINS complex subunit 2	GINS2	ENSG00000131153
GTP binding protein 2	GTPBP2	ENSG00000172432
G2 and S-phase expressed 1	GTSE1	ENSG00000075218
Glycophorin A	GYPA	ENSG00000170180
Glycophorin B	GYPB	ENSG00000250361
H3.3 histone A	H3-3A	ENSG00000163041
Holliday junction recognition protein	HJURP	ENSG00000123485
Hydroxymethylbilane synthase	HMBS	ENSG00000256269

Gene Name	Symbol	Ensembl ID
High mobility group box 2	HMGB2	ENSG00000164104
High mobility group nucleosomal binding domain 2	HMGN2	ENSG00000198830
Kell metalloendopeptidase	KEL	ENSG00000197993
Kinesin family member 2C	KIF2C	ENSG00000142945
Kinesin family member 4A	KIF4A	ENSG00000090889
Kinesin family member 18B	KIF18B	ENSG00000186185
Kinesin family member 20A	KIF20A	ENSG00000112984
Kinesin family member 22	KIF22	ENSG00000079616
Kruppel like factor 1	KLF1	ENSG00000105610
Kruppel like factor 15	KLF15	ENSG00000163884
Lamin B receptor	LBR	ENSG00000143815
DNA ligase 1	LIG1	ENSG00000105486
Lamin B1	LMNB1	ENSG00000113368
LSM6 homolog	LSM6	ENSG00000164167
LYL1 basic helix-loop-helix family member	LYL1	ENSG00000104903
Mitotic arrest deficient 2 like 1	MAD2L1	ENSG00000164109
Minichromosome maintenance complex component 2	MCM2	ENSG00000073111
Minichromosome maintenance complex component 3	MCM3	ENSG00000112118
Minichromosome maintenance complex component 4	MCM4	ENSG00000104738
Minichromosome maintenance complex component 5	MCM5	ENSG00000100297
Minichromosome maintenance complex	MCM6	ENSG0000076003
Minichromosome maintenance complex component 7	MCM7	ENSG00000166508
Maternal embryonic leucine zipper kinase	MELK	ENSG00000165304
MHC class I polypeptide-related sequence B	MICB	ENSG00000204516
MIS18 kinetochore protein A	MIS18A	ENSG00000159055
Marker of proliferation Ki-67	MKI67	ENSG00000148773
Non-SMC condensing I complex subunit D2	NCAPD2	ENSG00000010292
Non-SMC condensing complex subunit D3	NCAPD3	ENSG00000151503
Non-SMC condensing II complex subunit G2	NCAPG2	ENSG00000146918
Nuclear factor, erythroid 2	NFE2	ENSG00000123405
Nuclear receptor binding SET domain protein 2	NSD2	ENSG00000109685
Nudix hydrolase 1	NUDT1	ENSG00000106268
Nucleoporin 37	NUP37	ENSG00000075188
Nucleoporin 210	NUP210	ENSG00000132182
Nucleolar and spindle associated protein 1	NUSAP1	ENSG00000137804
Opa interacting protein 5	OIP5	ENSG00000104147
Origin recognition complex subunit 6	ORC6	ENSG00000091651
PCNA clamp associated factor	PCLAF	ENSG00000166803
Proliferating cell nuclear antigen	PCNA	ENSG00000132646
Platelet factor 4	PF4	ENSG00000163737
Phosphogluconate dehydrogenase	PGD	ENSG00000142657
Plekstrin	PLEK	ENSG00000115956
DNA polymerase epsilon 2, accessory subunit	POLE2	ENSG00000100479
Pro-platelet basic protein	PPBP	ENSG00000163736
Peptidylprolyl isomerase H	PPIH	ENSG00000171960
Protein regulator of cytokinesis 1	PRC1	ENSG00000198901
Proteasome 26S subunit, non-ATPase 9	PSMD9	ENSG00000110801
Securin	PTTG1	ENSG00000164611
Rac GTPase activating protein 1	RACGAP1	ENSG00000161800
RAD51 associated protein 1	RAD51AP	ENSG00000111247
Replication factor C subunit 3	RFC3	ENSG00000133119

Gene Name	Symbol	Ensembl ID
Replication factor C subunit 4	RFC4	ENSG00000163918
Ring finger and WD repeat domain 3	RFWD3	ENSG00000168411
Rh associated glycoprotein	RHAG	ENSG00000112077
Rh blood group CcEe antigens	RHCE	ENSG00000188672
Rh blood group D antigen	RHD	ENSG00000187010
Replication protein A3	RPA3	ENSG00000106399
Ribose-5-phosphate isomerase A	RPIA	ENSG00000153574
Ribonuclease P/MRP subunit p30	RPP30	ENSG00000148688
Ribonuclease reductase regulatory subunit M2	RRM2	ENSG00000171848
SHC binding and spindle associated 1	SHCBP1	ENSG00000171241
Structural maintenance of chromosomes 4	SMC4	ENSG00000113810
SNF8 subunit of ESCRT-II	SNF8	ENSG00000159210
Small nuclear riboprotein polypeptides B and B1	SNRPB	ENSG00000125835
Small nuclear ribonucleoprotein D1 polypeptide	SNRPD1	ENSG00000167088
Spectrin alpha, erythrocytic 1	SPTA1	ENSG00000163554
Serine and arginine rich splicing factor 2	SRSF2	ENSG00000161547
Transforming acidic coiled-coil containing protein 3	TACC3	ENSG00000013810
TAL bHLH transcription factor 1	TAL1	ENSG00000162367
Transcription factor 3	TCF3	ENSG00000071564
Transcription factor Dp-1	TFDP1	ENSG00000198176
Timeless circadian regulator	TIMELESS	ENSG00000111602
DNA topoisomerase II alpha	TOP2A	ENSG00000131747
TPX2 microtubule nucleation factor	TPX2	ENSG00000088325
Tripartite motif containing 10	TRIM 10	ENSG00000204613
Tripartite motif containing 58	TRIM58	ENSG00000162722
tRNA methyltransferase 5	TRMT5	ENSG00000126814
Trophinin associated protein	TROAP	ENSG00000135451
Translocator protein 2	TSPO2	ENSG0000011212
Thymidylate synthetase	TYMS	ENSG00000176890
Ubiquitin conjugating enzyme E2C	UBEC2C	ENSG00000175063
VRK serine/threonine kinase 1	VRK1	ENSG00000100749
ZW10 interacting kinetochore protein	ZWINT	ENSG00000122952

Appendix 2 – Reference

Venet, D., Dumont, J. E. & Detours, V. Most random gene expression signatures are significantly associated with breast cancer outcome. *PLoS Comput. Biol.* **7**, (2011).